

The University of Nottingham

Department of Molecular Therapeutics and Formulation

School of Pharmacy

Non-covalent polymer-protein complexes for pulmonary protein delivery

Alejandro Nieto Orellana, MPharm

Thesis submitted to the University of Nottingham

for the degree of Doctor of Philosophy

June 2017

A mis padres Pedro y Pepi
y a mis hermanos Pedro y Samuel

Abstract

Pulmonary delivery of protein and peptide therapeutics has recently received increasing attention to treat both local and systemic diseases. However, to further increase its current clinical impact, numerous challenges including protein degradation, pulmonary clearance and immunogenicity, still need to be addressed. To this aim, in the present work we developed novel non-covalent polymer-protein nanocomplexes to allow reversible conjugation of proteins, and investigate their potential to protect and release them at the target site following pulmonary administration.

Accordingly, a family of structurally related block copolymers $mPEG_{2k}$-poly(glutamic acid) with linear A-B ($mPEG_{2k}$-*lin*-polyGA) and miktoarm A-B_3 ($mPEG_{2k}$-*mik*-$(polyGA)_3$) structure was first synthesised to assess the effect of macromolecular topology of the copolymers on electrostatic polymer-protein complexation, using lysozyme as the model protein substrate. ($mPEG_{2k}$-*lin*-GA) and ($mPEG_{2k}$-*mik*-$(GA)_3$)-lysozyme nanocomplexes were then formulated into dry powders suitable for pulmonary delivery by spray-drying, using different aerosol excipients. The aerodynamic properties of these dry powders, their ability to efficiently release the nanocomplexes in aqueous environment and their capacity to protect lysozyme from proteolytic enzymes were evaluated.

Finally, to improve uptake of nanocomplexes by lung epithelial cells cyanocobalamin (vitamin B_{12}) ligands were introduced within the $mPEG_{2k}$-polyGA copolymers, and the resulting targeted macromolecules were

complexed with lysozyme. These targeted nanocomplexes were then formulated into dry powders and their ability to enhance lysozyme uptake by Calu-3 lung epithelial cells was assessed *in vitro*, along with their effect on activation of the complement system. Finally, (vitB_{12}- PEG_{3k}-polyGA)-lysozyme dry powder formulations were tested *in vivo* through administration to healthy BALB/c mice, and pulmonary protein deposition/retention and local pulmonary tolerance were evaluated.

Taken together, this study indicates that if complexing polymers are appropriately designed, efficient non-covalent complexation of proteins and peptides can be achieved. Importantly, inclusion within polymer complexes can protect proteins from proteolytic degradation, and when suitable targeted ligands are introduced, increase protein cellular uptake in the lung epithelium, and enhance protein retention in the lungs with minimal toxicity.

Acknowledgements

Firstly, a whole-hearted thank you to my supervisors Drs Snow Stolnik, “Beppe” Mantovani, Cynthia Bosquillon, Franco Falcone and Nick Childerhouse. Snow, thank you for your energy, enthusiasm, support and motivation through all my PhD. Your guidance and ability to bring out the best in myself has importantly contributed to my personal and professional growth. Beppe, there are no words to express my gratitude towards you. You were more than a supervisor, you were a big support here in UK. I would not be here today without the moments we spent together during all my “heart attack” periods. Thanks for having always time to make me laugh and release out all my stress. Cynthia, everything started when you replied to my email 4 years ago. Big thank you for all your help, support and all the chats we had together. Franco, thank you for your helpful advises on gel electrophoresis. Nick, thank you for giving me the opportunity to work within your team at Vectura and more important, thanks for making me feel at home. Thanks for your advices and comments on pulmonary delivery aspects. They were really important to me. Also, I would like to extend my thanks and appreciation to my internal assessor Dr. Maria Marlow for her very helpful advices and opinion on the project.

My sincerest gratitude and upmost respect goes to my family and friends for their never-ending love and encouragement throughout my life. I apologise for not being always present, but surely the future will bring us closer

together. I would like to especially dedicate this work to my parents Pedro and Pepi and my brothers Pedro and Samuel. Papa, mama, gracias por hacerme la persona que soy hoy en día. Por apoyarme en cada decisión que he tomado y motivarme a conseguir mis sueños. Cada día me siento un afortunado por teneros como padres. Bonitos... habéis sido un modelo a seguir para mí y quizá sea esta sea una de las razones por la que hoy estoy aquí. Me habéis guiado en la dirección correcta durante toda mi vida y seguramente no hubiera llegado tan lejos si no fuera por vosotros. Papa, mama, Pedrito, Mue, espero que estéis tan orgullosos de mí como yo lo estoy de vosotros. GRACIAS.

Marta, una de las personas más importantes en mi vida. Gracias por ser mi apoyo, mi motivación y la calma en mi tempestad. Gracias por estar a mi lado día a día. Gracias por ser mi compañera de viaje.

Finally, I would like to thank people that have been my family here in Nottingham: Paola, Nora, JB, Rosa, Patricia, Ruggero, Ioanna, Vincenzo, Francesca, Iria, Nuno, Hiteshri.... and especially to my best “coleguita” Joao! Por fin lo conseguimos!!!

A todos MUCHISIMAS GRACIAS/THANK YOU VERY MUCH!

Table of Contents

Abstract.....I

Acknowledgments.....III

Table of Contents.....V

List of Figures.....VIII

List of Tables.....XVIII

List of Schemes.....XIX

Abbreviations.....XX

Chapter 1: Literature review and objectives.....1

1.1. Introduction.....3
1.1.1. Protein therapeutics.....3
1.1.2. Pulmonary protein delivery.....5
1.1.2.1. Anatomy and physiology of the respiratory system.....5
1.1.2.2. Advantages of pulmonary delivery.....8
1.1.2.3. Pulmonary protein delivery: limitations.....8
1.1.2.3.1. Mucociliary escalator.....9
1.1.2.3.2. Alveolar macrophages.....10
1.1.2.3.3. Lung proteases.....10
1.1.2.3.4. Airway epithelium.....12
1.1.3. Polymeric nanosystems.....14
1.1.3.1. Polymer-protein interactions.....15
1.1.3.1.1. Covalent polymer-protein conjugates.....16
1.1.3.1.2. Electrostatic interactions.....17
1.1.4. Devices for pulmonary delivery.....19
1.1.4.1. Pressured Metered Dose Inhalers (pMDIs).....19
1.1.4.2. Nebulisers.....20
1.1.4.3. Dry Powder Inhalers (DPIs).....22
1.2. Aims and objectives of the PhD.....27
1.3. References.....28

Chapter 2: Effect of polymer topology on non-covalent polymer-protein complexation: miktoarm *versus* linear mPEG-poly(glutamic acid) copolymers.....42

2.1. Introduction.....44

2.2. Experimental section....48
2.3. Results and Discussion....60
2.3.1. Synthesis of miktoarm and linear $mPEG_{2k}$-poly(glutamic acid) copolymers....60
2.3.2. Polymer-protein complexes characterisation....65
2.3.3. Lysozyme conformation in polymer-protein complexes : intrinsic fluorescence studies....71
2.3.4. Lysozyme activity assay....72
2.3.5. Toxicity of $mPEG_{2k}$-poly(glutamic acid) copolymers....75
2.3.5.1. Metabolic activity (MTS assay)....76
2.3.5.2. Membrane integrity (LDH assay)....78
2.3.5.3. Apoptotic assay (Annexin V-FITC/PI assay)....79
2.4. Concluding remarks....82
2.5. References....84

Chapter 3: Dry powder formulations of non-covalent protein complexes with linear or miktoarm copolymers for pulmonary delivery....90

3.1. Introduction....92
3.2. Experimental section....96
3.3. Results and Discussion....102
3.3.1. Characterisation of dry powders....102
3.3.2. Aerosolisation performance....111
3.3.3. Nanocomplexes recovery, protein activity and protein protection against proteolytic enzymes....114
3.4. Concluding remarks....120
3.5. References....121

Chapter 4: PEG-poly(glutamic acid) copolymers for targeted delivery of proteins....126

4.1. Introduction....128
4.2. Experimental section....133
4.3. Results and Discussion....152
4.3.1. Synthesis of targeted linear and miktoarm $vitB_{12}$-PEG_{3k}-poly(glutamic acid) copolymers....152
4.3.2. *In vitro* protein internalisation by the airway epithelium....161
4.3.3. Complement activation....167
4.3.4. Local pulmonary tolerance of polymer-protein nanocomplexes-based dry powder formulations in healthy mice....168
4.3.5. *In vivo* pulmonary deposition and retention of polymer-protein nanocomplexes-based dry powder formulations in healthy mice....172
4.4. Concluding remarks....175
4.5. References....176

Chapter 5: Concluding remarks and Future prospects.....181

5.1. Concluding remarks and Future prospects.....182
5.2. References.....188

Chapter 6: Supporting Information.....189

6.1. Material and Methods of Chapter 2.....191
6.1.1. Material.....191
6.1.2. Instrumentation.....192
6.1.3. Characterisation of copolymers and corresponding precursors.....194
6.1.4. TEM analysis.....204
6.1.5. Circular dichroism.....205
6.1.6. Synthesis of mPEG-lysozyme covalent conjugates.....205
6.1.7. Metabolic activity (MTS assay).....208
6.1.8. Membrane integrity (LDH assay).....208
6.1.9. Apoptosis assay (Annexin V-FITC/PI assay).....209
6.1.10. Stability of ($mPEG_{2k}$-polyGA)-lysozyme nanocomplexes in DMEM.....209
6.2. Material and Methods of Chapter 3.....210
6.2.1. Material.....210
6.2.2. Particle size distribution of nanocomplexes.....210
6.3. Material and Methods of Chapter 4.....211
6.3.1. Material.....211
6.3.2. Instrumentation.....212
6.3.3. Characterisation of copolymers and corresponding precursors.....214
6.3.4. Lysozyme-Cy5: Reaction conditions.....223
6.3.5. *In vivo* pulmonary deposition and retention of polymer-protein nanocomplexes-based dry powder formulations in healthy mice.....225
6.4. References.....229

List of Figures

Chapter 1

Figure 1.1. Global biotech market estimate. Source: DTTL life sciences and health care industry group analysis of industry report: global biotechnology, IBISWorld, January 2015……4

Figure 1.2. Illustration of the respiratory system (Respiratory-system, 2001)…7

Figure 1.3. Subdivisions and structure of intrapulmonary airways. Taken from (Martin, 2008).....7

Figure 1.4. Schematic representation of the main mechanisms for protein clearance after pulmonary protein administration: mucociliary clearance, macrophage uptake and proteolytic degradation. Adapted from (Depreter et al., 2013)……9

Figure 1.4. Schematic representation of protein delivery to the airway epithelium. After aerosol particles land and disintegrate on lung lining fluids, proteins must cross the lung epithelium to reach systemic circulation, or alternatively penetrate inside epithelial cells, to exert their therapeutic action. To this end, proteins need to overcome effective clearance mechanisms including proteolytic degradation and mucociliary clearance. Adapted from (Ruge et al., 2013).....13

Figure 1.6. Schematic representation of polymer-protein interactions by covalent and electrostatic interactions. Protein molecular structure was taken from protein data bank (PDB database entry lysozyme, 1HEL)……..16

Figure 1.7. Representation of a typical pressurised metered dose inhaler (pMDI). Taken from (Newman, 2005)……..20

Figure 1.8. Representation of typical (A) jet and (B) ultrasonic nebulisers. Taken from (O'Callaghan and Barry, 1997)……..22

Figure 1.9. Principle of DPI design. Typically, the formulation is composed of micronised drug combined with larger carrier particles which are dispensed by a metering system. Particles are dispersed either by just the respiratory influx of the patient (passive) or with the help of different mechanisms (active) into the patient's airways. After that, drug particles separate from the carrier particles and are carried into the lung. Taken from (Telko and Hickey, 2005).....24

Chapter 2

Figure 2.1. Schematic representation of electrostatic polymer-protein complexation. Protein molecular structure was taken from protein data bank (PDB database entry lysozyme, 1HEL)……..44

Figure 2.2. Examples of miktoarm copolymer topologies, where polymer arms change by the molecular weight and the chemical groups. A, B and C refers to different polymer composition and " ' " refers to different polymer length. Adapted from (Khanna et al., 2010)……..45

Figure 2.3. ^{1}H NMR spectrum of miktoarm mPEG$_{2k}$-*mik*-(GA$_{10}$)$_3$ in D$_2$O……..64

Figure 2.4. Electrophoretic separation at pH 2.0 (A) and pH 7.4 (B) of free protein from linear mPEG$_{2k}$-*lin*-GA$_{10}$ and mPEG$_{2k}$-*lin*-GA$_{30}$, and miktoarm mPEG$_{2k}$-*mik*-(GA$_{10}$)$_3$ and mPEG$_{2k}$-*mik*-(GA$_{30}$)$_3$-derived complexes in a 1% agarose gel, run 2 h at 100 mA in Tris-Acetate-EDTA buffer……66

Figure 2.5. Particle size distribution of mPEG$_{2k}$-*lin*-GA$_{10}$, mPEG$_{2k}$-*lin*-GA$_{30}$, mPEG$_{2k}$-*mik*-(GA$_{10}$)$_3$ and mPEG$_{2k}$-*mik*-(GA$_{30}$)$_3$-derived complexes with lysozyme at charge ratio 1.0 (A) and 2.5 (B). D_H is the average hydrodynamic diameter ± SD of polymer-protein nanocomplexes as assessed by nanoparticle tracking analysis (NTA)……70

Figure 2.6. Tryptophan fluorescence spectra of lysozyme after complexation with linear mPEG$_{2k}$-*lin*-GA$_{10}$ and mPEG$_{2k}$-*lin*-GA$_{30}$, and miktoarm mPEG$_{2k}$-*mik*-(GA$_{10}$)$_3$ and mPEG$_{2k}$-*mik*-(GA$_{30}$)$_3$ copolymers at charge ratio 2.5 in 10 mM phosphate buffer pH 7.4. Polymer-protein complexes (blue), native lysozyme (red) and denatured protein (black). All spectra recorded at room temperature……72

Figure 2.7. A. Lysozyme enzymatic activity of linear mPEG$_{2k}$-*lin*-GA$_{10}$ and mPEG$_{2k}$-*lin*-GA$_{30}$, and miktoarm mPEG$_{2k}$-*mik*-(GA$_{10}$)$_3$ and mPEG$_{2k}$-*mik*-(GA$_{30}$)$_3$-derived complexes. Free protein (red), free polymer (black), and 0.1 (green), 0.5 (orange), 1.0 (grey) and 2.5 (pink) polymer-protein charge ratio *r*. OD$_{460nm}$ represents the optical density of the samples at λ = 460 nm. B. Lysozyme enzymatic activity of selected complexes at polymer-protein charge ratio of 2.5 – with either linear mPEG$_{2k}$-*lin*-GA$_{30}$, and miktoarm mPEG$_{2k}$-*mik*-(GA$_{10}$)$_3$ – before and after polymer de-complexation by addition of poly(allyl amine) (240 µg mL^{-1}, 4.2 mM of protonable amino groups)……..74

Figure 2.8. MTS assay in A549 and Calu-3 cells after treatment with free mPEG$_{2k}$-polyGA copolymers and (mPEG$_{2k}$-polyGA)-lysozyme nanocomplexes for A) 4 h and B) 24 h. (mPEG$_{2k}$-*lin*-GA$_{10}$) (green), (mPEG$_{2k}$-*lin*-GA$_{30}$) (blue), (mPEG$_{2k}$-*mik*-(GA$_{10}$)$_3$) (grey), mPEG$_{2k}$-*mik*-(GA$_{30}$)$_3$ (pink)-derived complexes or copolymer……77

Figure 2.9. Percentage of total LDH released from A549 and Calu-3 cells after treatment with free mPEG$_{2k}$-polyGA copolymers and (mPEG$_{2k}$-polyGA)-

lysozyme nanocomplexes for 4 h. mPEG$_{2k}$-*lin*-GA$_{10}$ (green), mPEG$_{2k}$-*lin*-GA$_{30}$ (blue), mPEG$_{2k}$-*mik*-(GA$_{10}$)$_3$ (grey), mPEG$_{2k}$-*mik*-(GA$_{30}$)$_3$ (pink)-derived complexes or copolymer……79

Figure 2.10. Examples of Annexin V-FITC/PI double staining flow cytometry analysis of necrosis and apoptosis in A549 cells and Calu-3 cells after 4 h treatment with mPEG$_{2k}$-polyGA copolymers. A-C: A549 cells; D-F Calu-3 cells; A, D: Untreated cells; B, E: mPEG$_{2k}$-*mik*-(GA$_{10}$)$_3$ copolymers; C, F: (mPEG$_{2k}$-*mik*-(GA$_{10}$)$_3$)-lysozyme nanocomplexes. FL1 and FL3 represents Annexin V-FITC and propidium iodide staining, respectively. I1: necrosis; I2: late apoptosis; I3: viable cells and I4: early apoptosis……81

Figure 2.11. Percentages of apoptosis (left panels) and necrosis (right panels) in A549 cells and Calu-3 cells after treatment with mPEG$_{2k}$-polyGA copolymers, both free and complexed with lysozyme for 4 h. Solid bars: free mPEG$_{2k}$-polyGA copolymers. Hatched bars: (mPEG$_{2k}$-polyGA)-lysozyme nanocomplexes. Untreated cells (black), mPEG$_{2k}$-*lin*-GA$_{10}$ (green), mPEG$_{2k}$-*lin*-GA$_{30}$ (blue), mPEG$_{2k}$-*mik*-(GA$_{10}$)$_3$ (grey) and mPEG$_{2k}$-*mik*-(GA$_{30}$)$_3$ (pink)-derived complexes or copolymer……81

Chapter 3

Figure 3.1. Schematic representation of the main mechanisms for protein clearance after pulmonary protein administration: mucociliary clearance, macrophage uptake and proteolytic degradation. Adapted from (Depreter et al., 2013)……94

Figure 3.2. Assembly of non-covalent polymer-protein ionic complexes and their formulation as dry powders by spray-drying……95

Figure 3.3. Representative scanning electron microscopy (SEM) images of dry powders containing un-complexed lysozyme (A, B and C), and (mPEG$_{2k}$-*mik*-(GA$_{30}$)$_3$)-lysozyme nanocomplexes (D, E and F). Excipients: (A, D) mannitol + 10% (*w/w*) leucine, (B, E) trehalose + 10% (*w/w*) leucine and (C, F) mannitol. All formulations contained 6.6% (w/w) phosphate buffer salts……..107

Figure 3.4. Protein encapsulation efficiency in trehalose, trehalose + leucine, mannitol and mannitol + leucine dry powders. Free un-complexed lysozyme (red), and mPEG$_{2k}$-*lin*-GA$_{10}$ (green), mPEG$_{2k}$-*lin*-GA$_{30}$ (blue), mPEG$_{2k}$-*mik*-(GA$_{10}$)$_3$ (grey) and mPEG$_{2k}$-*mik*-(GA$_{30}$)$_3$ (pink)-derived complexes. All formulations contained 6.6% (*w/w*) phosphate buffer salts. All experiments were carried out in quadruplicate……108

Figure 3.5. Moisture content of dry powders investigated in this study. Free un-complexed lysozyme (red), and mPEG$_{2k}$-*lin*-GA$_{10}$ (green), mPEG$_{2k}$-*lin*-GA$_{30}$ (blue), mPEG$_{2k}$-*mik*-(GA$_{10}$)$_3$ (grey) and mPEG$_{2k}$-*mik*-(GA$_{30}$)$_3$ (pink)-derived complexes. All formulations contained 6.6% (*w/w*) phosphate buffer salts……109

Figure 3.6. Fine particle fraction (FPF) (solid bars) and emitted dose (ED) (hatched bars) of trehalose, trehalose + leucine, mannitol and mannitol + leucine dry powders. Control (black), lysozyme (red), mPEG$_{2k}$-*lin*-GA$_{10}$ (green), mPEG$_{2k}$-*lin*-GA$_{30}$ (blue), mPEG$_{2k}$-*mik*-(GA$_{10}$)$_3$ (grey) and mPEG$_{2k}$-*mik*-(GA$_{30}$)$_3$ (pink)-derived complexes. 'Control' denotes blank powder formulation that contains only excipient without lysozyme or copolymer, and 'Lysozyme' denotes dry powder formulation that contains no copolymer. All formulations contained 6.6% (w/w) phosphate buffer salts. All experiments were carried out in triplicate. FPF and ED values from mannitol dry powders were obtained from single, double or triple measurements due to low material quantity obtained. One-way ANOVA was used for statistical analysis. * $p < 0.1$, ** $p < 0.01$ *** $p < 0.001$, **** $p < 0.0001$……113

Figure 3.7. Nanoparticle tracking analysis (NTA) of dry powder formulations following incubation in phosphate buffer (PB, 10 mM, pH 7.4) at 70 µg mL^{-1} protein concentration in (mPEG$_{2k}$-polyGA)-lysozyme nanocomplexes for 15 min. (A) Particle size distribution of nanocomplexes before spray-drying. (B) Particle size distribution of nanocomplexes recovered from mannitol + leucine-based dry powders. mPEG$_{2k}$-*lin*-GA$_{10}$ (green), mPEG$_{2k}$-*lin*-GA$_{30}$ (blue), mPEG$_{2k}$-*mik*-(GA$_{10}$)$_3$ (grey) and mPEG$_{2k}$-*mik*-(GA$_{30}$)$_3$ (pink)-derived complexes.....115

Figure 3.8. Lysozyme enzymatic activity. Solid bars: lysozyme activity after incubation of the dry powders in PB, hatched bars: lysozyme activity after incubation of the dry powders in the presence of poly(allyl amine). Trehalose, trehalose + leucine, mannitol and mannitol + leucine dry powders investigated in this study. Lysozyme (red), mPEG$_{2k}$-*lin*-GA$_{10}$ (green), mPEG$_{2k}$-*lin*-GA$_{30}$ (blue), mPEG$_{2k}$-*mik*-(GA$_{10}$)$_3$ (grey) and mPEG$_{2k}$-*mik*-(GA$_{30}$)$_3$ (pink)-derived complexes. 'Lysozyme' denotes dry powder formulation that contains no copolymer. All experiments were carried out in triplicate. Un-complexed free lysozyme was used as a reference (100% enzymatic activity). One-way ANOVA was used for statistical analysis. * $p < 0.1$, ** $p < 0.01$ *** $p < 0.001$, **** $p < 0.0001$……117

Figure 3.9. (mPEG$_{2k}$-polyGA)-lysozyme complexes: protection against lysozyme proteolytic degradation. Lysozyme activity was measured after incubation of the dry powders in the presence of trypsin for 3 h, followed by treatment with poly(allyl amine) for 1 h. Trehalose, trehalose + leucine, mannitol and mannitol + leucine dry powders investigated in this study. Un-complexed lysozyme (red), mPEG$_{2k}$-*lin*-GA$_{10}$ (green), mPEG$_{2k}$-*lin*-GA$_{30}$ (blue), mPEG$_{2k}$-*mik*-(GA$_{10}$)$_3$ (grey) and mPEG$_{2k}$-*mik*-(GA$_{30}$)$_3$ (pink)-derived complexes. All experiments were carried out in triplicate. Un-complexed free lysozyme was used as a reference (100% enzymatic activity). One-way ANOVA was used for statistical analysis. * $p < 0.1$, ** $p < 0.01$ *** $p < 0.001$, **** $p < 0.0001$.....119

Chapter 4

Figure 4.1. Chemical structure of cyanocobalamin (vitamin B_{12}) and targeted and non-targeted PEG-poly(glutamic acid) copolymers used in this part of this work……132

Figure 4.2. Graphic representation of the spraying process of dry powder formulations on top of Calu-3 cell monolayers using a Penn-Century® device……145

Figure 4.3. Characterisation of clicked product (20), product (21) and B_{12}-functionalised PEG-poly(GA) copolymers (13) and (18): A, B and C) HSQC and D) 1D NMR spectra of the α-CH_2 signals of the dibenzocyclooctyne-carbamate before and after click reaction……160

Figure 4.4. Particle size distribution of non-targeted and targeted nanocomplexes. Targeted polymer-protein nanocomplexes were composed of $mPEG_{2k}$-polyGA (85% mol:mol) and $vitB_{12}$-PEG_{3k}-polyGA (15% mol:mol) copolymers. D_H is the average hydrodynamic diameter ± SD of polymer-protein nanocomplexes as assessed by nanoparticle tracking analysis (NTA)……161

Figure 4.5. Cellular uptake in Calu-3 monolayers of un-complexed lysozyme compared to lysozyme complexed with targeted $vitB_{12}$-PEG_{3k}-polyGA copolymers alone, or in competition experiment with an excess of free vitamin B_{12}, and lysozyme complexed with non-targeted $mPEG_{2k}$-polyGA copolymers. All samples were added in solution on top of the cells. "Un-complexed lysozyme" corresponds to samples without polymers. One-way ANOVA was used for statistical analysis. ** $p < 0.01$, *** $p < 0.001$……163

Figure 4.6. Dry powder distribution after spraying them using a Penn-Century® device onto Transwell® inserts. Four different Transwell® inserts were used at once for each formulation. Dry powders containing (A) un-complexed lysozyme, (B) $mPEG_{2k}$-*lin*-GA_{30}, (C) $mPEG_{2k}$-*mik*-$(GA_{10})_3$, (D) $vitB_{12}$-PEG_{3k}-*lin*-polyGA and (E) $vitB_{12}$-PEG_{3k}-*mik*-poly$(GA)_3$-derived nanocomplexes. Each formulation was sprayed twice (2 mg per dose). Each square contains 900 small coloured images. These colours indicate the percentage of the Transwell® insert surface covered by particles. Blue: 0.01% of particles; orange: 5% particles; red: 10% particles. White small squares corresponds to 0% particles or focus issues with the microscope during the analysis. All dry powder contain 6.6% (*w/w*) phosphate buffer salts, 10% (*w/w*) leucine and up to 100% (*w/w*) trehalose……165

Figure 4.7. Representative scanning electron microscopy (SEM) images of dry powders before (A) and after (B) spraying them using a Penn-Century® device. "Un-complexed lysozyme" refers to formulations without copolymers. All dry powders contain 6.6% (*w/w*) phosphate salts, 10% (*w/w*) leucine and up to 100% (*w/w*) trehalose……166

Figure 4.8. Cell uptake in Calu-3 cells of un-complexed lysozyme formulated into dry powders compared to lysozyme complexed with targeted vitB_{12}-PEG_{3k}-polyGA and non-targeted mPEG_{2k}-polyGA copolymers, both formulated into dry powders. All dry powder samples were directly applied on top of the Calu-3 cells grown in AIC conditions. "Un-complexed lysozyme" corresponds to dry powders without polymers. All dry powders contain 6.6% (*w/w*) phosphate salts, 10% (*w/w*) leucine and up to 100% (*w/w*) trehalose. One-way ANOVA was used for statistical analysis. *** $p < 0.001$, **** $p < 0.0001$……166

Figure 4.9. Complement activation at 37˚C by un-complexed lysozyme, (vitB_{12}-PEG_{3k}-*lin*-polyGA)-lysozyme and (vitB_{12}-PEG_{3k}-*mik*-poly$(GA)_3$)-lysozyme nanocomplexes. Lysozyme concentration was kept constant to 1116 µg mL^{-1} for all samples. "Un-complexed lysozyme" corresponds to formulations without copolymers. One-way ANOVA was used for statistical analysis. *** $p < 0.001$, **** $p < 0.0001$……..168

Figure 4.10. Pro-inflammatory cytokine IL-1β, IL-6, and TNF-α gene expression in lung tissues, following endotracheal administration of dry powder formulations. Results are shown for untreated mice, (negative control) or those treated with LPS (positive control), empty DP (no polymer, no protein), UDP-P (no polymer) and UDP-L1 (with targeted nanocomplexes). One-way ANOVA was used for statistical analysis. *** $p < 0.001$, **** $p < 0.0001$……170

Figure 4.11. Bronchoalveolar lavage fluid analysis: differential cell count and representative images of the different cells found in the bronchoalveolar lavage fluid following endotracheal administration in healthy mice of dry powder formulations three times a week for three consecutive weeks (2 mg per dose). Mice were not treated (negative control) or treated with LPS (positive control), empty UDP (no polymer, no protein), UDP-P (no polymer) and UDP-L1 (with targeted nanocomplexes). One-way ANOVA was used for statistical analysis. *** $p < 0.001$, **** $p < 0.0001$……..171

Figure 4.12. Distribution of fluorescent lysozyme in the lungs of healthy mice after 0, 3 and 14 h after pulmonary administration. Examples of a 7-µm longitudinal lung cryo-section that was observed using a fluorescent microscope at 200 x magnification. The images show the distribution of red labelled lysozyme-Cy5 (on an Alexa Fluor 568 filter) in the blue fluorescent lung tissue (on a DAPI filter) of healthy mice after administration of 2 mg dry powder formulations: (i) LDP-L1 (targeted nanocomplexes), (ii) LDP-L2 (non-targeted nanocomplexes) and (iii) LDP-P (no polymer) using the pulmonary delivery device……174

Chapter 5

Figure 5.1. Particle size distribution of mPEG_{2k}-*lin*-GA_{30}, mPEG_{2k}-*mik*-$(GA_{10})_3$, vitB_{12}-PEG_{3k}-*lin*-polyGA and vitB_{12}-PEG_{3k}-*mik*-poly$(GA)_3$-derived complexes with RNAse A at polymer-protein charge ratio 2.5. D_H is the average hydrodynamic diameter ± SD of polymer-protein nanocomplexes as assessed

by nanoparticle tracking analysis (NTA). Protein concentration was kept constant (70 μg mL^{-1}) for all samples……187

Figure 5.2. MTS assay in Calu-3 cells after 4 and 24 h treatment with un-complexed RNAse A (red), linear (blue) and miktoarm (grey) copolymers complexed with RNAse A. Polymer-protein nanocomplexes were composed of $mPEG_{2k}$-polyGA (85% mol:mol) and $vitB_{12}$-PEG_{3k}-polyGA (15% mol:mol) copolymers. RNAse A concentration was kept constant (200 μg mL^{-1}) for all the samples. One-way ANOVA was used for statistical analysis. ** $p < 0.01$, **** $p < 0.0001$……187

Chapter 6

Figure S1. ^{1}H NMR spectrum of 3,4,5-tris(allyloxy)benzoic acid methyl ester (1) in $CDCl_3$……194

Figure S2. ^{13}C NMR spectrum of 3,4,5-tris(allyloxy)benzoic acid methyl ester (1) in $CDCl_3$……194

Figure S3. FT-IR spectrum of 3,4,5-tris(allyloxy)benzoic acid methyl ester (1) (neat)……195

Figure S4. Mass spectrum (ESI-MS) of 3,4,5-tris(allyloxy)benzoic acid methyl ester (1)……195

Figure S5. ^{1}H NMR spectrum of 3,4,5-tris(allyloxy)benzoic acid (2) in $CDCl_3$……196

Figure S6. ^{13}C NMR spectrum of 3,4,5-tris(allyloxy)benzoic acid (2) in $CDCl_3$……196

Figure S7. FT-IR spectrum of 3,4,5-tris(allyloxy)benzoic acid (2) (neat)……197

Figure S8. Mass spectrum (ESI-MS) of 3,4,5-tris(allyloxy)benzoic acid (2)……197

Figure S9. FT-IR spectrum of 3,4,5-tris(allyloxy)benzoyl chloride (3) (neat)…198

Figure S10. ^{1}H NMR spectrum of $mPEG_{2k}$ triallyl ether (4) in $CDCl_3$……198

Figure S11. FT-IR spectrum of $mPEG_{2k}$ triallyl ether (4) (neat)……199

Figure S12. ^{1}H NMR spectrum of triaminoPEG$_{2k}$ (5) in CD_3OD……199

Figure S13. Mass spectrum (MALDI-TOF) of methoxypolyethylene glycol amine 2,000……200

Figure S14. Mass spectrum (MALDI-TOF) of $mPEG_{2k}$ triallyl ether (4)……200

Figure S15. Mass spectrum (MALDI-TOF) of triaminoPEG$_{2k}$ (5)……201

Figure S16. ^{1}H NMR spectrum of γ-benzyl-L-glutamate *N*-carboxy-anhydride (NCA) in $CDCl_3$……..201

Figure S17. ^{13}C NMR spectrum of γ-benzyl-L-glutamate *N*-carboxy-anhydride (NCA) in $CDCl_3$……..202

Figure S18. FT-IR spectrum of γ-benzyl-L-glutamate N-carboxy-anhydride (NCA) (neat)……...202

Figure S19. ^{1}H NMR spectrum of miktoarm $mPEG_{2k}$-*mik*-$(GA_{30})_3$ copolymer in D_2O……..203

Figure S20. ^{1}H NMR spectrum of linear $mPEG_{2k}$-*lin*-GA_{10} copolymer in D_2O……..203

Figure S21. ^{1}H NMR spectrum of linear $mPEG_{2k}$-*lin*-GA_{30} copolymer in D_2O……..204

Figure S22. TEM images of ($mPEG_{2k}$-*lin*-GA_{30})-lysozyme complexes prepared at *r*: 2.5, as described in instrumentation section (Supporting Information, section 6.1.2)……204

Figure S23. Circular dichroism spectra for free linear $mPEG_{2k}$-*lin*-GA_{10}, $mPEG_{2k}$-*lin*-GA_{30} and miktoarm $mPEG_{2k}$-*mik*-$(GA_{10})_3$ copolymers (A) and their respective complexes with lysozyme (B). Complexes were prepared at different charge ratios *r*: 0.1, 1.0 and 2.5. Free lysozyme (red), *r*: 0.1 (blue), *r*: 1.0 (black) and *r*: 2.5 (green)……..205

Figure S24. SDS-PAGE of dialysed PEGylated lysozyme at different $mPEG_{2k}$-lysozyme molecule ratios (4.6, 5.2, 6.2, 6.3), as determined by TNBS assay……..207

Figure S25. Enzymatic activity of lysozyme-$(mPEG_{2k})_{5.2}$, lysozyme-$(mPEG_{2k})_{6.2}$, lysozyme-$(mPEG_{2k})_{6.3}$ conjugate PEGylated proteins containing different amounts of $mPEG_{2k}$ chains per lysozyme molecule: 5.18, 6.23 and 6.30. All experiments were carried out in triplicate……208

Figure S26. MTS assay in A549 and Calu-3 cells after 4 and 24 hours treatment with un-complexed lysozyme……..208

Figure S27. Percentage of total LDH released from A549 and Calu-3 cells after 4 hours treatment with un-complexed lysozyme……..208

Figure S28. Percentage of apoptosis and necrosis in A549 and Calu-3 cells after 4 hours treatment with free lysozyme. Control untreated cells (black) and un-complexed lysozyme (red)……209

Figure S29. Particle size distribution of (mPEG$_{2k}$-polyGA)-lysozyme nanocomplexes in phosphate buffer (PB) and phenol red-free DMEM. Polymer-protein nanocomplexes were prepared in PB and then diluted (40x) either in phenol red-free DMEM or PB. Polymer-protein nanocomplexes were incubated for 4 h at 37°C prior analysis by NTA. Final protein concentration was kept constant (70 μg mL^{-1}) in both media……209

Figure S30. Nanoparticle tracking analysis (NTA) of dry powder formulations following incubation in phosphate buffer (PB, 10 mM, pH 7.4) at 70 μg mL^{-1} protein concentration in (mPEG$_{2k}$-polyGA)-lysozyme nanocomplexes for 15 min. Particle size distribution of nanocomplexes recovered from (A) trehalose, (B) trehalose + leucine and (C) mannitol-based dry powders. mPEG$_{2k}$-*lin*-GA$_{10}$ (green), mPEG$_{2k}$-*lin*-GA$_{30}$ (blue), mPEG$_{2k}$-*mik*-(GA$_{10}$)$_3$ (grey) and mPEG$_{2k}$-*mik*-(GA$_{30}$)$_3$ (pink)-derived complexes……210

Figure S31. ^{1}H NMR spectrum of hydroxyl-PEG$_{3k}$ triallyl ether (6) in MeOD……214

Figure S32. ^{1}H NMR spectrum of triamino-hydroxyl-PEG$_{3k}$ (7) in MeOD……215

Figure S33. ^{1}H NMR spectrum of hydroxyl-PEG$_{3k}$-*mik*-poly(benzyl-glutamic acid)$_3$ (8) in CDCl$_3$……215

Figure S34. ^{1}H NMR spectrum of p-toluene-sulfonyl-PEG$_{3k}$-*mik*-poly(benzyl-glutamic acid)$_3$ (9) in CDCl$_3$……216

Figure S35. FT-IR spectrum of azide-PEG$_{3k}$-*mik*-poly(benzyl-glutamic acid)$_3$ copolymer (10) (net)……216

Figure S36. ^{1}H NMR spectrum of azide-PEG$_{3k}$-*mik*-poly(glutamic acid)$_3$ (11) in D$_2$O……217

Figure S37. ^{1}H NMR spectrum of alkyne vitamin B$_{12}$ (12) in D$_2$O……217

Figure S38. Mass spectrum (ESI-MS) of purified alkyne vitamin B$_{12}$ (12)……218

Figure S39. RP-HPLC chromatographs of alkyne vitamin B$_{12}$ (top) and vitamin B$_{12}$ starting material (bottom). Water/acetonitrile was used as mobile phase in gradient from 5% to 90% (*v/v*) of acetonitrile and UV detection at λ = 360 nm……218

Figure S40. ^{1}H NMR spectrum of vitB$_{12}$-PEG$_{3k}$-*mik*-poly(glutamic acid)$_3$ in (13) D$_2$O……219

Figure S41. SEC chromatogram of vitB_{12}-PEG_{3k}-*mik*-poly(GA)$_3$ copolymer (top) and free alkyne vitamin B_{12} (bottom). Water/acetonitrile was used as mobile phase in gradient from 5% to 90% (*v/v*) of acetonitrile and UV detection at λ = 360 nm……219

Figure S42. ^{1}H NMR spectrum of hydroxyl-PEG_{3k}-*lin*-poly(benzyl-glutamic acid)$_3$ (14) in $CDCl_3$……220

Figure S43. ^{1}H NMR spectrum of *p*-toluene-sulfonyl-PEG_{3k}-*lin*-poly(benzyl-glutamic acid)$_3$ (15) in $CDCl_3$……220

Figure S44. FT-IR spectrum of azide-PEG_{3k}-*lin*-poly(benzyl-glutamic acid)$_3$ (16) copolymer (net)……221

Figure S45. ^{1}H NMR spectrum of azide-PEG_{3k}-*lin*-poly(glutamic acid) (17) in D_2O……221

Figure S46. ^{1}H NMR spectrum of vitB_{12}-PEG_{3k}-*lin*-poly(glutamic acid) (18) in D_2O……222

Figure S47. SEC chromatogram of vitB_{12}-PEG_{3k}-*lin*-poly(GA) copolymer (top) and free alkyne vitamin B_{12} (bottom). Mobile phase water/acetonitrile in gradient from 5% to 90% (v/v) of acetonitrile and UV detection at λ = 360 nm……222

Figure S48. Percentage of PEG_{3k}-polyGA copolymers end-functionalisation with vitamin B_{12} as estimated by UV-vis spectrophotometry with detection at λ = 540 nm. Graphic shows the calibration curve utilised for this calculation, built using serial dilutions of cyanocobalamin. Samples of known copolymer concentration were analysed at λ = 540 nm and the resulting reading was compared to the theoretical value calculated assuming 100% vitamin B_{12} end-functionalisation……223

Figure S49. Distribution of fluorescent lysozyme in the lungs of healthy mice after 0 h, 3 h and 14 h after pulmonary administration. Each slide represents a 7-µm longitudinal lung cryo-section that was observed using a fluorescent microscope at 200 x magnification. The images show the distribution of red labelled lysozyme-Cy5 (on an Alexa Fluor 568 filter) in the blue fluorescent lung tissue (on a DAPI filter) of healthy mice after administration of 2 mg dry powder formulations: (i) LDP-L1 (targeted nanocomplexes), (ii) LDP-L2 (non-targeted nanocomplexes) and (iii) LDP-P (no polymer) using the pulmonary delivery device……228

List of Tables

Chapter 2

Table 2.1. Composition, architecture, M_n, and polydispersity of $mPEG_{2k}$-polyGA copolymers prepared in this study……63

Chapter 3

Table 3.1. Effect of the different formulations used in this study on spray-drying yield, particle size (D_{50}) and span values. All formulations contained 6.6% (*w/w*) phosphate buffer salts and experiments were carried out in triplicate unless specified……106

Table 3.2. Thermal behaviour of dry powders used in this study. All formulations contained 6.6% (*w/w*) phosphate buffer salts. Experiments were made in duplicate……110

Chapter 4

Table 4.1. Emitted dose, particle size (D_{50}) and uniformity of mass delivered of dry powder formulations tested in this study. All formulations contain 10% (*w/w*) leucine, 6.6% (*w/w*) buffer salts and up to 100% (*w/w*) trehalose……148

Table 4.2. Composition of the dry powder formulations used in the *in vivo* studies……151

Table 4.3. Particle size (D_{90}) of dry powders after spraying them using a Penn-Century® device into Transwell® inserts. Four Transwell® inserts were used at once for each formulation. Each formulation was sprayed twice (2 mg per dose). All dry powder contain 6.6% (*w/w*) phosphate buffer salts, 10% (*w/w*) leucine and up to 100% (*w/w*) trehalose……165

Chapter 6

Table S1. Percentage of lysozyme amino groups reacted with $mPEG_{2k}$, as estimated by TNBS assay……206

List of Schemes

Chapter 1

Scheme 1.1. Polymer-protein conjugation by covalent coupling: general approach and examples of functional groups involved in the chemical conjugation (Trzebicka et al., 2017). Protein molecular structure was taken from protein data bank (PDB database entry lysozyme, 1HEL).....17

Chapter 2

Scheme 2.1. Polymer structures used in this part of this study.....47

Scheme 2.2. Reactions and conditions. a) allyl bromide, K_2CO_3, acetonitrile, heated to reflux, 3 h; b) NaOH, MeOH/CH_2Cl_2, 14 h; c) oxalyl chloride, DMF, CH_2Cl_2, 1 h; d) methoxypolyethylene glycol amine 2.0 kDa, triethylamine, CH_2Cl_2, overnight; e) cysteamine hydrochloride, DPAP, MeOH, UV at λ = 365 nm, 3 h; f) and g) 1) γ-benzyl-L-glutamate NCA, THF, 0°C, 5 days and 2) NaOH, H_2O/THF, 2 days.....62

Scheme 2.3. Mechanism of MTS assay. This assay involves the reduction of tetrazolium compound (MTS) by active mitochondrial enzymes to form formazan products.....76

Chapter 4

Scheme 4.1. Reactions and conditions for the synthesis of vitB_{12}-PEG_{3k}-*mik*-poly$(GA)_3$ and vitB_{12}-PEG_{3k}-*lin*-polyGA copolymers. a) *O*-(2-aminoethyl)polyethylene glycol 3.0 kDa, DMTMM, MeOH, 2 days; b) cysteamine hydrochloride, DPAP, MeOH, UV at λ = 365 nm, 3 h; c and h) γ-benzyl-L-glutamate NCA, CH_2Cl_2, room temperature, 5 days; d and i) *p*-toluene sulfonyl chloride, triethylamine, CH_2Cl_2, 12 h; e and j) sodium azide, DMSO, 24 h; f and k) NaOH, H_2O/THF, 2 days; g and l) α-dibenzocyclooctyne-vitamin B_{12}, DMSO/H_2O, overnight.....156

Scheme 4.2. Synthesis of model clicked 1,2,3-triazole (20).....158

Scheme 4.3. Synthesis of vitB_{12} model clicked 1,2,3-triazole (21).....158

Abbreviations

Asp	Aspartic acid
BCA	Bicinchoninic acid
CD	Circular dichroism
$CDCl_3$	Deuterated chloroform
$CHCl_3$	Chloroform
CH_2Cl_2	Dichloromethane
Đ	Polydispersity index
D_2O	Deuterium oxide
DCM	Dichloromethane
DI	Deionised
DLS	Dynamic light scattering
DMEM	Dulbecco's modified eagle medium
DMF	Dimethylformamide
DMSO	Dimethyl sulfoxide
DMTMM	4-(4,6-dimethoxy-1,3,5-triazin-2-yl)-4-methylmorpholinium chloride
DPAP	2,2-dimethoxy-2-phenylacetophenone
DPBS	Dulbecco's phosphate buffer saline
DPI	Dry powder inhaler
DSC	Differential scanning calorimetry
ED	Emitted dose
EDTA	Ethylendiaminetetraacetic acid
ESI-MS	Electrospray ionisation mass spectrometry
Et_2O	Diethylether

Et_3N	Triethylamine
EtOAc	Ethyl acetate
FDA	Food and drug administration
FT-IR	Fourier transform infrared spectroscopy
FBS	Foetal bovine serum
FPF	Fine particle fraction
GA	Glutamic acid
GI	Gastrointestinal
HBSS	Hank's balanced salt solution
HCl	Hydrochloric acid
HPLC	High performance liquid chromatography
K_2CO_3	Potassium carbonate
LDH	Lactate dehydrogenase
LDP	Labelled dry powders
Lin	Linear
MALDI-TOF-MS	Matrix-assisted laser desorption/ionisation time of flight mass spectrometry
MeOH	Methanol
MeOD	Deuterated methanol
$MgSO_4$	Magnesium sulfate
Mik	Miktoarm
Mn	Number average molecular weight
Mp	Peak molecular weight
MTS	3-(4,5-dimethyl-2-yl)-5-(3-carboxymethoxyphenyl)-2-(4-sulfophenyl)-2H-tetrazolium, inner salt
Mw	Weight average molecular weight
MWCO	Molecular weight cut-off

NaH_2PO_4	Sodium phosphate monobasic
Na_2HPO_4	Sodium phosphate dibasic
NaN_3	Sodium azide
$NaNO_3$	Sodium nitrate
NaOH	Sodium hydroxide
NCA	*N*-carboxyanhydride
NMR	Nuclear magnetic resonance
NTA	Nanoparticle tracking analysis
OD	Optical density
PB	Phosphate buffer
PBS	Phosphate buffer saline
PEG	Poly(ethylene glycol)
PEO	Poly(ethylene oxide)
PI	Propidium iodide
pMDI	Pressured metered dose inhaler
Ppm	Parts per million
r	Relative molar charge ratio
SD	Standard deviation
SEC	Size exclusion chromatography
SEM	Scanning electron microscopy
TAE	TRIS-acetate-EDTA
TEER	Transepithelial Electrical Resistance
TEM	Transmission electron microscopy
T_g	Glass Transition Temperature
TGA	Thermo-gravimetric analysis
THF	Tetrahydrofuran

TLC	Thin layer chromatography
T_m	Melting temperature
Trp	Tryptophan
UDP	Unlabelled dry powders
UV	Ultraviolet
$VitB_{12}$ or B_{12}	Vitamin B_{12}, cyanocobalamin
λ_{em}	Emission wavelength
λ_{ex}	Excitation wavelength

CHAPTER 1

Literature review and objectives

The overall aim of the work presented in this thesis is the development of new polymeric nanovectors for the delivery of protein therapeutics to the lungs. Pulmonary delivery of biopharmaceuticals has a considerable potential for treating both local and systemic diseases. However, despite the increasing interest from both academia and industry, numerous challenges still need to be addressed for this approach to increase its clinical impact. These include intrinsic protein properties – e.g. sensitivity to denaturation, immunogenicity and poor permeation through biological membranes – and extrinsic factors related to pulmonary delivery itself, such as difficulties in reaching the intended pulmonary targets due to mucociliary escalator and proteolytic degradation in the lungs.

A number of strategies have been investigated to overcome these challenges. This chapter introduces the concept of pulmonary protein delivery, its advantages over other drug delivery routes, and how polymeric systems have been investigated to overcome some of these challenges. Finally, the different strategies and devices used to deliver these formulations into the lungs are discussed.

Table of Contents

1.1. Introduction.....3
1.1.1. Protein therapeutics.....3
1.1.2. Pulmonary protein delivery.....5
1.1.2.1. Anatomy and physiology of the respiratory system.....5
1.1.2.2. Advantages of pulmonary delivery.....8
1.1.2.3. Pulmonary protein delivery: Limitations.....8
1.1.2.3.1. Mucociliary escalator.....9
1.1.2.3.2. Alveolar macrophages.....10
1.1.2.3.3. Lung proteases.....10
1.1.2.3.4. Airway epithelium.....12
1.1.3. Polymeric nanosystems.....14
1.1.3.1. Polymer-protein interactions.....15
1.1.3.1.1. Covalent polymer-protein conjugates.....16
1.1.3.1.2. Electrostatic interactions.....17
1.1.4. Devices for pulmonary delivery.....19
1.1.4.1. Pressured Metered Dose Inhalers (pMDIs).....19
1.1.4.2. Nebulisers.....20
1.1.4.3. Dry Powder Inhalers (DPIs).....22
1.2. Aims and objectives of the PhD.....27
1.3. References.....28

1.1. Introduction

1.1.1. Protein therapeutics

Proteins are the most abundant macromolecules in living cells (Lodish et al., 2000). They participate actively in countless intracellular and extracellular functions, participating in the transport and storage of small molecules (e.g. the transport of oxygen by haemoglobin), providing intracellular and extracellular scaffolding support, acting as channels and receptors in membranes, and catalysing biochemical reactions (Cooper, 2000). Dysfunction in their biological performance is responsible for many diseases in humans, including diabetes and tyrosinemia (Walsh, 2010, Leader et al., 2008).

Biotechnology, molecular biology and genetic engineering have experienced a dramatic development in the past few decades, allowing for a better understanding of the biological role of proteins, and the large-scale production of protein therapeutics (2010, Leader et al., 2008). The first example of protein/peptide production in an industrial scale is insulin, and dates backs to 1923 (Sarmento et al., 2006). In 2007, the global market for biotech drugs revenue was around 75 billion of dollars (Malik, 2008) and is expected to reach over 400 billion of dollars by 2019 (Figure 1.1).

However, protein-based drugs can suffer from poor bioavailability due to a range of factors which include sensitivity to denaturation, immunogenicity and poor permeability through biological membranes, compared to many low molecular weight drugs (Wang, 1999).

Consequently, parenteral delivery to date remains the main administration route. However, even in this case proteins and peptides can suffer from short *in vivo* half-life – in the range of few minutes to few hours following systemic administration – due to poor stability, proteolytic degradation, immunogenicity, or rapid renal excretion if their size is smaller than the threshold for renal glomerular filtration (~60 kDa for globular proteins) (Pisal et al., 2010, Pawar et al., 2004, Zalta et al., 2002). Thus, frequent administration is often required, which leads to poor patient compliance, especially with chronic or prolonged treatments, and increase of therapy costs (Klingler et al., 2009, Amidi et al., 2010).

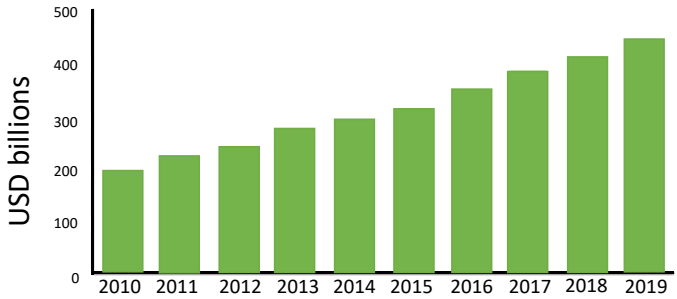


Figure 1.1. Global biotech market estimate. Source: DTTL life sciences and health care industry group analysis of industry report: global biotechnology, IBISWorld, January 2015.

To overcome these drawbacks, alternative non-invasive routes have been investigated, such as oral, nasal and pulmonary. Although the oral route would be preferred to maximise patient compliance, orally delivered protein therapeutics suffer from rapid degradation in the gastrointestinal tract and very poor permeation through the gut epithelium (Mahato et al., 2003, Yamanaka and Leong, 2008, Fruton, 2002, Bruno et al., 2013). Intranasal administration is widely studied for local and systemic therapies due to the avoidance of first-

pass metabolism (Meredith et al., 2015). Also, the possibility of using this route for delivering drugs directly into the brain has received special attention (Ugwoke et al., 2005). However, protein bioavailability is typically low due to the presence of proteolytic enzymes in the nasal mucosal cavity, poor membrane permeability, fast mucociliary clearance and small surface area for absorption (Lochhead and Thorne, 2012).

Pulmonary delivery, due to the physiological characteristics of the respiratory system, represents a promising non-invasive route for the administration of proteins. Moreover, being suitable for both local – e.g. for the treatment of many diseases including asthma and cystic fibrosis – and systemic drug delivery, pulmonary administration can be used in a plethora of clinical settings (Goel et al., 2013, Patil and Sarasija, 2012, Fellner et al., 2016, Pham et al., 2015, Depreter et al., 2013). For local drug delivery, several proteins – e.g. DNase, cyclosporin A and interleukin-2 (IL-2) – have been investigated to treat cystic fibrosis, asthma and pulmonary metastases of renal cell carcinoma, respectively (Chan et al., 1997, Rohatagi et al., 2000, Merimsky et al., 2004). The following paragraphs will discuss both advantages and current limitations of this administration route.

1.1.2. Pulmonary protein delivery

1.1.2.1. Anatomy and physiology of the respiratory system

The respiratory tract is divided into the upper respiratory system, composed by the oropharynx, the nasopharynx, the pharynx and associated structures, and the lower respiratory system, which includes the larynx, trachea, bronchi and

lungs (El-Sherbiny et al., 2015) (Figure 1.2). Subdivisions from trachea to alveoli sacs contribute to ensure efficient oxygen transport into the blood (R.J. and Thompson, 2007) (Figure 1.3).

The epithelium composition evolves along the respiratory tract (R.J. and Thompson, 2007). In the trachea and bronchi, the epithelium is composed by basal, goblet and ciliated cells. The mucus, produced by goblet cells, is propelled by beating cilia towards the pharynx where it is swallowed or expectorated, a process called the mucociliary escalator. Ciliated cells are present up to the bronchioles whereas goblet cells are only present in the trachea and bronchi, turning in deeper areas into club cells (formerly known as Clara cells). The latter secrete proteins and intervene in the regulation of the immune system, cellular regeneration and metabolism of xenobiotics (Hickey, 2007). From the terminal bronchioles to the alveoli, cells are no longer ciliated. There are two types of cells in the alveoli epithelium: pneumocytes type I which are uniform and liable to make gas exchange, and pneumocytes type II which are disperse and are responsible for the production of pulmonary surfactant – a surface-active lipoprotein complex (phospholipoprotein) (Zhao et al., 2010) – which decreases the superficial tension in the alveoli (Hickey, 2007, Hickey, 2003). In addition, macrophages are present in the alveoli area (around five or seven macrophages per alveolus in lungs of non-smokers (Stone et al., 1992)), the main function of which is the phagocytosis of inhaled particles, microorganisms, and other foreign particles. Moreover, macrophages are able to secrete enzymes and inflammation mediators (Hickey, 2003).

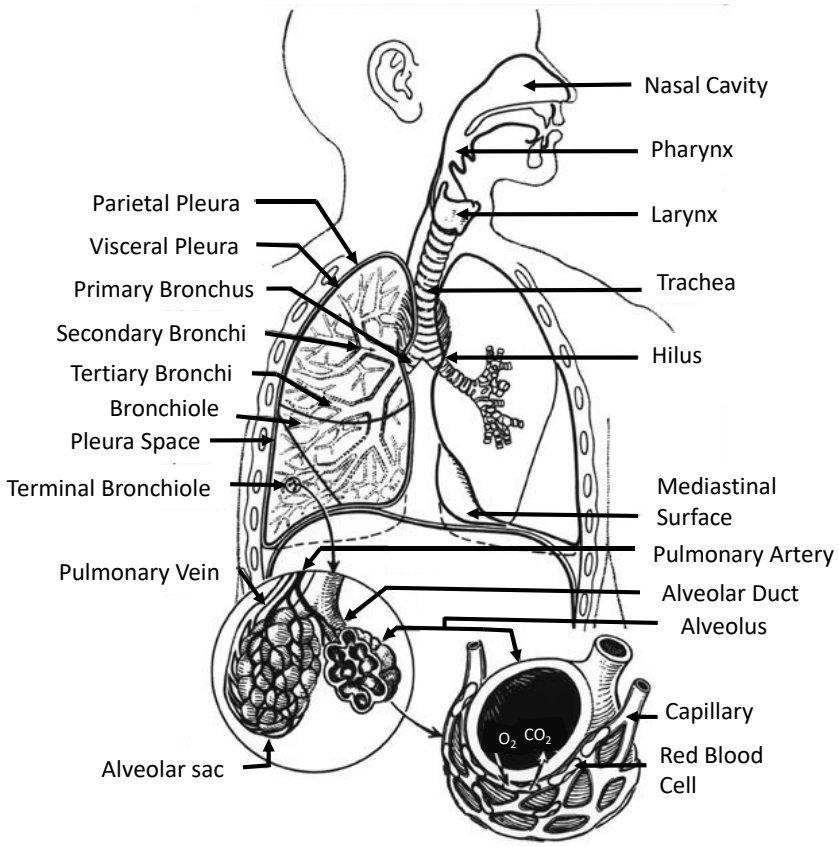


Figure 1.2. Illustration of the respiratory system (Respiratory-system, 2001).

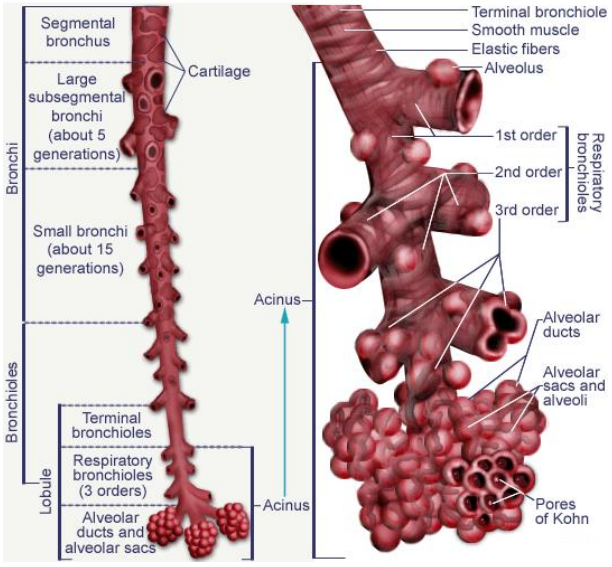


Figure 1.3. Subdivisions and structure of intrapulmonary airways. Taken from (Martin, 2008).

1.1.2.2. Advantages of pulmonary delivery

As discussed above, pulmonary delivery has great potential for non-invasive protein delivery, for the treatment of many diseases. Local targeted delivery in lungs avoids protein/peptide dilution in the blood, can improve the efficacy and decrease systemic side effects (Sharma et al., 2001, Gagnadoux et al., 2008). Rapid onset of action and absence of first-pass metabolism are also important advantages of this route (Cryan et al., 2007, Cefalu, 2004). Importantly, the enzymatic activity in the lungs is lower than that in the gastrointestinal tract leading to a reduction of unwanted degradation of pulmonary administered drugs.

Additionally, the lung complex structure provides a higher surface area for absorption (around 75-140 m^2 in adults) compared to other non-invasive routes such as nasal and buccal delivery (around 180 and 100 cm^2, respectively) (Wearley, 1991, Jitendra et al., 2011). Also, the great blood supply and the very thin alveolar epithelium (around 0.1-0.5 µm thick), permit a rapid drug absorption if systemic therapies are required (Bailey and Berkland, 2009, Amidi et al., 2010, Cryan et al., 2007).

1.1.2.3. Pulmonary protein delivery: limitations

Despite the many advantages offered by pulmonary administration, the respiratory system also possess several physiological and immunological barriers designed to decrease the deposition of particles in the lungs, and ensure sterility and minimise infections and morbidities. The main mechanisms

of protein clearance include the mucociliary escalator and the presence of alveolar macrophages and proteolytic enzymes (Figure 1.4).

Moreover, for systemic therapies, an additional issue is the need to pass through biological membranes, which is particularly challenging due to the large molecular weight and hydrophilicity of proteins (Hussain et al., 2004b).

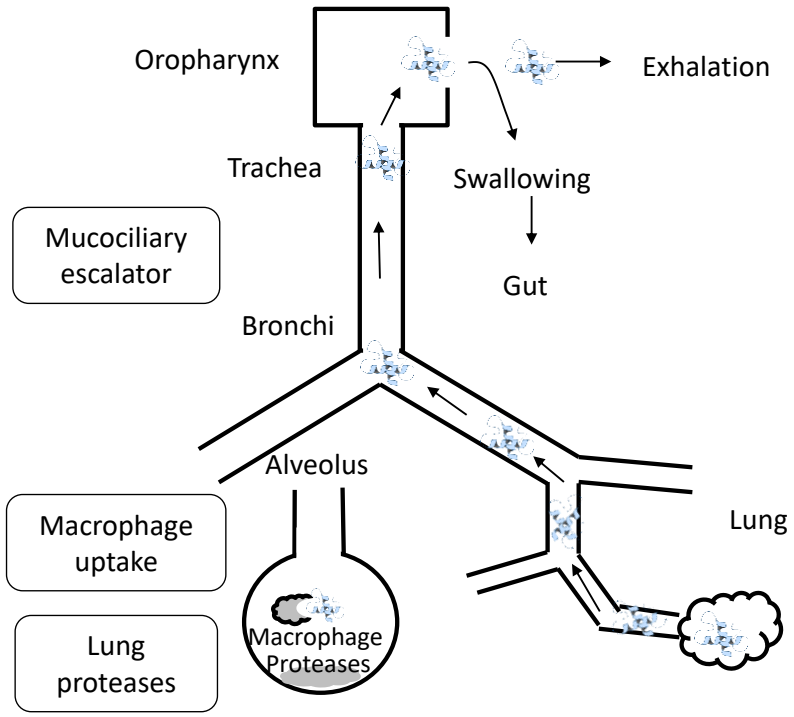


Figure 1.4. Schematic representation of the main mechanisms for protein clearance after pulmonary protein administration: mucociliary clearance, macrophage uptake and proteolytic degradation. Adapted from (Depreter et al., 2013).

1.1.2.3.1. Mucociliary escalator

Mucociliary clearance is an important barrier for the removal of foreign molecules and particles from the lungs. This process starts from the mucus produced by goblet cells in trachea and bronchi that trap inhaled molecules and particles and divert them to the pharynx and eventually to the gastrointestinal

tract (Yu and Chien, 1997, Hoiby et al., 2010). Insoluble particles larger than 6 μm are normally removed by this mechanism, whilst smaller particles can reach the bronchial epithelium or be directly deposited in the alveolar region. In healthy lungs, the production of mucus is around 10-20 mL per day (Toremalm, 1960, Foster et al., 1980). However, the rate of mucociliary clearance is reduced in older people and can be affected by lung diseases (Lowery et al., 2013, Labiris and Dolovich, 2003a).

1.1.2.3.2. Alveolar macrophages

An important clearance mechanism in the lungs involves resident alveolar macrophages (Hoiby et al., 2010). Alveolar macrophages are able to phagocytise and degrade deposited particles and/or simply transport them to the mucociliary escalator and the lymphatic system (Lombry et al., 2004, Zhang et al., 2011). In the lungs, particles between 1.5 and 3 μm are easily recognised by macrophages, whilst particles below 70 nm are usually not phagocytised (Azarmi et al., 2008, Yang et al., 2008, Oberdorster et al., 2005).

1.1.2.3.3. Lung proteases

In lungs, specific clearance mechanism for peptides and proteins, involves pulmonary peptidases and proteases (Van der Walle, 2011, Giannoni et al., 2006). These have been found in humans and other mammalians such as dogs and rabbits, and include cathepsin B, collagenase, elastase chymotrypsin, aminopeptidase P, neutrophil proteases and a range of carboxipeptidases (Janoff et al., 1983, Fujita et al., 1990, Stratford and Lee, 1986, Wall and Lanutti, 1993, Orlowski et al., 1981). These proteolytic enzymes can therefore affect the

efficacy of protein therapeutics in a number of ways. For example, peptides with less than 30 amino acids in their structure generally have poor bioavailability due to their destruction by pulmonary peptidases (Patton et al., 1998). However, proteins with molecular weights between 6 and 50 kDa are relatively resistant to most peptidases (Patton et al., 2004).

Peptidases are involved in different biological processes, including T-cell activation and inflammatory responses. However, their amount in lungs is significantly lower than that in the gastrointestinal tract (Patton et al., 2004). Also, the amount of metabolic enzymes differs from patients. For example, smokers induce more production of enzymes than non-smokers patients, which can have an effect on the fate and efficacy of inhaled protein and peptide therapeutics (Thorley and Tetley, 2007).

Addition of enzyme inhibitors (i.e. nafamostat mesilate, bacitracin, chymostatin, leupeptin and bestatin) to the formulation has been investigated to protect protein and peptide therapeutics and increase their local concentration and their bioavailability after pulmonary administration (Siekmeier and Scheuch, 2009, Kobayashi et al., 1994). For example, bacitracin has shown the inhibition of degradation of pulmonary delivered gonadorelin and buserelin mediated by aminopeptidases such as trypsin and chymotrypsin (Raehs et al., 1988). Also, when co-administered with nafamostat mesilate, the bioavailability of insulin was found to be twice higher than that obtained with insulin administered alone (Okumura et al., 1992). However, the lung contains a number of endogenous proteins such as mucins and collectins which are

responsible for the rheological properties of the mucus and are present in the pulmonary surfactant. Additionally, they have an important role in lung defense mechanisms. The addition of exogenous proteases inhibitors could destabilise this natural balance and therefore affect airway surface liquid homeostasis (Garcia-Verdugo et al., 2010).

1.1.2.3.4. Airway epithelium

Delivery of protein therapeutics to the airway epithelium for local or systemic action has been investigated for a range of clinical applications, including the treatment of pulmonary metastases of renal cell carcinoma, diabetes and osteoporosis (Patton, 2000, Onoue et al., 2008, Pfutzner and Forst, 2005, Skubitz and Anderson, 2000). In general, macromolecules smaller than 22 kDa are commonly absorbed by paracellular transport (transport between the cells), transcytosis (transport through the cells) and endocytosis while larger macromolecules are excluded from the first-mentioned pathway, taking hours to days to be absorbed (Amidi et al., 2010, Wang and Zhang, 2004). However, delivery of protein-based drugs to the target sites in sufficient amount to achieve the intended therapeutic effects can be a challenge due to the structure and the nature of the airway epithelium (Leader et al., 2008). To this aim, suitable delivery systems are often utilised (Figure 1.5).

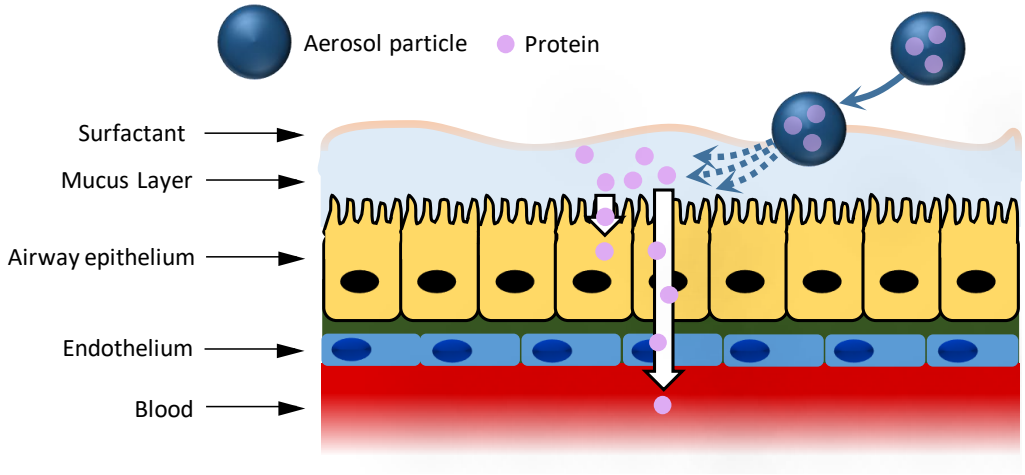


Figure 1.5. Schematic representation of protein delivery to the airway epithelium. After aerosol particles land and disintegrate on lung lining fluids, proteins must cross the lung epithelium to reach systemic circulation, or alternatively penetrate inside epithelial cells, to exert their therapeutic action. To this end, proteins need to overcome effective clearance mechanisms including proteolytic degradation and mucociliary clearance. Adapted from (Ruge et al., 2013).

The use of excipients such as absorption enhancers (i.e. surface-active agents, fatty acids and cyclodextrins) have been investigated to improve the bioavailability of peptide and protein formulations after pulmonary administration (Hussain et al., 2004a, Kobayashi et al., 1996, Kobayashi et al., 1994). For example, when co-administered with sodium taurocholate (32 mM) the bioavailability of insulin in beagle dogs was nine times higher than that obtained with insulin control formulations (23.2±4.4% *vs.* 2.6±0.3%) (Johansson et al., 2002). Also, the presence of non-ionic surfactant lauryl ether (1% solution) provided an increased bioavailability of recombinant human granulocyte colony-stimulation factor (G-CSF) after intratracheal administration (Machida et al., 2000, Hussain et al., 2004b). However, absorption enhancers could in some cases lead to permanent disruption of the alveolar epithelium, benefiting the entry of exogenous allergens and molecules inhaled during the process of breathing (Aungst, 2012).

Some proteins and peptides are naturally internalised by cells. Protein transduction domains (PTDs) or cell-penetrating peptides (CPPs) are present in a range of pathogens, and include herpes-virus derived VP22, human immunodeficiency virus I transcriptional activator (HIV-TAT) and the *Drosophilia* homeotic transcription protein antennapedia (Antp) (Derossi et al., 1996, Vives et al., 1997, Phelan et al., 1998). Interestingly, these pathogen-derived peptides have been combined or merged with protein therapeutics to enhance intracellular delivery. To date, the main challenge in this approach remains to achieve efficient endosomal escape and cytosol translocation of the internalised protein drugs (Patel et al., 2007, Green et al., 2003).

Polymer-based nanosystems are one of the most promising strategies to overcome the aforementioned limitations. Both advantages and limitations of this therapeutic approach will be presented in the following section.

1.1.3. Polymeric nanosystems

Polymeric nanosystems are gaining much interest as pulmonary protein delivery systems (Menon et al., 2014, Youn et al., 2009, Loira-Pastoriza et al., 2014, Paranjpe and Muller-Goymann, 2014, Sivadas et al., 2008, Pirooznia et al., 2012, Al-Qadi et al., 2012). Huang et *al*. developed chitosan-insulin particles with an average diameter of around 400 nm, zeta potential of approximately +42 mV and encapsulation efficiencies of 95.5%. When pulmonary administered to diabetic rats, the formulation produced a hypoglycemic effect similar to subcutaneous delivery of insulin solution but prolonged in time (Huang et al., 2009). In another study, insulin-loaded DL-lactide/glycolide

(PLGA) nanospheres, with average diameter of around 400 nm, showed an important reduction in systemic levels of glucose, which persists for a period longer than 48 h, compared to the nebulised aqueous solution of insulin as reference (6 h) (Kawashima et al., 1999). Insulin-loaded poly(DL-lactic-*co*-glycolic acid) nanospheres granulated with mannitol also had a stronger and prolonged pharmacologic effect compared to the inhalation of insulin solution (Yamamoto et al., 2007). Indeed, when properly designed, polymers can actually protect incorporated proteins from extreme environmental conditions such as proteolytic enzymes and increase the bioavailability at the targeted sites (Asensi et al., 2002, Anand et al., 2007, Hamid Akash et al., 2015, Bertrand et al., 2014). However, the stability and the toxicological profile of polymeric systems need to be investigated in a case-by-case. For example, polymeric materials with slow degradation profiles can promote their accumulation in the lungs, resulting in long-term toxicity (Sivadas et al., 2008, Armstrong et al., 1996, Lee et al., 2015). Also, positively charged polymers can produce high cytotoxicity on different cells and tissues (Fischer et al., 2003, Lv et al., 2006).

1.1.3.1. Polymer-protein interactions

A number of routes for covalent and non-covalent polymer conjugation have been investigated (Pelegri-O'Day et al., 2014, Qi and Chilkoti, 2015, Trzebicka et al., 2017, Gauthier and Klok, 2010, van Rijn, 2013). The latter mostly exploited hydrophobic polymer-protein interactions (Salmaso et al., 2012, Ambrosio et al., 2016, Salmaso et al., 2014), lectin-glycopolymer recognition (Antonik et al., 2016), and electrostatic complexation (Harada and Kataoka,

1998, Tsiourvas et al., 2012, Coue and Engbersen, 2011, Lee et al., 2008). The latter relies on interaction between polymers presenting multiple copies of charged repeating units, and oppositely charged amino acids at the surface of proteins or peptides (Figure 1.6).

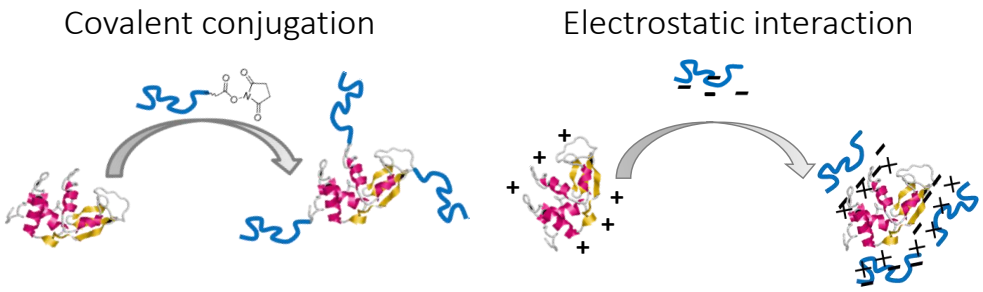


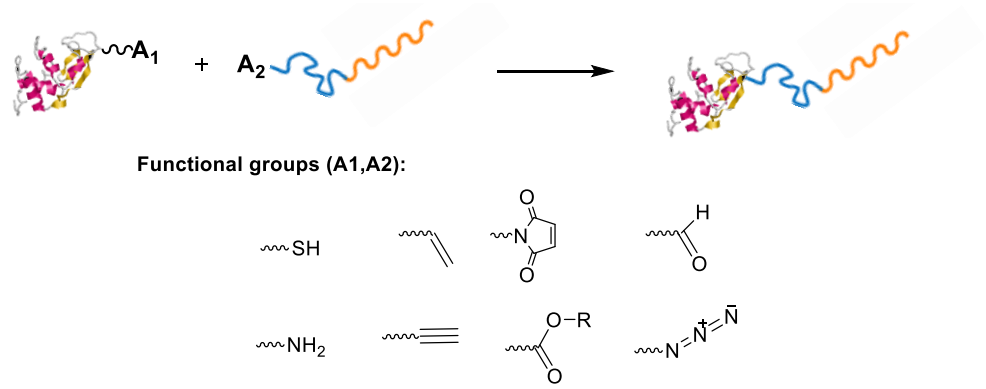
Figure 1.6. Schematic representation of polymer-protein interactions by covalent and electrostatic interactions. Protein molecular structure was taken from protein data bank (PDB database entry lysozyme, 1HEL).

1.1.3.1.1. Covalent polymer-protein conjugates

Proteins can be covalently conjugated to a range of natural and synthetic polymers *via* different synthetic approaches (Klok, 2005, van Rijn, 2013). Polymers can be covalently linked to proteins at specific or randomly distributed accessible amino acids, depending on the chosen conjugation approach, and nature of the targeted amino acid (Scheme 1.1).

PEGylation, where poly(ethylene glycol) (PEG) is the conjugating polymer of choice, is one successful example of such an approach. PEGylation can increase the protein/peptide half-life by reducing its immunogenicity and increasing the plasma stability, and, for small protein and peptides, by decreasing the rate of their renal glomerular filtration (Mero et al., 2009, Veronese, 2001). This has resulted in 12 PEGylated protein and peptide therapeutics being approved by

the FDA (Swierczewska et al., 2015). However, covalent polymer conjugation is not suitable for all proteins, as it can potentially decrease their therapeutic efficacy due to irreversible modification of key amino acid responsible for the protein bioactivity, or steric shielding of protein active sites (Gombotz and Pettit, 1995, Zhang et al., 2014, Greenwald et al., 2003). Moreover, this strategy may requires several synthetic and purification steps (Gauthier and Klok, 2010), which adds additional costs and is not ideal for fragile protein therapeutics (Frokjaer and Otzen, 2005).



Scheme 1.1. Polymer-protein conjugation by covalent coupling: general approach and examples of functional groups involved in the chemical conjugation (Trzebicka et al., 2017). Protein molecular structure was taken from protein data bank (PDB database entry lysozyme, 1HEL).

1.1.3.1.2. Electrostatic interactions

Non-covalent polymer-protein complexes, especially ionic polymer-protein complexes, have been investigated as alternatives to covalent conjugation (Harada and Kataoka, 1998, Tsiourvas et al., 2012, Coue and Engbersen, 2011, Lee et al., 2008). These complexes can be formed by interactions between polymer multiple charged groups and oppositely charged amino acid residues present in peptide and protein macromolecules. When these charged species

are formed upon protonation/deprotonation of ionisable residues, the pH of the environment these conjugates are dissolved in can have an important effect on both the assembly process, and stability of the resulting polymer-protein complexes.

Ionic polymer-protein complexes present two main advantages compared to covalent conjugates: (i) polymer-protein complexes are achieved by simple mixing of protein/peptide and polymer solutions. Thus, often complex synthetic routes for the attachment of end-functionalised polymers to proteins or peptides and subsequent characterisation of conjugates are not required. (ii) The intrinsically reversible nature of these interactions can allow complex disassembly under specific conditions - e.g. those found in the proximity of the intended biological target - which can offer therapeutic advantages.

Stable complexes in nanometre size range have been assembled from PEG-polyanion/polycation copolymers and charged macromolecules including proteins (Harada and Kataoka, 1998) and DNA (Harada-Shiba et al., 2002). Protein nanocomplexes with average diameter of around 50 nm were produced from lysozyme and PEG-*b*-poly(aspartic acid) (Harada and Kataoka, 1998) or insulin and oligolysine or oligoarginine-type homopeptide functionalised with PEG (Tsiourvas et al., 2012).

However, despite these pioneering studies, the field of non-covalent polymer conjugation is still in its infancy, largely due to the lack of current technologies to generate complexes that are sufficiently stable to allow efficient delivery *in*

vivo. Within this context, biocompatibility of the added polymers is also one key element to consider.

1.1.4. Devices for pulmonary delivery

For successful development of inhalation therapies, a number of factors - drug, drug formulation and administration device - must be optimised. Devices must aerosolise the drug in particle size distribution and concentration suitable to allow optimal deposition and dose in the targeted region of the lung (Labiris and Dolovich, 2003b). Therefore, the selection of the correct device is key to achieve the intended therapeutic performance of pulmonary delivered drugs. Modern inhalation devices can be divided in three main categories: pressurised metered-dose inhalers (pMDIs) and nebulisers for liquid formulations, and dry powder inhalers (DPIs) for solid formulations (Labiris and Dolovich, 2003b, Ibrahim et al., 2015).

1.1.4.1. Pressurised Metered Dose Inhalers (pMDIs)

pMDIs are the inhalers which are most commonly utilised to treat local respiratory diseases such as chronic obstructive pulmonary disease (COPD) and asthma (Lavorini et al., 2011, Ibrahim et al., 2015). First developed during the 1950s (Anderson, 2005), they are typically used to deliver solutions, suspensions, and more rarely emulsions. The main components of pMDIs are the canister, metering valve, actuator and a mouth piece (Vaswani and Creticos, 1998) (Figure 1.7). When the pMDI is not active, the chamber is filled with the liquid propellant-drug mixture by an inner valve. The latter closes as the patient presses the canister for dose actuation, and the outer valve opens to deliver

the metered propellant-drug mixture in an aerosol form (Cummings, 1999, Stein et al., 2014). The metering valve is responsible for the delivery of an accurate aerosol dose (20-100 µL).

Although widely utilised in a number of therapeutic settings, at present the applicability of pMDIs to deliver protein/peptide therapeutics appear to be limited, as most of these drugs possess limited solubility in the hydrofluoroalkane propellants which are used with pMDIs. Also, this class of devices often suffers from high oropharyngeal deposition (Lavorini, 2013) and poor hand-breath coordination (Newman, 2004).

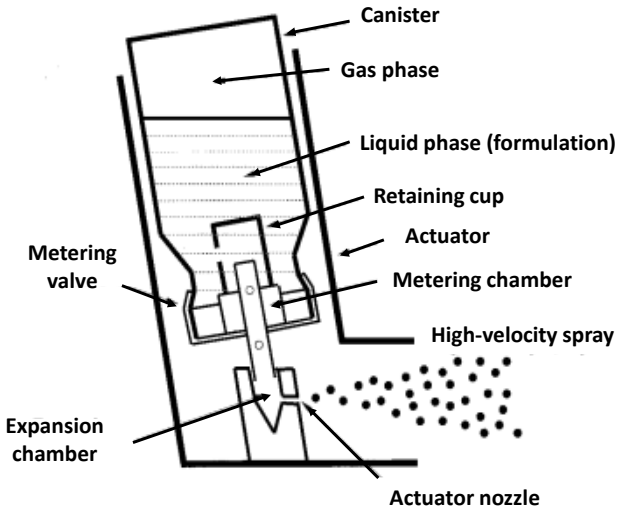


Figure 1.7. Representation of a typical pressurised metered dose inhaler (pMDI). Taken from (Newman, 2005).

1.1.4.2. Nebulisers

Similar to pMDIs, nebulisers are used to deliver solutions and suspensions. There are two main types of nebulisers, jet and ultrasonic (Figure 1.8), and they differ from the source used to generate an aerosol from a liquid (O'Callaghan

and Barry, 1997a, Boe et al., 2001). In jet nebulisers, an airstream goes at high velocity through a capillary tube, generating a low-pressure that helps the liquid to be aerosolised (Watts et al., 2008). Baffles, which are placed in different positions of the jet nebuliser, will break the droplets into smaller aerosol particles until they are small enough to leave the device. The main problems of these systems include the frequent need for a compressor to generate the aerosol and the noise that this can produce (Rubin and Williams, 2014). In ultrasonic nebulisers, vibration of piezoelectric crystals creates sound waves that can break the liquid into small droplets. Usually these are more costly devices, and also have the tendency to increase the temperature of the nebulised drug solution, which is inappropriate for thermolabile compounds such as proteins. They are also less efficient with viscous liquids and suspensions (Dolovich and Dhand, 2011, Davies et al., 2014). Finally, the performance can vary between different types of nebulisers (Lavorini, 2013).

Despite the ability of pMDIs and nebulisers to deliver different kind of molecules into the lungs including dornase alpha (Pulmozyme®), the main limitation for protein delivery is the often poor stability of protein formulations in aqueous solutions. Many mechanisms of protein degradation are believed to be water-mediated, including de-aminations and hydrolysis (Depreter et al., 2013). Moreover, solutions and suspensions are highly susceptible to microbial growth which can promote the contamination of pulmonary devices, especially those used for chronic treatments (Jarvis et al., 2014). Therefore, dry powder

inhalers (DPIs) are now being increasingly investigated for the delivery of proteins and peptides to the lungs.

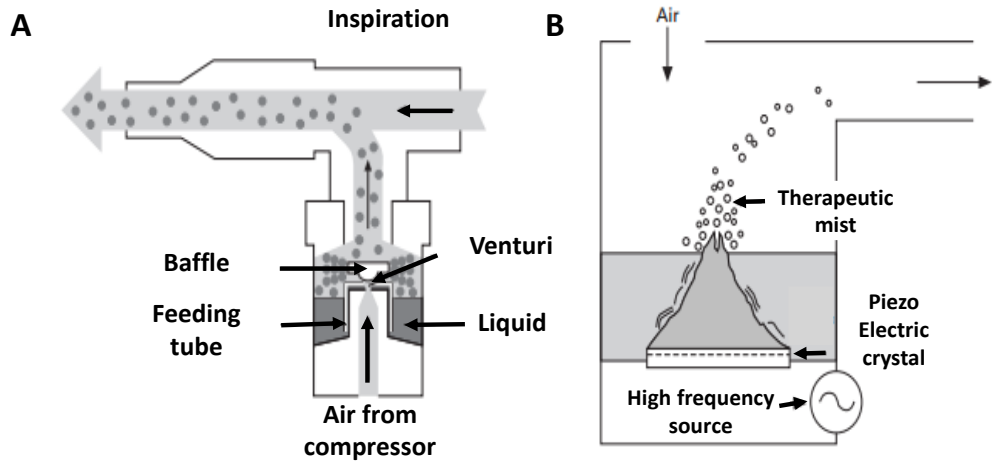


Figure 1.8. Representation of typical (A) jet and (B) ultrasonic nebulisers. Taken from (O'Callaghan and Barry, 1997b).

1.1.4.3. Dry Powder Inhalers (DPIs)

DPIs are devices which have been developed after the ban of the chlorofluorocarbons propellants, known to be implicated in atmospheric ozone depletion, in pMDIs devices (Molina and Rowland, 1974), and also with the objective to overcome problems associated with poor hand-breath coordination which can cause poorly reproducible dosing (Newman, 2004). There is a wide range of DPIs on the market, from single-dose devices loaded by the patient (e.g. Aerolizer, Rotahaler) to multiunit doses loaded in a blister pack (e.g. Diskhaler), in blisters on a strip which moves through the inhaler (e.g. Diskus) or in reservoir-type systems (e.g. Turbuhaler) (Figure 1.9). Formulations are usually composed of a mixture of drugs and excipients under a powder form, with particles with typical aerodynamic diameter in the 1-5 µm range.

The patient's inspiratory effort creates the energy to disaggregate large carrier particles into small drug particles, and disperse them as aerosols. DPIs can efficiently coordinate release of the drug with the act of inhalation.

Being essentially solvent free, dry powder formulations hold great potential for the delivery of protein and peptide therapeutics – e.g. insulin, heparin, parathyroid hormone (PTH) and human growth hormone (hGH) – into the lungs (Bosquillon et al., 2004, Bosquillon et al., 2001, Codrons et al., 2003, Codrons et al., 2004, Quattrin et al., 2004, Qi et al., 2004). For example, Afrezza®, a monomeric inhaled insulin developed by Mannkind (Valencia, CA, USA) to treat Type I and II diabetes was approved by the FDA in 2014 (Klonoff, 2014). This formulation is administered with the Dreamboat® DPI device. Advantages include better stability of protein formulations in dried state, as undesired reactions (i.e. hydrolysis and de-aminations) caused by the presence of water, changes of temperature and pH are minimised or suppressed. Additionally, dried proteins are less susceptible to shear-induced denaturation, surface adsorption and precipitation during storage and transport (Ohtake et al., 2011).

Different techniques have been developed to obtain dry powder formulations of proteins suitable for efficient pulmonary delivery. At present, the most widespread technique is freeze-drying, which is utilised for clinically available insulin inhaled protein (Afrezza®) (Pfutzner and Forst, 2005), and for others protein therapeutics under investigation, such as rhDNAse and Anti-IgE (Costantino et al., 2000, Yu et al., 2006).

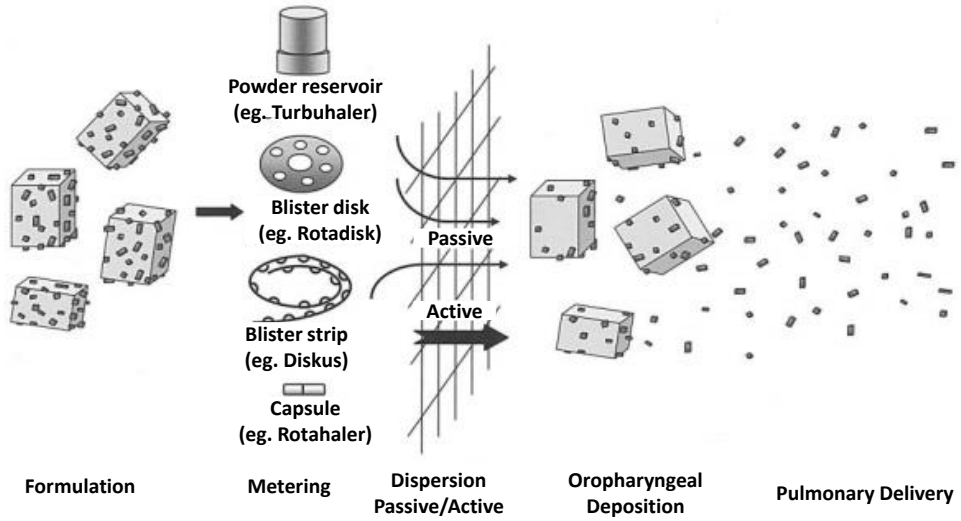


Figure 1.9. Principle of DPI design. Typically, the formulation is composed of micronised drug combined with larger carrier particles which are dispensed by a metering system. Particles are dispersed either by just the respiratory influx of the patient (passive) or with the help of different mechanisms (active) into the patient's airways. After that, drug particles separate from the carrier particles and are carried into the lung. Taken from (Telko and Hickey, 2005).

However, this technique is not suitable for all proteins as in some specific cases it can promote denaturation and protein aggregation (Abdul-Fattah et al., 2007). Also, this technique can lead not well-defined particles during the dehydration step (Depreter et al., 2013). When this occur, additional size reduction steps, such as jet milling or high pressure homogenisation, are often required, which adds further costs.

Another technique for the formulation of dry powders consists on the use of supercritical fluid drying. It is a relatively new technique and it has been used to dry a wide range number of proteins including cyclosporine A, lysozyme, myoglobin, insulin and human IgG (Tandya et al., 2006, Jovanovic et al., 2006, Jovanovic et al., 2008, Thiering et al., 2000, Nesta et al., 2000, Sellers et al., 2001). The most widely supercritical fluid used for pharmaceutical applications is CO_2, because of its low critical temperature and pressure, and the fact that is

also non-toxic, non-flammable and non-expensive (Shoyele and Cawthorne, 2006b). However, some proteins have a very limited solubility in supercritical CO_2. This could be an advantage when CO_2 is used as an anti-solvent, but again potential toxicity of organic solvents needed in this case, such as DMF and DMSO, can limit the applicability of this technique (Jackson and Mantsch, 1991, Shoyele and Cawthorne, 2006a). Also, poor control of the size and morphology of the particles has been reported (Depreter et al., 2013). Additionally, this technique in some cases can lead to protein degradation and reduced biological activity (Nesta et al., 2000, Sellers et al., 2001).

Spray-drying is arguably the technique which is currently receiving the greatest attention for the formulation of protein-based dry powders (Depreter et al., 2013), due to its scalability, cost-effectiveness and relative simplicity (Sou et al., 2011). Spray-drying generates dry powders from liquid formulations such as solutions, suspensions and emulsions (Beck-Broichsitter et al., 2012). In this process, the liquid feed is atomised by pressurised air, producing fine droplets which are then dried by hot air. Finally, a cyclone helps the dry powder collection (Chow et al., 2007, Nandiyanto and Okuyama, 2011). Commonly, the resulting dry powders are composed of a mixture of protein therapeutics and excipients, which are used to enhance the powder dispersion and therefore the delivery into the lungs (Figure 1.9). Moreover, spray-drying allows the formulation of well-defined particles in size, morphology, surface properties and density, providing suitable aerodynamic properties for inhalation that cannot be achieved with any other manufacturing process (Sou et al., 2011).

Exubera® (Nektar Therapeutics /Pfizer) was the first inhaled insulin developed by spray-drying and reached the market in 2006. The formulation was composed of insulin (60%), mannitol, glycine, Na citrate and NaOH. However, Exubera® was withdrawn in 2007 (Bailey and Barnett). Its low bioavailability and a lack of evidence of its superiority over subcutaneous insulin led to an increase on the therapy costs and unexpected low sales. Thus, further research on the field of pulmonary protein delivery is needed to overcome all the drawbacks currently observed.

1.2. Aims and objectives of the PhD

The overall aim of this PhD project is the development of non-covalent polymer-protein complexes suitable for pulmonary delivery of protein therapeutics. These novel nanocomplexes need to be assembled in aqueous conditions from the desired protein or peptide, and then be formulated into dry powders. Ideally, upon administration, these formulations should be able to quickly release their protein payload at their pulmonary target, and should be eventually cleared from the lungs to avoid a long accumulation there and thus, minimise potential local toxicity. The main objectives of this thesis therefore included:

1) Design libraries of synthetic copolymers with different structure able to interact non-covalently with proteins.
2) Investigate the ability of the resulting polymer-protein nanocomplexes to be incorporated into dry powder formulations by spray-drying, evaluate their aerodynamic properties and study their ability to protect protein therapeutics from physical and enzymatic insults.
3) Engineer a sub-family of polymer-protein nanocomplexes incorporating targeting agents and evaluate their capacity to potentially increase the delivery of proteins into the lung epithelium with minimum local toxicity both *in vitro* and *in vivo*.

1.3. References

2010. *EvaluatePharma®: World preview to 2016,* London, UK.

ABDUL-FATTAH, A. M., KALONIA, D. S. & PIKAL, M. J. 2007. The challenge of drying method selection for protein pharmaceuticals: product quality implications. *J Pharm Sci,* 96**,** 1886-916.

AL-QADI, S., GRENHA, A., CARRION-RECIO, D., SEIJO, B. & REMUNAN-LOPEZ, C. 2012. Microencapsulated chitosan nanoparticles for pulmonary protein delivery: in vivo evaluation of insulin-loaded formulations. *J Control Release,* 157**,** 383-90.

AMBROSIO, E., BARATTIN, M., BERSANI, S., SHUBBER, S., UDDIN, S., VAN DER WALLE, C. F., CALICETI, P. & SALMASO, S. 2016. A novel combined strategy for the physical PEGylation of polypeptides. *J Control Release,* 226**,** 35-46.

AMIDI, M., MASTROBATTISTA, E., JISKOOT, W. & HENNINK, W. E. 2010. Chitosan-based delivery systems for protein therapeutics and antigens. *Adv Drug Deliv Rev,* 62**,** 59-82.

ANAND, P., KUNNUMAKKARA, A. B., NEWMAN, R. A. & AGGARWAL, B. B. 2007. Bioavailability of curcumin: problems and promises. *Mol Pharm,* 4**,** 807-18.

ANDERSON, P. J. 2005. History of aerosol therapy: liquid nebulization to MDIs to DPIs. *Respir Care,* 50**,** 1139-50.

ANTONIK, P. M., EISSA, A. M., ROUND, A. R., CAMERON, N. R. & CROWLEY, P. B. 2016. Noncovalent PEGylation via Lectin-Glycopolymer Interactions. *Biomacromolecules,* 17**,** 2719-25.

ARMSTRONG, D. J., ELLIOTT, P. N., FORD, J. L., GADSDON, D., MCCARTHY, G. P., ROSTRON, C. & WORSLEY, M. D. 1996. Poly-(D,L-lactic acid) microspheres incorporating histological dyes for intra-pulmonary histopathological investigations. *J Pharm Pharmacol,* 48**,** 258-62.

ASENSI, M., MEDINA, I., ORTEGA, A., CARRETERO, J., BANO, M. C., OBRADOR, E. & ESTRELA, J. M. 2002. Inhibition of cancer growth by resveratrol is related to its low bioavailability. *Free Radic Biol Med,* 33**,** 387-98.

AUNGST, B. J. 2012. Absorption Enhancers: Applications and Advances. *The AAPS Journal,* 14**,** 10-18.

AZARMI, S., ROA, W. H. & LOBENBERG, R. 2008. Targeted delivery of nanoparticles for the treatment of lung diseases. *Adv Drug Deliv Rev,* 60**,** 863-75.

BAILEY, C. J. & BARNETT, A. H. Inhaled insulin: new formulation, new trial. *The Lancet,* 375**,** 2199-2201.

BAILEY, M. M. & BERKLAND, C. J. 2009. Nanoparticle formulations in pulmonary drug delivery. *Med Res Rev,* 29**,** 196-212.

BECK-BROICHSITTER, M., SCHWEIGER, C., SCHMEHL, T., GESSLER, T., SEEGER, W. & KISSEL, T. 2012. Characterization of novel spray-dried polymeric particles for controlled pulmonary drug delivery. *J Control Release,* 158**,** 329-35.

BERTRAND, N., WU, J., XU, X., KAMALY, N. & FAROKHZAD, O. C. 2014. Cancer nanotechnology: the impact of passive and active targeting in the era of modern cancer biology. *Adv Drug Deliv Rev,* 66**,** 2-25.

BOE, J., DENNIS, J. H., O'DRISCOLL, B. R., BAUER, T. T., CARONE, M., DAUTZENBERG, B., DIOT, P., HESLOP, K. & LANNEFORS, L. 2001. European Respiratory Society Guidelines on the use of nebulizers. *Eur Respir J,* 18**,** 228-42.

BOSQUILLON, C., LOMBRY, C., PRÉAT, V. & VANBEVER, R. 2001. Influence of formulation excipients and physical characteristics of inhalation dry powders on their aerosolization performance. *Journal of Controlled Release,* 70**,** 329-339.

BOSQUILLON, C., PREAT, V. & VANBEVER, R. 2004. Pulmonary delivery of growth hormone using dry powders and visualization of its local fate in rats. *J Control Release,* 96**,** 233-44.

BRUNO, B. J., MILLER, G. D. & LIM, C. S. 2013. Basics and recent advances in peptide and protein drug delivery. *Therapeutic delivery,* 4**,** 1443-1467.

CEFALU, W. T. 2004. Concept, strategies, and feasibility of noninvasive insulin delivery. *Diabetes Care,* 27**,** 239-46.

CODRONS, V., VANDERBIST, F., UCAKAR, B., PREAT, V. & VANBEVER, R. 2004. Impact of formulation and methods of pulmonary delivery on absorption of parathyroid hormone (1-34) from rat lungs. *J Pharm Sci,* 93**,** 1241-52.

CODRONS, V., VANDERBIST, F., VERBEECK, R. K., ARRAS, M., LISON, D., PREAT, V. & VANBEVER, R. 2003. Systemic delivery of parathyroid hormone (1-34) using inhalation dry powders in rats. *J Pharm Sci,* 92**,** 938-50.

COOPER, G. 2000. *The Cell: A Molecular Approach. 2nd edition*, Sunderland (MA): Sinauer Associates

COSTANTINO, H. R., FIROUZABADIAN, L., HOGELAND, K., WU, C., BEGANSKI, C., CARRASQUILLO, K. G., CÓRDOVA, M., GRIEBENOW, K., ZALE, S. E. & TRACY, M. A. 2000. Protein Spray-

Freeze Drying. Effect of Atomization Conditions on Particle Size and Stability. *Pharmaceutical Research,* 17**,** 1374-1382.

COUE, G. & ENGBERSEN, J. F. 2011. Functionalized linear poly(amidoamine)s are efficient vectors for intracellular protein delivery. *J Control Release,* 152**,** 90-8.

CRYAN, S. A., SIVADAS, N. & GARCIA-CONTRERAS, L. 2007. In vivo animal models for drug delivery across the lung mucosal barrier. *Adv Drug Deliv Rev,* 59**,** 1133-51.

CUMMINGS, R. H. 1999. Pressurized metered dose inhalers: chlorofluorocarbon to hydrofluoroalkane transition-valve performance. *J Allergy Clin Immunol,* 104**,** S230-6.

CHAN, H. K., CLARK, A., GONDA, I., MUMENTHALER, M. & HSU, C. 1997. Spray dried powders and powder blends of recombinant human deoxyribonuclease (rhDNase) for aerosol delivery. *Pharm Res,* 14**,** 431-7.

CHOW, A. H., TONG, H. H., CHATTOPADHYAY, P. & SHEKUNOV, B. Y. 2007. Particle engineering for pulmonary drug delivery. *Pharm Res,* 24**,** 411-37.

DAVIES, L. A., NUNEZ-ALONSO, G. A., MCLACHLAN, G., HYDE, S. C. & GILL, D. R. 2014. Aerosol delivery of DNA/liposomes to the lung for cystic fibrosis gene therapy. *Hum Gene Ther Clin Dev,* 25**,** 97-107.

DEPRETER, F., PILCER, G. & AMIGHI, K. 2013. Inhaled proteins: challenges and perspectives. *Int J Pharm,* 447**,** 251-80.

DEROSSI, D., CALVET, S., TREMBLEAU, A., BRUNISSEN, A., CHASSAING, G. & PROCHIANTZ, A. 1996. Cell internalization of the third helix of the Antennapedia homeodomain is receptor-independent. *J Biol Chem,* 271**,** 18188-93.

DOLOVICH, M. B. & DHAND, R. 2011. Aerosol drug delivery: developments in device design and clinical use. *Lancet,* 377**,** 1032-45.

EL-SHERBINY, I. M., EL-BAZ, N. M. & YACOUB, M. H. 2015. Inhaled nano- and microparticles for drug delivery. *Global Cardiology Science & Practice,* 2015**,** 2.

FELLNER, R. C., TERRYAH, S. T. & TARRAN, R. 2016. Inhaled protein/peptide-based therapies for respiratory disease. *Molecular and Cellular Pediatrics,* 3**,** 16.

FISCHER, D., LI, Y., AHLEMEYER, B., KRIEGLSTEIN, J. & KISSEL, T. 2003. In vitro cytotoxicity testing of polycations: influence of polymer structure on cell viability and hemolysis. *Biomaterials,* 24**,** 1121-1131.

FOSTER, W. M., LANGENBACK, E. & BERGOFSKY, E. H. 1980. Measurement of tracheal and bronchial mucus velocities in man: relation to lung clearance. *J Appl Physiol Respir Environ Exerc Physiol,* 48**,** 965-71.

FROKJAER, S. & OTZEN, D. E. 2005. Protein drug stability: a formulation challenge. *Nat Rev Drug Discov,* 4**,** 298-306.

FRUTON, J. S. 2002. A history of pepsin and related enzymes. *Q Rev Biol,* 77**,** 127-47.

FUJITA, J., NELSON, N. L., DAUGHTON, D. M., DOBRY, C. A., SPURZEM, J. R., IRINO, S. & RENNARD, S. I. 1990. Evaluation of elastase and antielastase balance in patients with chronic bronchitis and pulmonary emphysema. *Am Rev Respir Dis,* 142**,** 57-62.

GAGNADOUX, F., HUREAUX, J., VECELLIO, L., URBAN, T., LE PAPE, A., VALO, I., MONTHARU, J., LEBLOND, V., BOISDRON-CELLE, M., LERONDEL, S., MAJORAL, C., DIOT, P., RACINEUX, J. L. & LEMARIE, E. 2008. Aerosolized chemotherapy. *J Aerosol Med Pulm Drug Deliv,* 21**,** 61-70.

GARCIA-VERDUGO, I., DESCAMPS, D., CHIGNARD, M., TOUQUI, L. & SALLENAVE, J.-M. 2010. Lung protease/anti-protease network and modulation of mucus production and surfactant activity. *Biochimie,* 92**,** 1608-1617.

GAUTHIER, M. A. & KLOK, H.-A. 2010. Polymer-protein conjugates: an enzymatic activity perspective. *Polymer Chemistry,* 1**,** 1352-1373.

GIANNONI, E., SAWA, T., ALLEN, L., WIENER-KRONISH, J. & HAWGOOD, S. 2006. Surfactant Proteins A and D Enhance Pulmonary Clearance of Pseudomonas aeruginosa. *American Journal of Respiratory Cell and Molecular Biology,* 34**,** 704-710.

GOEL, A., BABOOTA, S., SAHNI, J. K. & ALI, J. 2013. Exploring targeted pulmonary delivery for treatment of lung cancer. *International Journal of Pharmaceutical Investigation,* 3**,** 8-14.

GOMBOTZ, W. R. & PETTIT, D. K. 1995. Biodegradable polymers for protein and peptide drug delivery. *Bioconjug Chem,* 6**,** 332-51.

GREEN, I., CHRISTISON, R., VOYCE, C. J., BUNDELL, K. R. & LINDSAY, M. A. 2003. Protein transduction domains: are they delivering? *Trends Pharmacol Sci,* 24**,** 213-5.

GREENWALD, R. B., CHOE, Y. H., MCGUIRE, J. & CONOVER, C. D. 2003. Effective drug delivery by PEGylated drug conjugates. *Advanced Drug Delivery Reviews,* 55**,** 217-250.

HAMID AKASH, M. S., REHMAN, K. & CHEN, S. 2015. Natural and Synthetic Polymers as Drug Carriers for Delivery of Therapeutic Proteins. *Polymer Reviews,* 55**,** 371-406.

HARADA-SHIBA, M., YAMAUCHI, K., HARADA, A., TAKAMISAWA, I., SHIMOKADO, K. & KATAOKA, K. 2002. Polyion complex micelles as vectors in gene therapy--pharmacokinetics and in vivo gene transfer. *Gene Ther,* 9**,** 407-14.

HARADA, A. & KATAOKA, K. 1998. Novel Polyion Complex Micelles Entrapping Enzyme Molecules in the Core: Preparation of Narrowly-Distributed Micelles from Lysozyme and Poly(ethylene glycol)−Poly(aspartic acid) Block Copolymer in Aqueous Medium. *Macromolecules,* 31**,** 288-294.

HICKEY, A. J. 2003. *Pharmaceutical Inhalation Aerosol Technology, Second Edition*, Taylor & Francis.

HICKEY, A. J. 2007. *Inhalation Aerosols: Physical and Biological Basis for Therapy*, Taylor & Francis.

HOIBY, N., CIOFU, O. & BJARNSHOLT, T. 2010. Pseudomonas aeruginosa biofilms in cystic fibrosis. *Future Microbiol,* 5**,** 1663-74.

HUANG, X., DU, Y.-Z., YUAN, H. & HU, F.-Q. 2009. Preparation and pharmacodynamics of low-molecular-weight chitosan nanoparticles containing insulin. *Carbohydrate Polymers,* 76**,** 368-373.

HUSSAIN, A., ARNOLD, J. J., KHAN, M. A. & AHSAN, F. 2004a. Absorption enhancers in pulmonary protein delivery. *Journal of Controlled Release,* 94**,** 15-24.

HUSSAIN, A., ARNOLD, J. J., KHAN, M. A. & AHSAN, F. 2004b. Absorption enhancers in pulmonary protein delivery. *J Control Release,* 94**,** 15-24.

IBRAHIM, M., VERMA, R. & GARCIA-CONTRERAS, L. 2015. Inhalation drug delivery devices: technology update. *Medical Devices (Auckland, N.Z.),* 8**,** 131-139.

JACKSON, M. & MANTSCH, H. H. 1991. Beware of proteins in DMSO. *Biochim Biophys Acta,* 1078**,** 231-5.

JANOFF, A., RAJU, L. & DEARING, R. 1983. Levels of elastase activity in bronchoalveolar lavage fluids of healthy smokers and nonsmokers. *Am Rev Respir Dis,* 127**,** 540-4.

JARVIS, S., IND, P. W., THOMAS, C., GOONESEKERA, S., HAFFENDEN, R., ABDOLRASOULI, A., FIORENTINO, F. & SHINER, R. J. 2014. Microbial contamination of domiciliary nebulisers and clinical implications in chronic obstructive pulmonary disease. *BMJ Open Respiratory Research,* 1.

JITENDRA, SHARMA, P. K., BANSAL, S. & BANIK, A. 2011. Noninvasive Routes of Proteins and Peptides Drug Delivery. *Indian Journal of Pharmaceutical Sciences,* 73**,** 367-375.

JOHANSSON, F., HJERTBERG, E., EIREFELT, S., TRONDE, A. & HULTKVIST BENGTSSON, U. 2002. Mechanisms for absorption enhancement of inhaled insulin by sodium taurocholate. *Eur J Pharm Sci,* 17**,** 63-71.

JOVANOVIC, N., BOUCHARD, A., HOFLAND, G. W., WITKAMP, G. J., CROMMELIN, D. J. & JISKOOT, W. 2006. Distinct effects of sucrose and trehalose on protein stability during supercritical fluid drying and freeze-drying. *Eur J Pharm Sci,* 27**,** 336-45.

JOVANOVIC, N., BOUCHARD, A., HOFLAND, G. W., WITKAMP, G. J., CROMMELIN, D. J. & JISKOOT, W. 2008. Stabilization of IgG by supercritical fluid drying: optimization of formulation and process parameters. *Eur J Pharm Biopharm,* 68**,** 183-90.

KAWASHIMA, Y., YAMAMOTO, H., TAKEUCHI, H., FUJIOKA, S. & HINO, T. 1999. Pulmonary delivery of insulin with nebulized DL-lactide/glycolide copolymer (PLGA) nanospheres to prolong hypoglycemic effect. *J Control Release,* 62**,** 279-87.

KLINGLER, C., MULLER, B. W. & STECKEL, H. 2009. Insulin-micro- and nanoparticles for pulmonary delivery. *Int J Pharm,* 377**,** 173-9.

KLOK, H.-A. 2005. Biological–synthetic hybrid block copolymers: Combining the best from two worlds. *Journal of Polymer Science Part A: Polymer Chemistry,* 43**,** 1-17.

KLONOFF, D. C. 2014. Afrezza Inhaled Insulin: The Fastest-Acting FDA-Approved Insulin on the Market Has Favorable Properties. *Journal of Diabetes Science and Technology,* 8**,** 1071-1073.

KOBAYASHI, S., KONDO, S. & JUNI, K. 1994. Study on pulmonary delivery of salmon calcitonin in rats: effects of protease inhibitors and absorption enhancers. *Pharm Res,* 11**,** 1239-43.

KOBAYASHI, S., KONDO, S. & JUNI, K. 1996. Pulmonary delivery of salmon calcitonin dry powders containing absorption enhancers in rats. *Pharm Res,* 13**,** 80-3.

LABIRIS, N. R. & DOLOVICH, M. B. 2003a. Pulmonary drug delivery. Part I: Physiological factors affecting therapeutic effectiveness of aerosolized medications. *British Journal of Clinical Pharmacology,* 56**,** 588-599.

LABIRIS, N. R. & DOLOVICH, M. B. 2003b. Pulmonary drug delivery. Part II: The role of inhalant delivery devices and drug formulations in therapeutic effectiveness of aerosolized medications. *British Journal of Clinical Pharmacology,* 56**,** 600-612.

LAVORINI, F. 2013. The Challenge of Delivering Therapeutic Aerosols to Asthma Patients. *ISRN Allergy,* 2013**,** 102418.

LAVORINI, F., CORRIGAN, C. J., BARNES, P. J., DEKHUIJZEN, P. R., LEVY, M. L., PEDERSEN, S., ROCHE, N., VINCKEN, W. & CROMPTON, G. K. 2011. Retail sales of inhalation devices in European countries: so much for a global policy. *Respir Med,* 105**,** 1099-103.

LEADER, B., BACA, Q. J. & GOLAN, D. E. 2008. Protein therapeutics: a summary and pharmacological classification. *Nat Rev Drug Discov,* 7**,** 21-39.

LEE, A. L. Z., WANG, Y., YE, W.-H., YOON, H. S., CHAN, S. Y. & YANG, Y.-Y. 2008. Efficient intracellular delivery of functional proteins using cationic polymer core/shell nanoparticles. *Biomaterials,* 29**,** 1224-1232.

LEE, W.-H., LOO, C.-Y., TRAINI, D. & YOUNG, P. M. 2015. Inhalation of nanoparticle-based drug for lung cancer treatment: Advantages and challenges. *Asian Journal of Pharmaceutical Sciences,* 10**,** 481-489.

LOCHHEAD, J. J. & THORNE, R. G. 2012. Intranasal delivery of biologics to the central nervous system. *Adv Drug Deliv Rev,* 64**,** 614-28.

LODISH, H., BERK, A., ZIPURSKY, S., MATSUDAIRA, P., BALTIMORE, D. & DARNELL, P. 2000. *Molecular Cell Biology. 4th edition,* New York, W. H. Freeman.

LOIRA-PASTORIZA, C., TODOROFF, J. & VANBEVER, R. 2014. Delivery strategies for sustained drug release in the lungs. *Advanced Drug Delivery Reviews,* 75**,** 81-91.

LOMBRY, C., EDWARDS, D. A., PREAT, V. & VANBEVER, R. 2004. Alveolar macrophages are a primary barrier to pulmonary absorption of macromolecules. *Am J Physiol Lung Cell Mol Physiol,* 286**,** L1002-8.

LOWERY, E. M., BRUBAKER, A. L., KUHLMANN, E. & KOVACS, E. J. 2013. The aging lung. *Clinical Interventions in Aging,* 8**,** 1489-1496.

LV, H., ZHANG, S., WANG, B., CUI, S. & YAN, J. 2006. Toxicity of cationic lipids and cationic polymers in gene delivery. *Journal of Controlled Release,* 114**,** 100-109.

MACHIDA, M., HAYASHI, M. & AWAZU, S. 2000. The Effects of Absorption Enhancers on the Pulmonary Absorption of Recombinant Human Granulocyte Colony-Stimulating Factor (rhG-CSF) in Rats. *Biol Pharm Bull,* 23 (1)**,** 84-86.

MAHATO, R. I., NARANG, A. S., THOMA, L. & MILLER, D. D. 2003. Emerging trends in oral delivery of peptide and protein drugs. *Crit Rev Ther Drug Carrier Syst,* 20**,** 153-214.

MALIK, N. N. 2008. Drug discovery: past, present and future. *Drug Discov Today,* 13**,** 909-12.

MARTIN, J. 2008. *Pumonary Ventilation. McGill Molson Medical Informatics*.

MENON, J. U., RAVIKUMAR, P., PISE, A., GYAWALI, D., HSIA, C. C. W. & NGUYEN, K. T. 2014. Polymeric nanoparticles for pulmonary protein and DNA delivery. *Acta Biomaterialia,* 10**,** 2643-2652.

MEREDITH, M. E., SALAMEH, T. S. & BANKS, W. A. 2015. Intranasal Delivery of Proteins and Peptides in the Treatment of Neurodegenerative Diseases. *AAPS J,* 17**,** 780-7.

MERIMSKY, O., GEZ, E., WEITZEN, R., PERETZ, T., RUBINOV, R., BEN-SHAHAR, M., HAYAT, H., KATSENELSON, R., MERMERSHTEIN, V. & LOVEN, D. 2004. Targeting pulmonary metastases of renal cell carcinoma by inhalation of Interleukin-2 (IL-2). *Journal of Clinical Oncology,* 22**,** 4662-4662.

MERO, A., SCHIAVON, O., PASUT, G., VERONESE, F. M., EMILITRI, E. & FERRUTI, P. 2009. A Biodegradable Polymeric Carrier Based on PEG for Drug Delivery. *Journal of Bioactive and Compatible Polymers,* 24**,** 220-234.

MOLINA, M. J. & ROWLAND, F. S. 1974. Stratospheric sink for chlorofluoromethanes: chlorine atomc-atalysed destruction of ozone. *Nature,* 249**,** 810-812.

NANDIYANTO, A. B. D. & OKUYAMA, K. 2011. Progress in developing spray-drying methods for the production of controlled morphology particles: From the nanometer to submicrometer size ranges. *Advanced Powder Technology,* 22**,** 1-19.

NESTA, D. P., ELLIOTT, J. S. & WARR, J. P. 2000. Supercritical fluid precipitation of recombinant human immunoglobulin from aqueous solutions. *Biotechnol Bioeng,* 67**,** 457-64.

NEWMAN, S. P. 2004. Dry powder inhalers for optimal drug delivery. *Expert Opin Biol Ther,* 4**,** 23-33.

NEWMAN, S. P. 2005. Principles of metered-dose inhaler design. *Respir Care,* 50**,** 1177-90.

O'CALLAGHAN, C. & BARRY, P. W. 1997a. The science of nebulised drug delivery. *Thorax,* 52 Suppl 2**,** S31-44.

O'CALLAGHAN, C. & BARRY, P. W. 1997b. The science of nebulised drug delivery. *Thorax,* 52**,** S31-S44.

OBERDORSTER, G., OBERDORSTER, E. & OBERDORSTER, J. 2005. Nanotoxicology: an emerging discipline evolving from studies of ultrafine particles. *Environ Health Perspect,* 113**,** 823-39.

OHTAKE, S., KITA, Y. & ARAKAWA, T. 2011. Interactions of formulation excipients with proteins in solution and in the dried state. *Adv Drug Deliv Rev,* 63**,** 1053-73.

OKUMURA, K., IWAKAWA, S., YOSHIDA, T., SEKI, T. & KOMADA, F. 1992. Intratracheal delivery of insulin. Absorption from solution and aerosol by rat lung. *Int J Pharm,* 88**,** 63-73.

ONOUE, S., HASHIMOTO, N. & YAMADA, S. 2008. Dry powder inhalation systems for pulmonary delivery of therapeutic peptides and proteins. *Expert Opinion on Therapeutic Patents,* 18**,** 429-442.

ORLOWSKI, M., ORLOWSKI, J., LESSER, M. & KILBURN, K. H. 1981. Proteolytic enzymes in bronchopulmonary lavage fluids: cathepsin B-like activity and prolyl endopeptidase. *J Lab Clin Med,* 97**,** 467-76.

PARANJPE, M. & MULLER-GOYMANN, C. C. 2014. Nanoparticle-mediated pulmonary drug delivery: a review. *Int J Mol Sci,* 15**,** 5852-73.

PATEL, L. N., ZARO, J. L. & SHEN, W. C. 2007. Cell penetrating peptides: intracellular pathways and pharmaceutical perspectives. *Pharm Res,* 24**,** 1977-92.

PATIL, J. S. & SARASIJA, S. 2012. Pulmonary drug delivery strategies: A concise, systematic review. *Lung India : Official Organ of Indian Chest Society,* 29**,** 44-49.

PATTON, J. S. 2000. Pulmonary delivery of drugs for bone disorders. *Adv Drug Deliv Rev,* 42**,** 239-48.

PATTON, J. S., FISHBURN, C. S. & WEERS, J. G. 2004. The lungs as a portal of entry for systemic drug delivery. *Proc Am Thorac Soc,* 1**,** 338-44.

PATTON, J. S., NAGARAJAN, S. & CLARK, A. 1998. *Pulmonary absorption and metabolism of peptides and proteins, in: Dalby, R.N. Byron, P.R. Farr, S.J. Respiratory Drug Delivery VI,* Interpharm Press, Bufflao Grove, IL, USA, pp. 17-24.

PAWAR, R., BEN-ARI, A. & DOMB, A. J. 2004. Protein and peptide parenteral controlled delivery. *Expert Opin Biol Ther,* 4**,** 1203-12.

PELEGRI-O'DAY, E. M., LIN, E.-W. & MAYNARD, H. D. 2014. Therapeutic Protein–Polymer Conjugates: Advancing Beyond PEGylation. *Journal of the American Chemical Society,* 136**,** 14323-14332.

PFUTZNER, A. & FORST, T. 2005. Pulmonary insulin delivery by means of the Technosphere drug carrier mechanism. *Expert Opin Drug Deliv,* 2**,** 1097-106.

PHAM, D.-D., FATTAL, E. & TSAPIS, N. 2015. Pulmonary drug delivery systems for tuberculosis treatment. *International Journal of Pharmaceutics,* 478**,** 517-529.

PHELAN, A., ELLIOTT, G. & O'HARE, P. 1998. Intercellular delivery of functional p53 by the herpesvirus protein VP22. *Nat Biotechnol,* 16**,** 440-3.

PIROOZNIA, N., HASANNIA, S., LOTFI, A. S. & GHANEI, M. 2012. Encapsulation of alpha-1 antitrypsin in PLGA nanoparticles: in vitro characterization as an effective aerosol formulation in pulmonary diseases. *J Nanobiotechnology,* 10**,** 20.

PISAL, D. S., KOSLOSKI, M. P. & BALU-IYER, S. V. 2010. DELIVERY OF THERAPEUTIC PROTEINS. *Journal of pharmaceutical sciences,* 99**,** 2557-2575.

QI, Y. & CHILKOTI, A. 2015. Protein–polymer conjugation — moving beyond PEGylation. *Current Opinion in Chemical Biology,* 28**,** 181-193.

QI, Y., ZHAO, G., LIU, D., SHRIVER, Z., SUNDARAM, M., SENGUPTA, S., VENKATARAMAN, G., LANGER, R. & SASISEKHARAN, R. 2004. Delivery of therapeutic levels of heparin and low-molecular-weight heparin through a pulmonary route. *Proc Natl Acad Sci U S A,* 101**,** 9867-72.

QUATTRIN, T., BELANGER, A., BOHANNON, N. J. & SCHWARTZ, S. L. 2004. Efficacy and safety of inhaled insulin (Exubera) compared with subcutaneous insulin therapy in patients with type 1 diabetes: results of a 6-month, randomized, comparative trial. *Diabetes Care,* 27**,** 2622-7.

R.J., A. & THOMPSON, D. C. 2007. *Physiology and pharmacology of the airways. In: Hickey A.J. (Ed.), Inhalation aerosols – Physical and biological basis for therapy - Second edition. Informa Healthcare, New York, pp 83-126*.

RAEHS, S. C., SANDOW, J., WIRTH, K. & MERKLE, H. P. 1988. The adjuvant effect of bacitracin on nasal absorption of gonadorelin and buserelin in rats. *Pharm Res,* 5**,** 689-93.

RESPIRATORY-SYSTEM. 2001. Available: https://visualsonline.cancer.gov/preview.cfm?imageid=1773&fileformat=jpg.

ROHATAGI, S., CALIC, F., HARDING, N., OZOUX, M. L., BOURIOT, J. P., KIRKESSELI, S., DELEIJ, L. & JENSEN, B. K. 2000. Pharmacokinetics, pharmacodynamics, and safety of inhaled cyclosporin A (ADI628) after single and repeated administration in healthy male and female subjects and asthmatic patients. *J Clin Pharmacol,* 40**,** 1211-26.

RUBIN, B. K. & WILLIAMS, R. W. 2014. Emerging aerosol drug delivery strategies: from bench to clinic. *Adv Drug Deliv Rev,* 75**,** 141-8.

RUGE, C. A., KIRCH, J. & LEHR, C. M. 2013. Pulmonary drug delivery: from generating aerosols to overcoming biological barriers-therapeutic possibilities and technological challenges. *Lancet Respir Med,* 1**,** 402-13.

SALMASO, S., BERSANI, S., MASTROTTO, F., TONON, G., SCHREPFER, R., GENOVESE, S. & CALICETI, P. 2012. Self-assembling nanocomposites for protein delivery: supramolecular interactions between PEG-cholane and rh-G-CSF. *J Control Release,* 162**,** 176-84.

SALMASO, S., BERSANI, S., SCOMPARIN, A., BALASSO, A., BRAZZALE, C., BARATTIN, M. & CALICETI, P. 2014. A novel soluble supramolecular system for sustained rh-GH delivery. *J Control Release,* 194**,** 168-77.

SARMENTO, B., RIBEIRO, A., VEIGA, F. & FERREIRA, D. 2006. Development and characterization of new insulin containing polysaccharide nanoparticles. *Colloids Surf B Biointerfaces,* 53**,** 193-202.

SELLERS, S. P., CLARK, G. S., SIEVERS, R. E. & CARPENTER, J. F. 2001. Dry powders of stable protein formulations from aqueous solutions prepared using supercritical CO(2)-assisted aerosolization. *J Pharm Sci,* 90**,** 785-97.

SHARMA, S., WHITE, D., IMONDI, A. R., PLACKE, M. E., VAIL, D. M. & KRIS, M. G. 2001. Development of inhalational agents for oncologic use. *J Clin Oncol,* 19**,** 1839-47.

SHOYELE, S. A. & CAWTHORNE, S. 2006a. Particle engineering techniques for inhaled biopharmaceuticals. *Advanced Drug Delivery Reviews,* 58**,** 1009-1029.

SHOYELE, S. A. & CAWTHORNE, S. 2006b. Particle engineering techniques for inhaled biopharmaceuticals. *Adv Drug Deliv Rev,* 58**,** 1009-29.

SIEKMEIER, R. & SCHEUCH, G. 2009. Treatment of systemic diseases by inhalation of biomolecule aerosols. *J Physiol Pharmacol,* 60 Suppl 5**,** 15-26.

SIVADAS, N., O'ROURKE, D., TOBIN, A., BUCKLEY, V., RAMTOOLA, Z., KELLY, J. G., HICKEY, A. J. & CRYAN, S. A. 2008. A comparative study of a range of polymeric microspheres as potential carriers for the inhalation of proteins. *Int J Pharm,* 358**,** 159-67.

SKUBITZ, K. M. & ANDERSON, P. M. 2000. Inhalational interleukin-2 liposomes for pulmonary metastases: a phase I clinical trial. *Anticancer Drugs,* 11**,** 555-63.

SOU, T., MEEUSEN, E. N., DE VEER, M., MORTON, D. A., KAMINSKAS, L. M. & MCINTOSH, M. P. 2011. New developments in dry powder pulmonary vaccine delivery. *Trends Biotechnol,* 29**,** 191-8.

STEIN, S. W., SHETH, P., HODSON, P. D. & MYRDAL, P. B. 2014. Advances in metered dose inhaler technology: hardware development. *AAPS PharmSciTech,* 15**,** 326-38.

STONE, K. C., MERCER, R. R., GEHR, P., STOCKSTILL, B. & CRAPO, J. D. 1992. Allometric relationships of cell numbers and size in the mammalian lung. *Am J Respir Cell Mol Biol,* 6**,** 235-43.

STRATFORD, R. E. & LEE, V. H. L. 1986. Aminopeptidase activity in homogenates of various absorptive mucosae m the albino rabbit: implications in peptide delivery. *International Journal of Pharmaceutics,* 30**,** 73-82.

SWIERCZEWSKA, M., LEE, K. C. & LEE, S. 2015. What is the future of PEGylated therapies? *Expert Opinion on Emerging Drugs,* 20**,** 531-536.

TANDYA, A., DEHGHANI, F. & FOSTER, N. R. 2006. Micronization of cyclosporine using dense gas techniques. *The Journal of Supercritical Fluids,* 37**,** 272-278.

TELKO, M. J. & HICKEY, A. J. 2005. Dry powder inhaler formulation. *Respir Care,* 50**,** 1209-27.

THIERING, R., DEHGHANI, F., DILLOW, A. & FOSTER, N. R. 2000. The influence of operating conditions on the dense gas precipitation of model proteins. *J Chem Technol Biotechnol,* 75**,** 29-41.

THORLEY, A. J. & TETLEY, T. D. 2007. Pulmonary epithelium, cigarette smoke, and chronic obstructive pulmonary disease. *International Journal of Chronic Obstructive Pulmonary Disease,* 2**,** 409-428.

TOREMALM, N. G. 1960. The daily amoung of tracheo-bronchial secretions in man. A method for continuous tracheal aspiration in laryngectomized and tracheotomized patients. *Acta Otolaryngol Suppl,* 158**,** 43-53.

TRZEBICKA, B., SZWEDA, R., KOSOWSKI, D., SZWEDA, D., OTULAKOWSKI, Ł., HALADJOVA, E. & DWORAK, A. 2017. Thermoresponsive polymer-peptide/protein conjugates. *Progress in Polymer Science,* 68**,** 35-76.

TSIOURVAS, D., SIDERATOU, Z., STERIOTI, N., PAPADOPOULOS, A., NOUNESIS, G. & PALEOS, C. M. 2012. Insulin complexes with PEGylated basic oligopeptides. *J Colloid Interface Sci,* 384**,** 61-72.

UGWOKE, M. I., AGU, R. U., VERBEKE, N. & KINGET, R. 2005. Nasal mucoadhesive drug delivery: background, applications, trends and future perspectives. *Adv Drug Deliv Rev,* 57**,** 1640-65.

VAN DER WALLE, C. 2011. *Peptide and Protein Delivery.* Boston: Academic Press.

VAN RIJN, P. 2013. Polymer Directed Protein Assemblies. *Polymers,* 5**,** 576.

VASWANI, S. K. & CRETICOS, P. S. 1998. Metered dose inhaler: past, present, and future. *Ann Allergy Asthma Immunol,* 80**,** 11-9; quiz 19-20.

VERONESE, F. M. 2001. Peptide and protein PEGylation: a review of problems and solutions. *Biomaterials,* 22**,** 405-17.

VIVES, E., BRODIN, P. & LEBLEU, B. 1997. A truncated HIV-1 Tat protein basic domain rapidly translocates through the plasma membrane and accumulates in the cell nucleus. *J Biol Chem,* 272**,** 16010-7.

WALSH, G. 2010. Biopharmaceutical benchmarks 2010. *Nat Biotechnol,* 28**,** 917-24.

WALL, D. A. & LANUTTI, A. T. 1993. High levels of exopeptidase activity are present in rat and canine bronchoalveolar lavage fluid. *International Journal of Pharmaceutics,* 97**,** 171-181.

WANG, W. 1999. Instability, stabilization, and formulation of liquid protein pharmaceuticals. *Int J Pharm,* 185**,** 129-88.

WANG, Z. & ZHANG, Q. 2004. Transport of proteins and peptides across human cultured alveolar A549 cell monolayer. *Int J Pharm,* 269**,** 451-6.

WATTS, A. B., MCCONVILLE, J. T. & WILLIAMS, R. O., 3RD 2008. Current therapies and technological advances in aqueous aerosol drug delivery. *Drug Dev Ind Pharm,* 34**,** 913-22.

WEARLEY, L. L. 1991. Recent progress in protein and peptide delivery by noninvasive routes. *Crit Rev Ther Drug Carrier Syst,* 8**,** 331-94.

YAMAMOTO, H., HOSHINA, W., KURASHIMA, H., TAKEUCHI, H., KAWASHIMA, Y., YOKOYAMA, T. & TSUJIMOTO, H. 2007. Engineering of poly(DL-lactic-co-glycolic acid) nanocomposite particles for dry powder inhalation dosage forms of insulin with the spray-fluidized bed granulating system. *Advanced Powder Technology,* 18**,** 215-228.

YAMANAKA, Y. J. & LEONG, K. W. 2008. Engineering strategies to enhance nanoparticle-mediated oral delivery. *J Biomater Sci Polym Ed,* 19**,** 1549-70.

YANG, W., PETERS, J. I. & WILLIAMS, R. O., 3RD 2008. Inhaled nanoparticles--a current review. *Int J Pharm,* 356**,** 239-47.

YOUN, Y. S., LEE, K. C., BAE, Y. H., NA, K. & LEE, E. S. 2009. Advanced Pulmonary Delivery of Peptides or Proteins Using Polymeric Particles. *Delivery Technologies for Biopharmaceuticals.* John Wiley & Sons, Ltd.

YU, J. & CHIEN, Y. W. 1997. Pulmonary drug delivery: physiologic and mechanistic aspects. *Crit Rev Ther Drug Carrier Syst,* 14**,** 395-453.

YU, Z., JOHNSTON, K. P. & WILLIAMS III, R. O. 2006. Spray freezing into liquid versus spray-freeze drying: Influence of atomization on protein aggregation and biological activity. *European Journal of Pharmaceutical Sciences,* 27**,** 9-18.

ZALTA, A. H., SWEENEY, C. P., ZALTA, A. K. & KAUFMAN, A. H. 2002. Intracameral tissue plasminogen activator use in a large series of eyes with valved glaucoma drainage implants. *Arch Ophthalmol,* 120**,** 1487-93.

ZHANG, F., LIU, M. R. & WAN, H. T. 2014. Discussion about several potential drawbacks of PEGylated therapeutic proteins. *Biol Pharm Bull,* 37**,** 335-9.

ZHANG, J., WU, L., CHAN, H. K. & WATANABE, W. 2011. Formation, characterization, and fate of inhaled drug nanoparticles. *Adv Drug Deliv Rev,* 63**,** 441-55.

ZHAO, C.-Z., FANG, X.-C., WANG, D., TANG, F.-D. & WANG, X.-D. 2010. Involvement of type II pneumocytes in the pathogenesis of chronic obstructive pulmonary disease. *Respiratory Medicine,* 104**,** 1391-1395.

CHAPTER 2

Effect of polymer topology on non-covalent polymer-protein complexation: miktoarm *versus* linear mPEG-poly(glutamic acid) copolymers

In this chapter, a family of structurally related block copolymers of $mPEG_{2k}$-poly(glutamic acid) with linear A-B ($mPEG_{2k}$-*lin*-polyGA) and miktoarm A-B_3 ($mPEG_{2k}$-*mik*-$(polyGA)_3$) structure was synthesised to assess the effect of macromolecular topology of the copolymers on electrostatic polymer-protein complexation. Their ability to efficiently bind lysozyme model protein, the effect of polymer complexation on protein integrity and their *in vitro* toxicological profile were investigated.

Table of Contents

2.1. Introduction.....44
2.2. Experimental section.....48
2.3. Results and Discussion.....60
2.3.1. Synthesis of miktoarm and linear $mPEG_{2k}$-poly(glutamic acid) copolymers.....60
2.3.2. Polymer-protein complexes characterisation.....65
2.3.3. Lysozyme conformation in polymer-protein complexes : intrinsic fluorescence studies.....71
2.3.4. Lysozyme activity assay.....72
2.3.5. Toxicity of $mPEG_{2k}$-poly(glutamic acid) copolymers.....75
2.3.5.1. Metabolic activity (MTS assay).....76
2.3.5.2. Membrane integrity (LDH assay).....78
2.3.5.3. Apoptotic assay (Annexin V-FITC/PI assay).....79
2.4. Concluding remarks.....82
2.5. References.....84

2.1. Introduction

As discussed in the Introduction Chapter (Chapter 1, section 1.1.3), polymer-protein complexes assembled through electrostatic interactions (Figure 2.1) are an attractive class of protein conjugates which is being investigated as an alternative to covalent polymer conjugation.

Complexes are typically assembled using linear (co)polymers (Coue and Engbersen, 2011, Tsiourvas et al., 2012, Lee et al., 2008), whilst the use of macromolecules with more complex topologies such as dendrimer (Hourani and Kakkar, 2010), graft (Hawker, 1995) or miktoarm (Khanna et al., 2010) structures, all of which could provide unique protein binding modalities, has been largely unexplored. To this end, in this part of this thesis work a family of copolymers with either linear A-B, or miktoarm A-B_3 structure was designed and their structure-function relationship for reversible protein complexation was investigated. The results presented in this chapter were recently published on Polymer Chemistry (Nieto-Orellana et al., 2017).

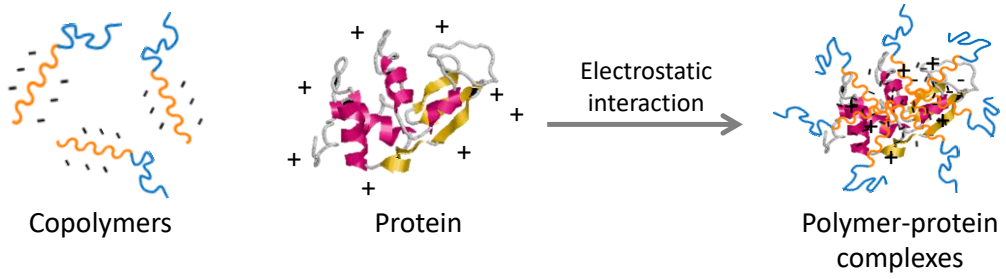


Figure 2.1. Schematic representation of electrostatic polymer-protein complexation. Protein molecular structure was taken from protein data bank (PDB database entry lysozyme, 1HEL).

Miktoarm star polymers – often simply referred to as miktoarm polymers – are star-shaped polymers where two or more macromolecular arms differ from their chemical composition, size, or both (Figure 2.2) (Altintas et al., 2012, Khanna et al., 2010, Blasco et al., 2014). The growing interest in miktoarm polymers, compared to other polymer architectures, comes from the possibility to incorporate both a variable number of polymer arms, and a plethora of chemical functionalities within one single macromolecule (Blasco et al., 2014). Studies have specifically focussed on the differences in self-assembly modalities of amphiphilic miktoarm copolymers compared to their linear analogues (Pispas et al., 2000, Yun et al., 2003).

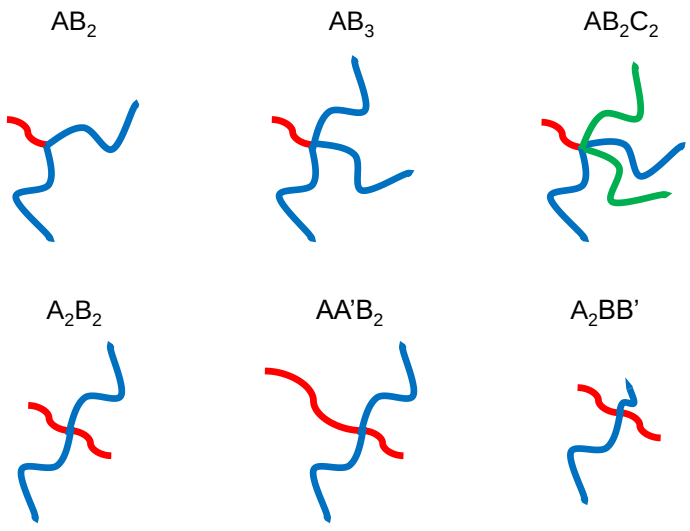


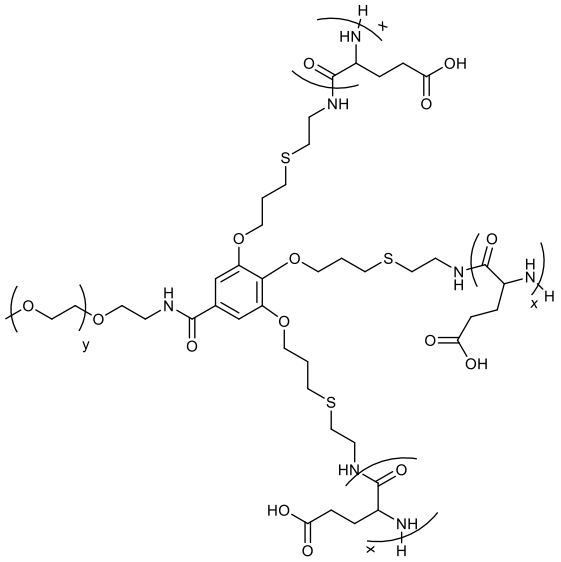
Figure 2.2. Examples of miktoarm copolymer topologies, where polymer arms change by the molecular weight and the chemical groups. A, B and C refers to different polymer composition and " ' " refers to different polymer length. Adapted from (Khanna et al., 2010).

The use of miktoarm polymers to engineer drug delivery vectors and formulations is still in its infancy, with known examples being limited to micellar and polymersomal nanovectors (Soliman et al., 2011, Soliman et al., 2010, Nederberg et al., 2009, Yin et al., 2009). Bae and co-workers synthesised a

library of Y-shaped AB_2 copolymers incorporating one PEG chain and two PLGA arms, which could be assembled into 33-75 nm polymersomes, and which could encapsulate doxorubicin hydrochloride and released it in a controlled fashion (Yin et al., 2009). Importantly, due to their macromolecular structure these miktoarm copolymers could form polymersomes in a much broader range of PEG volume fractions (0.2−0.7) than their linear diblock counterparts (0.2−0.4).

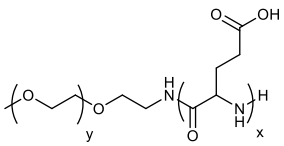
In this chapter, a novel family of $mPEG_{2k}$-poly(glutamic acid) copolymers with either miktoarm $A\text{-}B_3$ ($mPEG_{2k}$-*mik*-$(polyGA)_3$) or linear A-B ($mPEG_{2k}$-*lin*-polyGA) structure was synthesised (Scheme 2.1). The polyanion poly(glutamic acid) arm(s) was designed to provide ionic complexation with model protein lysozyme whilst the PEG_{2k} block infers steric stabilisation and minimises, or, ideally, prevents secondary aggregation of the complexes (Harada and Kataoka, 1998). Poly(glutamic acid) is a widely investigated polymer (Shih et al., 2004, Melancon and Li, 2011), and was chosen in this work because of its low toxicity – *e.g.* it has been used as macromolecular carrier in poly(GA)-paclitaxel conjugates that are being investigated in clinical trials for the treatment of a range of malignancies, including esophageal (Ng et al., 2010, Dipetrillo et al., 2012), ovarian (Sabbatini et al., 2008, Morgan et al., 2008), non-small-cell lung cancer (O'Brien et al., 2008, Albain et al., 2006, Paz-Ares et al., 2008, Langer et al., 2008), and gliobastoma multiforme – and the presence of multiple ionisable carboxylic acid groups along its polymer chain which potentially could allow complexation of proteins presenting positively charged surface residues. These copolymers were then investigated for their ability to form nanocomplexes

with egg white lysozyme model protein with the aim of identifying a structure-function relationship for this novel group of complexing copolymers.



$mPEG_{2k}$-*mik*-$(GA_{10})_3$ y:45; x:10

$mPEG_{2k}$-*mik*-$(GA_{30})_3$ y:45; x:30



$mPEG_{2k}$-*lin*-GA_{10} y:45; x:10

$mPEG_{2k}$-*lin*-GA_{30} y:45; x:30

Scheme 2.1. Polymer structures used in this part of this study.

2.2. Experimental section

3,4,5-tris(allyloxy)benzoic acid methyl ester (1). Methyl 3,4,5-trihydroxybenzoate (4.5 g, 25 mmol, 1.0 eq.) and K_2CO_3 (16.4 g, 119 mmol, 4.8 eq.), were added to a round bottomed flask. Anhydrous acetonitrile (125 mL) and allyl bromide (21.0 g, 174 mmol, 7.0 eq.) were then added to the mixture under N_2 atmosphere *via* syringe. The mixture was then heated to reflux and stirred whilst protected from the light. After 3 hours ^{1}H Nuclear Magnetic Resonance (NMR) showed completed conversion of the aromatic alcohol functionalities into their corresponding allyl ethers. Volatiles were then removed under reduced pressure. Toluene (200 mL) was added to the resulting residue, and the insoluble salts were filtered off and washed with additional portions of toluene (3x100 mL). The toluene fractions were combined, and the solvent removed under pressure to give the desired product **(1)** as an oil which was used for the next step without further purification. Yield 7.5 g, quant. ^{1}H NMR (400 MHz, $CDCl_3$, δ, ppm): 7.28 (s, 2H, $CH_{aromatic}$), 6.14-6.01 (m, 3H_{allyl}), 5.47-5.16 (m, 6H_{allyl}), 4.65-4.59 (m, 6H, OCH_2), 3.88 (s, 3H, CH_3O). ^{13}C NMR (101 MHz, $CDCl_3$, δ, ppm): 166.7, 152.4, 142.0, 134.3, 133.1, 125.1, 118.0, 117.8, 108.9, 74.2, 70.0, 52.3. ESI-TOF mass spectrometry: expected m/z [M-H$^+$] theor. 305.13, found 305.12. FT-IR: 1715 cm^{-1}($\upsilon_{C=O}$).

3,4,5-tris(allyloxy)benzoic acid (2). To a solution of ester **(1)** (7.5 g, 25 mmol) in CH_2Cl_2/MeOH (9:1 *v/v*, 20 mL), 160 mL of a 3.33 M solution of NaOH in methanol was added into a round bottomed flask obtaining a final alkali concentration of 2.82 M. The mixture was stirred at room temperature, and

after 14 hours TLC (petroleum ether/ethyl acetate 6:4) revealed the absence of starting material **(1)**. The solvents were then removed under reduced pressure; the resulting residue was mixed with distilled water (200 mL) and extracted with diethyl ether (3x100 mL) in order to remove any traces of unreacted ester starting material **(1)**. The aqueous phase was then acidified with HCl 2M to pH 2 and extracted with dichloromethane (3x100 mL). The combined organic layers were dried over $MgSO_4$, filtered, and the solvent removed under reduced pressure to give **(2)** as an oil (6.0 g, 84%). ^{1}H NMR (400 MHz, $CDCl_3$, δ, ppm): 7.35 (s, 2H, C$H_{aromatic}$), 6-14-6.03 (m, 3H_{allyl}), 5.47-5.16 (m, 6H_{allyl}), 4.66-4.62 (m, 6H, OCH_2) ^{13}C NMR (101 MHz, $CDCl_3$, δ, ppm): 171.4, 152.4, 142.0, 134.3, 133.1, 123.9.1, 118.0, 117.8, 108.9, 74.2, 70.0. ESI-TOF mass spectrometry: expected m/z [M-H$^+$] 291.32, found 291.41. FT-IR: 1687 cm^{-1} ($\upsilon_{C=O}$).

3,4,5-tris(allyloxy)benzoyl chloride (3). Compound **(2)** (1.0 g, 3.4 mmol, 1.0 eq.) was dissolved in anhydrous dichloromethane (50 mL). Anhydrous DMF catalyst (2 drops) and oxalyl chloride (0.66 g, 5.2 mmol, 1.5 eq.) were added to the solution under N_2 atmosphere *via* syringe. The mixture was stirred at room temperature for 1 h, until evolution of gas could no longer be observed. The volatiles were then removed under reduced pressure, and the residue was redissolved in dichloromethane and the solvent removed under reduced pressure. This procedure was repeated several times in order to remove all traces of residual oxalyl chloride and provide analytically pure **(3)** as orange viscous oil, which was used for next step without further purification. Yield: 1.0 g, quant. ^{1}H NMR (400 MHz, $CDCl_3$, δ, ppm): 7.35 (s, 2H, C$H_{aromatic}$), 6.08-5.97

(m, 3H_{allyl}), 5.44-5.15 (m, 6H_{allyl}), 4.66-4.58 (m, 6H, OCH_2). ^{13}C NMR (101 MHz, $CDCl_3$, δ, ppm): 167.6, 152.4, 144.3, 133.9, 132.6, 127.7.1, 118.4, 118.2, 110.9, 74.3, 70.2. FT-IR: 1749 cm^{-1} ($\upsilon_{C=O}$).

mPEG$_{2k}$ triallyl ether (4). Methoxypolyethylene glycol amine 2.0 kDa (1.5 g, 0.75 mmol) was dissolved in toluene (50 mL) and solvent was then removed under reduced pressure. This procedure was repeated five times, to remove traces of water from the PEG starting material, before starting the reaction. Compound **(3)** (1.00 g, 3.20 mmol, 4.2 eq.), methoxypolyethylene glycol amine 2.0 kDa (1.50 g, 0.75 mmol, 1.0 eq.) and anhydrous triethylamine (0.70 g, 6.9 mmol, 9.2 eq.) were dissolved in anhydrous dichloromethane (50 mL) under inert atmosphere. The mixture was stirred at room temperature overnight, after which time ^{1}H NMR analysis showed that the reaction was complete (aromatics signals shifted from 7.35 to 7.04 ppm). The solvent was then removed under reduced pressure, and the resulting residue suspended in 60 mL of water. Insoluble starting material **(3)** and potential compounds derived from it were removed by filtration, and the aqueous solution was extracted with Et_2O (3x100 mL) to remove triethylamine and other non-water soluble impurities, and finally with dichloromethane (3x100 mL). Removal of the solvent from the combined organic layers gave **(4)** as a waxy solid (1.6 g, 92%). ^{1}H NMR (400 MHz, $CDCl_3$, δ, ppm): 7.04 (s, 2H, C$H_{aromatic}$), 6.75 (bs, 1H, N*H*CO) 6.08-5.97 (m, 3H_{allyl}), 5.44-5.15 (m, 6H_{allyl}), 4.64-4.57 (m, 6H, OCH_2), 3.64-3.50 (s, 194H, OCH_2 of PEG), 3.37 (s, 3H, OCH_3 of methoxy PEG).

TriaminoPEG$_{2k}$ (5). mPEG$_{2k}$ triallyl ether **(4)** (1.6 g, 0.69 mmol, 1.0 eq.), cysteamine hydrochloride (0.90 g, 12 mmol, 16.0 eq.) and 2,2-dimethoxy-2-phenylacetophenone (DPAP) (0.060 g, 0.23 mmol, 0.3 eq.) were dissolved in methanol (5 mL). The mixture was then irradiated using a 36 Watt UV Lamp equipped with 4 X 9 W Light bulbs at 365 nm for 3 hours, until allyl signals could no longer be detected by ^{1}H NMR. Methanol was then evaporated under reduced pressure and the resulting residue was suspended in water. The mixture was extracted with ethyl acetate in order to remove traces of DPAP and corresponding decomposition products. After saturation with NaCl the aqueous phase was extracted with isopropanol:dichloromethane 3:1 vol:vol. Solvent removal under reduced pressure from the combined organic layers provided **(5)** as solid (1.5 g, 76%). ^{1}H NMR (400 MHz, CD_3OD, δ, ppm): 7.24 (s, 2H, C*H*$_{aromatic}$), 4.22 (t, *J* = 6.0 Hz, 4H, OC*H*$_2$CH$_2$CH$_2$S), 4.14 (t, *J* = 5.8 Hz, 2H, OC*H*$_2$CH$_2$CH$_2$S), 3.85-3.50 (s, 236H, OC*H*$_2$ of PEG), 3.35 (s, 3H, OC*H*$_3$ of methoxy PEG), 3.20 (t, *J* = 6.7 Hz, 6H, C*H*$_2$N), 2.90-2.78 (m, 12H, C*H*$_2$S), 2.18 (m, 4H, OCH$_2$C*H*$_2$CH$_2$S), 1.97 (m, 2H, OCH$_2$C*H*$_2$CH$_2$S).

γ-Benzyl-L-glutamate *N*-carboxyanhydride (NCA). L-Glutamic acid γ-benzyl ester (13.7 g, 57.8 mmol) was added to a dry round bottomed flask. Anhydrous THF (200 mL) and triphosgene (6.8 g, 23 mmol) were then added under nitrogen atmosphere. The mixture was heated at 50°C under stirring. The reaction mixture turned clear in about 1 h. The solution was then cooled down to room temperature and bubbled with nitrogen for 2 h to remove traces of gaseous co-products (during this process the outlet was connected to a NaOH$_{aq}$ trap). The

solution was then concentrated under vacuum to a ~ 10 mL volume, precipitated with petroleum ether, filtered, washed with petroleum ether and recrystallised from THF:petroleum ether 1:1 (*v/v*) at 0°C to give the desired product as crystalline solid (5.2 g, 35%). The residual mother liquor contained more γ-benzyl-L-glutamate *N*-carboxyanhydride, which however did not crystallise under these conditions. ^{1}H NMR (400 MHz, $CDCl_3$, δ, ppm): 7.40-7.31 (m, 5H, C$H_{aromatic}$), 6.59 (s, 1H, N*H*), 5.13 (s, 2H, CH_2O), 4.38 (ddd, *J* = 6.5, 5.4, 0.8 Hz, 1H, C*H*NH), 2.59 (t, *J* = 6.9 Hz, 2H, CH_2), 2.31-2.06 (m, 2H, CH_2). ^{13}C NMR (101 MHz, $CDCl_3$, δ, ppm): 172.5, 169.5, 151.9, 135.3, 128.8, 128.7, 128.5, 67.2, 57.0, 30.0, 27.0. FT-IR: 1651, 1737, 1790, 1856 and 1965 cm^{-1}.

mPEG$_{2k}$-poly(glutamic acid) copolymers: typical polymerisation conditions and hydrolysis of benzyl ester repeating units. TriaminoPEG$_{2k}$ initiator **(5)** (50 mg, 0.019 mmol) or commercially available methoxypolyethyleneglycol amine 2.0 kDa (50 mg, 0.025 mmol) were dissolved in dry THF (50 mL) in a round bottom flask and cooled to 0°C. γ-Benzyl-L-glutamate NCA (628 mg, 2.39 mmol), (250 mg, 0.940 mmol), (333 mg, 1.25 mmol), or (83 mg, 0.32 mmol) to form mPEG$_{2k}$-*mik*-(GA$_{30}$)$_3$, mPEG$_{2k}$-*mik*-(GA$_{10}$)$_3$, mPEG$_{2k}$-*lin*-GA$_{30}$, and mPEG$_{2k}$-*lin*-GA$_{10}$ copolymers, respectively was dissolved in anhydrous THF (100 mL), cooled to 0°C and added to the solution containing the amino-PEG initiator. The mixture was stirred in a water ice bath at 0°C under inert atmosphere. After 5 days at 0°C the conversion was found to be ~ 70% as judged by ^{1}H NMR analysis. 6, 2.35, 3.13, or 0.79 mL of 1.0 M NaOH aqueous solution to hydrolyse benzyl ester repeating units in mPEG$_{2k}$-*mik*-(GA$_{30}$)$_3$, mPEG$_{2k}$-*mik*-(GA$_{10}$)$_3$, mPEG$_{2k}$-*lin*-

GA_{30}, and $mPEG_{2k}$-*lin*-GA_{10} copolymers respectively, (2.5 equiv. of NaOH per benzyl group) were then slowly added under vigorous stirring. The reaction was left to stir for 2 days at room temperature, then the solvents were removed under reduced pressure. The residue was dissolved in distilled water (50 mL) and the resulting solution was dialysed (MWCO 1 kDa for linear $mPEG_{2k}$-*lin*-GA_{10} copolymers or 3.5 kDa for $mPEG_{2k}$-*lin*-GA_{30}, $mPEG_{2k}$-*mik*-$(GA_{10})_3$ and $mPEG_{2k}$-*mik*-$(GA_{30})_3$ copolymers). The solution was then freeze-dried and analysed by ^{1}H NMR in D_2O and Size Exclusion Chromatography (SEC) using aqueous 0.10 M $NaNO_3$, 0.02 NaN_3, pH 10 (Perdih et al., 2014) as the mobile phase.

$mPEG_{2k}$-*mik*-$(GA_{30})_3$ yield: 178 mg, 60%. ^{1}H NMR (400 MHz, D_2O, δ, ppm): 7.15 (s, 2H, C*H*$_{aromatic}$), 4.38-3.99 (m, 88H, HNC*H*CO and 6H, CH_2NH), 3.70-3.47 (s, 158H, OC*H*$_2$ of PEG), 3.3 (s, 3H, OC*H*$_3$ of PEG), 3.18-2.90 (m, 12H, C*H*$_2$SC*H*$_2$), 2.4-1.6 (m, 607H, C*H*$_2$C*H*$_2$COOH and 6H, C*H*$_2$). $M_{n,NMR}$ = 15.5 kDa, M_{nSEC} = 7.0 kDa, Đ = 1.27.

$mPEG_{2k}$-*mik*-$(GA_{10})_3$ yield: 120 mg, 90%. ^{1}H NMR (400 MHz, D_2O, δ, ppm): 7.15 (s, 2H, C*H*$_{aromatic}$), 4.38-3.99 (m, 31H, HNC*H*CO and 6H, C*H*$_2$NH), 3.70-3.47 (s, 180H, OC*H*$_2$ of PEG), 3.3 (s, 3H, C*H*$_3$O of PEG), 3.18-2.90 (m, 12H, C*H*$_2$SC*H*$_2$), 2.4-1.6 (m, 126H, C*H*$_2$C*H*$_2$COOH and 6H, C*H*$_2$NH). $M_{n,NMR}$ = 7.2 kDa, $M_{n,SEC}$ = 4.7 kDa, Đ = 1.28.

$mPEG_{2k}$-*lin*-GA_{30} yield: 140 mg, 80%. ^{1}H NMR (400 MHz, D_2O, δ, ppm): 4.38-3.99 (m, 39H, HNC*H*CO), 3.70-3.47 (s, 165H, OC*H*$_2$ of PEG), 3.3 (s, 3H, C*H*$_3$O of PEG), 2.4-1.6 (m, 161H, C*H*$_2$C*H*$_2$COOH). $M_{n,NMR}$ = 7.7 kDa, $M_{n,SEC}$ = 1.9 kDa, Đ = 1.26.

mPEG$_{2k}$-*lin*-GA$_{10}$ yield: 71 mg, 81%. ^{1}H NMR (400 MHz, D_2O, δ, ppm): 4.38-3.99 (m, 14H, HNC*H*CO), 3.70-3.47 (s, 1770H, OCH_2 of PEG), 3.3 (s, 3H, CH_3O of PEG), 2.4-1.6 (m, 77H, CH_2CH_2COOH). $M_{n,NMR}$ = 3.9 kDa, $M_{n,SEC}$ = 2.2 kDa, Đ = 1.24.

Preparation of polymer-protein nanocomplexes. Association was assessed at different polymer-protein mixing ratios (*r* = 0.1, 0.25, 0.5, 1.0, 1.5, 2.0 and 2.5) where *r* was the ratio between the number of glutamic acid residues present in the copolymer and the number of lysine and arginine residues in lysozyme. Polymer and protein stock solutions were prepared by separately dissolving them in phosphate buffer (PB, 10 mM, pH 7.4; Na_2HPO_4 8.1 mM, $NaH_2PO_4{\cdot}2H_2O$ 1.47 mM) at a concentration of 10 mg mL^{-1} and 14.5 mg mL^{-1}, respectively, and appropriate aliquots mixed in order to achieve the desired *r* values. Protein concentration was kept constant at 300 µg mL^{-1} in all mixing ratios, unless otherwise stated. The mixtures were stored overnight at room temperature prior to further characterisation.

Agarose gel electrophoresis. Polymer-protein complexes were prepared as described above at the same mixing ratios. Protein concentration was kept constant (300 µg mL^{-1}). 50 µL of complexes solution were loaded onto 1% (*w/v*) agarose gel with 25 µL of solution of 25 mg mL^{-1} ethidium bromide and the electrophoresis was ran with TRIS-acetate-EDTA (TAE) buffer at 100 mA for 2 hours. The resulting gel was stained with Coomassie blue and visualised on an ultraviolet transilluminator. Free lysozyme and free polymers were used as controls.

To perform agarose gel electrophoresis with complexes at acid pH, polymer-protein associations were prepared as described before using a phosphate buffer at pH 2 (10 mM, pH 2.0). The procedure was the same as described before.

Nanoparticle Tracking Analysis (NTA). The hydrodynamic diameter of complexes was measured by NTA using a Nanosight LM14. All measurements were performed at 25°C. NTA 2.0 Build 127 software was used for data acquisition and analysis. The samples were measured for 80 s. Mean size (±SD) values correspond to the arithmetic values calculated for all the particles analysed by the software. Polymer-protein nanocomplexes were prepared as described before using ratios of 1.0 and 2.5, in phosphate buffer (10 mM, pH 7.4). Protein concentration was kept constant (70 μg mL^{-1}) for all measurements. Free protein and polymers were used as controls.

Intrinsic fluorescence spectroscopy. Protein tryptophan fluorescence spectra were measured using a Cary Eclipse Fluorescence Spectrophotometer. The excitation wavelength was 280 nm. Slits were 5.0 and 10.0 nm for excitation and emission, respectively. Polymer-protein nanocomplexes were prepared as described before using a charge ratio of 2.5. Protein concentration was kept constant (70 μg mL^{-1}).

Circular dichroism (CD) spectroscopy. CD spectra were recorded on an Applied Photo-physics Chirascan circular dichroism spectropolarimeter using a 1 mm path length quartz cuvette. CD measurements were performed at 25°C over a range of 180-250 nm using a response time of 1 s, 1 nm pitch and 0.5 nm

bandwidth. The recorded spectra represent a smoothed average of three scans, zero-corrected at 250 nm and normalised (Molar ellipticity θ is quoted in 105 deg cm^2 $dmol^{-1}$). The absorbance of the buffer was subtracted from the recorded spectra. Polymer-protein complexes were prepared as described before using a charge ratio of 0.1, 1.0 and 2.5. Protein concentration was kept constant (37 μg mL^{-1}).

Lysozyme enzymatic activity assay. A turbidimetric enzymatic assay was performed by measuring the decrease in optical density of an aqueous suspension of *Micrococcus lysodeikticus* lyophilised cells, a natural substrate for lysozyme, in PB. Polymer-protein complexes were prepared as described before at ratios 0.1, 0.5, 1.0 and 2.5. Lysozyme concentration was kept constant (37 μg mL^{-1}). PB (20 mL) solution was added to 10 mg of lyophilised cells. 300 μL of this substrate suspension were added to 150 μL of nanocomplex suspension and the decrease in optical density at λ = 460 nm was measured as a function of time. Free polymers and free lysozyme were used as controls at the same concentration as in the samples. All kinetics experiments were carried out in triplicate.

To recover lysozyme from the nanocomplexes, 480 μg of poly(allyl amine) (M_w ~ 17 kDa, 20 wt. % solution in H_2O) were added to 2 mL of the nanocomplex suspension and the resulting solution mixture was maintained under very gentle agitation for 1 h at room temperature. Lysozyme activity of the resulting solution was then measured as described above.

Cell culture conditions and sample preparation. Human alveolar cells (A549) and human airway epithelial cells (Calu-3) were routinely cultured in Dulbecco's Modified Eagle's Medium (DMEM) and DMEM/F-12 medium, respectively. Both mediums were supplemented with Foetal Bovine Serum (FBS, 10% *v/v*), non-essential amino acids (1% *v/v*), L-glutamine (1% *v/v*), penicillin (100 units mL^{-1}) and streptomycin (100 µg mL^{-1}). Dulbecco's Phosphate-Buffered Saline (DPBS) and trypsin/EDTA were used to wash and detach adherent cells in the process of cell splitting. Cells were always incubated at 37°C and 5% CO_2.

Samples tested – polymer, protein and polymer-protein nanocomplexes at relative molar charge ratio 2.5 – were prepared in PB and diluted in non-supplemented medium (dilution factor 40x). The stability of polymer-protein nanocomplexes in medium was confirmed by NTA analysis (see Supporting Information, Figure S29).

Determination of the metabolic activity via MTS assay. A549 or Calu-3 cells were seeded in 96-well plates at 2-3.10^4 cells per well and permitted to grow for 24 h. Medium was then removed, cells washed with DPBS and samples, at polymer concentrations ranging from 25 to 200 µg mL^{-1}, added to the cells (200 µl per well) for 4 hours. After that, medium was removed, cells washed with DPBS and 120 µL of MTS solution (20 µL MTS + 100 µL medium) were added. After 3 h incubation, the optical density was read at 490 nm. Experiments were carried out in triplicate.

To evaluate the metabolic activity after 24 h, cells were incubated with samples for 4 h as previously described. After washing them with DPBS, 200 µL of

supplemented medium were added. After 20 h incubation, cells were washed again with DPBS and 120 µL of MTS solution were added as described above. Experiments were carried out in triplicate.

Controls for both experiments were performed using 4% (*v/v*) Triton X-100 and untreated cells, indicating 0% metabolic activity (positive control) and 100% metabolic activity (negative control), respectively. The metabolic activity was calculated using the following formula:

$$\%\ Metabolic\ activity = \frac{\mathrm{S} - \mathrm{P}}{\mathrm{N} - \mathrm{P}}\ \mathrm{X}\ 100$$

where S, N and P are the absorbance of treated cells, negative control and positive control, respectively.

Determination of membrane integrity via LDH assay. A549 or Calu-3 cells were seeded in 96-well plates at 2-3.10^4 cells per well and permitted to grow for 24 h. Medium was then removed, cells washed with DPBS and samples, at polymer concentrations ranging from 25 to 200 µg mL^{-1}, added to the cells (200 µl per well) for 4 hours. After that, the plate was centrifuged 4 min at 1,500 rpm, 50 µL of supernatant were disposed in a new 96-well plate and 100 µL of a LDH kit solution were added according to the manufacturer's instructions (*in vitro* toxicology assay kit, lactic dehydrogenase based, Sigma Aldrich). The mixture was incubated during 30 min at room temperature. After that, 15 µL of 1 M HCl were added to quench the reaction. The absorbance was measured at 490 nm. Controls were performed using 4% (*v/v*) Triton X-100 and untreated cells indicating 100% LDH release (positive control) and 0% LDH release (negative

control) respectively. Experiments were carried out in triplicate. The percentage of LDH release was calculated using the following formula:

$$\% \text{ LDH Release} = \frac{S - N}{P - N} \text{ x } 100$$

where S, N and P are the absorbance of treated cells, negative control and positive control, respectively.

Annexin V-FITC/propidium iodide apoptosis assay. A549 and Calu-3 cells were seeded in 24-well plates at 4-6.10^5 cells per well and permitted to grow for 24 h. Medium was then removed, cells washed with DPBS and samples at polymer concentration of 200 µg mL^{-1} added to the cells (500 µl per well) for 4 hours. Medium was then removed, cells washed with DPBS, detached with trypsin/EDTA and washed twice again with DPBS. Afterwards, cells were re-suspended in 500 µL binding buffer and 5 µL of Annexin V-FITC were then added to the suspension. After 10 minutes incubation at 4°C in the dark, 10 µL of propidium iodide (100 µg mL^{-1}) were added and incubated for 5 minutes at 4°C. The flow cytometry analysis was performed within 15 minutes. Experiments were carried out in triplicate, with more than 10,000 cells measured in each sample.

2.3. Results and Discussion

2.3.1. Synthesis of miktoarm and linear $mPEG_{2k}$-poly(glutamic acid) copolymers

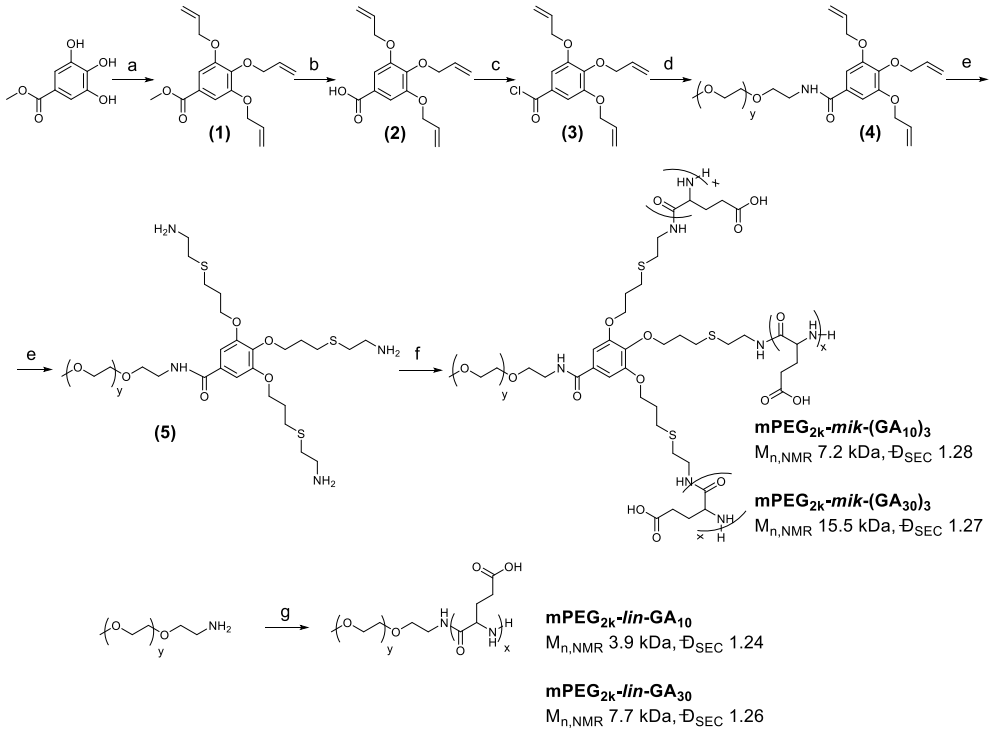
In this study, we synthesised two novel A-B_3 miktoarm star copolymers consisting of one 2.0 kDa monomethoxy polyethylene glycol ($mPEG_{2k}$) arm (A) and three poly(glutamic acid) poly(GA) branches (B) of variable chain length. The chain length of polyethylene glycol block was kept constant at 2.0 kDa. Due to the hydrophilic nature of this polymer, longer PEG chains could potentially decrease cellular uptake while smaller sizes might negatively affect the stability of the formulated polymer-protein nanocomplexes. Glutamic acid repeating units were utilised here as potential binding sites for the complexation of positively charged amino acids in protein structure. Formation of polymer-protein complexes was expected to occur through electrostatic interactions, and be especially favoured at a pH window between the pKa of carboxylic groups of poly(glutamic acid) and the isoelectric point (pI) of the selected protein. In this work, the length of the hydrophilic $mPEG_{2k}$ A block was kept constant and that of protein-binding polyGA arms was systematically varied.

Methyl 3,4,5-trihydroxybenzoate (gallic acid methyl ester) was used as the starting point to generate the core of the miktoarm polymers synthesised in this study. Reaction with allyl bromide using potassium carbonate as a base afforded the triallyl ether **(1)** (Kaplánek et al., 2009) in virtually quantitative yield (Scheme 2.2). Hydrolysis of **(1)** with methanolic NaOH gave the acid **(2)** which was then converted in its correspondent acid chloride **(3)** with oxalyl

chloride, using DMF as the catalyst. Whilst both ^{1}H and ^{13}C NMR analyses were found not suitable to differentiate between **(2)** and **(3)**, FT-IR showed the disappearance of the band at 1687 cm^{-1} for the acid moiety of **(2)**, and the appearance of a new band at 1749 cm^{-1} of the C=O stretching of the acid chloride group of **(3)**. The latter was then reacted with methoxypolyethylene glycol amine 2.0 kDa in anhydrous dichloromethane using triethylamine as the acid scavenger to give **(4)**. Thiol-ene (Dondoni, 2008) addition in the presence of cysteamine hydrochloride and 2,2-dimethoxy-2-phenylacetophenone (DPAP) photoinitiator under irradiation at λ = 365 nm in methanol for 3 hours gave the desired $mPEG_{2k}$-triamino initiator **(5)**. Quantitative conversion of triallyl $mPEG_{2k}$ **(4)** into **(5)** was achieved after careful optimisation of the thiol-ene reaction conditions, especially in terms of amount of solvent required, alkyne:photoinitiator molar ratio, and reaction time.

Polymerisation of α-amino acid-*N*-carboxyanhydrides (NCAs) has emerged in recent years as one of the most efficient and versatile routes to synthesise homopolypeptides. The polymerisation requires a nucleophilic initiator, typically a primary amine and proceeds by sequential nucleophilic ring-opening of the monomer(s) NCA ring, affording well-defined polymers with low polydispersities (Habraken et al., 2012). However, loss of control can occur via several mechanisms. For example, dry conditions are essential as water can act as an initiator and start the polymerisation process. Habraken et al. showed that NCA polymerisation at 0°C leads to poly(glutamic acid) with very high fidelity in amino-end groups required to achieve control over the

polymerisation process, leading to well-defined polymers with low polydispersities. However, at higher temperatures pyroglutamates end-groups were generated, leading to unwanted chain termination and broader molecular weight distributions (Habraken et al., 2010).



Scheme 2.2. Reactions and conditions. a) allyl bromide, K_2CO_3, acetonitrile, heated to reflux, 3 h; b) NaOH, MeOH/CH_2Cl_2, 14 h; c) oxalyl chloride, DMF, CH_2Cl_2, 1 h; d) methoxypolyethylene glycol amine 2.0 kDa, triethylamine, CH_2Cl_2, overnight; e) cysteamine hydrochloride, DPAP, MeOH, UV at λ = 365 nm, 3 h; f) and g) 1) γ-benzyl-L-glutamate NCA, THF, 0°C, 5 days and 2) NaOH, H_2O/THF, 2 days.

In the present study, a family of $mPEG_{2k}$-polyGA copolymers with miktoarm and linear macromolecular structures was prepared from initiators **(5)** and $mPEG_{2k}NH_2$, respectively. The number of glutamic acid (GA) monomer units in B block arms were either 10 or 30 in both linear and miktoarm copolymers (Table 2.1).

Table 2.1. Composition, architecture, M_n, and polydispersity of $mPEG_{2k}$-polyGA copolymers prepared in this study.

Polymer	Architecture	$M_{n,\,Theo}$ (kDa)[a]	$M_{n,NMR}$ (kDa)[b]	$M_{n,SEC}$ (kDa)[c]	$Đ_{SEC}$[c]
$mPEG_{2k}$-*mik*-$(GA_{10})_3$	miktoarm	7.0	7.2	4.7	1.28
$mPEG_{2k}$-*mik*-$(GA_{30})_3$	miktoarm	14.8	15.5	7.0	1.27
$mPEG_{2k}$-*lin*-GA_{10}	linear	3.3	3.9	2.2	1.24
$mPEG_{2k}$-*lin*-GA_{30}	linear	7.1	7.7	1.9	1.26

[a]Calculated from $[Monomer]_0/[Initiator]_0$ and conversion values for each polymerisation run. [b]Copolymers composition estimated by ^1H NMR in D_2O. [c]Determined by SEC aqueous 0.10 M $NaNO_3$, 0.02 (*w/v*) NaN_3, pH 10 as the mobile phase, in a system calibrated with 0.2-130 kDa PEO standards.

Linear $mPEG_{2k}$-*lin*-GA_{10} and $mPEG_{2k}$-*lin*-GA_{30} copolymers were synthesised using commercially available monoamino $mPEG_{2k}$ (2.0 kDa) as the polymerisation initiator, whilst for miktoarm $mPEG_{2k}$-*mik*-poly$(GA)_3$ copolymers a tri-functional initiator **(5)** was required. All polymerisation reactions were carried out at 0°C and monitored by ^1H NMR, by following the disappearance of the α-CH proton signal of the NCA monomer at 4.4 ppm. The polymerisations were stopped at ~70% conversion, which generally occurred within 5 days.

Treatment of the reaction crude product with $NaOH_{aq}$ afforded the required $mPEG_{2k}$-polyGA copolymers, which were purified by dialysis against deionised water (MWCO 1-3.5 kDa).

A typical ^1H NMR spectrum of a $mPEG_{2k}$-poly(GA) copolymer is shown in Figure 2.3. $M_{n,NMR}$ were calculated by comparing the integral of the ethylene repeating

units of $mPEG_{2k}$ with that of the CHN groups in the glutamic acid repeating units, and were found to be in good agreement with the theoretical ones, calculated from the initial ($mPEG_{2k}$ initiator):(glutamic acid N-carboxyanhydride monomer) molar ratios and the final monomer conversions.

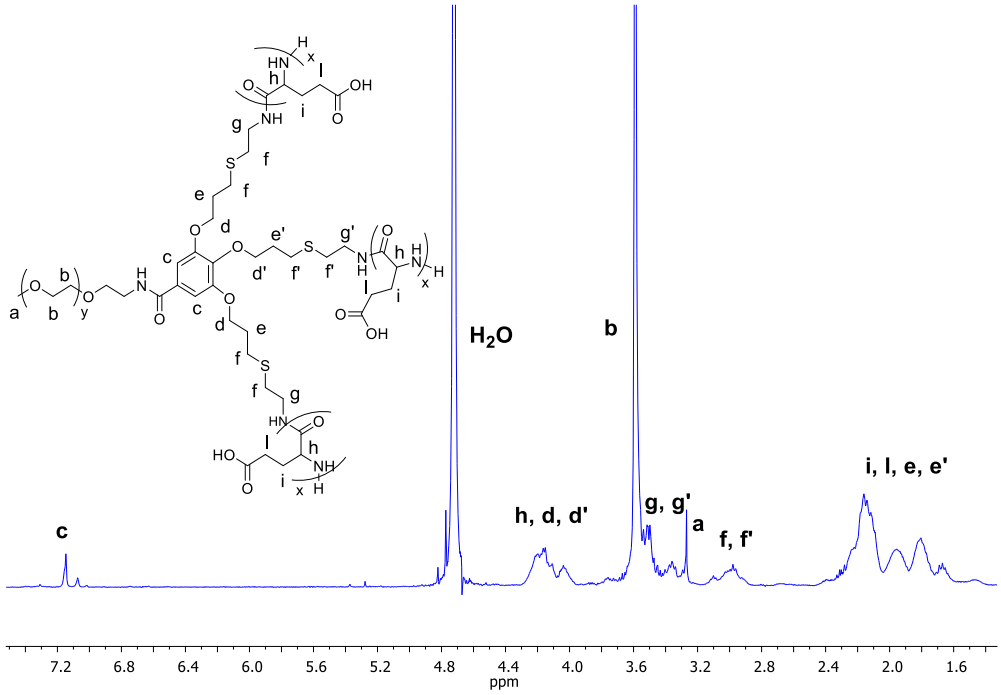


Figure 2.3. ^{1}H NMR spectrum of miktoarm $mPEG_{2k}$-*mik*-$(GA_{10})_3$ in D_2O.

^{1}H NMR confirmed that the $M_{n,NMR}$ of all copolymers was in line with the expected theoretical values (Table 2.1). Therefore, the total number of glutamic acid repeating units in $mPEG_{2k}$-*lin*-GA_{10}, $mPEG_{2k}$-*lin*-GA_{30}, $mPEG_{2k}$-*mik*-$(GA_{10})_3$ and $mPEG_{2k}$-*mik*-$(GA_{30})_3$ copolymers were confirmed to be 10, 30, 30 and 90, respectively. However, the exact number of glutamic acid repeating units per polypeptide chain in miktoarm copolymers could not be confirmed. SEC analysis using aqueous 0.10 M $NaNO_3$, 0.02 (*w/v*) NaN_3, pH 10 mobile phase (Perdih et al., 2014) showed a lower average molecular mass, $M_{n,SEC}$, which

could be ascribed to the difference in relative hydrodynamic volume between $mPEG_{2k}$-polyGA copolymers and mPEG narrow standards used to calibrate the SEC.

2.3.2. Polymer-protein complexes characterisation

Next, the ability of $mPEG_{2k}$-polyGA copolymers to complex model protein, lysozyme, was assessed. This protein was chosen in this study due to its very high isoelectric point (pI: 11.3) (Wetter and Deutsch, 1951) – with net positive charge (+7.5) at physiological pH (Kuehner et al., 1999) which potentially could allow its complexation with polyanionic macromolecules – and its high stability in solution. Hen egg-white lysozyme is a 129 amino acid, 14.3 kDa protein (Canfield, 1963) with 6 lysine and 11 arginine residues (Masuda et al., 2005) exposed at the surface of the protein.

In this study polymer-protein complexes were studied by incubating $mPEG_{2k}$-polyGA copolymers and lysozyme in 10 mM phosphate buffer, pH 7.4 or pH 2.0. Association was assessed in the 0.1-2.5 range of mixing ratios *r*, defined as the relative charge ratio between the number of glutamic acid monomer units in $mPEG_{2k}$-polyGA copolymers (mostly negatively charged at pH 7.4), and the number of lysine and arginine residues in the lysozyme (positively charged at both pH 7.4 and 2.0).

Poly(glutamic acid) possesses mostly a α-helix conformation (~ 3.6 residues per turn) at pH < 5, in aqueous media, whilst at pH > 6 it exhibits a random coil conformation (Kukula et al., 2002). This coil-to-helix conformation transition

depends on several factors, including pH, chain length, concentration and temperature (Krejtschi and Hauser, 2011, Gooding et al., 2013). At pH 7.4 poly(GA) is expected to assume mostly a random coil conformation due to Coulombic repulsion between ionised glutamate sidechains (Gooding et al., 2013), thus potentially further favouring protein complexation. The protein concentration was kept constant (300 µg mL^{-1}) whilst the polymer concentration was varied to obtain the desired *r* values.

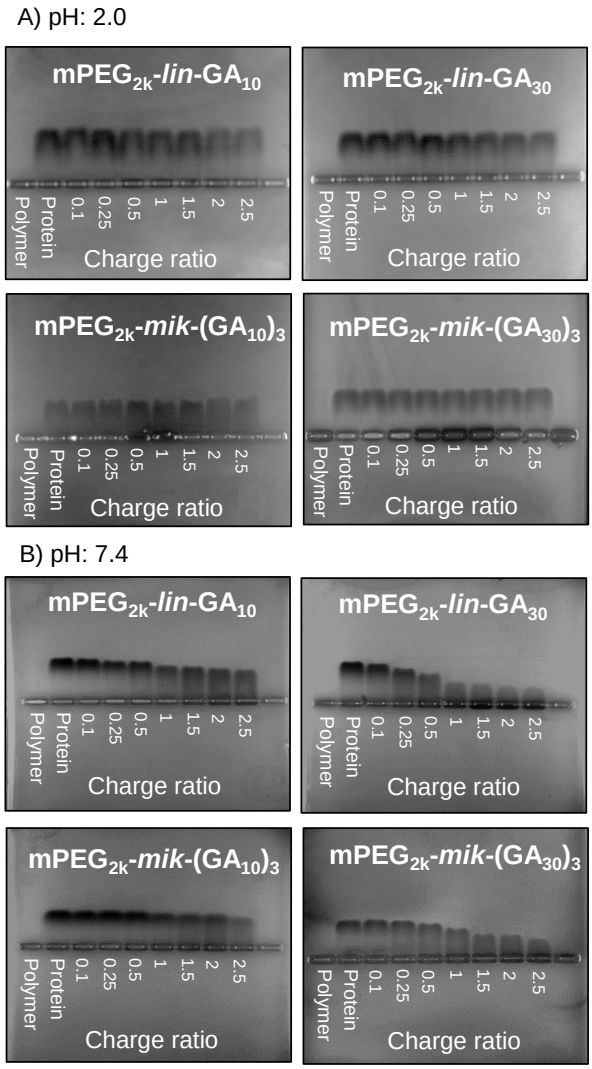


Figure 2.4. Electrophoretic separation at pH 2.0 (A) and pH 7.4 (B) of free protein from linear $mPEG_{2k}$-*lin*-GA_{10} and $mPEG_{2k}$-*lin*-GA_{30}, and miktoarm $mPEG_{2k}$-*mik*-$(GA_{10})_3$ and $mPEG_{2k}$-*mik*-$(GA_{30})_3$-derived complexes in a 1% agarose gel, run 2 h at 100 mA in Tris-Acetate-EDTA buffer.

Protein complexation was first assessed by agarose gel electrophoresis in an electrophoretic mobility shift assay (Figure 2.4). The efficiency of ($mPEG_{2k}$-polyGA)-protein complexation was found to be pH-dependent, with no complexation observed at pH 2.0 (Figure 2.4 A), where carboxylic groups of the glutamic acid repeating units exist in their protonated uncharged form, and are hence unable to engage with positively charged Lys and Arg protein residues. Taken together with evidence of ($mPEG_{2k}$-polyGA)-protein complexation under pH 7.4 conditions (Figure 2.4 B) these results further confirm that the complexation process was indeed driven by ionic interactions between the species. The pH 7.4 gels followed a general pattern, where bands were observed at low *r* ratios, indicating the presence of either weakly complexed, or free protein. As the amount of copolymer increased at higher *r* ratios, the free protein bands gradually became dimmer, indicating greater level of complexation with the copolymer, until they eventually disappear. At higher *r* ratios increased staining could be seen in the wells, which was suggestive of the presence of large and/or of neutral complexes which prevented their migration out of the well.

These results suggested a dependence of protein complexation on the molecular composition and architecture of the complexing copolymer. Low level of complexation was found for linear $mPEG_{2k}$-*lin*-GA_{10} which was not significantly improved by the use of a miktoarm $mPEG_{2k}$-*mik*-$(GA_{10})_3$ copolymer, containing three arms of GA_{10}. Intriguingly, the same number of GA monomeric units (30) but arranged in a linear chain of $mPEG_{2k}$-*lin*-GA_{30} copolymer produced

a superior complexation whereby, from approximately $r \geq 1.0$, no free protein could be observed in the gel. Further increase in the number of GA_{30} branches in $mPEG_{2k}$-*mik*-$(GA_{30})_3$ miktoarm resulted in a gel pattern similar to that observed for $mPEG_{2k}$-*lin*-GA_{30}.

The particle size of ($mPEG_{2k}$-polyGA)-lysozyme complexes at 1.0 and 2.5 ratios were analysed by nanoparticle tracking analysis (NTA). In the present study, NTA was found to be superior to dynamic light scattering (DLS) to estimate the size of relatively polydisperse samples of polymer-protein complexes in solution, as reported previously (Dragovic et al., 2011). For $r = 2.5$ all ($mPEG_{2k}$-polyGA)-lysozyme complexes were found to possess average diameter in the 50-200 nm range (Figure 2.5) with relatively broad particle size distribution. At $r = 1.0$ $mPEG_{2k}$-*lin*-GA_{10}, $mPEG_{2k}$-*lin*-GA_{30} and $mPEG_{2k}$-*mik*-$(GA_{30})_3$ copolymers showed a hydrodynamic diameter between 50 and 150 nm whilst the presence of larger polymer-protein complexes was detected with $mPEG_{2k}$-*mik*-$(GA_{10})_3$. Neither unmodified lysozyme nor free $mPEG_{2k}$-polyGA copolymers could be detected by NTA, further confirming that the sizes analysed were polymer-protein complexes.

TEM images of representative ($mPEG_{2k}$-*lin*-GA_{30})-lysozyme complexes at $r = 2.5$ illustrate the presence of numerous complexes in the size range of 30-50 nm, as well as existence of some larger aggregates (Supporting Information, Fig. S22).

Taken together, agarose gel electrophoresis, particle size analysis and TEM suggest that binding of the copolymers to lysozyme initiated 'controlled

assembly' into complexes made of multiple molecules of lysozyme and copolymers. This agrees with previous work where $mPEG_{12k}$-*lin*-Asp_{18} copolymers were utilised to form stable lysozyme complexes consisting of 36 and 42 molecules of lysozyme and mPEG-poly(Asp), respectively (Harada and Kataoka, 1998). One could propose that the presence of PEG_{2k} may prevent higher order aggregation of ($mPEG_{2k}$-polyGA)-protein complexes when their overall charge is close to neutral, as previously suggested for $mPEG_{5k}$–poly(*N,N*-dimethylaminoethyl methacrylate) (PAMA) copolymer when complexing L-asparaginase (Kurinomaru et al., 2012).

Current literature indicates that protein binding efficiency and size of the resulting ionic complexes depend on a complex interplay between a number of parameters, including size and charge density of both polymers and proteins, pH, ionic strength, [polymer]:[protein] molar ratio, and, for PEG-containing block copolymers, the relative size of PEG and polyionic blocks. Under the complexation conditions of the present work (pH > 6), random coil conformation of polyglutamic acid chain would be expected (Kukula et al., 2002) to allow for its relative conformational freedom an interaction with surface groups of lysozyme, however it is not clear at this point if the chain would have such a flexibility to as to 'wrap around' the protein to form multiple interactive contacts (Park et al., 1992). The superior complexation of linear GA_{30} relative to both linear $polyGA_{10}$ and miktoarm $poly(GA_{10})_3$ copolymers might be pointing to such a 'wrapping' and formation of multiple contacts as the chain length is increased. Positively charged amino acid residues of lysozyme appear

distributed throughout the protein surface (Wilson et al., 1992) rather than creating 'charged patches'; this may favour creation of interactive contacts with polyGA$_{30}$ linear chain of mPEG$_{2k}$-*lin*-GA$_{30}$ rather than 'grouped' anion charges in miktoarm mPEG$_{2k}$-*mik*-(GA$_{10}$)$_3$.

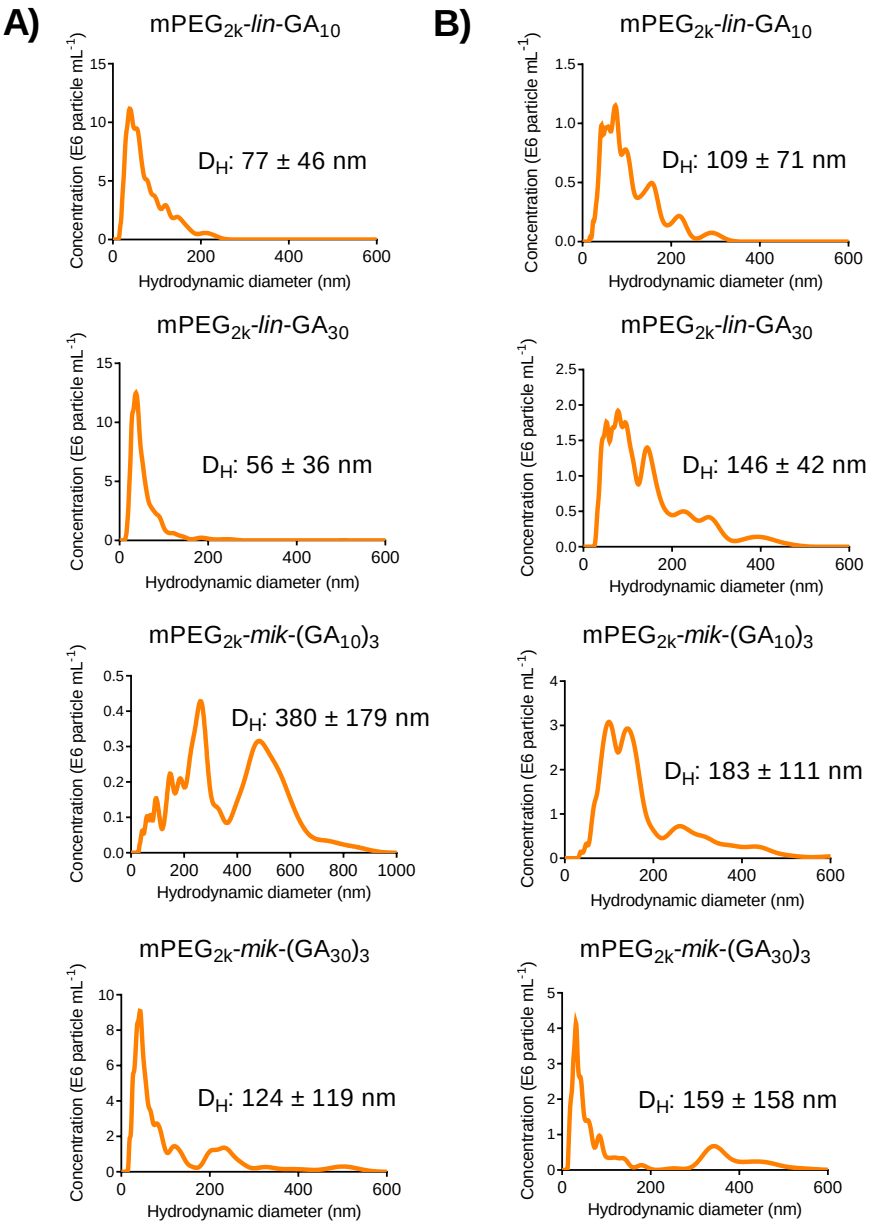


Figure 2.5. Particle size distribution of mPEG$_{2k}$-*lin*-GA$_{10}$, mPEG$_{2k}$-*lin*-GA$_{30}$, mPEG$_{2k}$-*mik*-(GA$_{10}$)$_3$ and mPEG$_{2k}$-*mik*-(GA$_{30}$)$_3$-derived complexes with lysozyme at charge ratio 1.0 (A) and 2.5 (B). D_H is the average hydrodynamic diameter ± SD of polymer-protein nanocomplexes as assessed by nanoparticle tracking analysis (NTA).

2.3.3. Lysozyme conformation in polymer-protein complexes: intrinsic fluorescence studies

Protein intrinsic fluorescence studies were carried out to investigate whether the conformation of lysozyme was affected by polymer complexation. Selected fluorescence spectra of polymer-protein complexes at a 2.5 ratio are shown in Figure 2.6. Spectra are dominated by tryptophan fluorescence due to the presence of six tryptophan residues – Trp-28, Trp-62, Trp-63, Trp-108, Trp-111 and Trp-123 – within the lysozyme structure. The maximum of fluorescence emission λ_{max} of tryptophan-containing native proteins typically falls in the 308-350 nm range, the exact position depending on burial of individual tryptophan residues within protein domains. Protein unfolding typically results in exposure of tryptophan residues to more polar and solvent exposed local environments, leading to a red shift of fluorescence λ_{max}, typically in the 345-355 nm range (Eftink, 1994). At 25°C native lysozyme in 10 mM phosphate buffer, pH 7.4 showed a maximum emission at λ = 344 nm. However, upon heating at 95°C for 120 min, λ_{max} shifted to 350 nm. This bathochromic shift has been observed before, and was ascribed to unfolding of lysozyme (Chi and Asher, 1998, Imoto et al., 1972). For ($mPEG_{2k}$-polyGA)-lysozyme complexes, a slight hypsochromic (blue) shift of λ_{max} was observed, irrespective of the polymer macromolecular architecture and length of polyGA protein-binding arm(s), suggesting that upon complexation lysozyme did not unfold (Figure 2.6). This blue shift may indicate that within these complexes tryptophan residues were actually exposed to a more nonpolar environment (Imoto et al., 1972).

Circular dichroism experiments on (mPEG$_{2k}$-polyGA)-lysozyme complexes proved less informative due to significant overlap between the spectra of the poly(glutamic acid) moiety and lysozyme (Supporting Information, Figure S23). However, although not conclusive, the data indicated that, at least for low polymer-protein ratios, no detectable protein unfolding occurred, which is in agreement with the intrinsic tryptophan fluorescence results.

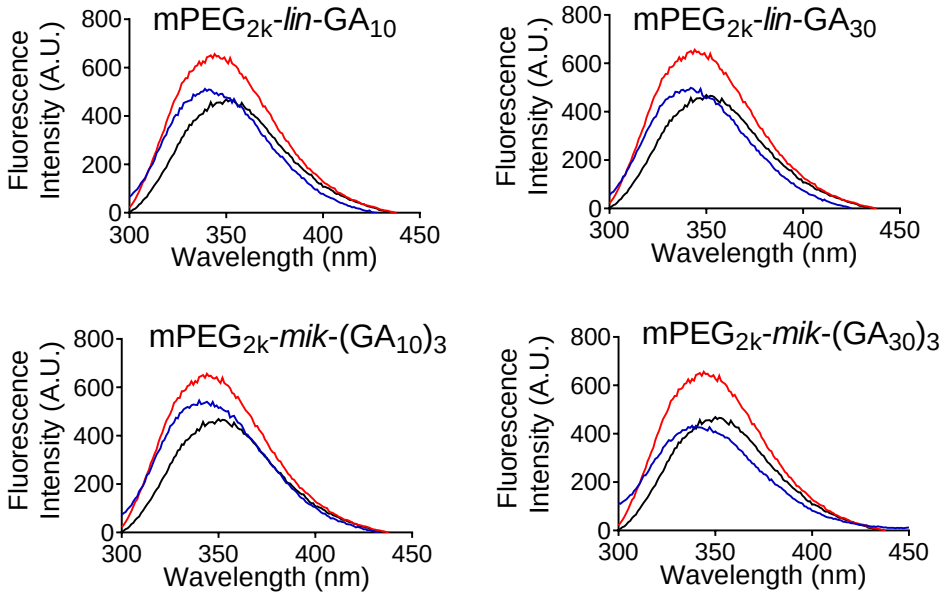


Figure 2.6. Tryptophan fluorescence spectra of lysozyme after complexation with linear mPEG$_{2k}$-*lin*-GA$_{10}$ and mPEG$_{2k}$-*lin*-GA$_{30}$, and miktoarm mPEG$_{2k}$-*mik*-(GA$_{10}$)$_3$ and mPEG$_{2k}$-*mik*-(GA$_{30}$)$_3$ copolymers at charge ratio 2.5 in 10 mM phosphate buffer pH 7.4. Polymer-protein complexes (**blue**), native lysozyme (**red**) and denatured protein (**black**). All spectra were recorded at room temperature.

2.3.4. Lysozyme activity assay

Lysozyme exerts its antimicrobial activity by selectively cleaving β-1,4-glycosidic bonds between *N*-acetylmuramic acid and *N*-acetylglucosamine, often found in bacterial cell walls (Rees and Sternberg, 1984). The effect of protein complexation on the residual enzymatic activity of lysozyme at various polymer-protein ratios was assessed using *Micrococcus lysodeikticus*

lyophilised cell walls at the substrate. For all $mPEG_{2k}$-polyGA investigated, lytic activity decreased after polymer-protein complexation (Figure 2.7) suggesting that enzyme was located towards the "core" of these assemblies, where the enzyme active centre was less accessible (Harada and Kataoka, 1999). A decrease in lytic activity due to protein denaturation (Masschalck et al., 2001), or changes in its secondary structure seemed unlikely, given the results from our intrinsic fluorescence studies. Similar decrease in lysozyme enzymatic activity was seen in complexation with polyanionic poly(acrylic acid) (Tomita et al., 2010).

A more pronounced decrease in lysozyme activity at higher polymer-protein ratios suggests an increased complexation level (Figure 2.7 A), which can be supported by gel electrophoresis data showing more pronounced protein sequestration at higher polymer-protein ratios (Figure 2.4 B). ($mPEG_{2k}$-*lin*-GA_{30})-lysozyme complexes showed the highest reduction in enzymatic activity, again indicating the importance of copolymer architecture and the length of protein-binding polyGA moiety on sheltering of the enzyme catalytic pocket.

For comparative purposes, irreversible covalent PEGylation of lysozyme was carried out using methoxy PEG_{2k} succinimidyl carbonate to generate conjugates with average number of mPEG chains ranging from 5.2-6.3 per lysozyme macromolecule. These conjugates were found to possess minimal or no residual enzymatic activity, as confirmed by *Micrococcus lysodeikticus* turbidimetric assay (Supporting Information, section 6.1.6). This is in agreement with previous work, which indicated that some lysine residues – e.g.

Lys97 – are located in a region responsible for substrate specificity (Gregoritza et al., 2016).

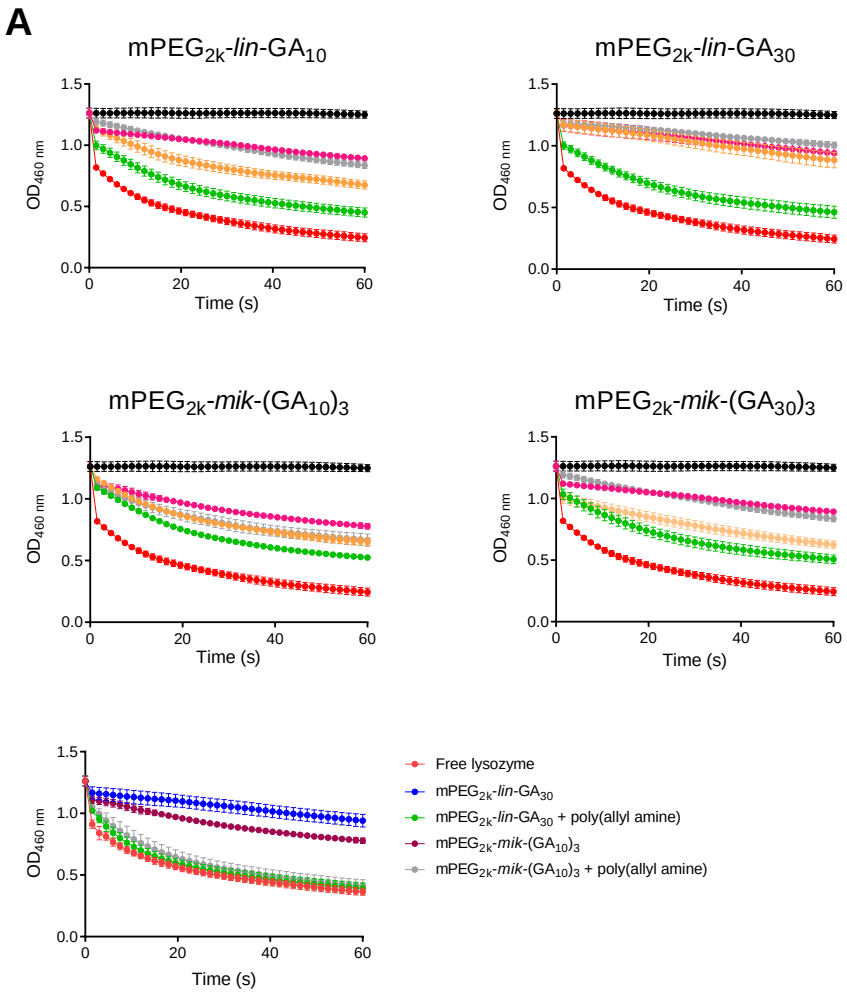


Figure 2.7. A. Lysozyme enzymatic activity of linear mPEG$_{2k}$-*lin*-GA$_{10}$ and mPEG$_{2k}$-*lin*-GA$_{30}$, and miktoarm mPEG$_{2k}$-*mik*-(GA$_{10}$)$_3$ and mPEG$_{2k}$-*mik*-(GA$_{30}$)$_3$-derived complexes. Free protein (**red**), free polymer (**black**), and 0.1 (**green**), 0.5 (**orange**), 1.0 (**grey**) and 2.5 (**pink**) polymer-protein charge ratio *r*. OD$_{460nm}$ represents the optical density of the samples at λ = 460 nm. B. Lysozyme enzymatic activity of selected complexes at polymer-protein charge ratio of 2.5 – with either linear mPEG$_{2k}$-*lin*-GA$_{30}$, and miktoarm mPEG$_{2k}$-*mik*-(GA$_{10}$)$_3$ – before and after polymer de-complexation by addition of poly(allyl amine) (240 µg mL^{-1}, 4.2 mM of protonable amino groups).

By contrast to PEG-conjugated lysozyme, full enzymatic activity was recovered upon de-complexation of lysozyme from the (mPEG$_{2k}$-polyGA)-protein nanocomplexes by addition of 17 kDa poly(allyl amine), a known complexant for polyanionic polymers (Tomita et al., 2010) (Figure 2.7 B). Thus, these data

confirmed that initial decrease of enzymatic activity was indeed due to inclusion of lysozyme within polymer nanocomplexes which limited the accessibility of its catalytic pocket, and subsequent complete recovery of activity clearly indicate that polymer complexation induced no irreversible protein unfolding or denaturation confirming this advantage of the complexation approach adopted.

2.3.5. Toxicity of $mPEG_{2k}$-poly(glutamic acid) copolymers

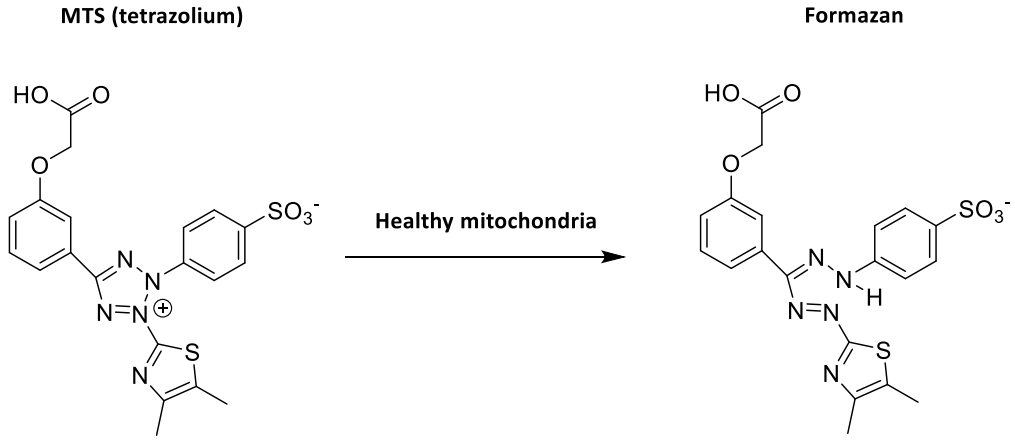
Despite the many advantages presented by polymer-protein nanocomplexes, they may have high reactivity with cellular components. In fact, polymer cytotoxicity can be induced by several factors such as the material itself and its physicochemical properties such as charge, hydrophilicity and length (Shin et al., 2015). Then, the toxicological profile of each polymer and polymer-based nanocomplex have to be carefully investigated.

In this part of this thesis work, the toxicological profile of $mPEG_{2k}$-polyGA copolymers, both free and complexed with lysozyme, was investigated on lung epithelial A549 and Calu-3 cell lines. Cell-polymer incubation time was set at 4 h for all the toxicological assays performed in this chapter (MTS, LDH and Annexin V/PI). Longer periods of time were not considered due to the absence of FBS in cell medium (cell viability might be affected after 5 h in serum free medium). FBS was removed from medium to eliminate polymer-serum competitive interactions and therefore maximise the contact between cells and polymer.

Polymer concentrations in the range of 25-200 µg mL^{-1} were chosen for these initial toxicological studies. They covered the range of polymer concentrations that we intended to use for subsequent *in vitro* (1-10 µg mL^{-1}) and *in vivo* studies (100 µg). Future toxicological studies will likely extend this range to include higher concentrations.

2.3.5.1. Metabolic activity (MTS assay)

The ability of cells to reduce a tetrazolium reagent (MTS) to formazan gives an indication of the mitochondria integrity and therefore of the metabolic activity of cells (Wang et al., 2010). Indeed, MTS is reduced by viable cells to generate a formazan product (Scheme 2.3). This reduction happens due to dehydrogenase enzymes found in the mitochondria, and the resulting formazan reduced product is soluble in the medium, and can be quantified by a colorimetric method.



Scheme 2.3. Mechanism of MTS assay. This assay involves the reduction of tetrazolium compound (MTS) by active mitochondrial enzymes to form formazan products.

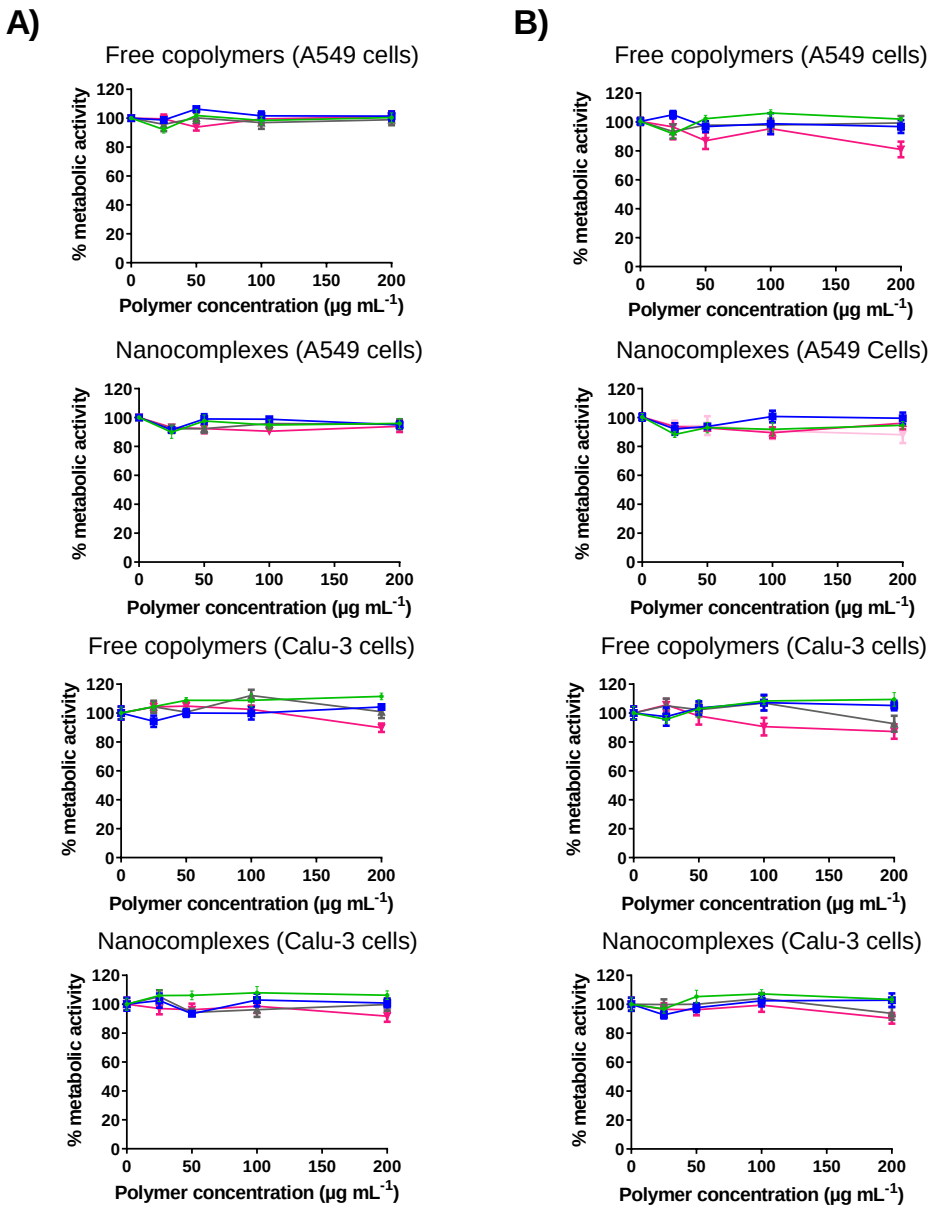


Figure 2.8. MTS assay in A549 and Calu-3 cells after treatment with free mPEG$_{2k}$-polyGA copolymers and (mPEG$_{2k}$-polyGA)-lysozyme nanocomplexes for A) 4 h and B) 24 h. (mPEG$_{2k}$-*lin*-GA$_{10}$) (**green**), (mPEG$_{2k}$-*lin*-GA$_{30}$) (**blue**), (mPEG$_{2k}$-*mik*-(GA$_{10}$)$_3$) (**grey**), mPEG$_{2k}$-*mik*-(GA$_{30}$)$_3$ (**pink**)-derived complexes or copolymer.

The metabolic activity of A549 and Calu-3 cells was evaluated after 4 and 24 h treatment with mPEG$_{2k}$-polyGA copolymers and (mPEG$_{2k}$-polyGA)-lysozyme nanocomplexes (Figure 2.8). After 4 h treatment, the metabolic activity was found to be between 80 and 100% in both cell lines, and similar results were also observed after 24 h treatment. These data therefore indicates that

$mPEG_{2k}$-polyGA copolymers, both free and complexed with lysozyme, does not have any metabolic effect on lung epithelial cells at polymer concentrations up to 200 µg mL^{-1}. Control free lysozyme, at the same concentrations than that in the polymer-protein nanocomplexes, did not affect the metabolic activity of lung epithelial cells (Supporting Information, Figure S26).

2.3.5.2. Membrane integrity (LDH assay)

LDH is a colorimetric assay which allows assessing the integrity of cell membranes. Lactate dehydrogenase is a stable cytosolic enzyme which is released into the media when a disruption of membranes occurs. The amount of LDH in the media can be estimated with a 30 min coupled enzymatic assay that results in the conversion of a tetrazolium salt into a colored formazan product which can be quantified by measuring its absorbance at λ = 490 nm. The amount of formazan is proportional to the damage of cell membranes.

The membrane damage of A549 and Calu-3 cells after 4 h treatment with $mPEG_{2k}$-polyGA copolymers, both free and complexed with lysozyme, was investigated (Figure 2.9). As observed with the metabolic activity assay, both free and complexed $mPEG_{2k}$-polyGA copolymers, at concentrations up to 200 µg mL^{-1}, did not show any significant effect on the membrane integrity of lung epithelial cells. Indeed, after treatment less than 1% of LDH was released from both cell type for all samples tested indicating no membrane damage. Control free lysozyme, at the same concentrations than that in polymer-protein nanocomplexes, did not affect the membrane integrity of lung epithelial cells (Supporting Information, Figure S27).

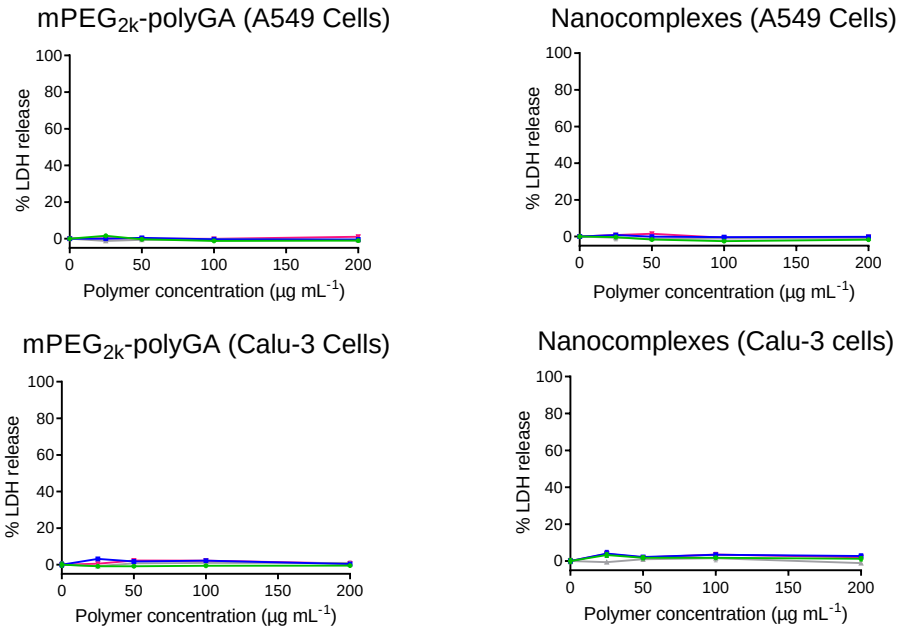


Figure 2.9. Percentage of total LDH released from A549 and Calu-3 cells after treatment with free $mPEG_{2k}$-polyGA copolymers and ($mPEG_{2k}$-polyGA)-lysozyme nanocomplexes for 4 h. $mPEG_{2k}$-*lin*-GA_{10} (**green**), $mPEG_{2k}$-*lin*-GA_{30} (**blue**), $mPEG_{2k}$-*mik*-$(GA_{10})_3$ (**grey**), $mPEG_{2k}$-*mik*-$(GA_{30})_3$ (**pink**)-derived complexes or copolymer.

2.3.5.3. Apoptotic assay (Annexin V-FITC/PI assay)

To quantify cell apoptosis, A549 and Calu-3 cells exposed to $mPEG_{2k}$-polyGA copolymers and ($mPEG_{2k}$-polyGA)-lysozyme nanocomplexes were stained using Annexin V-FITC/propidium iodide double staining and analysed by flow cytometry. Annexin V, a calcium-dependent phospholipid-binding protein with affinity for phosphatidylserine, can be used as a sensitive probe to detect the presence of this phospholipid on the cell membrane. Within cell membranes, phosphatidylserine is not evenly distributed, but is found preferentially in the inner leaflet of the plasma membrane and in endocytic membranes (Leventis and Grinstein, 2010). Apoptotic cells lose the asymmetry of their plasma membrane, which results in increased exposure of phosphatidylserine on the

outside surface. Annexin V can therefore act as a marker for apoptosis. Propidium iodide (PI) is a non-specific DNA intercalating agent, which does not penetrate through membranes when cells are alive. Thus, PI can be used as a marker for necrotic cells and distinguish from apoptotic and living cells. Figure 2.10 shows a generic example of the data generated by flow cytometry with these double staining assay.

Lung epithelial cells were exposed for 4 hours to $mPEG_{2k}$-polyGA copolymers, both free and complexed with lysozyme, and the necrotic and apoptotic effects of the latter is shown in Figure 2.11. For both A549 and Calu-3 cells, all samples tested showed more than 80% viable cells. Also, when compared to untreated cells, no significant apoptotic or necrotic cells were observed after treatment with free $mPEG_{2k}$-polyGA copolymers or ($mPEG_{2k}$-polyGA)-lysozyme complexes, at polymer concentrations of 200 μg mL^{-1}. Control free lysozyme, at the same concentrations than that in polymer-protein nanocomplexes, was also confirmed not to be toxic on lung epithelial cells (Supporting Information, Figure S28).

Taken together these data, $mPEG_{2k}$-polyGA copolymers showed a safe profile in lung epithelial cells at concentrations up to 200 μg mL^{-1} and are very encouraging as polymer cytotoxicity can often be a critical limitation for the development of drug delivery systems (Fischer et al., 2003).

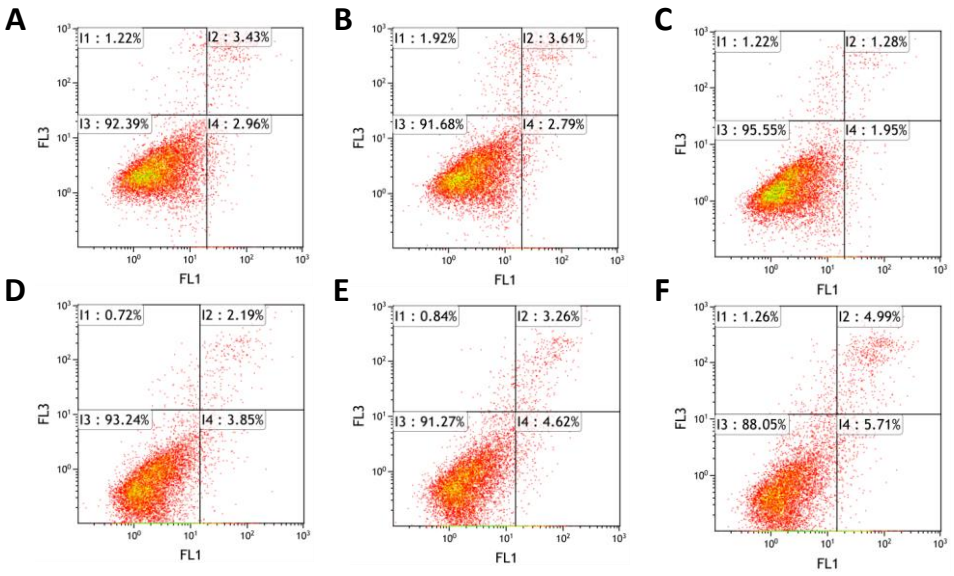


Figure 2.10. Examples of Annexin V-FITC/PI double staining flow cytometry analysis of necrosis and apoptosis in A549 cells and Calu-3 cells after 4 h treatment with mPEG$_{2k}$-polyGA copolymers. A-C: A549 cells; D-F Calu-3 cells; A, D: Untreated cells; B, E: mPEG$_{2k}$-*mik*-(GA$_{10}$)$_3$ copolymers; C, F: (mPEG$_{2k}$-*mik*-(GA$_{10}$)$_3$)-lysozyme nanocomplexes. FL1 and FL3 represents Annexin V-FITC and propidium iodide staining, respectively. I1: necrosis; I2: late apoptosis; I3: viable cells and I4: early apoptosis.

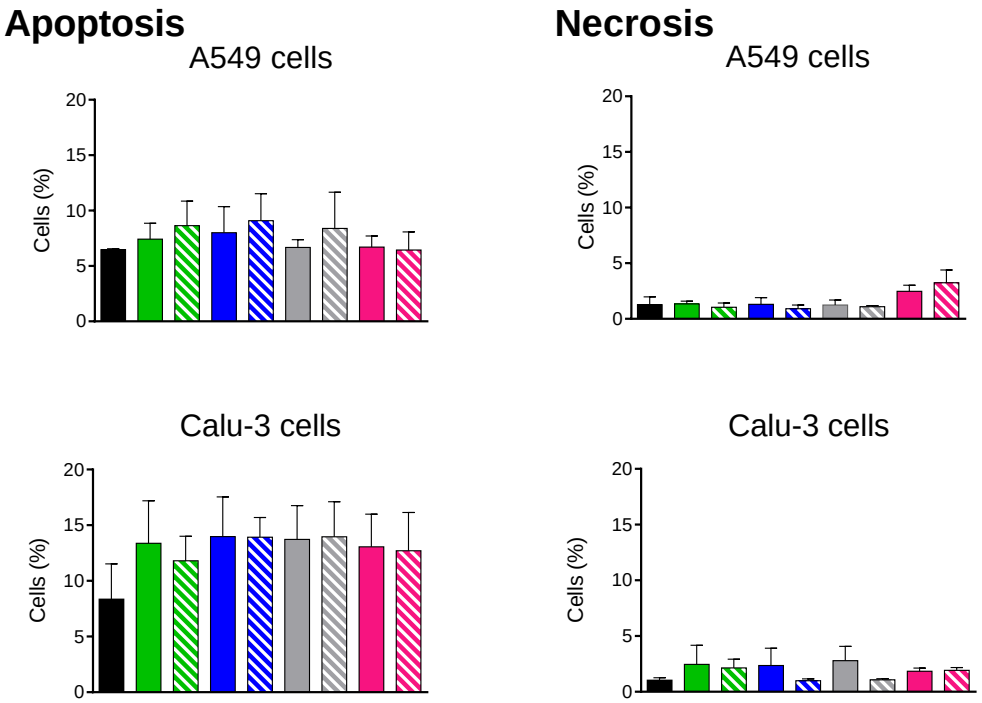


Figure 2.11. Percentages of apoptosis (left panels) and necrosis (right panels) in A549 cells and Calu-3 cells after treatment with mPEG$_{2k}$-polyGA copolymers, both free and complexed with lysozyme for 4 h. Solid bars: free mPEG$_{2k}$-polyGA copolymers. Hatched bars: (mPEG$_{2k}$-polyGA)-lysozyme nanocomplexes. Untreated cells (**black**), mPEG$_{2k}$-*lin*-GA$_{10}$ (**green**), mPEG$_{2k}$-*lin*-GA$_{30}$ (**blue**), mPEG$_{2k}$-*mik*-(GA$_{10}$)$_3$ (**grey**) and mPEG$_{2k}$-*mik*-(GA$_{30}$)$_3$ (**pink**)-derived complexes or copolymer.

2.4. Concluding remarks

In this chapter, a family of PEG-polyanion copolymers suitable for non-covalent and reversible complexation of proteins is presented. $mPEG_{2k}$-poly(glutamic acid) copolymers with different architecture - linear A-B and miktoarm $A-B_3$ - and different length of the protein-binding arms were synthesised by NCA polymerisation, and their ability to bind model protein (lysozyme) was investigated.

Electrophoresis and nanoparticle tracking analysis indicated that the length of protein-binding poly(glutamic acid) arms of the copolymers, as well as their macromolecular architecture, had a significant effect on complexation efficiency, where for copolymers with the same number of glutamic acid repeating units, polymers with linear architecture were more efficient, than their miktoarm analogues, to complex lysozyme model protein.

Importantly, upon polymer complexation the protein structural conformation appears to be conserved, and no detectable denaturation was observed. Enzymatic activity of the complexed protein was reduced, attributable to limited access of substrate to enzyme active site, and the extent of this reduction depends on the macromolecular architecture of the complexing copolymer.

Finally, linear and miktoarm $mPEG_{2k}$-polyGA copolymers have shown no toxicity at polymer concentrations up to 200 $\mu g\ mL^{-1}$.

This study identified a first structure-function relationship for a new family of $mPEG_{2k}$-poly(glutamic acid) polymers with various macromolecular architectures. Moreover, these polymers demonstrated to be suitable for protein complexation without affecting protein integrity and compromising cell viability. Therefore, next step will be to investigate the ability of these complexes to form efficient pulmonary protein formulations. This will be described in Chapter 3.

2.5. References

ALBAIN, K. S., BELANI, C. P., BONOMI, P., O'BYRNE, K. J., SCHILLER, J. H. & SOCINSKI, M. 2006. PIONEER: A Phase III Randomized Trial of Paclitaxel Poliglumex Versus Paclitaxel in Chemotherapy-Naive Women with Advanced-Stage Non-Small-Cell Lung Cancer and Performance Status of 2. *Clinical Lung Cancer,* 7**,** 417-419.

ALTINTAS, O., VOGT, A. P., BARNER-KOWOLLIK, C. & TUNCA, U. 2012. Constructing star polymers via modular ligation strategies. *Polymer Chemistry,* 3**,** 34-34.

BLASCO, E., SCHMIDT, B. V. K. J., BARNER-KOWOLLIK, C., PIÑOL, M. & ORIOL, L. 2014. A novel photoresponsive azobenzene-containing miktoarm star polymer: Self-assembly and photoresponse properties. *Macromolecules,* 47**,** 3693-3700.

CANFIELD, R. E. 1963. The Amino Acid Sequence of Egg White Lysozyme. *J Biol Chem,* 238**,** 2698-707.

COUE, G. & ENGBERSEN, J. F. 2011. Functionalized linear poly(amidoamine)s are efficient vectors for intracellular protein delivery. *J Control Release,* 152**,** 90-8.

CHI, Z. & ASHER, S. A. 1998. UV Raman Determination of the Environment and Solvent Exposure of Tyr and Trp Residues. *The Journal of Physical Chemistry B,* 102**,** 9595-9602.

DIPETRILLO, T., SUNTHARALINGAM, M., NG, T., FONTAINE, J., HORIBA, N., OLDENBURG, N., PEREZ, K., BIRNBAUM, A., BATTAFARANO, R., BURROWS, W. & SAFRAN, H. 2012. Neoadjuvant Paclitaxel Poliglumex, Cisplatin, and Radiation for Esophageal Cancer: A Phase 2 Trial. *American Journal of Clinical Oncology,* 35.

DONDONI, A. 2008. The emergence of thiol-ene coupling as a click process for materials and bioorganic chemistry. *Angew Chem Int Ed Engl,* 47**,** 8995-7.

DRAGOVIC, R. A., GARDINER, C., BROOKS, A. S., TANNETTA, D. S., FERGUSON, D. J., HOLE, P., CARR, B., REDMAN, C. W., HARRIS, A. L., DOBSON, P. J., HARRISON, P. & SARGENT, I. L. 2011. Sizing and phenotyping of cellular vesicles using Nanoparticle Tracking Analysis. *Nanomedicine,* 7**,** 780-8.

EFTINK, M. R. 1994. The use of fluorescence methods to monitor unfolding transitions in proteins. *Biophys J,* 66**,** 482-501.

FISCHER, D., LI, Y., AHLEMEYER, B., KRIEGLSTEIN, J. & KISSEL, T. 2003. In vitro cytotoxicity testing of polycations: influence of polymer structure on cell viability and hemolysis. *Biomaterials,* 24**,** 1121-1131.

GOODING, E. A., SHARMA, S., PETTY, S. A., FOUTS, E. A., PALMER, C. J., NOLAN, B. E. & VOLK, M. 2013. pH-dependent helix folding dynamics of poly-glutamic acid. *Chemical Physics,* 422**,** 115-123.

GREGORITZA, M., GOEPFERICH, A. M. & BRANDL, F. P. 2016. Polyanions effectively prevent protein conjugation and activity loss during hydrogel cross-linking. *Journal of Controlled Release,* 238**,** 92-102.

HABRAKEN, G. J. M., HEISE, A. & THORNTON, P. D. 2012. Block Copolypeptides Prepared by N-Carboxyanhydride Ring-Opening Polymerization. *Macromol Rapid Commun,* 33**,** 272-286.

HABRAKEN, G. J. M., PEETERS, M., DIETZ, C. H. J. T., KONING, C. E. & HEISE, A. 2010. How controlled and versatile is N-carboxy anhydride (NCA) polymerization at 0 °C? Effect of temperature on homo-, block- and graft (co)polymerization. *Polymer Chemistry,* 1**,** 514.

HARADA, A. & KATAOKA, K. 1998. Novel Polyion Complex Micelles Entrapping Enzyme Molecules in the Core: Preparation of Narrowly-Distributed Micelles from Lysozyme and Poly(ethylene glycol)−Poly(aspartic acid) Block Copolymer in Aqueous Medium. *Macromolecules,* 31**,** 288-294.

HARADA, A. & KATAOKA, K. 1999. On−Off Control of Enzymatic Activity Synchronizing with Reversible Formation of Supramolecular Assembly from Enzyme and Charged Block Copolymers. *J Am Chem Soc,* 121**,** 9241-9242.

HAWKER, C. J. 1995. Architectural Control in "Living" Free Radical Polymerizations: Preparation of Star and Graft Polymers. *Angewandte Chemie International Edition in English,* 34**,** 1456-1459.

HOURANI, R. & KAKKAR, A. 2010. Advances in the elegance of chemistry in designing dendrimers. *Macromol Rapid Commun,* 31**,** 947-74.

IMOTO, T., FORSTER, L. S., RUPLEY, J. A. & TANAKA, F. 1972. Fluorescence of Lysozyme: Emissions from Tryptophan Residues 62 and 108 and Energy Migration. *Proc Natl Acad Sci U S A,* 69**,** 1151-1155.

KAPLÁNEK, R., HAVLÍK, M., KRÁL, V., MARTÁSEK, P. & BŘÍZA, T. 2009. Methyl Gallate as the Framework for the Construction of Fluorous Building Blocks. *Synthetic Communications,* 40**,** 247-256.

KHANNA, K., VARSHNEY, S. & KAKKAR, A. 2010. Miktoarm star polymers: advances in synthesis, self-assembly, and applications. *Polymer Chemistry,* 1**,** 1171-1185.

KREJTSCHI, C. & HAUSER, K. 2011. Stability and folding dynamics of polyglutamic acid. *Eur Biophys J,* 40**,** 673-85.

KUEHNER, D. E., ENGMANN, J., FERGG, F., WERNICK, M., BLANCH, H. W. & PRAUSNITZ, J. M. 1999. Lysozyme Net Charge and Ion Binding in Concentrated Aqueous Electrolyte Solutions. *The Journal of Physical Chemistry B,* 103**,** 1368-1374.

KUKULA, H., SCHLAAD, H., ANTONIETTI, M. & FÖRSTER, S. 2002. The Formation of Polymer Vesicles or "Peptosomes" by Polybutadiene-block-poly(l-glutamate)s in Dilute Aqueous Solution. *J Am Chem Soc,* 124**,** 1658-1663.

KURINOMARU, T., TOMITA, S., KUDO, S., GANGULI, S., NAGASAKI, Y. & SHIRAKI, K. 2012. Improved Complementary Polymer Pair System: Switching for Enzyme Activity by PEGylated Polymers. *Langmuir,* 28**,** 4334-4338.

LANGER, C. J., O'BYRNE, K. J., SOCINSKI, M. A., MIKHAILOV, S. M., LEŚNIEWSKI-KMAK, K., SMAKAL, M., CIULEANU, T. E., ORLOV, S. V., DEDIU, M., HEIGENER, D., EISENFELD, A. J., SANDALIC, L., OLDHAM, F. B., SINGER, J. W. & ROSS, H. J. 2008. Phase III Trial Comparing Paclitaxel Poliglumex (CT-2103, PPX) in Combination with Carboplatin Versus Standard Paclitaxel and Carboplatin in the Treatment of PS 2 Patients with Chemotherapy-Naïve Advanced Non-small Cell Lung Cancer. *Journal of Thoracic Oncology,* 3**,** 623-630.

LEE, A. L. Z., WANG, Y., YE, W.-H., YOON, H. S., CHAN, S. Y. & YANG, Y.-Y. 2008. Efficient intracellular delivery of functional proteins using cationic polymer core/shell nanoparticles. *Biomaterials,* 29**,** 1224-1232.

LEVENTIS, P. A. & GRINSTEIN, S. 2010. The distribution and function of phosphatidylserine in cellular membranes. *Annu Rev Biophys,* 39**,** 407-27.

MASSCHALCK, B., HOUDT, R. V., HAVER, E. G. R. V. & MICHIELS, C. W. 2001. Inactivation of Gram-Negative Bacteria by Lysozyme, Denatured Lysozyme, and Lysozyme-Derived Peptides under High Hydrostatic Pressure. *Appl Environ Microbiol,* 67**,** 339-344.

MASUDA, T., IDE, N. & KITABATAKE, N. 2005. Structure-sweetness relationship in egg white lysozyme: role of lysine and arginine residues on the elicitation of lysozyme sweetness. *Chem Senses,* 30**,** 667-81.

MELANCON, M. P. & LI, C. 2011. MULTIFUNCTIONAL SYNTHETIC POLY(L-GLUTAMIC ACID)-BASED CANCER THERAPEUTIC AND IMAGING AGENTS. *Molecular imaging,* 10**,** 28-42.

MORGAN, M. A., DARCY, K. M., ROSE, P. G., DEGEEST, K., BOOKMAN, M. A., AIKINS, J. K., SILL, M. W., MANNEL, R. S., ALLIEVI, C. &

EGORIN, M. J. 2008. Paclitaxel poliglumex and carboplatin as first-line therapy in ovarian, peritoneal or fallopian tube cancer: A phase I and feasibility trial of the Gynecologic Oncology Group. *Gynecologic Oncology,* 110**,** 329-335.

NEDERBERG, F., APPEL, E., TAN, J. P., KIM, S. H., FUKUSHIMA, K., SLY, J., MILLER, R. D., WAYMOUTH, R. M., YANG, Y. Y. & HEDRICK, J. L. 2009. Simple approach to stabilized micelles employing miktoarm terpolymers and stereocomplexes with application in paclitaxel delivery. *Biomacromolecules,* 10**,** 1460-8.

NG, T., FONTAINE, J., SUNTHARALINGAM, M., DIPETRILLO, T., HORIBA, M. N., OLDENBURG, N. B., PEREZ, K., CHEN, W., HABR, F. & SAFRAN, H. 2010. Neoadjuvant paclitaxel poliglumex (PPX), cisplatin, and radiation (RT) for esophageal cancer. *Journal of Clinical Oncology,* 28**,** 4085-4085.

NIETO-ORELLANA, A., DI ANTONIO, M., CONTE, C., FALCONE, F. H., BOSQUILLON, C., CHILDERHOUSE, N., MANTOVANI, G. & STOLNIK, S. 2017. Effect of polymer topology on non-covalent polymer-protein complexation: miktoarm versus linear mPEG-poly(glutamic acid) copolymers. *Polymer Chemistry,* 8**,** 2210-2220.

O'BRIEN, M. E. R., SOCINSKI, M. A., POPOVICH, A. Y., BONDARENKO, I. N., TOMOVA, A., BILYNSKY˘ı, B. T., HOTKO, Y. S., GANUL, V. L., KOSTINSKY, I. Y., EISENFELD, A. J., SANDALIC, L., OLDHAM, F. B., BANDSTRA, B., SANDLER, A. B. & SINGER, J. W. 2008. Randomized Phase III Trial Comparing Single-Agent Paclitaxel Poliglumex (CT-2103, PPX) with Single-Agent Gemcitabine or Vinorelbine for the Treatment of PS 2 Patients with Chemotherapy-Naïve Advanced Non-small Cell Lung Cancer. *Journal of Thoracic Oncology,* 3**,** 728-734.

PARK, J. M., MUHOBERAC, B. B., DUBIN, P. L. & XIA, J. 1992. Effects of protein charge heterogeneity in protein-polyelectrolyte complexation. *Macromolecules,* 25**,** 290-295.

PAZ-ARES, L., ROSS, H., O'BRIEN, M., RIVIERE, A., GATZEMEIER, U., VON PAWEL, J., KAUKEL, E., FREITAG, L., DIGEL, W., BISCHOFF, H., GARCIA-CAMPELO, R., IANNOTTI, N., REITERER, P., BOVER, I., PRENDIVILLE, J., EISENFELD, A. J., OLDHAM, F. B., BANDSTRA, B., SINGER, J. W. & BONOMI, P. 2008. Phase III trial comparing paclitaxel poliglumex vs docetaxel in the second-line treatment of non-small-cell lung cancer. *Br J Cancer,* 98**,** 1608-1613.

PERDIH, P., ČEBAŠEK, S., MOŽIR, A. & ŽAGAR, E. 2014. Post-Polymerization Modification of Poly(L-glutamic acid) with D-(+)-Glucosamine. *Molecules,* 19.

PISPAS, S., HADJICHRISTIDIS, N., POTEMKIN, I. & KHOKHLOV, A. 2000. Effect of Architecture on the Micellization Properties of Block Copolymers: A2B Miktoarm Stars vs AB Diblocks. *Macromolecules,* 33**,** 1741-1746.

REES, A. R. & STERNBERG, M. J. E. 1984. *From Cells to Atoms: An Illustrated Introduction to Molecular Biology*, Blackwell Scientific Publications.

SABBATINI, P., SILL, M. W., O'MALLEY, D., ADLER, L. & SECORD, A. A. 2008. A phase II trial of paclitaxel poliglumex in recurrent or persistent ovarian or primary peritoneal cancer (EOC): A gynecologic oncology group study. *Gynecologic Oncology,* 111**,** 455-460.

SHIH, I. L., VAN, Y. T. & SHEN, M. H. 2004. Biomedical applications of chemically and microbiologically synthesized poly(glutamic acid) and poly(lysine). *Mini Rev Med Chem,* 4**,** 179-88.

SHIN, S., SONG, I. & UM, S. 2015. Role of Physicochemical Properties in Nanoparticle Toxicity. *Nanomaterials,* 5**,** 1351-1365.

SOLIMAN, G. M., SHARMA, A., MAYSINGER, D. & KAKKAR, A. 2011. Dendrimers and miktoarm polymers based multivalent nanocarriers for efficient and targeted drug delivery. *Chem Commun (Camb),* 47**,** 9572-87.

SOLIMAN, G. M., SHARMA, R., CHOI, A. O., VARSHNEY, S. K., WINNIK, F. M., KAKKAR, A. K. & MAYSINGER, D. 2010. Tailoring the efficacy of nimodipine drug delivery using nanocarriers based on A2B miktoarm star polymers. *Biomaterials,* 31**,** 8382-92.

TOMITA, S., ITO, L., YAMAGUCHI, H., KONISHI, G.-I., NAGASAKI, Y. & SHIRAKI, K. 2010. Enzyme switch by complementary polymer pair system (CPPS). *Soft Matter,* 6**,** 5320-5320.

TSIOURVAS, D., SIDERATOU, Z., STERIOTI, N., PAPADOPOULOS, A., NOUNESIS, G. & PALEOS, C. M. 2012. Insulin complexes with PEGylated basic oligopeptides. *J Colloid Interface Sci,* 384**,** 61-72.

WANG, P., HENNING, S. M. & HEBER, D. 2010. Limitations of MTT and MTS-Based Assays for Measurement of Antiproliferative Activity of Green Tea Polyphenols. *PLOS ONE,* 5**,** e10202.

WETTER, L. R. & DEUTSCH, H. F. 1951. Immunological studies on egg white proteins. IV. Immunochemical and physical studies of lysozyme. *J Biol Chem,* 192**,** 237-42.

WILSON, K. P., MALCOLM, B. A. & MATTHEWS, B. W. 1992. Structural and thermodynamic analysis of compensating mutations within the core of chicken egg white lysozyme. *Journal of Biological Chemistry,* 267**,** 10842-10849.

YIN, H., KANG, S.-W. & BAE, Y. H. 2009. Polymersome Formation from AB2 Type 3-Miktoarm Star Copolymers. *Macromolecules,* 42**,** 7456-7464.

YUN, J., FAUST, R., SZILÁGYI, L. S., KÉKI, S. & ZSUGA, M. 2003. Effect of Architecture on the Micellar Properties of Amphiphilic Block Copolymers: Comparison of AB Linear Diblock, A1A2B, and A2B Heteroarm Star Block Copolymers. *Macromolecules,* 36**,** 1717-1723.

CHAPTER 3

Dry powder formulations of non-covalent protein complexes with linear or miktoarm copolymers for pulmonary delivery

In this part of this thesis work, ($mPEG_{2k}$-*lin*-GA) and ($mPEG_{2k}$-*mik*-$(GA)_3$)-lysozyme nanocomplexes were formulated into dry powders by spray-drying using different aerosol excipients. The aerodynamic properties of these dry powders, their ability to efficiently release the nanocomplexes in aqueous environment and their capacity to protect lysozyme from proteolytic enzymes were investigated.

Table of Contents

3.1. Introduction.....92
3.2. Experimental section.....96
3.3. Results and Discussion.....102
3.3.1. Characterisation of dry powders.....102
3.3.2. Aerosolisation performance.....111
3.3.3. Nanocomplexes recovery, protein activity and protein protection against proteolytic enzymes.....114
3.4. Concluding remarks.....120
3.5. References.....121

3.1. Introduction

Polymeric nanoparticles have been extensively investigated as potential formulations for pulmonary delivery of protein therapeutics (Bailey and Berkland, 2009, Menon et al., 2014, Trapani et al., 2013, Lee et al., 2013), as they offer protection from degradation both during storage and *in vivo*, can enhance cell targeting (Fowler et al., 2013b, Fowler et al., 2013a, Li et al., 2017, Goodall et al., 2015, Kamaly et al., 2012) and reduce immunogenicity (Sung et al., 2007, Soppimath et al., 2001). However, polymeric materials with slow degradation profiles can potentially induce pulmonary accumulation of nanoparticles, especially when daily administration is needed (Dunne et al., 2000), resulting in long-term toxicity in the lungs (Sivadas et al., 2008, Armstrong et al., 1996). Within this context, formulations based on complexes with relatively shorter life-time in the lung, such as reversible polymer-protein nanocomplexes, could overcome the pulmonary accumulation issue while still providing protection against protein degradation and pulmonary clearance (Figure 1.3), and potential for cellular targeting and transcellular transport.

Nanocomplexes are commonly formulated in aqueous solutions. However, most of protein degradation mechanisms are believed to be water-mediated including de-aminations and hydrolysis (Depreter et al., 2013). Moreover, solutions and suspensions are susceptible to microbial growth which can promote the contamination of pulmonary devices, especially those used for chronic treatments (Jarvis et al., 2014). Within this context, dry powders are one attractive alternative for the delivery of protein therapeutics into the lungs.

Spray-drying is the most common technique utilised for the production of inhalable dry powder formulations of a number of drugs, including protein therapeutics (Maltesen et al., 2008, You et al., 2007). However, for efficient deposition in the lungs, particles must possess specific particle size, density and shape - collectively defined as the aerodynamic diameter (Carvalho et al., 2011). Most of the currently available commercial inhalation products use lactose as a carrier material (Pilcer et al., 2012). However, lactose may not be always suitable for formulations that contain primary amino groups, such as peptides and proteins, because of a range of potential side-reaction occurring at the sugar reducing end - e.g. Maillard reaction, especially when the processing of the formulation requires high temperatures (Littringer et al., 2012a). Therefore, non-reducing sugars such as mannitol and trehalose have been investigated as potential alternatives (Maury et al., 2005, Littringer et al., 2012b).

In the previous chapter, we showed that $mPEG_{2k}$-poly(glutamic acid) copolymers with linear A-B ($mPEG_{2k}$-*lin*-polyGA) and miktoarm A-B_3 ($mPEG_{2k}$-*mik*-poly$(GA)_3$) architectures can be successfully utilised for reversible protein complexation. At physiological pH the polyGA block(s) possess multiple copies of anionic carboxylate units, which can complex positively charged amino acids at the surface of proteins (lysozyme was used in this thesis as a protein model). In the present study, we aimed to investigate the suitability of these non-covalent polymer-protein nanocomplexes to be formulated into inhalable spray-dried powders for pulmonary delivery.

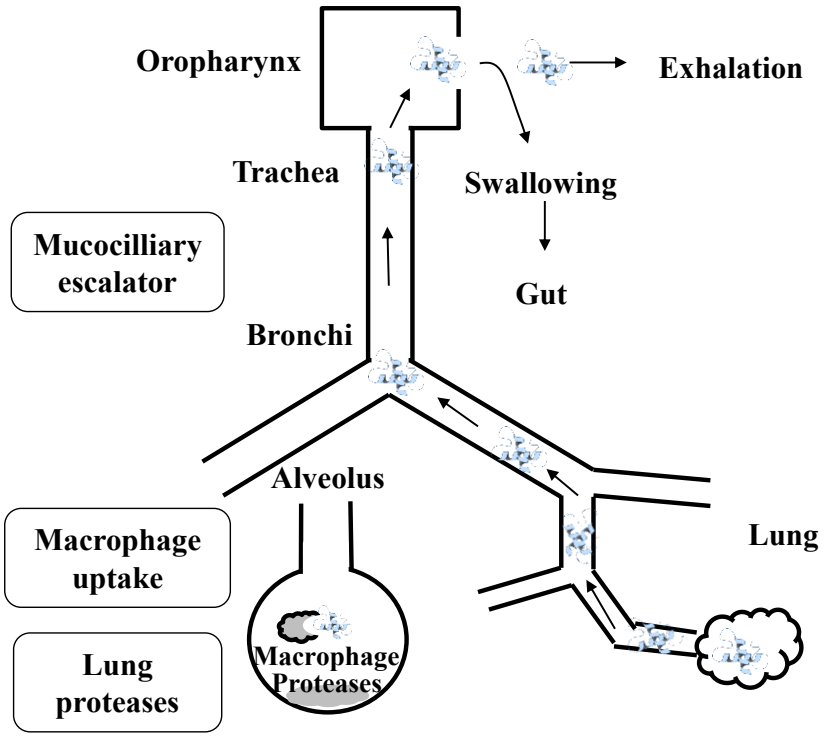


Figure 3.1. Schematic representation of the main mechanisms for protein clearance after pulmonary protein administration: mucociliary clearance, macrophage uptake and proteolytic degradation. Adapted from (Depreter et al., 2013).

The aerosolisation properties of these dry powders were investigated using trehalose, mannitol and/or leucine as aerosol excipients. As a disperser enhancer, leucine plays a crucial role in promoting de-aggregation of microparticles by limiting interparticulate forces, while trehalose and mannitol are common protective agents for biopharmaceuticals during both formulation and storage (Kibbe and Association, 2000, Bakaltcheva et al., Schüle et al., 2007, Torrado and Torrado, 2002, Ogain et al., 2011, Maa et al., 1997, Jin et al., 2010, Hulse et al., 2008).

The lung possesses a wide range of pulmonary peptidases which are involved in specific clearance mechanisms for proteins and peptides, facilitating in their degradation/inactivation. In this part of our work, we also aimed to investigate the ability of dry powder formulations to release nanocomplexes in aqueous

conditions and preserve protein activity in the presence of model protease trypsin.

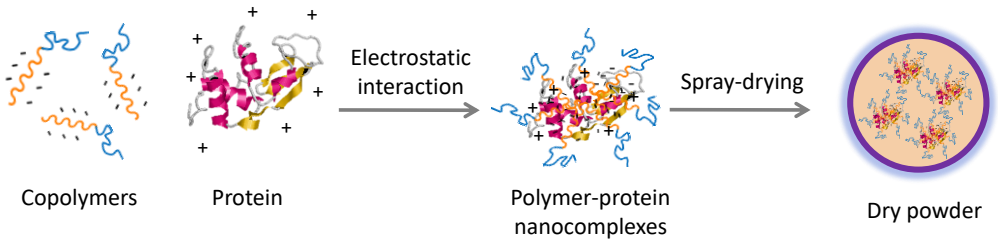


Figure 3.2. Assembly of non-covalent polymer-protein ionic complexes and their formulation as dry powders by spray-drying.

3.2. Experimental section

Synthesis of linear and miktoarm mPEG$_{2k}$-poly(glutamic acid) copolymers. Linear mPEG$_{2k}$-*lin*-GA$_{10}$ and mPEG$_{2k}$-*lin*-GA$_{30;}$ and miktoarm mPEG$_{2k}$-*mik*-(GA$_{10}$)$_3$ and mPEG$_{2k}$-*mik*-(GA$_{30}$)$_3$ copolymers were synthesised by ring-opening polymerisation of γ-benzyl-L-glutamate *N*-carboxyanhydride (NCA) monomer from appropriate ω-amino poly(ethylene glycol)s as described in Chapter 2, section 2.2.

Preparation of polymer-protein nanocomplexes. (mPEG$_{2k}$-polyGA)-lysozyme nanocomplexes were prepared at relative molar charge ratios r = 2.5, where r is the charge ratio between the number of glutamic acid residues present in the copolymer (negatively charged at physiological pH) and that of protein lysine and arginine residues (17 in total per protein molecule, positively charged at physiological pH) of lysozyme. Polymers and protein were separately dissolved in phosphate buffer (PB, 10 mM, pH 7.4) and appropriate aliquots were mixed to achieve r = 2.5.

Preparation of the liquid feed for spray-drying. 37.5 mL of nanocomplex suspension (2 mg mL^{-1}) were added to 37.5 mL of deionised water where the required excipients had been previously dissolved. The final total solid content of the suspension was always kept constant at 1% (*w/v*). The suspension was gently stirred for 30 min at room temperature prior to spray-drying. The components of the resulting dry powders were: 0-10% (*w/w*) nanocomplexes, 0-10% (*w/w*) leucine, 6.6% (*w/w*) phosphate buffer salts, and trehalose or mannitol as bulking agents (up to 100% (*w/w*)) (for specific ratios see Table 3.1).

Spray-drying conditions. A laboratory scale spray-drying equipment developed by Vectura Group plc (Chippenham, United Kingdom) was used to produce the dry powders. The optimal operating conditions were: total solids content: 1% (*w/v*), atomisation air flow rate: 15 L min^{-1}, atomisation air pressure: 2.5 bar, air outlet temperature: 65°C, liquid feed flow rate: 2.5 mL min^{-1}, drying air flow rate 17 kg h^{-1} and drying gas pressure: 2.0 bar. The resulting dry powder formulations were handled and stored at low humidity (< 30%).

The yield was calculated as the ratio between the weight of solids collected after spray-drying and that of the initial amount of ingredients used to prepare the aqueous solutions, expressed as a percentage (%).

Dry powder characterisation

Particle size distribution and morphology. Particle size distribution was measured by laser diffraction (ASPIROS Sympatec, Clausthal-Zellerfeld, Germany). Powders were dispersed through the measurement zone under a dispersion pressure of 2.0 bar using the R2 lens. The measurements were performed in triplicate. Size is reported as mean volumetric diameter (D_{50}) and distribution width is presented as span. Span index is calculated as follows:

$$\text{Span}=\frac{D_{90}-D_{10}}{D_{50}}$$

where D_{10}, D_{50} and D_{90} are the diameters below which 10%, 50% and 90% of the particle population lie, respectively. The morphology of the particles was visualised by scanning electron microscopy (SEM). The samples were mounted

onto aluminium stubs and sputter coated (20 nm) with gold/palladium target using a Quorum Q15 TES coating unit. The samples were viewed using a Hitachi S3000H Scanning Electron Microscope with an accelerating voltage of 10 kV.

Moisture content. Particle moisture content was measured immediately after spray-drying by thermogravimetric analysis under non-oxidising conditions using a TGA 4000. For the analysis, 10-20 mg of powder were heated from 20°C to 160°C at 10°C min^{-1} and then maintained at that temperature for 5 min before measurement.

Protein incorporation efficiencies. The amount of protein encapsulated in the dry powders was evaluated by bicinchoninic acid (BCA) assay. Dry powders were first incubated in phosphate buffer (PB, 10 mM, pH 7.4) for 1 h under gentle stirring, at room temperature – at a theoretical protein concentration of 15-25 µg mL^{-1} (mass of protein, assuming 100% protein incorporation). Then 150 µL of particle samples and 150 µL of BCA solution prepared as described by the manufacturer (BCA protein assay kit, ThermoFisher Technologies) were mixed and heated at 56°C for 60 min. Once cooled down to 25°C, the absorbance was measured at λ = 562 nm using a micro-plate reader (SpectraMax M2). All the absorbance values were corrected by subtracting the values measured for relevant blank samples. Each measurement was performed in quadruplicate. The protein encapsulation (%) was calculated as a percentage between the amount of protein in the dry powder, determined from a calibration curve, and the amount of protein present in the liquid feed.

Differential scanning calorimetry (DSC). Samples were prepared in closed aluminium pans. 2-3 mg of powders were first heated from 10°C to 60°C at 10°C min^{-1} and then cooled down to 10°C. This process was then repeated 3 times, increasing the temperature to 130°C, 140°C and 230°C, respectively. Glass transition (T_g), heat capacity (ΔCp), melting point (T_m) and enthalpy of melting (ΔH_m) were derived from the resulting thermograms.

In vitro **pulmonary deposition.** The aerodynamic properties of dry powders were assessed using a fast screening impactor (FSI, Copley Scientific). A standard dispersion procedure was conducted for 4 s at an air flow rate of 60 L min^{-1}. The cut-off aerodynamic diameter was 5 µm. An amount of 12 ± 1 mg of powder was loaded into blisters and aerosolised using a proprietary unit dose DPI (Vectura, UK). The emitted dose (ED) was calculated by accurately weighing the blister before and after aerosolisation. Particles with an aerodynamic diameter lower than 5 µm were deposited on a filter in the fine fraction collector. The filter was weighed before and after dispersion, in order to determine the fine particle fraction (FPF), which can be defined as the fraction (%) of the emitted dose (ED) with an aerodynamic diameter below 5 µm. Each powder was tested in triplicate.

Nanocomplexes recovery from dry powders in aqueous medium. To investigate whether the nanocomplexes could be recovered from the dry powders, the latter were incubated in phosphate buffer (PB, 10 mM, pH 7.4) for 15 min under gentle stirring at room temperature at a protein concentration of 70 µg mL^{-1} (as quantified by BCA assay). The hydrodynamic diameter of

nanocomplexes was then measured by nanoparticle tracking analysis (NTA) using a Nanosight LM14. All measurements were performed at 25°C. NTA 2.0 Build 127 software was used for data capturing and analysis. The samples were measured for 80 s.

Particle size distributions are represented here as normalised distributions where the most populated size is taken as 100%.

Lysozyme activity. The enzymatic activity of lysozyme, was measured by a turbidimetric enzymatic assay where the decrease in optical density of a suspension of *Micrococcus lysodeikticus* lyophilised cells, a natural substrate for lysozyme, in phosphate buffer (PB, 10 mM, pH 7.4) was monitored (Tomita et al., 2010). Nanocomplexes or free lysozyme were extracted from the dry powders as previously described and the protein concentration was adjusted to 37 µg mL^{-1} (as quantified by BCA assay). 10 mg of lyophilised cells were added to 20 mL of PB. 300 µL of this substrate suspension were added to 150 µL of nanocomplex suspension and the decrease in optical density (OD) was measured at λ = 460 nm as a function of time, for 60 sec. The (OD) decay plots from 0 to 10 sec were fitted to a linear equation and the enzymatic activities were then determined from the slope of the fitted line.

To recover lysozyme from the polymer complexes to assess its residual enzymatic activity, 480 µg of poly(allyl amine) were added to 2 mL of the nanocomplex suspension to sequester $mPEG_{2k}$-polyGA from lysozyme complexes, and the mixture was maintained under very gentle stirring for 1 h at room temperature. The lysozyme activity in the resulting solution was then

quantified as previously described. Un-complexed free lysozyme was used as a reference (100% enzymatic activity). All enzymatic activity experiments were carried out in triplicate.

(mPEG$_{2K}$-polyGA)-lysozyme complexes: stability against proteolytic degradation. Nanocomplexes were recovered from dry powders as previously described, and the protein concentration adjusted to 37 µg mL^{-1} (as quantified by BCA assay). 657 µg of trypsin were added to 4 mL of particle suspension and the mixture was kept at room temperature for 3 h under gentle stirring. 480 µg of poly(allyl amine) were then added to the suspension, and the mixture was gently stirred for 1 h. Lysozyme activity was then quantified as previously described. All enzymatic activity experiments were carried out in triplicate.

Statistical analysis. Measurements were carried out in triplicate, unless otherwise stated. Values are given as means ± SD. The statistical significance of the results was assessed using one-way analysis of variance (ANOVA), Dunnet's multiple comparisons test.

3.3. Results and Discussion

3.3.1. Characterisation of dry powders

The previous chapter discussed the ability of linear and miktoarm $mPEG_{2k}$-polyGA copolymers to non-covalently complex proteins under appropriate conditions. These initial studies showed that incorporated lysozyme protein was mostly located at the "core" of these assemblies, and that protein integrity was not affected by polymer complexation. Here, we further explored the therapeutic potential of this technology by investigating how ($mPEG_{2k}$-polyGA)-lysozyme nanocomplexes can be formulated into inhalable spray-dried powders. The resulting formulations were then characterised in terms of particle size, moisture content, thermal properties, encapsulation efficiency and aerodynamic properties, to assess their suitability to be incorporated into inhalable dry powder formulations.

As shown in Chapter 2, polymer-protein feed at relative molar charge ratio of 2.5 yielded the best polymer-protein complexation efficiencies. This ratio was therefore chosen for the formulation of polymer-protein nanocomplexes in this second part of this work. Nanocomplexes were first assembled and then formulated by spray drying into dry powders using different aerosol excipients – trehalose, mannitol and leucine – to form potentially inhalable dry powder of micron-sized particles. Trehalose was used as a bulking agent as it is a well-established stabiliser for bio-molecules that are sensitive to loss of activity and structural integrity via desiccation. Trehalose is a disaccharide consisting of two molecules of glucose linked through a α,α-1,1-glucoside bond. Not having a free

anomeric reducing end, trehalose does not react with primary amino groups, thus it is particularly suitable for the formulation of (poly)peptide therapeutics. In solid formulations, trehalose is believed to stabilise biological molecules by trapping them in a rigid, amorphous glass matrix with a high glass transition temperature (Ogain et al., 2011, Maa et al., 1997, Jin et al., 2010, Hulse et al., 2008). Indeed, a high glass transition temperature will give these matrices the ability to limit the mobility of dispersed bio-molecules, thus reducing protein-protein interactions which could lead to undesired protein aggregation, and by preserving the protein tridimensional structure (Chang and Pikal, 2009). Mannitol is a polyol and its use as a stabilising excipient in protein spray-dried formulations has been extensively reviewed (Kibbe and Association, 2000, Bakaltcheva et al., Schüle et al., 2007, Torrado and Torrado, 2002). It presents very low affinity to moisture and low chemical reactivity (Andya et al., 1999). Mannitol is listed as "generally recognised as safe" (GRAS) material by the US Food and Drug Administration (FDA) and has already been approved for inhalation (Exubera®, Pzifer UK). Both trehalose and mannitol can also form hydrogen bonds with proteins in the dry state to substitute the hydrogen bonds that water creates with proteins in solution, thus stabilising their tridimensional structure (Chang and Pikal, 2009, Weers et al., 2007, Vehring, 2008). Leucine, a hydrophobic amino acid, is a well-established disperser enhancer which is typically located on the surface of spray-dried micron-sized particles (typically < 10 μm), and possesses the ability to limit the interactions between them so as to facilitate their dispersion and aerosolisation (Li et al., 2003, Vehring, 2008).

In this work, four set of formulations – trehalose, trehalose + 10% (*w/w*) leucine, mannitol, and mannitol + 10% (*w/w*) leucine – each with 0-10% (*w/w*) nanocomplexes or 5% (*w/w*) un-complexed lysozyme were tested. To address it, 37.5 mL of nanocomplex suspension (10% *w/w*), un-complexed lysozyme (5% *w/w*), or phosphate buffer (PB, 10 mM, pH 7.4, control) were added to 37.5 mL deionised water where mannitol, trehalose and/or leucine were previously dissolved. The suspension was then spray-dried by using a custom-made laboratory scale spray-drying equipment. $mPEG_{2k}$-*lin*-GA_{10}, $mPEG_{2k}$-*lin*-GA_{30}, $mPEG_{2k}$-*mik*-$(GA_{10})_3$ and $mPEG_{2k}$-*mik*-$(GA_{30})_3$ copolymers having different molecular weights and topologies were chosen in this work to assess whether these polymer structural parameters had an effect on these dry powder formulations.

Initially, the yield of the spray-drying process, particle size (D_{50}), and particle size distribution (span) of dry powder formulations were investigated. High yields – defined as the percentage ratio between the mass of solids collected after spray-drying and that of the initial amount of components used to prepare the feed solutions – are desired from an industrial perspective. On the other hand, D_{50} – the size below which 50% of the particle population lie – and span values need to be in an optimal range, as they affect the aerodynamic diameter of the formulated dry powders, and therefore the amount of particles that will potentially reach the target site in the lungs. Table 3.1 shows that the presence of ($mPEG_{2k}$-polyGA)-lysozyme nanocomplexes, did not negatively affect the spray-drying yields of formulations containing trehalose and leucine excipient

combinations, compared to control dry powders prepared with (5% *w/w*) un-complexed lysozyme model protein. The use of nanocomplexes significantly increased the yield of mannitol + leucine formulations, from 30.9% using un-complexed lysozyme, to 60.9% for the nanocomplex samples. Yields between 40 and 60% are typically regarded as being satisfactory for lab-scale spray-dryers (Islam and Langrish, 2010). For samples formulated without leucine, lower and more variable spray-drying yields were observed using both free lysozyme and polymer-lysozyme nanocomplexes. No significant effect of ($mPEG_{2k}$-polyGA) polymer size and topology on final yield was observed.

Similarly, the presence of polymer-protein nanocomplexes in spray-dried powders, had no detrimental effect on their particle size distribution. For leucine-containing dry powders, particle sizes (D_{50}) were found to be in the 2-3 µm range, which is in the optimal range for inhalation purposes (Labiris and Dolovich, 2003). Except for dry powders containing $mPEG_{2k}$-*lin*-GA_{10} nanocomplexes without leucine, distribution width values (span) were always lower than 2, which is indicative of narrow particle size distributions (Palazzo et al., 2013).

Overall, these data showed that the presence of leucine was then key to maintain good yield and particle size values of dry powder formulations as previously shown elsewhere (Yang et al., 2015).

Table 3.1. Effect of the different formulations used in this study on spray-drying yield, particle size (D_{50}) and span values. All formulations contained 6.6% (*w/w*) phosphate buffer salts and experiments were carried out in triplicate unless specified.

Excipients (*w/w*)	Nanocomplexes (*w/w*)	Yield (%)[a]	D_{50} (µm)[b]	Span[c]
Up to 100% Trehalose	-	-	1.70 ± 0.01	1.95 ± 0.02
	5% Free lysozyme	36.0	1.99[d]	1.78[d]
	10% ($mPEG_{2k}$-*lin*-GA_{10})-Lys	15.3	2.48[d]	28.16[d]
	10% ($mPEG_{2k}$-*lin*-GA_{30})-Lys	18.3	1.49 ± 0.05[d]	1.17 ± 0.5[d]
	10% ($mPEG_{2k}$-*mik*-$(GA_{10})_3$)-Lys	20.9	1.45[d]	1.81[d]
	10% ($mPEG_{2k}$-*mik*-$(GA_{30})_3$)-Lys	21.5	1.30[d]	1.46[d]
Up to 100% Trehalose + 10% Leucine	-	-	2.50 ± 0.02	1.77 ± 0.01
	5% Free lysozyme	57.8	2.37 ± 0.03	1.74 ± 0.02
	10% ($mPEG_{2k}$-*lin*-GA_{10})-Lys	55.6	2.43 ± 0.06	1.59 ± 0.02
	10% ($mPEG_{2k}$-*lin*-GA_{30})-Lys	49.7	2.45 ± 0.02	1.61 ± 0.01
	10% ($mPEG_{2k}$-*mik*-$(GA_{10})_3$)-Lys	53.8	2.32 ± 0.07	1.67 ± 0.04
	10% ($mPEG_{2k}$-*mik*-$(GA_{30})_3$)-Lys	62.4	2.30 ± 0.02	1.73 ± 0.02
Up to 100% Mannitol	-	-	2.29 ± 0.03	1.88 ± 0.01
	5% Free lysozyme	11.5	5.79[d]	1.82[d]
	10% ($mPEG_{2k}$-*lin*-GA_{10})-Lys	4.0	-	-
	10% ($mPEG_{2k}$-*lin*-GA_{30})-Lys	20.7	6.61 ± 0.08[d]	1.70 ± 0.03[d]
	10% ($mPEG_{2k}$-*mik*-$(GA_{10})_3$)-Lys	5.7	-	-
	10% ($mPEG_{2k}$-*mik*-$(GA_{30})_3$)-Lys	8.6	-	-
Up to 100% Mannitol + 10% Leucine	-	-	2.45 ± 0.06	1.80 ± 0.05
	5% Free lysozyme	30.9	2.73 ± 0.04	1.75 ± 0.01
	10% ($mPEG_{2k}$-*lin*-GA_{10})-Lys	54.3	2.62 ± 0.04	1.94 ± 0.02
	10% ($mPEG_{2k}$-*lin*-GA_{30})-Lys	60.9	2.66 ± 0.14	1.74 ± 0.03
	10% ($mPEG_{2k}$-*mik*-$(GA_{10})_3$)-Lys	52.0	2.50 ± 0.01	1.70 ± 0.01
	10% ($mPEG_{2k}$-*mik*-$(GA_{30})_3$)-Lys	48.6	2.58 ± 0.06	1.63 ± 0.02

[a]Yield is calculated from the amount of solid mass obtained from the spray-drying divided by the total amount of solid ingredients delivered to the chamber of the spray-drier, expressed as a percentage (%). [b]Particle size distribution, D_{50}, denotes the size below which 50% of the particle population lie. [c]Span values lower than 2 indicate narrow particle size distributions. [d]Data obtained from single or duplicate measurements, due to low quantity of material obtained.

SEM analysis revealed that trehalose-based dry powders were generally of spherical shape with smooth surfaces, whilst particles formulated from mannitol had surfaces with typical crystalline structures (Figure 3.3) (Pourshahab et al., 2011). The presence of leucine was found to be key to retain a spherical morphology for the spray-dried powders, probably due to its presence on the surface of these particles which can lead a decrease on particle aggregation (Vehring, 2008), and, importantly, the presence of polymer-protein nanocomplexes had no detrimental impact on the morphology of the spray-dried powders.

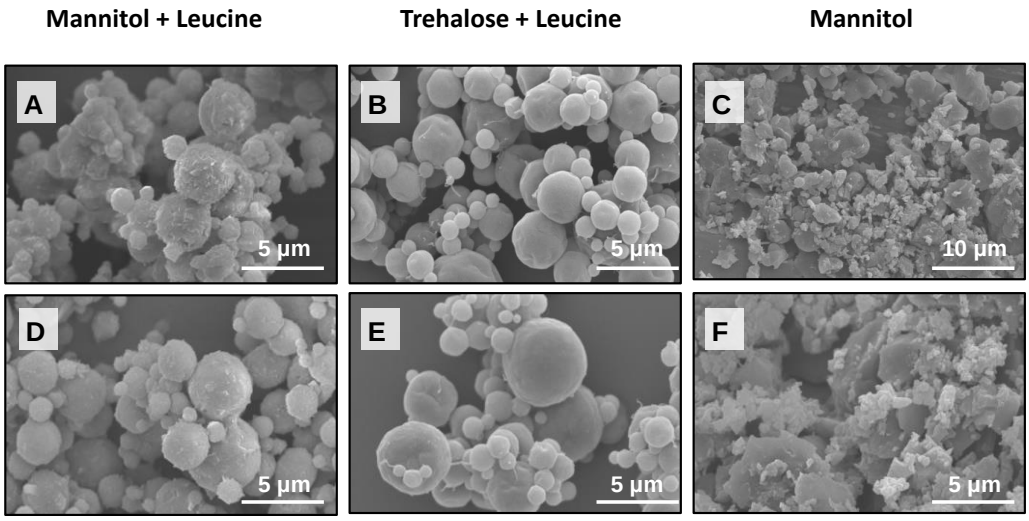


Figure 3.3. Representative scanning electron microscopy (SEM) images of dry powders containing un-complexed lysozyme (A, B and C), and (mPEG$_{2k}$-*mik*-(GA$_{30}$)$_3$)-lysozyme nanocomplexes (D, E and F). Excipients: (A, D) mannitol + 10% (*w/w*) leucine, (B, E) trehalose + 10% (*w/w*) leucine and (C, F) mannitol. All formulations contained 6.6% (w/w) phosphate buffer salts.

Polymer-protein nanocomplexes were found to be efficiently incorporated into dry powders with encapsulation efficiencies, defined as the ratio between the amount of protein added to the feed solution and the quantity of protein encapsulated inside of the dry powders, between 80 and 100% (Figure 3.4). No

significant effect of the complexing polymer architecture on the encapsulation efficiency was observed.

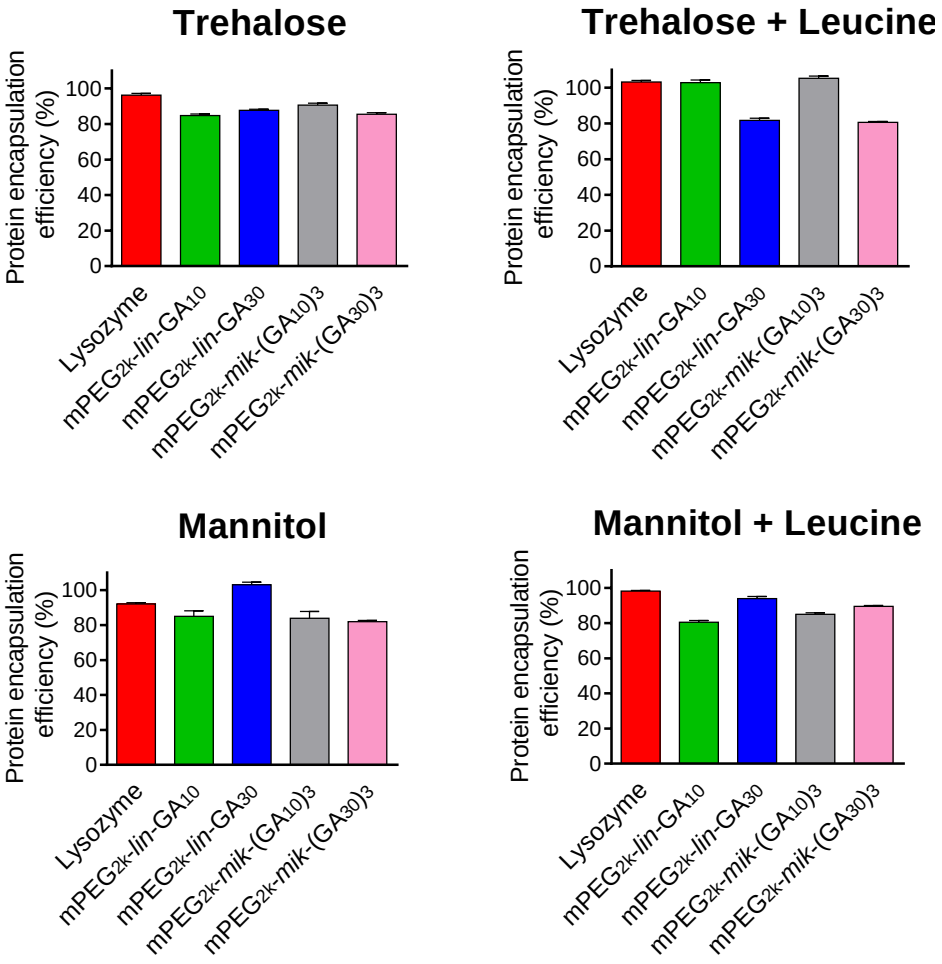


Figure 3.4. Protein encapsulation efficiency in trehalose, trehalose + leucine, mannitol and mannitol + leucine dry powders. Free un-complexed lysozyme (**red**), and mPEG$_{2k}$-*lin*-GA$_{10}$ (**green**), mPEG$_{2k}$-*lin*-GA$_{30}$ (**blue**), mPEG$_{2k}$-*mik*-(GA$_{10}$)$_3$ (**grey**) and mPEG$_{2k}$-*mik*-(GA$_{30}$)$_3$ (**pink**)-derived complexes. All formulations contained 6.6% (*w/w*) phosphate buffer salts. All experiments were carried out in quadruplicate.

Moisture content was found to be lower than 5% for all spray-dried powders, with values as low as 0.5% with mannitol particles (Figure 3.5). These results indicate that drying of these materials using the chosen operating conditions was efficient. Low moisture content is very desirable, as water can negatively affect the storage stability of dry powder formulations. For example, residual water contents after spray-drying can cause undesired stickiness and caking of

the dry powders, and can lower glass transition temperatures (Chang and Pikal, 2009). As dry powder formulations undergo the glass transition, at $T>T_g$, the molecular mobility increases, which can promote undesired protein interactions leading to protein aggregation and/or degradation (Depreter et al., 2013). Also, the presence of water may enhance other degradative reactions in protein therapeutics (Depreter et al., 2013).

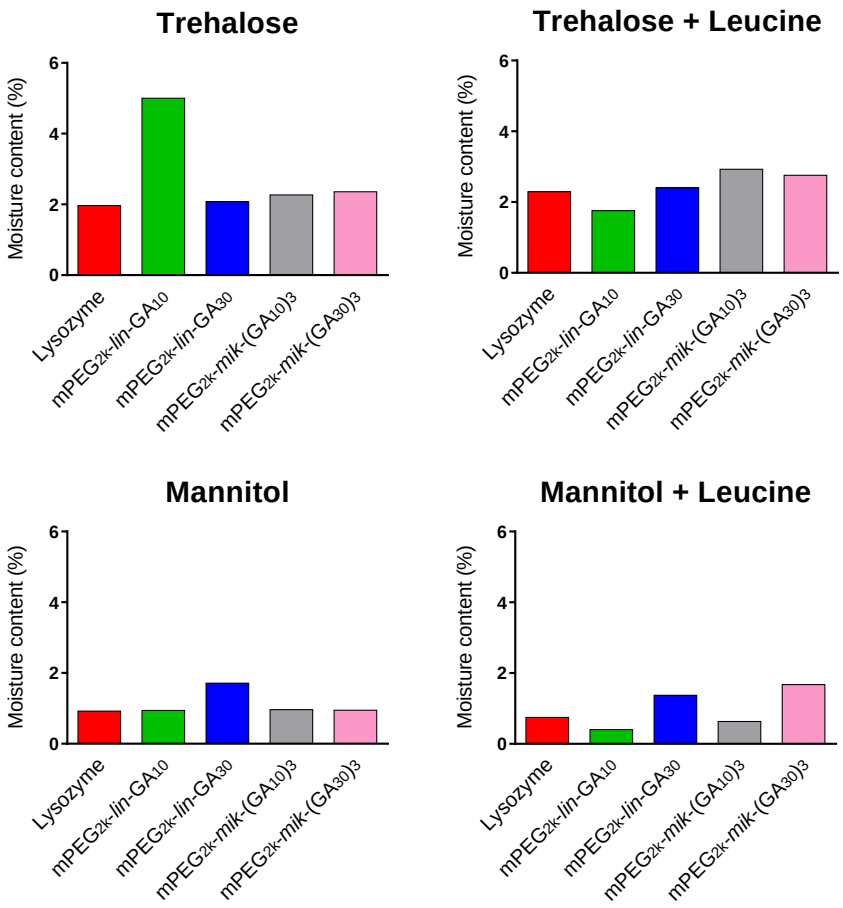


Figure 3.5. Moisture content of dry powders investigated in this study. Free un-complexed lysozyme (**red**), and mPEG$_{2k}$-*lin*-GA$_{10}$ (**green**), mPEG$_{2k}$-*lin*-GA$_{30}$ (**blue**), mPEG$_{2k}$-*mik*-(GA$_{10}$)$_3$ (**grey**) and mPEG$_{2k}$-*mik*-(GA$_{30}$)$_3$ (**pink**)-derived complexes. All formulations contained 6.6% (*w/w*) phosphate buffer salts.

Finally, differential scanning calorimetry (DSC) was used to evaluate the physical properties of the dry powder matrix in the 0-230°C range (Table 3.2).

Table 3.2. Thermal behaviour of dry powders used in this study. All formulations contained 6.6% (*w/w*) phosphate buffer salts. Experiments were made in duplicate.

Excipients (*w/w*)	Nanocomplexes (*w/w*)	Tg (˚C)	ΔCp (J/g ˚C)	Tm (˚C)	ΔH_m (J/g)
Up to 100% Trehalose	-	130.6 ± 0.1	0.42 ± 0.1	-	-
	5% Free lysozyme	127.4	0.61		
	10% ($mPEG_{2k}$-*lin*-GA_{10})-Lys	128.0 ± 0.2	0.20 ± 0.1		
	10% ($mPEG_{2k}$-*lin*-GA_{30})-Lys	125.9[a]	0.38[a]	-	-
	10% ($mPEG_{2k}$-*mik*-$(GA_{10})_3$)-Lys	127.0 ± 0.3	0.29 ± 0.1		
	10% ($mPEG_{2k}$-*mik*-$(GA_{30})_3$)-Lys	130.7 ± 1.0	0.31 ± 0.1	-	-
Up to 100% Trehalose + 10% Leucine	-	128.7 ± 0.5	0.31 ± 0.1	-	-
	5% Free lysozyme	126.4 ± 5.3	0.43 ± 0.1	-	-
	10% ($mPEG_{2k}$-*lin*-GA_{10})-Lys	124.2 ± 0.3	0.38 ± 0.1	-	-
	10% ($mPEG_{2k}$-*lin*-GA_{30})-Lys	126.7 ± 0.4	0.29 ± 0.1	-	-
	10% ($mPEG_{2k}$-*mik*-$(GA_{10})_3$)-Lys	129.15[a]	0.36[a]	-	-
	10% ($mPEG_{2k}$-*mik*-$(GA_{30})_3$)-Lys	129.5 ± 1.2	0.38 ± 0.1	-	-
Up to 100% Mannitol	-	-	-	162.4 ± 0.2	245.0 ± 8.7
	5% Free lysozyme	-	-	159.4 ± 0.1	222.9 ± 2.5
	10% ($mPEG_{2k}$-*lin*-GA_{10})-Lys			158.0 ± 0.1	182.7 ± 1.8
	10% ($mPEG_{2k}$-*lin*-GA_{30})-Lys	-	-	148.6 ± 0.6	110.3 ± 27.4
	10% ($mPEG_{2k}$-*mik*-$(GA_{10})_3$)-Lys	-	-	159.4 ± 0.1	210.3 ± 0.1
	10% ($mPEG_{2k}$-*mik*-$(GA_{30})_3$)-Lys			159.5 ± 0.1	206.9 ± 2.5
Up to 100% Mannitol + 10% Leucine	-	-	-	160.8 ± 0.1	213.7 ± 10.6
	5% Free lysozyme	-	-	158.0 ± 0.1	194.4 ± 2.1
	10% ($mPEG_{2k}$-*lin*-GA_{10})-Lys	-	-	158.7 ± 0.2	171.3 ± 36.1
	10% ($mPEG_{2k}$-*lin*-GA_{30})-Lys	-	-	147.9 ± 0.1	124.9 ± 1.3
	10% ($mPEG_{2k}$-*mik*-$(GA_{10})_3$)-Lys	-	-	158.0 ± 0.1	182.3 ± 9.8
	10% ($mPEG_{2k}$-*mik*-$(GA_{30})_3$)-Lys	-	-	158.2[a]	167.6[a]

[a]Single or double determinations due to poor material quantity obtained

Trehalose dry powders showed glass transition temperatures (T_g) between 124 and 131°C. These values are higher than that of dry pure trehalose (106°C, (Roe and Labuza, 2005)) likely due to the presence of phosphate buffer salts in these formulations (Ohtake et al., 2004). As previously discussed, from a formulation viewpoint this is very positive, as higher glass transition temperatures generally

increase the stability of protein formulations. An endothermic melting transition (T_m) between 148 and 162°C was found for formulations containing mannitol as excipient, and is typical for crystalline mannitol particles (Ong et al., 2014, Takada et al., 2009). The presence of leucine or polymer-protein nanocomplexes did not affect T_g or T_m values.

3.3.2. Aerosolisation performance

In the development of dry powders for pulmonary drug delivery, it is very important to evaluate whether a given particle formulation is suitable for deposition in the human respiratory tract. To this aim, in this study the Emitted Dose (ED) - the percentage of the mass of a formulation exiting a given device after inhalation - and Fine Particle Fraction (FPF) - the fraction of particles with an aerodynamic diameter below 5 µm (hence suitable for pulmonary delivery) - of our dry powder formulations developed were assessed.

In Emitted Dose experiments, ED were above 80% for dry powder formulations with (mPEG$_{2k}$-polyGA)-lysozyme nanocomplexes in trehalose without leucine, (with the sole exception of mPEG$_{2k}$-*lin*-GA$_{30}$ copolymers, Figure 3.6). However, in the absence of copolymers the ED decreased to 30-75% showing that in this case the presence of protein nanocomplexes had a beneficial effect on the properties of the resulting dry powder formulations. The emitted dose of all other formulations was very high, in the 80-100% range, independently of the complexing copolymer used.

Next, a quantification of fine particle fractions (FPF) was carried out. All leucine-free and mannitol formulations exhibited significantly lower FPF compared to trehalose-leucine based particles (Figure 3.6). It was not unexpected as high concentrations of trehalose results in poor aerosolisation properties due to the highly hygroscopic and adhesive nature of amorphous trehalose (Maa et al., 1997). Also, large amounts of mannitol can adversely affect the proportion of respirable fraction of spray-dried particles, likely due to the formation of particle aggregates (Bosquillon et al., 2001). This is in agreement with the low spray-drying yield observed in our experiments with leucine-free dry powder formulations (< 36%). Trehalose particles with leucine showed the highest FPF, achieving up to 68% with $mPEG_{2k}$-*lin*-GA_{10} copolymers. This was in line with the general consensus in the literature, where a small proportion of a surface active molecule (e.g. leucine) is believed to be important to improve the dispersability of particles (Lechuga-Ballesteros et al., 2008, Li et al., 2003, Lucas et al., Li et al., 2005). Leucine was also able to improve the FPF values obtained with mannitol particles. However, these remain much lower than those FPF values obtained with trehalose particles – ~ 30% *vs.* ~ 60%. Polymer architecture – linear *vs.* miktoarm - and size did not have a significant effect on the emitted dose ED, or on the FPF values of these dry powders.

Taken together, these initial characterisation results were very positive, showing that both polymer topology and size did not have a detrimental effect on the aerodynamic properties - ED and FPF - of the corresponding dry powder formulations.

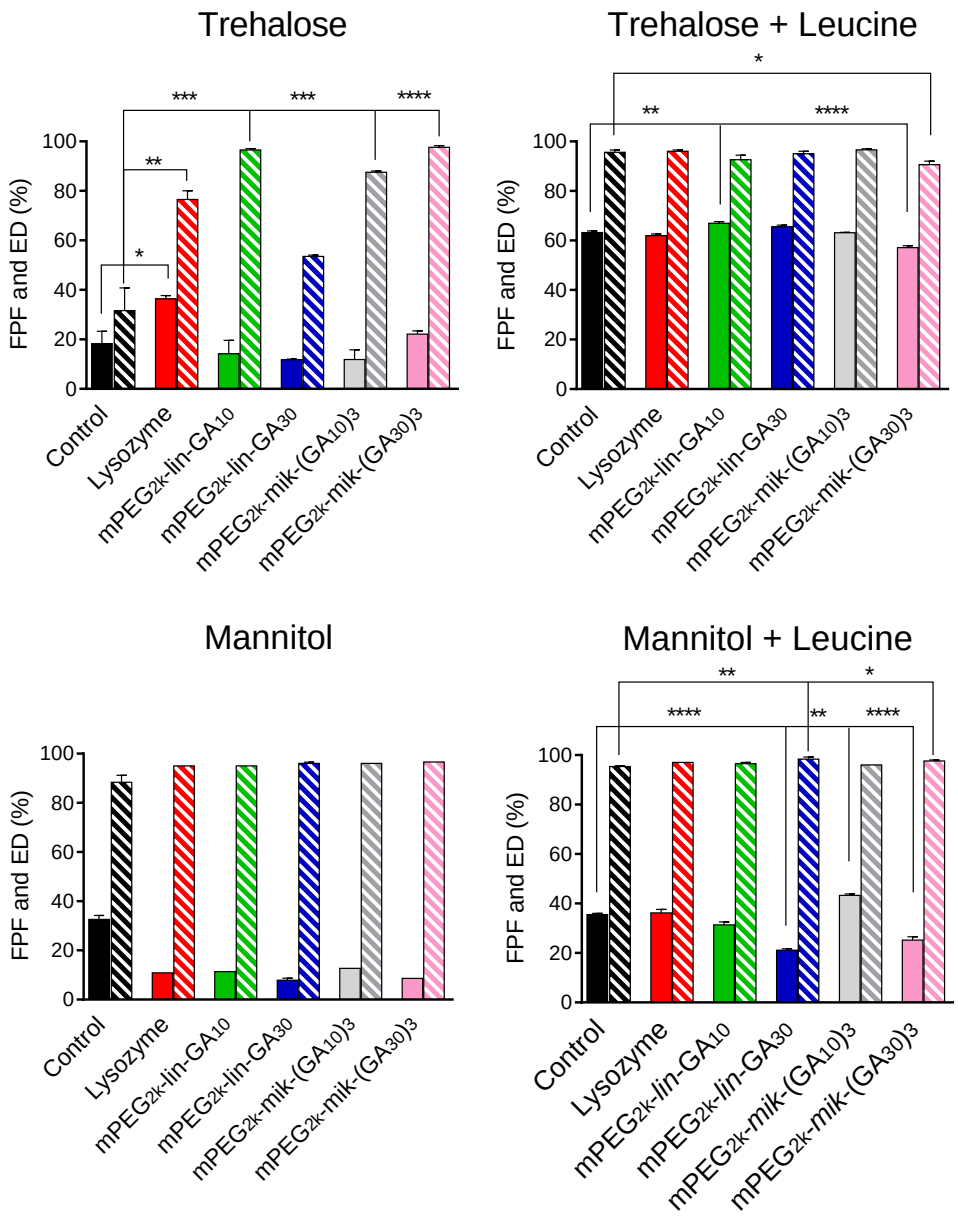


Figure 3.6. Fine particle fraction (FPF) (solid bars) and emitted dose (ED) (hatched bars) of trehalose, trehalose + leucine, mannitol and mannitol + leucine dry powders. Control (**black**), lysozyme (**red**), mPEG$_{2k}$-*lin*-GA$_{10}$ (**green**), mPEG$_{2k}$-*lin*-GA$_{30}$ (**blue**), mPEG$_{2k}$-*mik*-(GA$_{10}$)$_3$ (**grey**) and mPEG$_{2k}$-*mik*-(GA$_{30}$)$_3$ (**pink**)-derived complexes. 'Control' denotes blank powder formulation that contains only excipient without lysozyme or copolymer, and 'Lysozyme' denotes dry powder formulation that contains no copolymer. All formulations contained 6.6% (*w/w*) phosphate buffer salts. All experiments were carried out in triplicate. FPF and ED values from mannitol dry powders were obtained from single, double or triple measurements due to low material quantity obtained. One-way ANOVA was used for statistical analysis. * $p < 0.1$, ** $p < 0.01$ *** $p < 0.001$, **** $p < 0.0001$.

3.3.3. Nanocomplexes recovery, protein activity and protein protection against proteolytic enzymes

Once dry powders were characterised, their ability to efficiently release polymer-protein nanocomplexes in aqueous conditions was evaluated. It is generally acknowledged that the airway lining fluid has a pH of around 7 (Jayaraman et al., 2001), hence the potential of the dry powder formulations to deliver polymer-protein nanocomplexes was investigated by incubating them in phosphate buffer (PB, 10 mM, pH 7.4). Following incubation of the formulations for 15 min, the hydrodynamic diameter of the reconstituted nanocomplexes was measured by nanoparticle tracking analysis (NTA). As discussed in Chapter 2, NTA can be superior to DLS to estimate the size of relatively polydisperse nanocomplexes in solution (Dragovic et al., 2011). The particle size distribution of nanoparticles recovered by dissolution of dry powders was found to be in the 20-200 nm range, which is not significantly different to that found in ($mPEG_{2k}$-polyGA)-lysozyme nanocomplexes before spray-drying (Figure 3.7 and Supporting Information, Figure S30). This showed that under the conditions chosen for the preparation of these spray-dried formulations, the stability of the nanocomplexes was not compromised, and that they could be efficiently recovered upon dissolution of dry powders. These results are very remarkable, as the spray-drying process can affect the stability and size of nanoparticles once they are re-dispersed from dry powder formulations (Sham et al., 2004). No assemblies could be detected by NTA upon dissolution of control formulations of dry powders containing either un-complexed lysozyme or free $mPEG_{2k}$-polyGA copolymers, further confirming

that the nano-sized assemblies observed for the non-control formulations were indeed polymer-protein complexes.

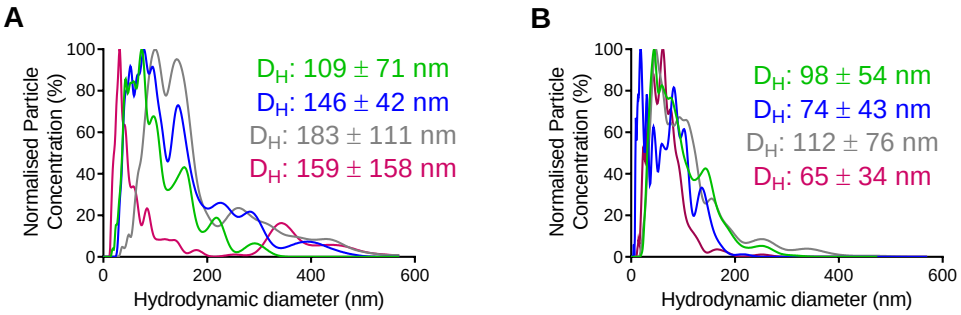


Figure 3.7. Nanoparticle tracking analysis (NTA) of dry powder formulations following incubation in phosphate buffer (PB, 10 mM, pH 7.4) at 70 µg mL^{-1} protein concentration in ($mPEG_{2k}$-polyGA)-lysozyme nanocomplexes for 15 min. (A) Particle size distribution of nanocomplexes before spray-drying. (B) Particle size distribution of nanocomplexes recovered from mannitol + leucine-based dry powders. $mPEG_{2k}$-*lin*-GA_{10} (**green**), $mPEG_{2k}$-*lin*-GA_{30} (**blue**), $mPEG_{2k}$-*mik*-$(GA_{10})_3$ (**grey**) and $mPEG_{2k}$-*mik*-$(GA_{30})_3$ (**pink**)-derived complexes.

Once nanocomplexes were recovered from dry powders and to evaluate that protein integrity was not compromised by spray-drying, the residual lysozyme enzymatic activity was studied by a turbidimetric assay using *Micrococcus lysodeikticus* freeze-dried cells as the substrate. All nanocomplexes recovered from the dry powders exhibited lower enzymatic activity when compared to un-complexed lysozyme recovered from the corresponding control sample (Figure 3.8). This result was expected as we previously observed (Chapter 2) that inclusion of lysozyme within polymer non-covalent complexes reduces its enzymatic activity. Although the underlying mechanism(s) has not been fully elucidated yet, it appears that this effect may be due to steric effects resulting in the enzyme active site becoming less accessible to substrate upon complexation with the copolymers. However, enzymatic activity could be recovered if suitable interaction between polyionic macromolecules and

polyglutamic acid and/or lysozyme occurs. Glycosaminoglycans are examples of polyionic macromolecules present in the lungs (Papakonstantinou and Karakiulakis, 2009). Also, lung lining fluid might contain charged species that can favoured the disassembly of polymer-protein complexes and release protein therapeutics at the site of action. However, the reproduction of real lung conditions in an *in vitro* model is a challenge due to the complexity of the respiratory system. Therefore, poly(allyl amine), due to its low price and relative availability, was chosen as a model polyion in this study. Upon addition, polycationic poly(allyl amine), which can sequester polyanionic polymers (Tomita et al., 2010) - poly(glutamic acid) block of ($mPEG_{2k}$-polyGA) copolymers in this case induced complex disassembly and release of lysozyme enzyme. These results showed that after de-complexation 70-100% of initial lysozyme activity was recovered (Figure 3.8). From a pulmonary protein delivery perspective this is very advantageous, as this suggests that these complexes could release their protein payload at the site of action, ready to exert its effect, if suitable dissociation conditions are achieved. However, as previously mentioned, the ability of these complexes to disassemble under similar conditions to those found in the respiratory system will need to be investigated to further confirm these data.

Although mannitol has been used to protect biopharmaceuticals, high concentrations of crystalline mannitol-based dry powders can affect protein stability (Costantino et al., 1998). In this study, we also observed that copolymers, especially $mPEG_{2k}$-*lin*-GA_{30} in mannitol + leucine dry powder

formulations, were able to provide partial or full recovery of lysozyme activity (80-100%) whilst un-complexed lysozyme in mannitol formulations only retained around 70-80% of the initial enzymatic activity (Figure 3.8). These findings suggest that un-complexed lysozyme can be partially degraded in formulations containing crystalline mannitol, and that protection could be achieved upon reversible complexation with mPEG$_{2k}$-polyGA copolymers.

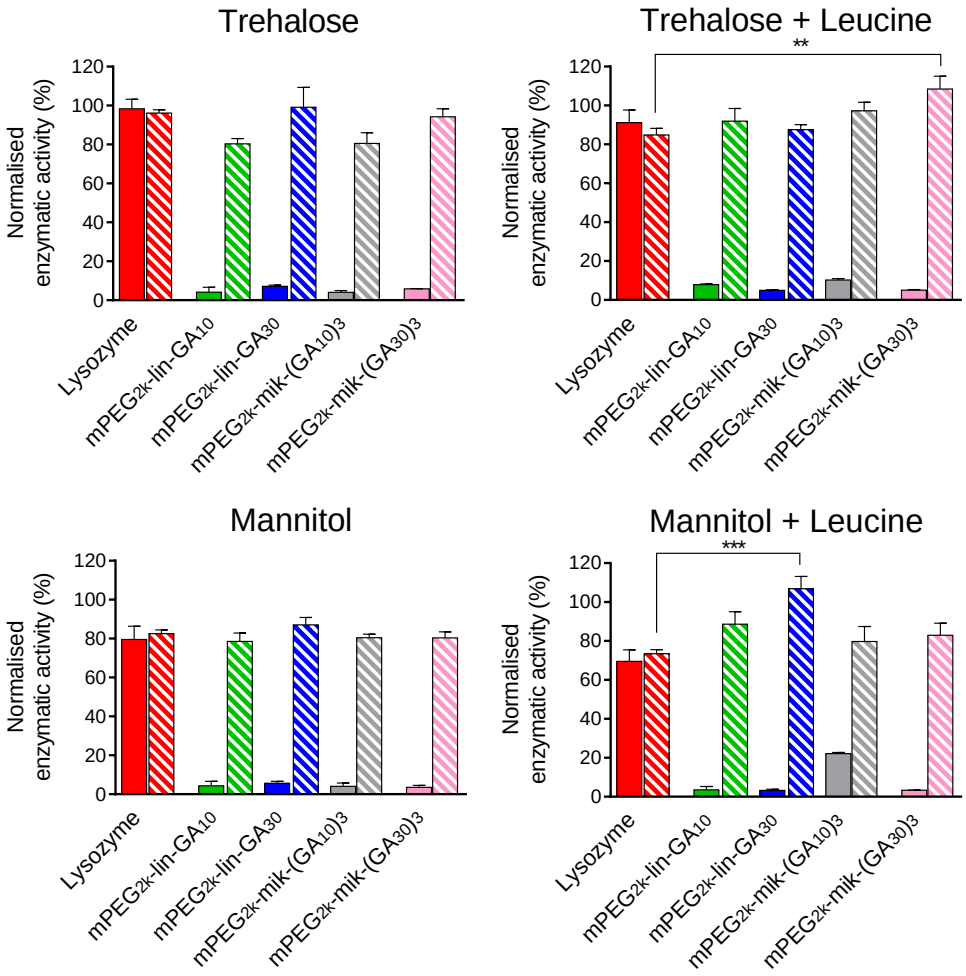


Figure 3.8. Lysozyme enzymatic activity. Solid bars: lysozyme activity after incubation of the dry powders in PB, hatched bars: lysozyme activity after incubation of the dry powders in the presence of poly(allyl amine). Trehalose, trehalose + leucine, mannitol and mannitol + leucine dry powders investigated in this study. Lysozyme (**red**), mPEG$_{2k}$-*lin*-GA$_{10}$ (**green**), mPEG$_{2k}$-*lin*-GA$_{30}$ (**blue**), mPEG$_{2k}$-*mik*-(GA$_{10}$)$_3$ (**grey**) and mPEG$_{2k}$-*mik*-(GA$_{30}$)$_3$ (**pink**)-derived complexes. 'Lysozyme' denotes dry powder formulation that contains no copolymer. All experiments were carried out in triplicate. Un-complexed free lysozyme was used as a reference (100% enzymatic activity). One-way ANOVA was used for statistical analysis. * $p < 0.1$, ** $p < 0.01$ *** $p < 0.001$, **** $p < 0.0001$.

Finally, the ability of (mPEG$_{2k}$-polyGA)-lysozyme complexes to protect the enzyme from proteolytic degradation was assessed. Apart from the generic particle removing mechanisms of the lungs such as the mucociliary escalator and macrophages, the respiratory system has also specific clearance mechanisms for proteins and peptides (Depreter et al., 2013). A range of pulmonary peptidases have been found in humans and other mammalians such as dogs and rabbits. These include cathepsin B, collagenase, elastase chymotrypsin, aminopeptidase P, neutrophil proteases and a range of carboxypeptidases (Janoff et al., 1983, Fujita et al., 1990, Stratford and Lee, 1986, Wall and Lanutti, 1993, Orlowski et al., 1981). In this study, we have chosen trypsin, which cleaves proteins specifically at the carboxyl side of lysine and arginine residues, as a model proteolytic enzyme. Lysozyme is particularly prone to undergo trypsin digestion due to its high content in these amino acids.

Dry powder formulations and trypsin were added to 4 mL of phosphate buffer (PB, 10 mM, pH 7.4) and the mixture was incubate at room temperature for 3 h under gentle stirring to allow both proteolysis of un-complexed lysozyme and trypsin auto-digestion. Poly(allyl amine) was then added to sequester mPEG$_{2k}$-polyGA copolymers and release lysozyme from the complexes, and the mixture was kept under gentle stirring for 1 h. In the absence of polymers, under these conditions lysozyme activity was found to be reduced to less than 40% of its initial value. However, all mPEG$_{2k}$-polyGA copolymers were able to protect lysozyme against enzymatic degradation, again with mPEG$_{2k}$-*lin*-GA$_{30}$ offering the greatest protection (~100%) (Figure 3.9).

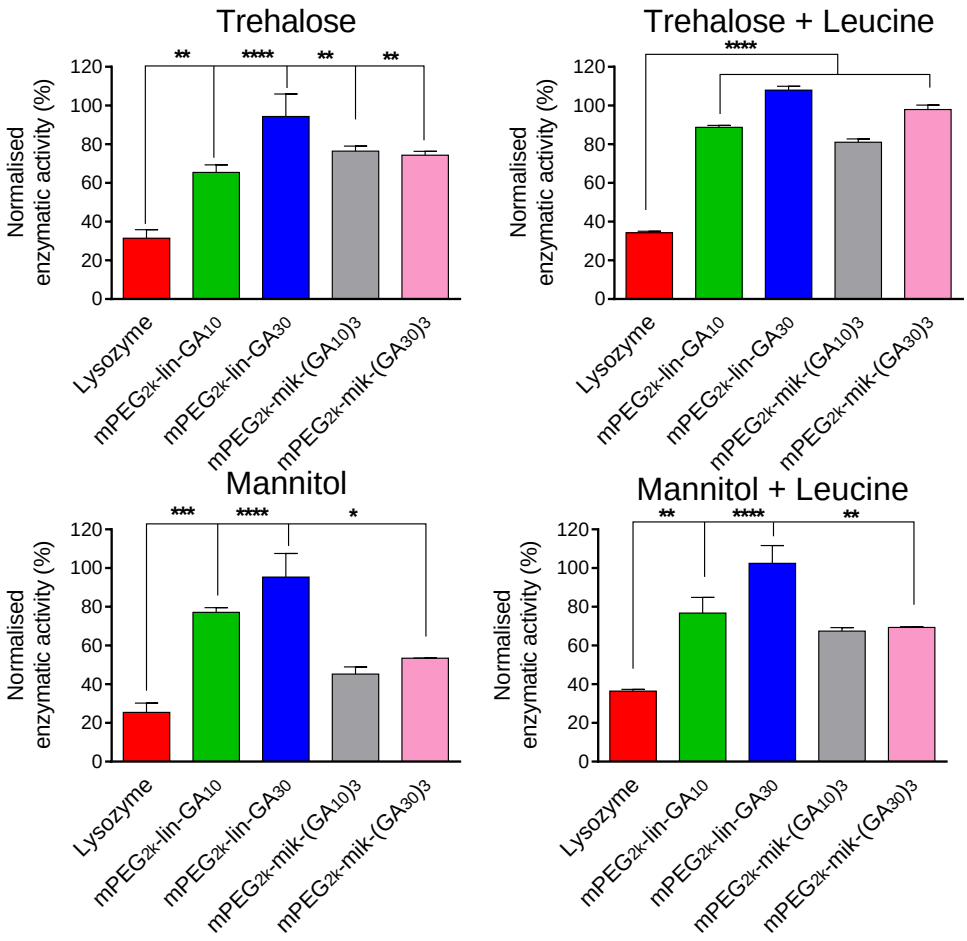


Figure 3.9. (mPEG$_{2k}$-polyGA)-lysozyme complexes: protection against lysozyme proteolytic degradation. Lysozyme activity was measured after incubation of the dry powders in the presence of trypsin for 3 h, followed by treatment with poly(allyl amine) for 1 h. Trehalose, trehalose + leucine, mannitol and mannitol + leucine dry powders were investigated in this study. Un-complexed lysozyme (**red**), mPEG$_{2k}$-*lin*-GA$_{10}$ (**green**), mPEG$_{2k}$-*lin*-GA$_{30}$ (**blue**), mPEG$_{2k}$-*mik*-(GA$_{10}$)$_3$ (**grey**) and mPEG$_{2k}$-*mik*-(GA$_{30}$)$_3$ (**pink**)-derived complexes. All experiments were carried out in triplicate. Un-complexed free lysozyme was used as a reference (100% enzymatic activity). One-way ANOVA was used for statistical analysis. * $p < 0.1$, ** $p < 0.01$ *** $p < 0.001$, **** $p < 0.0001$.

3.4. Concluding remarks

In this chapter, we demonstrated that (mPEG$_{2k}$-polyGA)-lysozyme nanocomplexes can be successfully formulated into inhalation dry powders. Typical inhalable aerosol excipients such as trehalose, mannitol and leucine were evaluated. Trehalose dry powders with leucine and polymer-protein nanocomplexes showed excellent aerodynamic properties with FPFs as high as 68%. Upon dissolution of dry powder formulations, lysozyme nanocomplexes could be efficiently recovered, with no negative effect on their particle size distribution. Finally, polymers, especially mPEG$_{2k}$-*lin*-GA$_{30}$, were able to protect proteins from proteolytic enzymes and from the crystalline structure of mannitol dry powders.

In the next chapter we will describe how these formulations can be further refined and utilised to overcome challenges associated to pulmonary delivery such as immunogenicity and low protein uptake by the airway epithelium.

3.5. References

ANDYA, J. D., MAA, Y.-F., COSTANTINO, H. R., NGUYEN, P.-A., DASOVICH, N., SWEENEY, T. D., HSU, C. C. & SHIRE, S. J. 1999. The Effect of Formulation Excipients on Protein Stability and Aerosol Performance of Spray-Dried Powders of a Recombinant Humanized Anti-IgE Monoclonal Antibody1. *Pharmaceutical Research,* 16**,** 350-358.

ARMSTRONG, D. J., ELLIOTT, P. N., FORD, J. L., GADSDON, D., MCCARTHY, G. P., ROSTRON, C. & WORSLEY, M. D. 1996. Poly-(D,L-lactic acid) microspheres incorporating histological dyes for intra-pulmonary histopathological investigations. *J Pharm Pharmacol,* 48**,** 258-62.

BAILEY, M. M. & BERKLAND, C. J. 2009. Nanoparticle formulations in pulmonary drug delivery. *Med Res Rev,* 29**,** 196-212.

BAKALTCHEVA, I., O'SULLIVAN, A. M., HMEL, P. & OGBU, H. Freeze-dried whole plasma: Evaluating sucrose, trehalose, sorbitol, mannitol and glycine as stabilizers. *Thrombosis Research,* 120**,** 105-116.

BOSQUILLON, C., LOMBRY, C., PRÉAT, V. & VANBEVER, R. 2001. Influence of formulation excipients and physical characteristics of inhalation dry powders on their aerosolization performance. *Journal of Controlled Release,* 70**,** 329-339.

CARVALHO, T. C., PETERS, J. I. & WILLIAMS, R. O., 3RD 2011. Influence of particle size on regional lung deposition--what evidence is there? *Int J Pharm,* 406**,** 1-10.

COSTANTINO, H. R., ANDYA, J. D., NGUYEN, P. A., DASOVICH, N., SWEENEY, T. D., SHIRE, S. J., HSU, C. C. & MAA, Y. F. 1998. Effect of mannitol crystallization on the stability and aerosol performance of a spray-dried pharmaceutical protein, recombinant humanized anti-IgE monoclonal antibody. *J Pharm Sci,* 87**,** 1406-11.

CHANG, L. L. & PIKAL, M. J. 2009. Mechanisms of protein stabilization in the solid state. *J Pharm Sci,* 98**,** 2886-908.

DEPRETER, F., PILCER, G. & AMIGHI, K. 2013. Inhaled proteins: challenges and perspectives. *Int J Pharm,* 447**,** 251-80.

DRAGOVIC, R. A., GARDINER, C., BROOKS, A. S., TANNETTA, D. S., FERGUSON, D. J., HOLE, P., CARR, B., REDMAN, C. W., HARRIS, A. L., DOBSON, P. J., HARRISON, P. & SARGENT, I. L. 2011. Sizing and phenotyping of cellular vesicles using Nanoparticle Tracking Analysis. *Nanomedicine,* 7**,** 780-8.

DUNNE, M., CORRIGAN, O. I. & RAMTOOLA, Z. 2000. Influence of particle size and dissolution conditions on the degradation properties of polylactide-co-glycolide particles. *Biomaterials,* 21**,** 1659-1668.

FOWLER, R., VLLASALIU, D., FALCONE, F. H., GARNETT, M., SMITH, B., HORSLEY, H., ALEXANDER, C. & STOLNIK, S. 2013a. Uptake and transport of B(12)-conjugated nanoparticles in airway epithelium(). *Journal of Controlled Release,* 172**,** 374-381.

FOWLER, R., VLLASALIU, D., TRILLO, F. F., GARNETT, M., ALEXANDER, C., HORSLEY, H., SMITH, B., WHITCOMBE, I., EATON, M. & STOLNIK, S. 2013b. Nanoparticle transport in epithelial cells: pathway switching through bioconjugation. *Small,* 9**,** 3282-94.

FUJITA, J., NELSON, N. L., DAUGHTON, D. M., DOBRY, C. A., SPURZEM, J. R., IRINO, S. & RENNARD, S. I. 1990. Evaluation of elastase and antielastase balance in patients with chronic bronchitis and pulmonary emphysema. *Am Rev Respir Dis,* 142**,** 57-62.

GOODALL, S., JONES, M. L. & MAHLER, S. 2015. Monoclonal antibody-targeted polymeric nanoparticles for cancer therapy – future prospects. *Journal of Chemical Technology & Biotechnology,* 90**,** 1169-1176.

HULSE, W. L., FORBES, R. T., BONNER, M. C. & GETROST, M. 2008. Do co-spray dried excipients offer better lysozyme stabilisation than single excipients? *Eur J Pharm Sci,* 33**,** 294-305.

ISLAM, M. I. U. & LANGRISH, T. A. G. 2010. An investigation into lactose crystallization under high temperature conditions during spray drying. *Food Research International,* 43**,** 46-56.

JANOFF, A., RAJU, L. & DEARING, R. 1983. Levels of elastase activity in bronchoalveolar lavage fluids of healthy smokers and nonsmokers. *Am Rev Respir Dis,* 127**,** 540-4.

JARVIS, S., IND, P. W., THOMAS, C., GOONESEKERA, S., HAFFENDEN, R., ABDOLRASOULI, A., FIORENTINO, F. & SHINER, R. J. 2014. Microbial contamination of domiciliary nebulisers and clinical implications in chronic obstructive pulmonary disease. *BMJ Open Respiratory Research,* 1.

JAYARAMAN, S., SONG, Y., VETRIVEL, L., SHANKAR, L. & VERKMAN, A. S. 2001. Noninvasive in vivo fluorescence measurement of airway-surface liquid depth, salt concentration, and pH. *Journal of Clinical Investigation,* 107**,** 317-324.

JIN, T. H., TSAO, E., GOUDSMIT, J., DHEENADHAYLAN, V. & SADOFF, J. 2010. Stabilizing formulations for inhalable powders of an adenovirus 35-vectored tuberculosis (TB) vaccine (AERAS-402). *Vaccine,* 28**,** 4369-4375.

KAMALY, N., XIAO, Z., VALENCIA, P. M., RADOVIC-MORENO, A. F. & FAROKHZAD, O. C. 2012. Targeted polymeric therapeutic nanoparticles: design, development and clinical translation. *Chemical Society reviews,* 41**,** 2971-3010.

KIBBE, A. H. & ASSOCIATION, A. P. 2000. *Handbook of Pharmaceutical Excipients*, American Pharmaceutical Association.

LABIRIS, N. R. & DOLOVICH, M. B. 2003. Pulmonary drug delivery. Part II: The role of inhalant delivery devices and drug formulations in therapeutic effectiveness of aerosolized medications. *British Journal of Clinical Pharmacology,* 56**,** 600-612.

LECHUGA-BALLESTEROS, D., CHARAN, C., STULTS, C. L., STEVENSON, C. L., MILLER, D. P., VEHRING, R., TEP, V. & KUO, M. C. 2008. Trileucine improves aerosol performance and stability of spray-dried powders for inhalation. *J Pharm Sci,* 97**,** 287-302.

LEE, C., CHOI, J. S., KIM, I., OH, K. T., LEE, E. S., PARK, E. S., LEE, K. C. & YOUN, Y. S. 2013. Long-acting inhalable chitosan-coated poly(lactic-co-glycolic acid) nanoparticles containing hydrophobically modified exendin-4 for treating type 2 diabetes. *Int J Nanomedicine,* 8**,** 2975-83.

LI, B., LI, Q., MO, J. & DAI, H. 2017. Drug-Loaded Polymeric Nanoparticles for Cancer Stem Cell Targeting. *Frontiers in Pharmacology,* 8**,** 51.

LI, H. Y., NEILL, H., INNOCENT, R., SEVILLE, P., WILLIAMSON, I. & BIRCHALL, J. C. 2003. Enhanced dispersibility and deposition of spray-dried powders for pulmonary gene therapy. *J Drug Target,* 11**,** 425-32.

LI, H. Y., SEVILLE, P. C., WILLIAMSON, I. J. & BIRCHALL, J. C. 2005. The use of amino acids to enhance the aerosolisation of spray-dried powders for pulmonary gene therapy. *J Gene Med,* 7**,** 343-53.

LITTRINGER, E. M., MESCHER, A., ECKHARD, S., SCHRÖTTNER, H., LANGES, C., FRIES, M., GRIESSER, U., WALZEL, P. & URBANETZ, N. A. 2012a. Spray Drying of Mannitol as a Drug Carrier—The Impact of Process Parameters on Product Properties. *Drying Technology,* 30**,** 114-124.

LITTRINGER, E. M., MESCHER, A., SCHROETTNER, H., ACHELIS, L., WALZEL, P. & URBANETZ, N. A. 2012b. Spray dried mannitol carrier particles with tailored surface properties--the influence of carrier surface roughness and shape. *Eur J Pharm Biopharm,* 82**,** 194-204.

LUCAS, P., ANDERSON, K., POTTER, U. J. & STANIFORTH, J. N. Enhancement of Small Particle Size Dry Powder Aerosol Formulations using an Ultra Low Density Additive. *Pharmaceutical Research,* 16**,** 1643-1647.

MAA, Y. F., COSTANTINO, H. R., NGUYEN, P. A. & HSU, C. C. 1997. The effect of operating and formulation variables on the morphology of spray-dried protein particles. *Pharm Dev Technol,* 2**,** 213-23.

MALTESEN, M. J., BJERREGAARD, S., HOVGAARD, L., HAVELUND, S. & VAN DE WEERT, M. 2008. Quality by design - Spray drying of insulin intended for inhalation. *Eur J Pharm Biopharm,* 70**,** 828-38.

MAURY, M., MURPHY, K., KUMAR, S., MAUERER, A. & LEE, G. 2005. Spray-drying of proteins: effects of sorbitol and trehalose on aggregation and FT-IR amide I spectrum of an immunoglobulin G. *Eur J Pharm Biopharm,* 59**,** 251-61.

MENON, J. U., RAVIKUMAR, P., PISE, A., GYAWALI, D., HSIA, C. C. W. & NGUYEN, K. T. 2014. Polymeric Nanoparticles for Pulmonary Protein and DNA Delivery. *Acta biomaterialia,* 10**,** 2643-2652.

OGAIN, O. N., LI, J., TAJBER, L., CORRIGAN, O. I. & HEALY, A. M. 2011. Particle engineering of materials for oral inhalation by dry powder inhalers. I-Particles of sugar excipients (trehalose and raffinose) for protein delivery. *Int J Pharm,* 405**,** 23-35.

OHTAKE, S., SCHEBOR, C., PALECEK, S. P. & DE PABLO, J. J. 2004. Effect of pH, counter ion, and phosphate concentration on the glass transition temperature of freeze-dried sugar-phosphate mixtures. *Pharm Res,* 21**,** 1615-21.

ONG, H. X., TRAINI, D., BALLERIN, G., MORGAN, L., BUDDLE, L., SCALIA, S. & YOUNG, P. M. 2014. Combined Inhaled Salbutamol and Mannitol Therapy for Mucus Hyper-secretion in Pulmonary Diseases. *The AAPS Journal,* 16**,** 269-280.

ORLOWSKI, M., ORLOWSKI, J., LESSER, M. & KILBURN, K. H. 1981. Proteolytic enzymes in bronchopulmonary lavage fluids: cathepsin B-like activity and prolyl endopeptidase. *J Lab Clin Med,* 97**,** 467-76.

PALAZZO, F., GIOVAGNOLI, S., SCHOUBBEN, A., BLASI, P., ROSSI, C. & RICCI, M. 2013. Development of a spray-drying method for the

formulation of respirable microparticles containing ofloxacin-palladium complex. *Int J Pharm,* 440**,** 273-82.

PAPAKONSTANTINOU, E. & KARAKIULAKIS, G. 2009. The 'sweet' and 'bitter' involvement of glycosaminoglycans in lung diseases: pharmacotherapeutic relevance. *British Journal of Pharmacology,* 157**,** 1111-1127.

PILCER, G., WAUTHOZ, N. & AMIGHI, K. 2012. Lactose characteristics and the generation of the aerosol. *Adv Drug Deliv Rev,* 64**,** 233-56.

POURSHAHAB, P. S., GILANI, K., MOAZENI, E., ESLAHI, H., FAZELI, M. R. & JAMALIFAR, H. 2011. Preparation and characterization of spray dried inhalable powders containing chitosan nanoparticles for pulmonary delivery of isoniazid. *J Microencapsul,* 28**,** 605-13.

ROE, K. D. & LABUZA, T. P. 2005. Glass Transition and Crystallization of Amorphous Trehalose-sucrose Mixtures. *International Journal of Food Properties,* 8**,** 559-574.

SCHÜLE, S., FRIEß, W., BECHTOLD-PETERS, K. & GARIDEL, P. 2007. Conformational analysis of protein secondary structure during spray-drying of antibody/mannitol formulations. *European Journal of Pharmaceutics and Biopharmaceutics,* 65**,** 1-9.

SHAM, J. O., ZHANG, Y., FINLAY, W. H., ROA, W. H. & LOBENBERG, R. 2004. Formulation and characterization of spray-dried powders containing nanoparticles for aerosol delivery to the lung. *Int J Pharm,* 269**,** 457-67.

SIVADAS, N., O'ROURKE, D., TOBIN, A., BUCKLEY, V., RAMTOOLA, Z., KELLY, J. G., HICKEY, A. J. & CRYAN, S. A. 2008. A comparative study of a range of polymeric microspheres as potential carriers for the inhalation of proteins. *Int J Pharm,* 358**,** 159-67.

SOPPIMATH, K. S., AMINABHAVI, T. M., KULKARNI, A. R. & RUDZINSKI, W. E. 2001. Biodegradable polymeric nanoparticles as drug delivery devices. *J Control Release,* 70**,** 1-20.

STRATFORD, R. E. & LEE, V. H. L. 1986. Aminopeptidase activity in homogenates of various absorptive mucosae m the albino rabbit: implications in peptide delivery. *International Journal of Pharmaceutics,* 30**,** 73-82.

SUNG, J. C., PULLIAM, B. L. & EDWARDS, D. A. 2007. Nanoparticles for drug delivery to the lungs. *Trends Biotechnol,* 25**,** 563-70.

TAKADA, A., NAIL, S. L. & YONESE, M. 2009. Influence of ethanol on physical state of freeze-dried mannitol. *Pharm Res,* 26**,** 1112-20.

TOMITA, S., ITO, L., YAMAGUCHI, H., KONISHI, G.-I., NAGASAKI, Y. & SHIRAKI, K. 2010. Enzyme switch by complementary polymer pair system (CPPS). *Soft Matter,* 6**,** 5320-5326.

TORRADO, S. & TORRADO, S. 2002. Characterization of physical state of mannitol after freeze-drying: effect of acetylsalicylic acid as a second crystalline cosolute. *Chem Pharm Bull (Tokyo),* 50**,** 567-70.

TRAPANI, A., DI GIOIA, S., DITARANTO, N., CIOFFI, N., GOYCOOLEA, F. M., CARBONE, A., GARCIA-FUENTES, M., CONESE, M. & ALONSO, M. J. 2013. Systemic heparin delivery by the pulmonary route using chitosan and glycol chitosan nanoparticles. *Int J Pharm,* 447**,** 115-23.

VEHRING, R. 2008. Pharmaceutical Particle Engineering via Spray Drying. *Pharmaceutical Research,* 25**,** 999-1022.

WALL, D. A. & LANUTTI, A. T. 1993. High levels of exopeptidase activity are present in rat and canine bronchoalveolar lavage fluid. *International Journal of Pharmaceutics,* 97**,** 171-181.

WEERS, J. G., TARARA, T. E. & CLARK, A. R. 2007. Design of fine particles for pulmonary drug delivery. *Expert Opin Drug Deliv,* 4**,** 297-313.

YANG, X.-F., XU, Y., QU, D.-S. & LI, H.-Y. 2015. The influence of amino acids on aztreonam spray-dried powders for inhalation. *Asian Journal of Pharmaceutical Sciences,* 10**,** 541-548.

YOU, Y., ZHAO, M., LIU, G. & TANG, X. 2007. Physical characteristics and aerosolization performance of insulin dry powders for inhalation prepared by a spray drying method. *J Pharm Pharmacol,* 59**,** 927-34.

CHAPTER 4

PEG-poly(glutamic acid) copolymers for targeted delivery of proteins

In this part of our study, $mPEG_{2k}$-polyGA copolymers were covalently linked to cyanocobalamin (vitamin B_{12}) ligand. The resulting targeted macromolecules were then complexed with lysozyme model protein to investigate their ability to efficiently deliver proteins into relevant epithelial cells, along with their effect on activation of the complement system. Next, targeted nanocomplexes were formulated into dry powders and their ability to enhance lysozyme uptake by Calu-3 lung epithelial cells was assessed *in vitro*. Finally, ($vitB_{12}$- PEG_{3k}-polyGA)-lysozyme dry powder formulations were tested *in vivo* through administration to healthy BALB/c mice, and pulmonary protein deposition/retention of these formulations was evaluated by analysing five non-serial cryo-sections of 7 µm per lung at various time points following endotracheal administration – 0, 3, and 14 h. Local pulmonary tolerance was also investigated after dry powder administrations in healthy BALB/c mice – three times a week for three consecutive weeks – by analysing bronchoalveolar lavage fluids in terms of cell composition and pro-inflammatory marker concentration (cytokines IL-1β, IL-6, and TNF-α).

Table of Contents

4.1. Introduction.....128
4.2. Experimental section.....133
4.3. Results and Discussion.....152
4.3.1. Synthesis of targeted linear and miktoarm vitB_{12}-PEG_{3k}-poly(glutamic acid) copolymers.....152
4.3.2. *In vitro* protein internalisation by the airway epithelium.....161
4.3.3. Complement activation.....167
4.3.4. Local pulmonary tolerance of polymer-protein nanocomplexes-based dry powder formulations in healthy mice.....168
4.3.5. *In vivo* pulmonary deposition and retention of polymer-protein nanocomplexes-based dry powder formulations in healthy mice.....172
4.4. Concluding remarks.....175
4.5. References.....176

4.1. Introduction

As discussed in Chapter 1, whilst pulmonary delivery is increasingly seen as an attractive, non-invasive route for the delivery of protein therapeutics, poor protein bioavailability and immunogenicity are challenges that still need to be addressed (Baker et al., 2010, Hussain et al., 2004). Absorption enhancers (i.e. surface-active agents and cyclodextrines) and protease inhibitors have been used to increase protein bioavailability after pulmonary administration (Kobayashi et al., 1996, Machida et al., 2000, Park et al., 2007b, Kobayashi et al., 1994). However, often they can also promote irreversible disruption of the epithelial layer, increase the absorption of toxins and cause toxicity and immunogenicity (Garcia-Verdugo et al., 2010, Park et al., 2007a, Huang et al., 2005).

Within this context, decorating therapeutic nanocarriers with natural compounds such as nutrients (i.e. vitamin B_{12}, and folate esters and amides) or endogenous molecules (i.e. albumin, IgG) can increase the interaction with epithelial cells (Russell-Jones et al., 1995, Tuma and Hubbard, 2003). Indeed, these molecules present specific pathways through the human epithelium which can be exploited for the delivery of therapeutic carriers. For example, studies have shown that PLGA or PLA-PEG nanoparticles decorated with either folate or IgG molecules on their surface, respectively, were delivered into the intestinal epithelium more efficiently than non-targeted control nanoparticles (Roger et al., 2012, Pridgen et al., 2013). Also, the presence of vitamin B_{12}-specific transport pathways has been confirmed in intestinal cell lines such as

Caco-2 cells (Dix et al., 1990, Ramanujam et al., 1991) and vitamin B_{12} receptors have been targeted for intestinal delivery of proteins (Russell-Jones et al., 1999, Chalasani et al., 2007a) and *in vitro* transport of nanoparticles across intestinal epithelium (Chalasani et al., 2007a, Chalasani et al., 2007b, Fowler et al., 2013c).

Relevant to targeted drug delivery to the airway epithelium, the presence of specific vitamin B_{12} receptors in Calu-3 cells (cubilin receptor and the transcobalamin II receptor) and A549 cells (cubilin receptor) was also confirmed (Fowler et al., 2013b, Vortherms et al., 2011). Cubilin and transcobalamin II receptors are expressed in different human tissues including the renal proximal tubule, visceral yolk sac and human intestinal epithelial cells and their role differs depending on the area in which they are located (i.e. re-absorption, conservation and transcytosis of different molecules (including vitamin B_{12})) (Sahali et al., 1992, Pons et al., 2000, Bose and Seetharam, 1997, Bose et al., 1997). However, the biological function of cubilin and transcobalamin II in the airway epithelium is still unclear. Within our group, these receptors were recently exploited to significantly increase uptake of vitamin B_{12}-decorated polystyrene nanoparticles compared to non-targeted control nanoparticles in Calu-3 epithelial cells (Fowler et al., 2013b). Despite these initial reports, the potential of this epithelial route for drug delivery to the airway epithelium has not been fully elucidated, and to the best of our knowledge no studies on protein delivery are currently available. This might be due, at least in part, to the challenging synthesis and purification of vitamin B_{12}

derivatives, compared to other common ligands such as folic acid and transferrin, which have also shown receptor expression and endocytotic activity in airway epithelial cells (Saeed et al., 2011, Moradi et al., 2012).

In this thesis work, cyanocobalamin (referred here as vitamin B_{12} or vitB_{12}) was covalently conjugated to mPEG_{2k}-polyGA with either linear A-B or miktoarm A-B_3 architecture (Figure 4.1), and the resulting targeted copolymers were utilised to complex lysozyme model protein. Targeted polymer-protein complexes were then formulated into dry powders to potentially enhance protein delivery into the lung epithelium. For our initial *in vitro* studies, Calu-3 cells were chosen as lung epithelial model cells and were grown in air-interface culture (AIC) conditions to promote mucus secretion (Grainger et al., 2006). Finally, the ability of these formulations to deposit and retain lysozyme in the lung of healthy BALB/c mice following pulmonary administration was evaluated.

As previously discussed, an undesired problem associated to pulmonary delivery of protein formulations can be the immunogenicity of drug delivery systems, protein cargoes, or both. Accordingly, immunogenic proteins can lead to reduced efficacy, inflammation, anaphylaxis and sometimes life-threatening autoimmunity. These side-effects can result from different factors, including the intrinsic nature of specific protein therapeutics, or their tendency to aggregate, either during storage or *in vivo*, which is known to increase their immunogenicity (Respaud et al., 2015). The complement system has key roles in innate and adaptive immune responses. Although most of complement proteins are generated in the liver as inactive precursor enzymes, the lung may

also act as a local source of complement proteins (Pandya and Wilkes, 2014). Different cells can be involved in this process such as alveolar type II epithelial cells (Strunk et al., 1988) and bronchiolar epithelial cells (Varsano et al., 2000). Also, inflammatory cytokines such as IL-1, IL-6 and TNF-α can initiate the synthesis of complement proteins in cells such as fibroblasts, epithelial cells and polymorphonuclear leukocytes (Volanakis, 1995). In this chapter, the immunogenicity of (mPEG$_{2k}$-polyGA)-lysozyme complexes and corresponding dry powder formulations was therefore assessed both *in vitro*, by measuring the residual haemolytic capacity of normal human serum (NHS) to study the complement activation, and *in vivo*, by analysing bronchoalveolar lavage fluids in terms of cell composition and pro-inflammatory marker concentration (cytokines IL-1β, IL-6, and TNF-α) after dry powder endotracheal administration three times a week for three consecutive weeks.

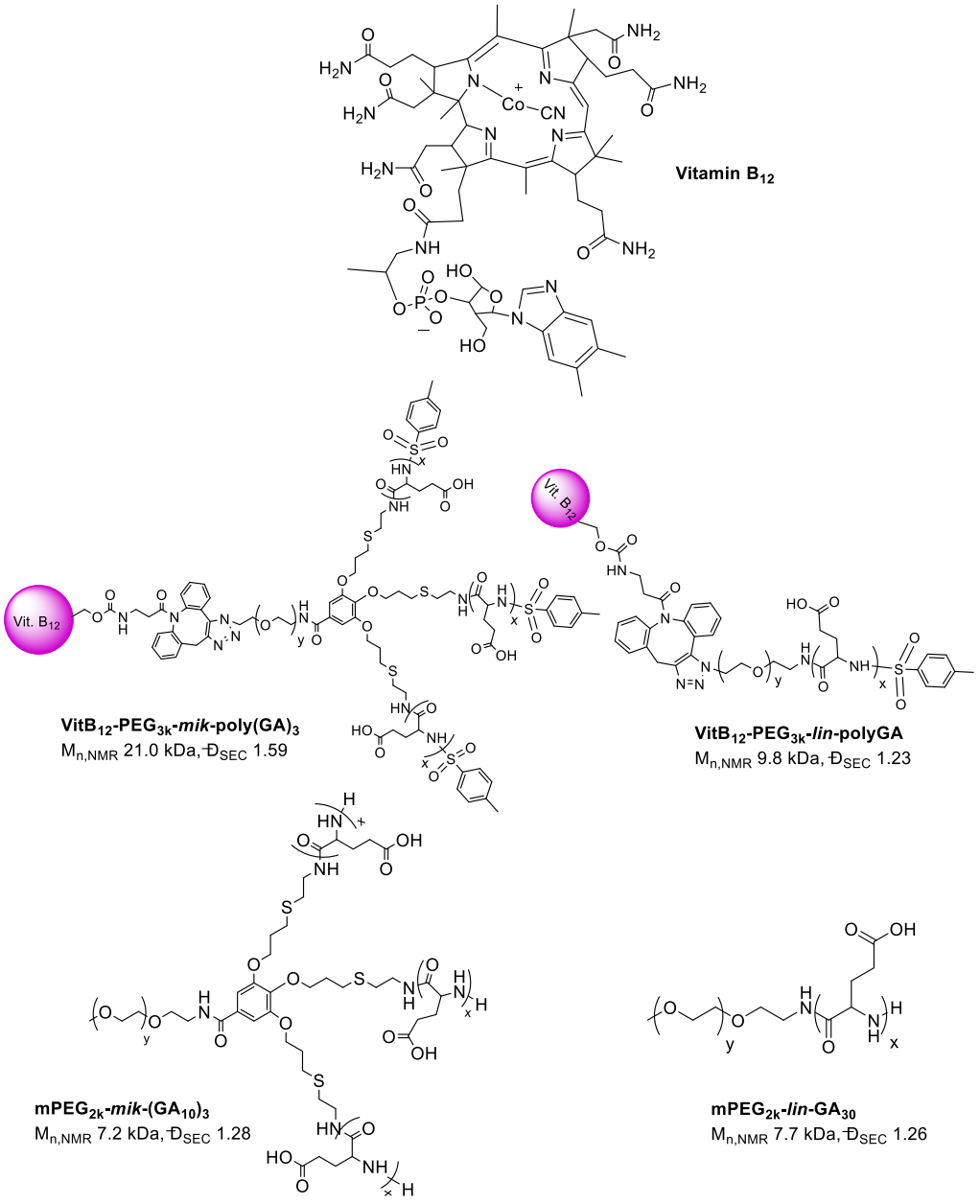


Figure 4.1. Chemical structure of cyanocobalamin (vitamin B_{12}) and targeted and non-targeted PEG-poly(glutamic acid) copolymers used in this part of this work.

4.2. Experimental section

3,4,5-tris(allyloxy)benzoic acid methyl ester **(1)**, 3,4,5-tris(allyloxy)benzoic acid **(2)**, and γ-benzyl-L-glutamate *N*-carboxyanhydride (NCA) were synthesised as described in Chapter 2, section 2.2.

Hydroxyl-PEG$_{3k}$ triallyl ether (6). *O*-(2-aminoethyl)polyethylene glycol 3.0 kDa (500 mg, 0.167 mmol) was dissolved in toluene (50 mL) and solvent was then removed under reduced pressure. This process was repeated five times in order to remove traces of water from the PEG starting material, before starting the reaction. 3,4,5-tris(allyloxy)benzoic acid **(2)** (73 mg, 0.25 mmol, 1.5 eq.), *O*-(2-aminoethyl)polyethylene glycol 3.0 kDa (500 mg, 0.167 mmol, 1.0 eq.) and 4-(4,6-dimethoxy-1,3,5-triazin-2-yl)-4-methylmorpholinium chloride (DMTMM) (70 mg, 0.25 mmol, 1.5 eq.) were dissolved in anhydrous methanol (50 mL) under inert atmosphere. The mixture was stirred for two days at room temperature, after which time ^{1}H NMR analysis showed that the reaction was complete (aromatics signals shifted from 7.35 to 7.20 ppm, with the latter integrating for 2H, after the peaks for the OCH_2CH_2 of PEG at 3.6 ppm were set to 356H). The solvent was then removed under reduced pressure and the resulting residue suspended in 60 mL of water. Insoluble materials were removed by filtration, and the aqueous solution was dialysed against deionised water (MWCO 1.0 kDa). The resulting solution was then freeze-dried to give polymer **(6)** as an off-white solid (425 mg, 78%). ^{1}H NMR (400 MHz, MeOD, δ, ppm): 7.20 (s, 2H, C$H_{aromatic}$), 6.19-6.04 (m, 3H, H_{allyl}), 5.55-5.15 (m, 6H, H_{allyl}), 4.68-4.56 (m, 6H, OCH_2), 3.70-3.55 (s, 356H, OCH_2 of PEG).

Triamino-hydroxyl-PEG$_{3k}$ (7). Hydroxyl-PEG$_{3k}$ triallyl ether **(6)** (425 mg, 0.129 mmol, 1.0 eq.), cysteamine hydrochloride (160 mg, 2.07 mmol, 16.0 eq.) and 2,2-dimethoxy-2-phenylacetophenone (DPAP) (10 mg, 0.039 mmol, 0.3 eq.) were dissolved in methanol (5 mL). The mixture was then irradiated using a 36 Watt UV Lamp equipped with 4 X 9 W Light bulbs at 365 nm for 3 hours, until allyl signals could no longer be detected by ^{1}H NMR. Methanol was then evaporated under reduced pressure and the resulting residue was suspended in water. The mixture was extracted with ethyl acetate to remove traces of DPAP and corresponding decomposition products. The aqueous layer was dialysed (MWCO 1.0 kDa) against deionised water for 3 days, then freeze-dried to give polymer **(7)** as an off-white solid (352 mg, 77%). ^{1}H NMR (400 MHz, MeOD, δ, ppm): 7.20 (s, 2H, C*H*$_{aromatic}$), 4.21-4.05 (m, 6H, OC*H*$_2$), 3.70-3.43 (s, 390H, OC*H*$_2$ of PEG), 3.11 (m, 6H, C*H*$_2$NH$_2$), 2.80 (m, 12H, C*H*$_2$S), 2.15-1.90 (m, 6H, OCH$_2$C*H*$_2$CH$_2$S).

Hydroxyl-PEG$_{3k}$-*mik*-poly(benzyl-glutamic acid)$_3$ (8). Triamino-hydroxyl-PEG$_{3k}$ **(7)** (91 mg, 0.026 mmol, 1.0 eq.) was dissolved in dry DCM (10 mL) in a round bottom flask. γ-Benzyl-L-glutamate NCA (821 mg, 3.12 mmol, 120 eq.) was then dissolved in anhydrous DCM (30 mL) and added to the solution containing the amino-PEG initiator. The mixture was stirred at room temperature under inert atmosphere. After 5 days the conversion was found to be ~ 80% as judged by ^{1}H NMR analysis. The solution was then concentrated under vacuum (5 mL) and precipitated with diethyl ether to give the desired product **(8)** as white solid (403 mg, 58%). ^{1}H NMR (400 MHz, CDCl$_3$, δ, ppm): 7.35-7.15 (bs, 370H,

C*H*$_{aromatic}$), 5.16-4.92 (bs, 148H, C(O)OC*H*$_2$Bn), 4.05-3.80 (bs, 74H, HNC*H*CO), 3.69-3.57 (s, 390H, OCH$_2$ of PEG), 2.75-1.97 (m, 296H, C*H*$_2$C*H*$_2$C(O)OBn).

***p*-toluenesulfonyl-PEG$_{3k}$-*mik*-poly(benzyl-glutamic acid)$_3$ (9)**. Hydroxyl-PEG$_{3k}$-*mik*-poly(benzyl-GA)$_3$ **(8)** (300 mg, 0.012 mmol, 1.0 eq.) was dissolved in dry DCM (50 mL) in a round bottom flask. While stirring, *p*-toluenesulfonyl chloride (23 mg, 0.12 mmol, 10.0 eq.) and triethylamine (1.8 g, 18 mmol, 150 eq.) were added to the solution containing the hydroxyl-PEG$_{3k}$-*mik*-poly(benzyl-GA)$_3$ compound. The reaction was stirred at room temperature under inert atmosphere for 12 h. The mixture was then neutralised with 1 M HCl, filtered and an excess of sodium bicarbonate as a solid was added. The suspension was stirred, filtered again and the solution was then concentrated (2 mL). The product **(9)** was recovered by precipitating it in diethyl ether (153 mg, 50%). ^{1}H NMR (400 MHz, CDCl$_3$, δ, ppm): 7.78-7.72 (s, 8H, C*H*$_{aromatic}$), 7.39-7.15 (bs, 430H, C*H*$_{aromatic}$), 7.11-7.06 (s, 8H, C*H*$_{aromatic}$), 5.16-4.92 (bs, 174H, C(O)OC*H*$_2$Bn), 4.02-3.84 (bs, 87H, HNC*H*CO), 3.67-3.60 (s, 390H, OC*H*$_2$ of PEG), 2.75-1.95 (m, 348H, C*H*$_2$C*H*$_2$C(O)OBn).

Azide-PEG$_{3k}$-*mik*-poly(benzyl-glutamic acid)$_3$ (10). *p*-toluenesulfonyl-PEG$_{3k}$-*mik*-poly(benzyl-GA)$_3$ **(9)** (150 mg, 0.00595 mmol, 1.0 eq.) was dissolved in anhydrous DMSO (5 mL) in a round bottom flask. Sodium azide (4 mg, 0.06 mmol, 10.0 eq.) was then added and the solution was stirred at room temperature under inert atmosphere for 24 h. After that, the mixture was precipitated in diethyl ether and dissolved in THF. The precipitated was filtered and the solvent was removed under reduced pressure to give the desired

product as a colourless polymer film **(10)** which was utilised for the subsequent step without further purification (98 mg, 64%). FT-IR: 2042 cm^{-1} (υ_{N3}).

Azide-PEG$_{3k}$-*mik*-poly(glutamic acid)$_3$ (11). Azide-PEG$_{3k}$-*mik*-poly(benzyl-GA)$_3$ **(10)** (98 mg, 0.0059 mmol) was dissolved in THF in a round bottom flask. 10 µL of a 1.0 M NaOH aqueous solution were then slowly added under vigorous stirring to hydrolyse the benzyl ester repeating units in azide-PEG$_{3k}$-*mik*-poly(benzyl-GA)$_3$ copolymer (2.5 equiv. of NaOH per benzyl group). The reaction was left to stir for 2 days at room temperature, then the solvents were removed under reduced pressure. The residue was dissolved in deionised water (25 mL) and the resulting solution was dialysed (MWCO 3.5 kDa) against deionised water for 3 days. The solution was then freeze-dried and polymer **(11)** was recovered as an off-white solid (60 mg, 95%).^{1}H NMR (400 MHz, D_2O, δ, ppm): 4.44-4.26 (bs, 100H, HNC*H*CO), 3.77-3.63 (s, 390H, OCH_2 of PEG), 2.38-1.85 (m, 456H, CH_2CH_2COOH).

Alkyne vitamin B$_{12}$ (12). Vitamin B_{12} (50 mg, 0.0369 mmol, 1.0 eq.) was dissolved in anhydrous DMSO (5 mL) under inert atmosphere. 1,1'-carbonyldiimidazole (CDI) (12 mg, 0.074 mmol, 2.0 eq.) was then added to the round bottom flask and the reaction was stirred at 30°C for 1.5 h prior addition of a solution of dibenzocyclooctyne-amine (30 mg, 0.11 mmol, 3.0 eq.) in anhydrous DMSO (5 mL). The resulting solution was kept under stirring at room temperature and protected from the light for 24 h, then precipitated in diethyl ether. The resulting red-purple solid was filtered, dissolved in methanol, and then purified by preparative-TLC (^{i}PrOH/*n*-BuOH/H_2O/NH_4OH 30/45/21/4),

using methanol to extract the product from silica. The resulting mixture was filtered to remove most of the silica in suspension, and the solvent was then removed under reduced pressure. Yield: 41 mg, 67%. Mass spectrometry and High-Performance Liquid Chromatography (HPLC) confirmed the purity of the product (Supporting Information, Figure S38 and S39): expected m/z [M-Na^{++}] theor. 851.85, found 851.33.

VitB_{12}-PEG_{3k}-*mik*-poly(glutamic acid)$_3$ (13). Azide-PEG_{3k}-*mik*-poly(GA)$_3$ **(11)** (40 mg, 0.0022 mmol, 1.0 eq.) was dissolved in deionised water (3 mL). Alkyne vitamin B_{12} (7 mg, 0.004 mmol, 2.0 eq.) was then dissolved in DMSO (3 mL) and added to the round bottom flask containing the copolymer. The mixture was stirred overnight at room temperature, protected from the light and then dialysed (MWCO 3.5 kDa) against deionised water for 5 days. The resulting solution was freeze-dried, and polymer **(13)** was isolated as a red-purple light solid (39 mg, 91%). ^{1}H NMR (400 MHz, D_2O, δ, ppm): 4.44-4.28 (bs, 110H, HNC*H*CO), 3.75-3.60 (s, 390H, OCH_2 of PEG), 2.52-1.90 (m, 502H, CH_2CH_2COOH). $M_{n,NMR}$ = 21.0 kDa, $M_{n,SEC}$ = 4.8 kDa, Đ = 1.59.

Heteronuclear single quantum coherence (HSQC) and 1D nuclear magnetic resonance (NMR) (Figure 4.3) and size exclusion chromatography (SEC) (Supporting Information, Figure S41) were used to confirm the success of the reaction and evaluate the absence of unreacted free alkyne vitamin B_{12}, respectively. The percentage (%) of PEG_{3k}-*mik*-poly(GA)$_3$ copolymers end-functionalisation with vitamin B_{12} was calculated from a calibration curve by using UV-Visible spectroscopy (Supporting Information, Figure S48).

Hydroxyl-PEG$_{3k}$-*lin*-poly(benzyl-glutamic acid) (14). Commercially available *O*-(2-aminoethyl)polyethylene glycol 3.0 kDa (200 mg, 0.0667 mmol, 1.0 eq.) was dissolved in dry DCM (10 mL) in a round bottom flask. γ-Benzyl-L-glutamate NCA (2.11 g, 8.04 mmol, 120 eq.) was then dissolved in anhydrous DCM (30 mL) and added to the solution containing the amino-PEG initiator. The mixture was stirred at room temperature under inert atmosphere. After 5 days the conversion was found to be ~ 25% as judged by ^{1}H NMR analysis. The solution was then concentrated under vacuum (5 mL) and precipitated with diethyl ether to give the desired product **(14)** as white solid (493 mg, 73%). ^{1}H NMR (400 MHz, $CDCl_3$, δ, ppm): 7.40-7.15 (bs, 170H, C*H*$_{aromatic}$), 5.13-4.93 (bs, 68H, C(O)OC*H*$_2$Bn) 4.00-3.80 (bs, 34H, HNC*H*CO), 3.72-3.56 (s, 390H, OC*H*$_2$ of PEG), 2.70-1.95 (m, 140H, C*H*$_2$C*H*$_2$C(O)OBn).

***p*-toluenesulfonyl-PEG$_{3k}$-*lin*-poly(benzyl-glutamic acid) (15)**. Hydroxyl-PEG$_{3k}$-*lin*-poly(benzyl-GA) **(14)** (300 mg, 0.030 mmol, 1.0 eq.) was dissolved in dry DCM (50 mL) in a round bottom flask. While stirring, *p*-toluenesulfonyl chloride (57 mg, 0.300 mmol, 10.0 eq.) and triethylamine (1.5 g, 15 mmol, 50.0 eq.) were added to the solution containing the hydroxyl-PEG$_{3k}$-poly(benzyl-GA) compound. The reaction was stirred at room temperature under inert atmosphere for 12 h. The mixture was then neutralised with 1 M HCl, filtered and an excess of sodium bicarbonate was added as a solid. The suspension was stirred, filtered, and the solution was then concentrated (2 mL). The product **(15)** was isolated by precipitation in diethyl ether (213 mg, 67%). ^{1}H NMR (400 MHz, $CDCl_3$, δ, ppm): 7.79-7.74 (s, 4H, C*H*$_{aromatic}$), 7.38-7.16 (s, 235H, C*H*$_{aromatic}$),

7.14-7.10 (s, 4H, C*H*$_{aromatic}$), 5.16-4.91 (bs, 94H, C(O)OC*H*$_2$Bn), 3.97-3.83 (bs, 47H, HNC*H*CO), 3.69-3.59 (bs, 390H, OCH_2 of PEG), 2.65-2.0 (m, 190H, C*H*$_2$C*H*$_2$C(O)OBn).

Azide-PEG$_{3k}$-*lin*-poly(benzyl-glutamic acid) (16). *p*-toluenesulfonyl-PEG$_{3k}$-*lin*-poly(benzyl-GA) **(15)** (200 mg, 0.0193 mmol, 1.0 eq.) was dissolved in anhydrous DMSO (5 mL) in a round bottom flask. Sodium azide (12 mg, 0.19 mmol, 10.0 eq.) was then added and the solution was stirred at room temperature under inert atmosphere for 24 h. The mixture was then precipitated in diethyl ether and dissolved in THF. The precipitated was filtered and the solvent was removed under reduced pressure to give the desired product as a colourless polymer film **(16)** which was utilised for the subsequent step without further purification (113 mg, 58%). FT-IR: 2089 cm^{-1} (υ_{N3}).

Azide-PEG$_{3k}$-*lin*-poly(glutamic acid) (17). Azide-PEG$_{3k}$-*lin*-poly(benzyl-GA) **(16)** (113 mg, 0.0136 mmol) was dissolved in THF in a round bottom flask. 28 µL of a 1.0 M NaOH aqueous solution were then slowly added under vigorous stirring to hydrolyse the benzyl ester repeating units in azide-PEG$_{3k}$-*lin*-poly(benzyl-GA) copolymer (2.5 equiv. of NaOH per benzyl group). The reaction was left to stir for 2 days at room temperature, then the solvents were removed under reduced pressure. The residue was dissolved in distilled water (25 mL) and the resulting solution was dialysed (MWCO 3.5 kDa) against deionised water for 3 days. The solution was then freeze-dried and polymer **(17)** was recovered as an off-white solid (76 mg, 95%). ^{1}H NMR (400 MHz, D_2O, δ, ppm): 7.76-7.66 (s, 2H,

C*H*$_{aromatic}$), 7.48-7.32 (s, 2H, C*H*$_{aromatic}$), 4.44-4.02 (bs, 31H, HNC*H*CO), 3.77-3.59 (s, 390H, OC*H*$_2$ of PEG), 2.48-1.83 (m, 189H, C*H*$_2$C*H*$_2$COOH).

VitB$_{12}$-PEG$_{3k}$-*lin*-poly(glutamic acid) (18). Azide-PEG$_{3k}$-*lin*-polyGA **(17)** (100 mg, 0.0136 mmol, 1.0 eq.) was dissolved in deionised water (3 mL). Alkyne vitamin B$_{12}$ (44 mg, 0.026 mmol, 2.0 eq.) was then dissolved in DMSO (3 mL) and added to the round bottom flask containing the copolymer. The mixture was stirred overnight at room temperature, protected from the light and then dialysed (MWCO 3.5 kDa) against deionised water for 5 days. The resulting solution was freeze-dried, and polymer **(18)** was isolated as a red-purple light solid (121 mg, 96%). ^{1}H NMR (400 MHz, D$_2$O, δ, ppm): 7.83-7.66 (s, 2H, C*H*$_{aromatic}$), 7.50-7.33 (s, 2H, C*H*$_{aromatic}$), 4.47-4.05 (bs, 37H, HNC*H*CO), 3.76-3.58 (s, 390H, OC*H*$_2$ of PEG), 2.50-1.86 (m, 176H, C*H*$_2$C*H*$_2$COOH). $M_{n,NMR}$ = 9.8 kDa, $M_{n,SEC}$ = 4.4 kDa, Đ = 1.23.

Heteronuclear single quantum coherence (HSQC) and 1D nuclear magnetic resonance (NMR) (Figure 4.3), and size exclusion chromatography (SEC) (Supporting Information, Figure S47) were used to confirm the success of the reaction and evaluate the absence of unreacted free alkyne vitamin B$_{12}$, respectively. The percentage (%) of PEG$_{3k}$-*lin*-polyGA copolymers end-functionalisation with vitamin B$_{12}$ was calculated from a calibration curve by using UV-Visible spectroscopy (Supporting Information, Figure S48).

mPEG$_{2k}$-polyGA copolymers. Non-targeted linear mPEG$_{2k}$-*lin*-GA$_{30}$ and miktoarm mPEG$_{2k}$-*mik*-(GA$_{10}$)$_3$ copolymers were synthesised as described in Chapter 2, section 2.2.

Ethyl (3-(1-(2-(2-(2-hydroxyethoxy)ethoxy)ethyl)-1,13-dihydro-8H-dibenzo[b,g][1,2,3]triazolo[4,5-d]azocin-8-yl)-3-oxopropyl)carbamate (20). Dibenzocyclooctyne-amine (20 mg, 0.072 mmol, 1.0 eq.) was dissolved in DCM (2 mL) and reacted with an excess of ethyl chloroformate (16 mg, 0.14 mmol, 2.0 eq.) and triethylamine (15 mg, 0.14 mmol, 2.0 eq.) for 24 h, to give compound **(19)**. Methanol (2 mL) was then added to quench the excess of ethyl chloroformate and 2-(2-(2-azidoethoxy)ethoxy)ethanol (25 mg, 0.145 mmol, 2.0 eq.) was added for 12 h. Purification by preparative TLC (^{i}PrOH/n-BuOH/H_2O/NH_4OH 30/45/21/4) gave the desired clicked product **(20)**.

Cyanocobalamin (3-(1-(2-(2-(2-hydroxyethoxy)ethoxy)ethyl)-1,13-dihydro-8H-dibenzo[b,g][1,2,3]triazolo[4,5-d]azocin-8-yl)-3-oxopropyl)carbamate (21). Alkyne vitamin B_{12} (10 mg, 0.0060 mmol, 2.0 eq.) was added to a solution of DMSO with 2-(2-(2-azidoethoxy)ethoxy)ethanol (3.1 mg, 0.018 mmol, 3.0 eq.). Purification by preparative TLC (^{i}PrOH/n-BuOH/H_2O/NH_4OH 30/45/21/4) gave the desired clicked product **(21)**.

Preparation of polymer-protein nanocomplexes. Non-targeted ($mPEG_{2k}$-polyGA)-lysozyme nanocomplexes were prepared at relative molar charge ratios r = 2.5 where r is the charge ratio between the number of glutamic acid residues present in the copolymer (negatively charged at physiological pH) and the 17 lysine and arginine residues (positively charged at physiological pH) of lysozyme. Polymer and protein stock solutions were prepared by separately dissolving them in phosphate buffer (PB, 10 mM, pH 7.4) at a concentration of

10 mg mL^{-1} and 14.5 mg mL^{-1}, respectively, and appropriate aliquots mixed in order to achieve *r* = 2.5.

To prepare targeted polymer-protein nanocomplexes, $mPEG_{2k}$-polyGA and $vitB_{12}$-PEG_{3K}-polyGA copolymers of the same topology (i.e. either linear or miktoarm) were mixed at relative molar ratios of 85:15, respectively, to prepare the required polymer stock solution. Polymers and lysozyme were then mixed at relative molar charge ratio of 2.5 as previously described.

Lysozyme was labelled with sulfo-Cyanine 5 NHS ester (Cy5) (Supporting Information, section 6.3.4) and complexed with copolymers as previously described to evaluate protein uptake *in vitro*, in Calu-3 cells, and protein deposition and retention *in vivo*, in healthy mice lungs.

Nanoparticle Tracking Analysis (NTA). Nanoparticle tracking analysis was carried out as described in Chapter 2, section 2.2.

Spray-drying conditions. Dry powders were formulated as described in Chapter 3, section 3.2. The components of the resulting dry powder formulations were: 0-10% (*w/w*) nanocomplexes or 5% (*w/w*) lysozyme, 10% (*w/w*) leucine, 6.6% (*w/w*) phosphate buffer salts and trehalose as bulking agent (up to 100% (*w/w*)).

Culture of cells on flasks. Human airway epithelial cells (Calu-3) were cultured in Dulbecco's Modified Eagle's Medium (DMEM)/F-12 medium. Medium was supplemented with Foetal Bovine Serum (FBS, 10% *v/v*), non-essential amino acids (1% *v/v*), L-glutamine (1% *v/v*), penicillin (100 units mL^{-1}) and

streptomycin (0.1 mg mL^{-1}). Dulbecco's Phosphate-Buffered Saline (DPBS) and trypsin/EDTA were used to wash and detach adherent cells in the process of cell splitting. Cells were always incubated at 37°C and 5% CO_2.

Culture of cells on Transwell® inserts. Calu-3 cells were seeded at $1 \cdot 10^6$ cells per cm^2 on Transwell® inserts (12 mm diameter, 0.4 μm pore size) and cultured for 21 days, with medium replacement every two days. Cells were cultured using air-interface culture (AIC) conditions - known to promote mucus secretion - which were created on day 2 post-seeding on Transwell® inserts. Culturing cells over 21 days period was considered important to ensure complete cell differentiation. Cell confluence and cell layer integrity before samples exposure was confirmed by transepithelial electrical resistance (TEER) measurements using an EVOM voltohmmeter. Cells included in the experiments always had values higher than 500 Ω cm^2.

Cellular uptake of lysozyme using polymer-protein nanocomplex suspension. Calu-3 cells were cultured on Transwell® inserts over 21 days as previously described. Polymer-protein nanocomplexes prepared as previously described were added to non-supplemented medium – final protein concentration 3 μg mL^{-1}. Following a routine measurement of TEER (to assess cell layer integrity and hence their suitability for inclusion in the experiments), the nanocomplex suspension (0.5 mL) was added to the apical chamber of the Transwell® insert and 0.5 mL of non-supplemented medium were added to the basolateral chamber. Cells were then incubated at 37°C for 3 h. After that, medium was removed, cells washed with DPBS, detached with trypsin/EDTA and washed

again with DPBS. Cells were analysed by flow cytometry in at least quadruplicate experiments, with more than 10,000 cells measured in each sample.

The effect of a competitive ligand on receptor-mediated uptake of targeted nanocomplexes was studied in the presence of free vitamin B_{12}. A vitamin B_{12} stock solution (2.0 mg mL^{-1}) was prepared by dissolving 10 mg of $vitB_{12}$ in 5.0 mL of non-supplemented medium, and 0.50 mL (1.0 mg of $vitB_{12}$) of it were added to the apical chamber of Transwell® inserts. Cells were then incubated at 37°C for 30 min following addition of targeted polymer-protein nanocomplex suspension (0.5 mL, final protein concentration 3 µg mL^{-1}). Cells were incubated again at 37°C for 3 h and analysed by flow cytometry as previously described. Experiments were made in at least quadruplicate, with more than 10,000 cells measured in each sample.

Cellular uptake of lysozyme using dry powder formulations. Calu-3 cells were cultured on Transwell® inserts over 21 days as previously described. Culture medium was then removed and dry powders were sprayed twice (2 mg per dose) using a Dry Powder Insufflator™ model DP4-M® (Penn-Century®) into the Transwell® inserts as follows:

Four Transwell® inserts were placed into a desiccator at equal distance from the centre (Figure 4.2) as previously shown within our group (Cingolani, 2017). 2 mg of dry powder formulations were then sprayed twice from a Penn-Century® device. Next, 0.5 mL of Hank's Balanced Salts Solution (HBSS) were added to the basolateral chamber of the Transwell® inserts and cells were

incubated at 37°C and 5% CO_2 for 3 h. Cells were then detached with trypsin/EDTA, washed twice with DPBS and lysozyme uptake was analysed by flow cytometry in quadruplicate experiments, with more than 10,000 cells measured in each sample.

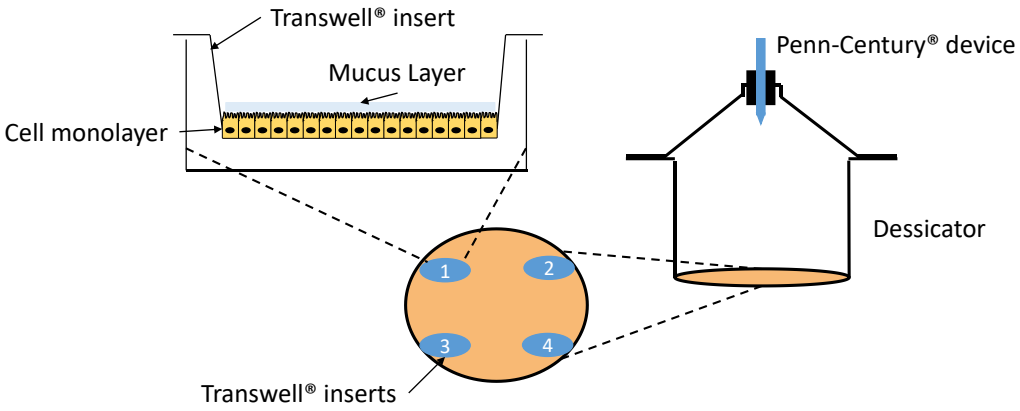


Figure 4.2. Graphic representation of the spraying process of dry powder formulations on top of Calu-3 cell monolayers using a Penn-Century® device.

To ensure that all Transwell® inserts placed into the desiccator receive similar dose, particle size (D_{90}) and particle distribution were investigated. 2 mg of dry powder formulations were sprayed twice from a Penn-Century® device as shown in Figure 4.2, and each Transwell® insert (without cells) was examined by optical microscopy. Images were then analysed by ImageJ Software to give D_{90} – diameter below which 90% of the particle population lie – and dry powder distribution.

Scanning electron microscopy (SEM) of dry powder formulations before and after spraying them using a Penn-Century® device was performed as previously described in Chapter 3, section 3.2.

Complement activation. ($VitB_{12}$-PEG_{3k}-polyGA)-lysozyme nanocomplexes or free lysozyme were kept in contact with normal human serum (NHS) and the residual haemolytic capacity was measured to study the complement activation. Sheep erythrocytes were sensitised by rabbit anti-sheep erythrocyte antibodies at a final dilution of 1/800 *v/v* and these sensitised sheep erythrocytes were suspended at a final concentration of $1 \cdot 10^8$ cells mL^{-1} in veronal-buffer saline (VBS^{2+}, containing 0.5 mM Mg^{2+} and 0.15 mM Ca^{2+}). VBS^{2+} and NHS were mixed with polymer-lysozyme nanocomplexes or free lysozyme at a final protein concentration of 1.116 mg mL^{-1} so that the final dilution of NHS in the reaction mixture was 1/4 (*v/v*) in a final volume of 400 µL. The suspension was incubated at 37°C for 60 min under gentle stirring. The mixture was then diluted 1/25 (*v/v*) in VBS^{2+} and different aliquots at different dilutions were added to a specific volume of sensitised sheep erythrocytes. The suspensions were incubated for 45 min at 37°C under gentle stirring and the reaction was then stopped by adding ice-cold NaCl (0.15 M). The mixture was centrifuged at 2,000 rpm for 5 minutes to precipitate un-lysed erythrocytes. The supernatant was collected and the optical density was measured at λ = 415 nm.

The presence of polymer or lysozyme without serum did not lead to hemolysis of the sensitised sheep erythrocytes at the polymer/protein concentration investigated. Sample without serum was used here as positive control (100% complement activation, 0% sensitised sheep erythrocytes lysis) and employed to correct the absorbance values from the samples. Sample with serum and

without particles was utilised as negative control (0% complement activation, 100% lysis). The data can be expressed in terms of CH50 units, defined as the serum dilution at which 50% haemolysis is observed. They can be calculated by a linear fit to a log-log version of the Von Krogh equation (Kazatchkine et al., 1986). In this study, the data was expressed as the percentage of complement activation relative to 100% complement activation observed with our positive control samples.

$$Complement\ activation\ (\%) = \frac{CH50_{sample} - CH50_{control}}{CH50_{control}}$$

where $CH50_{control}$ refers to CH50 of the positive controls (100% complement activation).

***In vivo* evaluation of nanocomplexes-based dry powder formulations**

In vivo experiments were designed based on our *in vitro* results, and done in collaboration with Drs Remi Rosière, Nathalie Wauthoz and Karim Amighi at the Free University of Brussels (Belgium), and materially carried out by our collaborators in Belgium. Results are discussed here for the sake of completeness.

Animals and husbandry conditions. Female BALB/c mice (Charles River, Arbresle, France) were kept under conventional housing conditions (22 ± 2°C, 55 ± 10% humidity, and 12-hours day/night cycle). All studies and manipulations were approved by the CEBEA ethical committee of the Faculty of Medicine, ULB (Commission d'Ethique du Bien-Etre Animal, Université libre

de Bruxelles, Belgium) (Ethical protocol N°585N). Laboratory federal agreement number: LA 1230568.

Dry powder formulations delivery from the dry powder insufflator

Aerosol particles generated from Dry Powder Insufflator™ model DP4-M® (Penn-Century®) were confirmed to be suitable for endotracheal administration into the mice by using a Spraytec® laser diffractometer. The emitted aerosol was presented directly and perpendicular to the laser beam for size measurement. For all formulations tested (Table 4.1) a loading powder mass of 2 mg was evaluated (n=10). High emitted dose values (> 80%), particle size D_{50} ≤ 5 µm and RSD values ≤ 25% were considered suitable for the administration of dry powder formulations into the mice.

Table 4.1. Emitted dose, particle size (D_{50}) and uniformity of mass delivered of dry powder formulations tested in this study. All formulations contain 10% (*w/w*) leucine, 6.6% (*w/w*) buffer salts and up to 100% (*w/w*) trehalose.

Formulation[a]	Nanocomplexes (*w/w*)	Emitted Dose (%)	Particle Size (D_{50}, µm)[b]	RSD (%)[c]
UDP	0% Nanocomplexes	83 ± 10	4.1 ± 0.2	≤ 25%
UDP-P	5% Lysozyme	93 ± 4	4.3 ± 0.6	≤ 25%
UDP-L1	10% Nanocomplexes	93 ± 7	4.4 ± 0.6	≤ 25%

[a] See UDP, UDP-P and UDP-L1 composition in Table 4.2.
[b] D_{50} represents the diameter below which 50% of the particle population lie.
[c] Uniformity of mass delivered (RSD, Relative Standard Deviation).

Local pulmonary tolerance of polymer-protein nanocomplexes-based dry powder formulations in healthy mice

Solutions and dry powder formulations were administered by the non-invasive endotracheal route using an aerosolising system (Microsprayer™ model IA-1C®) or a dry powder insufflator designed for mice (Dry Powder Insufflator™ model DP4-M®, Penn-Century®), respectively, as described elsewhere (Bivas-Benita et al., 2005, Rosiere et al., 2016).

Five groups were compared: (i) non-treated mice as negative control (n=6), (ii) mice treated with unlabeled dry powder (UDP) (n=5), (iii) mice treated with UDP-P (n=5), (iv) mice treated with UDP-L1 (n=5) and (v) mice treated with a lipopolysaccharide (LPS) solution (single administration of 1 µg) as positive control (n=6) (see compositions in Table 4.2). Mice treated with dry powders received 2 mg of dry powder administered three times a week for three consecutive weeks.

Bronchoalveolar lavage fluids (BALFs) were analysed in terms of cell composition and pro-inflammatory marker concentration (cytokines IL-1β, IL-6, and TNF-α) as previously described (Rosiere et al., 2016). Briefly, mice were euthanised by a lethal intraperitoneal injection of 12 mg sodium phenobarbital 8 h (for the LPS group) or 24 h (for the dry powder groups) after the last inhaled administration. BALFs were collected using a 20-gauge cannula (Surflo® catheter) with 3 flushes of 0.7 mL cold PBS and conserved on ice until cell count analysis. BALFs were centrifuged at 160 x g at 4°C, supernatants were collected and conserved at -80°C for cytokine quantification. Differential cell counts were

performed on cytospin preparations after staining with May Grünwald and Giemsa (Sigma-Aldrich). A total of 200 cells were counted per slide and were referred to as alveolar macrophages, lymphocytes or polymorphonuclear neutrophils according to their morphology. Cytokine concentrations were determined by ELISA for mouse IL-1 β, IL-6, and TNF-α (DuoSet® ELISA, RnD Systems) according to the manufacturer's protocols. The limits of quantification for the techniques used were 15.6 pg mL^{-1} for IL-1β and IL-6, and 31.3 pg mL^{-1} for TNF-α.

***In vivo* pulmonary deposition and retention.** The deposition of the dry powder formulations was evaluated after pulmonary delivery. Labelled dry powder formulations with sulfo-cyanine 5 (LDP-P, LDP-L1 and LDP-L2, see composition in Table 4.2) were administered to mice (2 mice per group) by the endotracheal route as described previously. After 0, 3, and 14 h, mice were sacrificed using sodium phenobarbital, and the lungs were collected and blocked using Optimum Cutting Temperature (OCT) solution (Tissue-Tek® OCT compound, Sakura). Five non-serial cryosections of 7 µm per lung were prepared and mounted on SuperFrost™ slides (Thermo Fischer Scientific) using a DAPI solution (DAPI Counterstain) and finally covered with a coverslip.

The slides were observed under a Leica SP8 confocal microscope. The images were processed using ImageJ Software.

Table 4.2. Composition of the dry powder formulations used in the *in vivo* studies.

Formulation	Nanocomplexes (*w/w*)	Leucine (% *w/w*)	Buffer salts *(% w/w)*	Trehalose (% *w/w*)
UDP	0% Nanocomplexes	10	6.6	Up to 100
UDP-P	5% Lysozyme	10	6.6	Up to 100
UDP-L1	10% Targeted nanocomplexes	10	6.6	Up to 100
LDP-P	5% Lysozyme-Cy5	10	6.6	Up to 100
LDP-L1	10% Targeted nanocomplexes-Cy5	10	6.6	Up to 100
LDP-L2	10% Non-targeted nanocomplexes-Cy5	10	6.6	Up to 100

All dry powder formulations with nanocomplexes contained 5% *w/w* lysozyme.

4.3. Results and Discussion

In this chapter, novel vitB_{12}-PEG_{3k}-polyGA copolymers were synthesised with the aim of creating polymer-protein nanocomplexes for targeted delivery of protein cargoes to specific epithelial cells. In the previous chapter, we showed that dry powder formulations of (mPEG_{2k}-polyGA)-protein nanocomplexes were able to protect proteins from degradation by proteolytic enzymes. Here, we further evolved these formulations by designing nanovectors bearing targeting ligands, and investigated their ability to enhance the cellular uptake of protein payloads in human airway epithelial cells (Calu-3) *in vitro*, and in a BALB/c mouse model *in vivo*.

4.3.1. Synthesis of targeted linear and miktoarm vitB_{12}-PEG_{3k}-poly(glutamic acid) copolymers

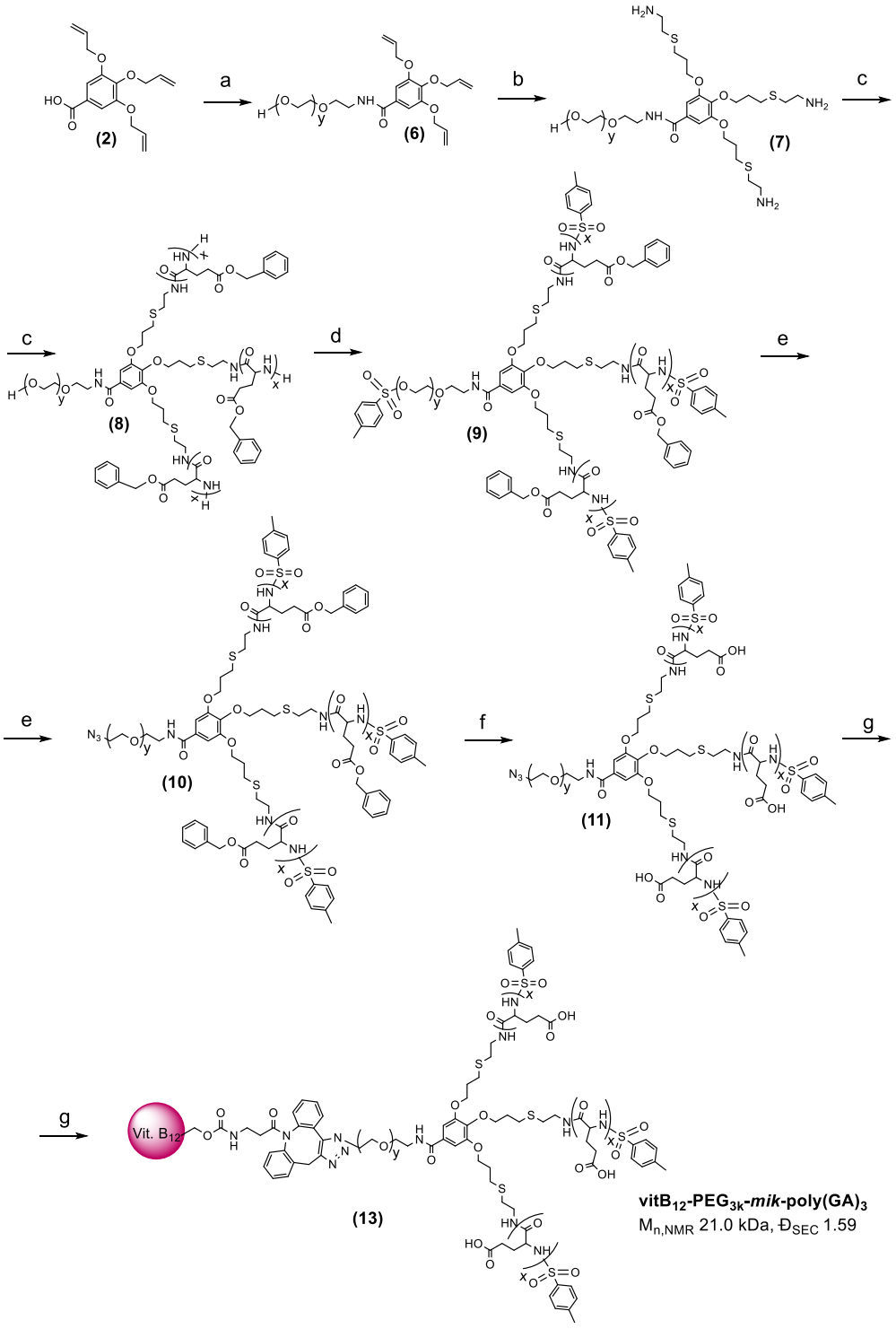
For the design of targeted protein-complexing copolymers novel A-B_3 targeted miktoarm copolymer consisting of vitamin B_{12} ligand, one chain of 3.0 kDa polyethylene glycol (PEG_{3k}) and three chains of poly(glutamic acid) was synthesised. Vitamin B_{12} was chosen here as the ligand, as previous studies within our group have shown its potential for enhancing receptor-mediated uptake by Calu-3 epithelial model cell line (Fowler et al., 2013b). The length of the polyethylene glycol block in targeted copolymers was 3.0 kDa, that is slightly longer than that of the non-targeted complexing copolymers to enhance the exposure of vitamin B_{12} at the surface of targeted polymer-protein nanocomplexes.

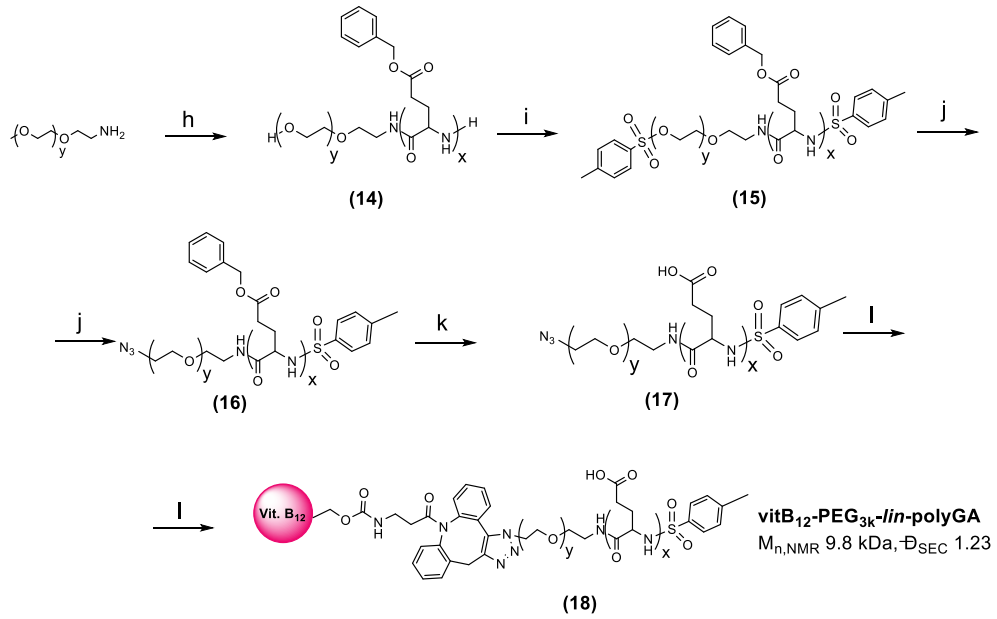
Methyl 3,4,5-trihydroxybenzoate (gallic acid methyl ester) was used as the starting point to generate the core of the targeted miktoarm copolymer required for polymer complexation. Reaction of gallic acid triallyl ether **(2)** with *O*-(2-aminoethyl)polyethylene glycol 3.0 kDa in anhydrous methanol and DMTMM as the coupling reagent afforded the PEG intermediate **(6)**. This was then subjected to thiol-ene (Dondoni, 2008) addition in the presence of 2,2-dimethoxy-2-phenylacetophenone (DPAP) photoinitiator and cysteamine hydrochloride, under irradiation at λ = 365 nm in methanol for 3 hours, to give hydroxyl-PEG_{3k}-triamino initiator **(7)**.

As for the synthesis of the non-targeted copolymers described in Chapter 2, *N*-carboxyanhydride (NCA) polymerisation of γ-benzyl-L-glutamate *N*-carboxyanhydride was chosen here to synthetise poly(benzyl-glutamic acid) (poly(benzyl-GA)) blocks. This polymerisation strategy requires a nucleophilic initiator, typically a primary amine. In this work, hydroxyl-PEG_{3k}-triamino **(7)** and commercially available *O*-(2-aminoethyl)polyethylene glycol 3.0 kDa were utilised to form miktoarm and linear copolymers, respectively. All polymerisations were carried out in DCM at room temperature and monitored by ^{1}H NMR by following the disappearance of the α-CH proton signal of the α-amino acid-*N*-carboxyanhydride (NCA) monomer at 4.4 ppm. In the polymerisation reactions described in Chapter 2, NCA polymerisations carried out at 0°C led very well defined poly(glutamic acid benzyl ester) chains with low polydispersities. However, in this case, possibly due to the presence of a hydroxyl group at the PEG end-chain, higher temperatures were required to

start the polymerisation process. The use of higher temperatures, can lead to less controlled polymerisations with broader molecular weight distributions (Habraken et al., 2010). This could explain the higher molecular weight and polydispersity found in the miktoarm copolymer (Scheme 4.1).

Miktoarm hydroxyl-PEG$_{3k}$-*mik*-poly(benzyl-GA)$_3$ **(8)** and linear hydroxyl-PEG$_{3k}$-*lin*-poly(benzyl-GA) **(14)** copolymers were then reacted with *p*-toluenesulfonyl chloride and triethylamine as the acid scavenger in anhydrous dichloromethane to give *p*-toluenesulfonyl-PEG$_{3k}$-*mik*-poly(benzyl-GA)$_3$ **(9)** and *p*-toluenesulfonyl-PEG$_{3k}$-*lin*-poly(benzyl-GA) **(15)**. A relatively large excess of TsCl (10.0 eq.) was employed in this step to simultaneously protect the polymer terminal amino groups as stable *p*-toluenesulfonamides, and activate the primary alcohol at the PEG chain end as a tosyl ester group. After purification, sodium azide was added to a solution of **(9)** and **(15)** in anhydrous DMSO. NMR analysis was found not to be suitable to confirm the presence of the azide group on the copolymers, due to the signal for newly formed CH_2N_3 moiety being too small in intensity, and hidden by the large signals of the polymer backbone. However, FT-IR showed the appearance of a new band at 2042 and 2089 cm^{-1} typical of azide groups (Mantovani et al., 2005), for azide-PEG$_{3k}$-*mik*-poly(benzyl-GA)$_3$ **(10)** and azide-PEG$_{3k}$-*lin*-poly(benzyl-GA) **(16)**, respectively. Quantitative hydrolysis of the polymer benzyl ester groups with NaOH gave azide-PEG$_{3k}$-*mik*-poly(GA)$_3$ **(11)** and azide-PEG$_{3k}$-*lin*-polyGA **(17)**.


(2)
(6)
(7)
(8)
(9)
(10)
(11)
(13)
Vit. B12
vitB12-PEG3k-mik-poly(GA)3
Mn,NMR 21.0 kDa, ÐSEC 1.59



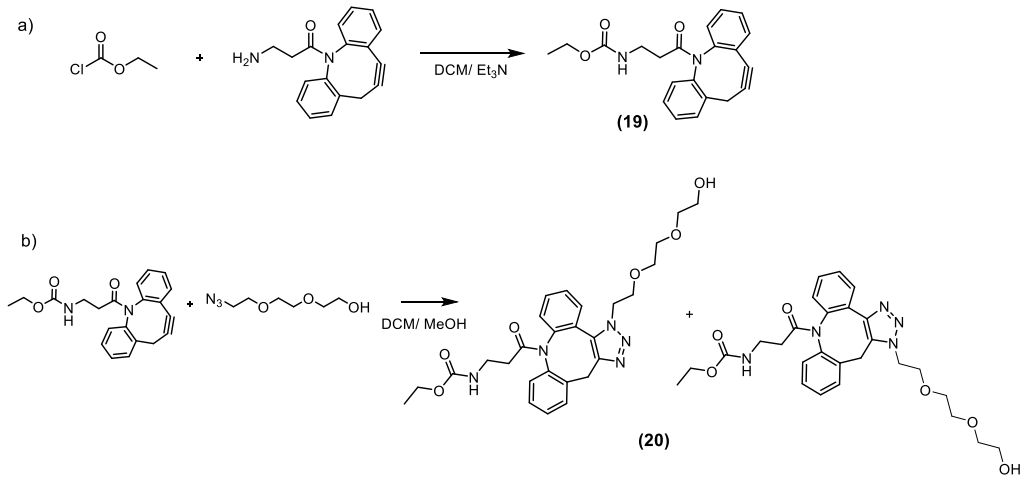
Scheme 4.1. Reactions and conditions for the synthesis of vitB$_{12}$-PEG$_{3k}$-*mik*-poly(GA)$_3$ and vitB$_{12}$-PEG$_{3k}$-*lin*-polyGA copolymers. a) *O*-(2-aminoethyl)polyethylene glycol 3.0 kDa, DMTMM, MeOH, 2 days; b) cysteamine hydrochloride, DPAP, MeOH, UV at λ = 365 nm, 3 h; c and h) γ-benzyl-L-glutamate NCA, CH_2Cl_2, room temperature, 5 days; d and i) *p*-toluenesulfonyl chloride, triethylamine, CH_2Cl_2, 12 h; e and j) sodium azide, DMSO, 24 h; f and k) NaOH, H_2O/THF, 2 days; g and l) alkyne vitamin B_{12}, DMSO/H_2O, overnight.

In this study, click chemistry was used for coupling polymer intermediates **(11)** and **(17)** with vitamin B_{12} to afford the desired targeted miktoarm vitB$_{12}$-PEG$_{3k}$-*mik*-poly(GA)$_3$ and linear vitB$_{12}$-PEG$_{3k}$-*lin*-polyGA copolymers. Click chemistry (Kolb et al., 2001) is a general term that refers to a family of chemical reactions characterised by very high efficiencies, inoffensive co-products and use of benign solvents such as water. Copper(I)-catalysed azide-alkyne 1,3-dipolar cycloaddition, where a 1-alkyne and organic azide react to form a 1,4-triazole, is arguably the most popular example of click reactions (Tiwari et al., 2016). However, efficient removal of residual copper catalyst from the final "clicked" product is very challenging. To circumvent this problem, here we chose a copper-free of the alkyne-azide cycloaddition, which utilises an activated alkyne which, being part of a highly strained cyclooctyne ring, is very reactive

and can lead to efficient and ultrafast click reaction even at room temperature and in the absence of catalysts. Accordingly, alkyne vitamin B_{12} **(12)** was synthesised by reacting vitamin B_{12} and CDI in DMSO for 30 min, followed by the addition of dibenzocyclooctyne-amine. The crude product was precipitated in diethyl ether, purified by preparative TLC using ^{i}PrOH/n-BuOH/H_2O/NH_4OH 30/45/21/4 as the mobile phase and characterised by mass spectrometry and HPLC (Supporting Information, Figure S38 and S39).

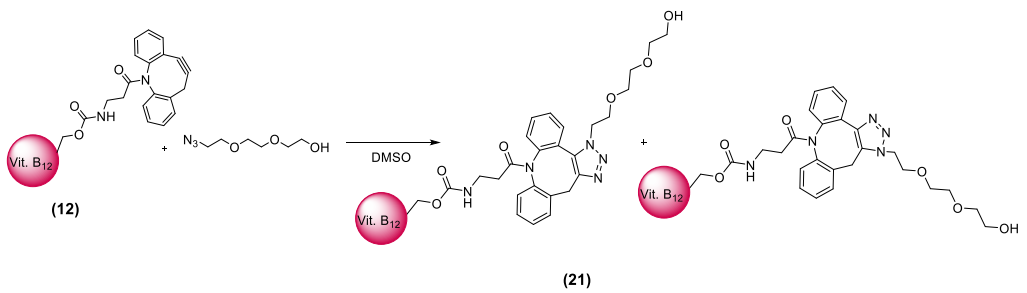
Reaction of azide-terminated polymers **(11)** and **(17)** with alkyne vitamin B_{12} in water/DMSO overnight at room temperature followed by purification by dialysis, led to the desired B_{12}-terminated polymers vitB_{12}-PEG_{3k}-*mik*-poly$(GA)_3$ **(13)** and vitB_{12}-PEG_{3k}-*lin*-polyGA **(18)**. The success of the cycloaddition reaction was confirmed by 2D ^{1}H-^{13}C HSQC and 1D ^{1}H NMR (Figure 4.3). HSQC NMR data are represented as 2D plots with axes defined by proton (^{1}H) and carbon (^{13}C) chemical shifts, giving much more detailed chemical fingerprints than those obtained in typical 1D ^{1}H NMR spectra. The complexity of the NMR spectra of the clicked polymers did not initially allow an easy interpretation of the NMR results. To circumvent this problem, simpler clicked model molecules were prepared to identify diagnostic NMR peaks suitable for the interpretation of the complex spectra of clicked polymers. Accordingly, 1,2,3-triazole **(20)** was synthesised in two steps from dibenzocyclooctyne-amine, as shown in Scheme 4.2. HSQC NMR confirmed the success of the click reaction, with shift of the α-CH_2 signals of the dibenzocyclooctyne-carbamate **(19)** at 5.2/56 ppm to 6.1/52

ppm ($^{1}H/^{13}C$ signals). Signals for both regioisomeric cycloadducts were clearly visible in the spectrum of the purified product **(20)** (Figure 4.3 A).



Scheme 4.2. Synthesis of model clicked 1,2,3-triazole **(20)**.

With a first set of signals identified for the regioisomeric cycloadducts **(20)**, a new model clicked compound **(21)** incorporating vitB$_{12}$, thus with chemical structure closer to that of the clicked polymers vitB$_{12}$-PEG$_{3k}$-*mik*-poly(GA)$_3$ **(13)** and vitB$_{12}$-PEG$_{3k}$-*lin*-polyGA **(18)**, was synthesised (Scheme 4.3). Similarly to what observed previously for model adducts **(20)**, signals from the α-CH$_2$ of the dibenzocyclooctyne-carbamate at 5.0/56 ppm shifted to 5.9/52 ppm in the clicked product **(21)** (Figure 4.3 B).



Scheme 4.3. Synthesis of vitB$_{12}$ model clicked 1,2,3-triazole **(21)**.

Once diagnostic NMR peaks for the clicked triazole moiety were identified, vitB$_{12}$-PEG$_{3k}$-*lin*-polyGA and vitB$_{12}$-PEG$_{3k}$-*mik*-poly(GA)$_3$ copolymers were similarly re-analysed. As previously observed, the α-CH$_2$ signals of the dibenzocyclooctyne-carbamate at 5.0/56 ppm shifted to 5.9/52 ppm in the linear PEG$_{3k}$-*lin*-GA copolymer, confirming the success of the click reaction (Figure 4.3 C). However, HSQC NMR could not be used to characterise miktoarm vitB$_{12}$-PEG$_{3k}$-*mik*-poly(GA)$_3$ due to poor signal intensity in the ^{13}C NMR. However, 1D ^{1}H NMR showed the appearance of a new peak at 5.9 pm analogous to that found in HSQC NMR spectra and thus confirming the success of the click reaction (Figure 4.3 D). The efficiency of the covalent coupling between vitamin B$_{12}$ and the copolymers was found to be 93 and 97% for vitB$_{12}$-PEG$_{3k}$-*lin*-polyGA and vitB$_{12}$-PEG$_{3k}$-*mik*-poly(GA)$_3$, respectively as revealed by UV-visible analysis (Supporting Information, Figure S48).

Targeted polymer-protein nanocomplexes – consisting of mPEG$_{2k}$-polyGA (85% mol:mol) and vitB$_{12}$-PEG$_{3k}$-polyGA (15% mol:mol) copolymers – and non-targeted nanocomplexes – consisting of mPEG$_{2k}$-polyGA copolymers (100%) – were then formulated at polymer-protein relative molar charge ratio of 2.5. mPEG$_{2k}$-*lin*-GA$_{30}$ and mPEG$_{2k}$-*mik*-(GA$_{10}$)$_3$, synthesised as described in Chapter 2, were utilised as non-targeted control copolymers. mPEG$_{2k}$-*lin*-GA$_{30}$ copolymer was selected here because in our previous experiments it showed the best lysozyme complexation efficiency, whereas mPEG$_{2k}$-*mik*-(GA$_{10}$)$_3$ possessing approximately the same average molecular mass as its linear mPEG$_{2k}$-*lin*-GA$_{30}$ analogue, was chosen as the miktoarm copolymer for these

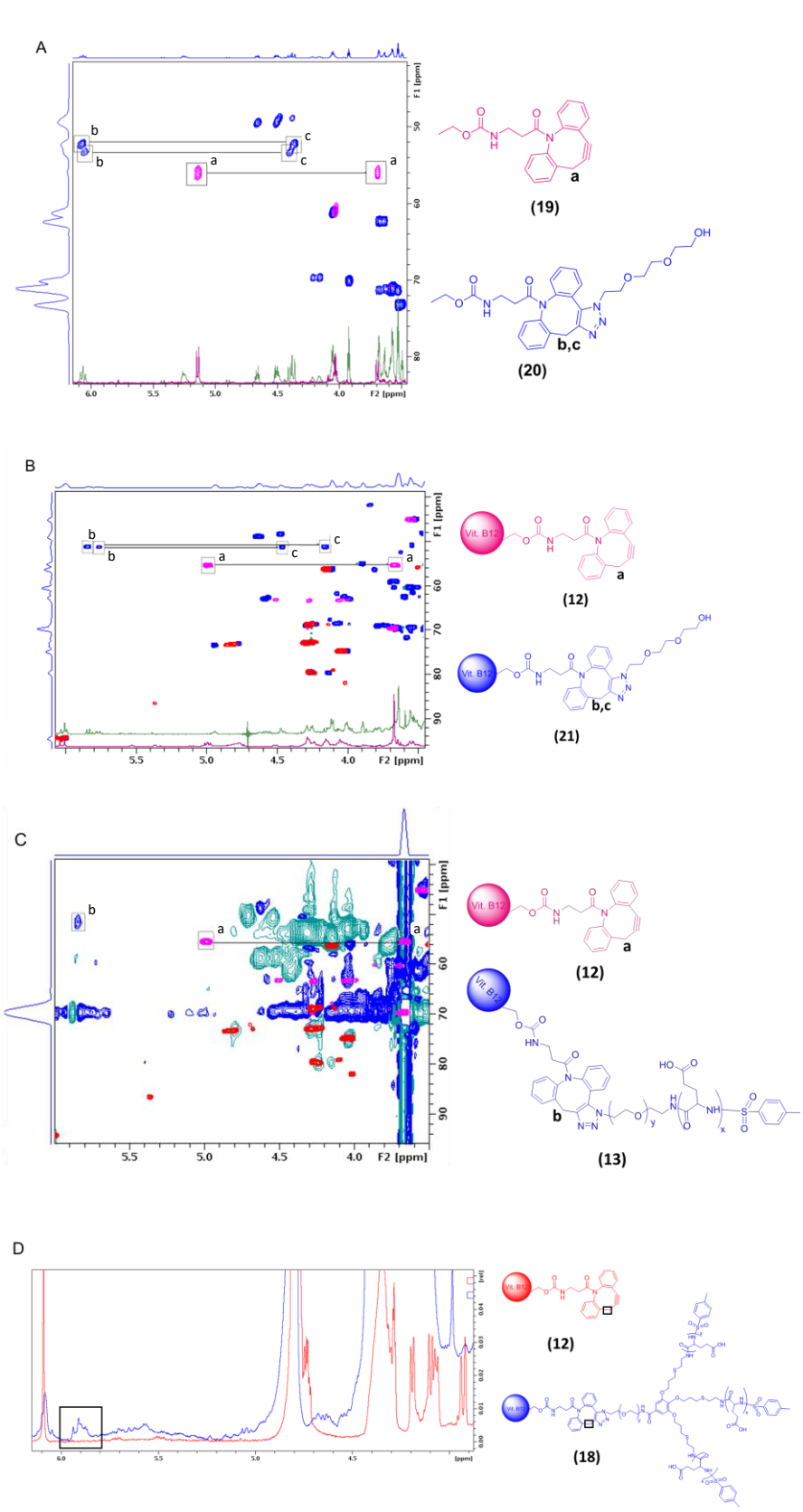


Figure 4.3. Characterisation of clicked product **(20)**, product **(21)** and B_{12}-functionalised PEG-poly(GA) copolymers **(13)** and **(18)**: A, B and C) HSQC and D) 1D NMR spectra of the α-CH_2 signals of the dibenzocyclooctyne-carbamate before and after click reaction.

studies. The presence of targeted vitB$_{12}$-PEG$_{3k}$-polyGA copolymers did not negatively affect the formation of polymer-protein nanocomplexes as sizes in the range of 50-200 nm were observed by NTA analysis (Figure 4.4). Neither unmodified lysozyme nor free copolymers could be detected by NTA, further confirming that the sizes analysed were polymer-protein complexes.

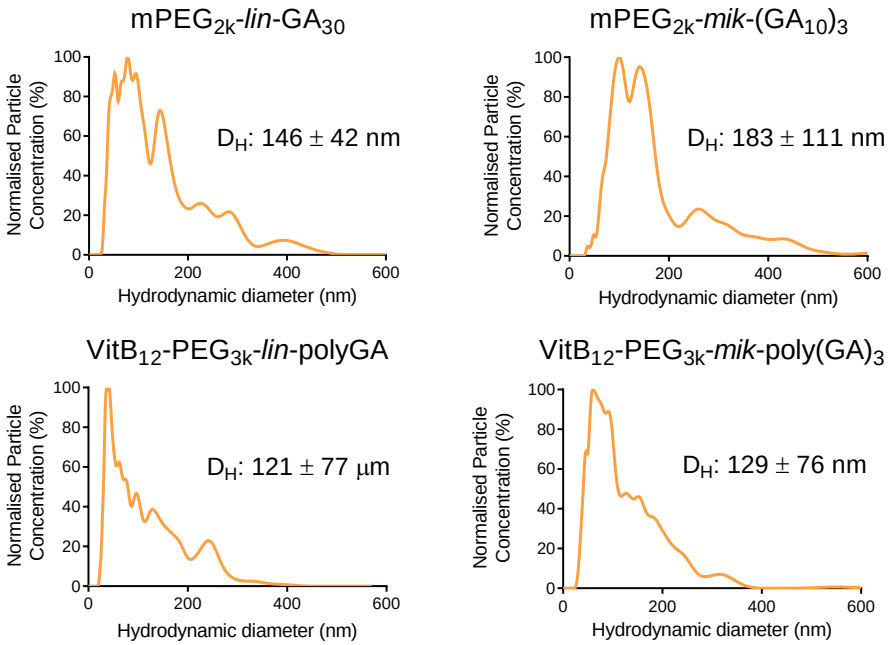


Figure 4.4. Particle size distribution of non-targeted and targeted nanocomplexes. Targeted polymer-protein nanocomplexes were composed of mPEG$_{2k}$-polyGA (85% mol:mol) and vitB$_{12}$-PEG$_{3k}$-polyGA (15% mol:mol) copolymers. D_H is the average hydrodynamic diameter ± SD of polymer-protein nanocomplexes as assessed by nanoparticle tracking analysis (NTA).

4.3.2. *In vitro* protein internalisation by the airway epithelium

Next, the ability of targeted (vitB$_{12}$-PEG$_{3k}$-polyGA)-lysozyme nanocomplexes to deliver proteins into the airway epithelium was assessed. Bronchial Calu-3 cells were chosen here as an airway epithelium cell model able to form tight polarised monolayers and promote mucus secretion when they are grown in air-interface culture (AIC) conditions (Grainger et al., 2006). Calu-3 cells have been utilised in a number of studies to screen potential formulations for drug

delivery to the respiratory epithelium (Foster et al., 2000, Forbes and Ehrhardt, 2005, Kreft et al., 2015). Calu-3 cells also express cubilin and transcobalamin II receptors, which have a key role in the cellular uptake of vitB_{12}-decorated nanoparticles (Fowler et al., 2013a).

In this study, Calu-3 cells were cultured in AIC conditions for 21 days to ensure complete cell differentiation, promote mucus secretion and therefore provide an *in vitro* model representative of the airway epithelium. For uptake experiments, lysozyme was fluorescently tagged with sulfo-Cyanine-NHS ester 5 (Cy5) and the fluorescence of treated cells – proportional to the amount of lysozyme-Cy5 internalised – was quantified by flow cytometry analysis. Formulations were applied on top of Calu-3 cells and incubated for 3 h, a time that was considered sufficient to achieve measurable cell uptake while maintaining cell integrity, as previously shown by our group (Fowler et al., 2013b).

Firstly, targeted vitB_{12}-PEG_{3k}-polyGA nanocomplexes in suspension (0.5 mL, protein concentration 3 µg mL^{-1}) were applied on top of Calu-3 cell monolayers and incubated for 3 h at 37°C. Cells were then collected from the Transwell® inserts and analysed by flow cytometry. Results showed that targeted vitB_{12}-PEG_{3k}-polyGA nanocomplexes were able to significantly increase lysozyme uptake by Calu-3 cells when compared to both free lysozyme and non-targeted $mPEG_{2k}$-polyGA nanocomplexes, independently of the polymer architecture used, with lysozyme uptake increasing by 46% (Figure 4.5). Importantly, in a competitive inhibition study, cellular uptake of targeted nanocomplexes was

decreased to the level of non-targeted nanocomplexes, in the presence of an excess of free vitamin B_{12}. Taken together, these data were in line with previous studies observed with vitamin B_{12} polystyrene nanoparticles (Fowler et al., 2013b) and indicate that the uptake of the targeted nanocomplexes was receptor-mediated.

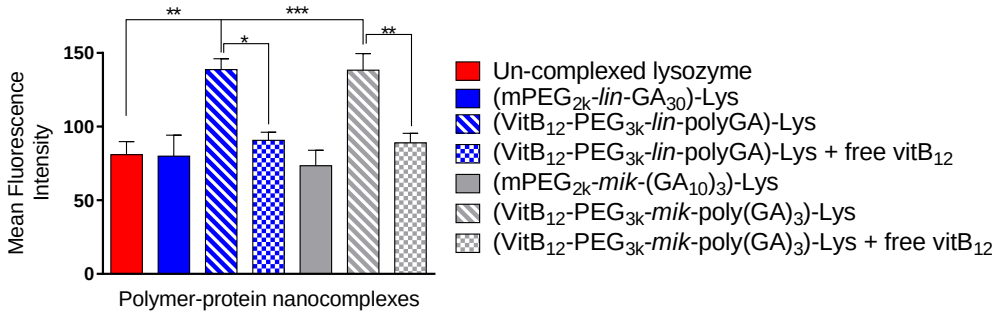


Figure 4.5. Cellular uptake in Calu-3 monolayers of un-complexed lysozyme compared to lysozyme complexed with targeted vitB$_{12}$-PEG$_{3k}$-polyGA copolymers alone, or in competition experiment with an excess of free vitamin B_{12}, and lysozyme complexed with non-targeted mPEG$_{2k}$-polyGA copolymers. All samples were added in solution on top of the cells. "Un-complexed lysozyme" corresponds to samples without polymers. One-way ANOVA was used for statistical analysis. ** $p < 0.01$, *** $p < 0.001$.

To further investigate the potential of these formulations to efficiently deliver proteins into the lung epithelium, targeted polymer-protein nanocomplexes were then formulated into dry powders. In Chapter 3, dry powder formulations composed of 6.6% (*w/w*) phosphate buffer salts, 10% (*w/w*) leucine and up to 100% (*w/w*) trehalose showed excellent aerodynamic properties – particle size (D_{50}) of ~ 2.5 µm and fine particle fraction between 60 and 70% –. Here, these excipients were therefore chosen to formulate targeted nanocomplexes-based dry powders. Once formulated, dry powders were directly sprayed on top of Calu-3 cell layers using four Transwell® inserts at once as shown in Figure 4.2. Particle size and particle distribution on the Transwell® inserts were confirmed

to be similar for all the formulations and for the four Transwell® inserts used in this study (Table 4.3 and Figure 4.6). Interestingly, the morphology of dry powders containing un-complexed lysozyme changed after spraying (Figure 4.7). However, copolymers were able to maintain the original spherical shape of the particles suggesting that PEG-polyGA copolymers can have an important effect on the stability of these dry powder formulations.

In uptake tests, formulations were then sprayed on top of Calu-3 cell monolayers, incubated 3 h at 37°C and analysed by flow cytometry as previously described. Results revealed that dry powders containing targeted vitB_{12}-PEG_{3k}-polyGA nanocomplexes enhanced lysozyme uptake compared to dry powders containing only lysozyme, or non-targeted mPEG_{2k}-polyGA nanocomplexes (Figure 4.8). These data were in line with those observed in cellular uptake studies using nanocomplex suspensions. This may suggest that dry powder formulations could disintegrate in the mucus layer secreted by Calu-3 cells, and release efficiently intact nanocomplexes as previously observed in the literature (Ruge et al., 2016). These results also correlate with the data observed in Chapter 3 where nanocomplexes were able to be efficiently released from dry powder formulations in an aqueous environment.

Table 4.3. Particle size (D_{90}) of dry powders after spraying them using a Penn-Century® device into Transwell® inserts. Four Transwell® inserts were used at once for each formulation. Each formulation was sprayed twice (2 mg per dose). All dry powder contain 6.6% (*w/w*) phosphate buffer salts, 10% (*w/w*) leucine and up to 100% (*w/w*) trehalose.

Dry powder	Transwell® insert 1 D_{90} (µm)	Transwell® insert 2 D_{90} (µm)	Transwell® insert 3 D_{90} (µm)	Transwell® insert 4 D_{90} (µm)
Free lysozyme	4.9	6.6	6.5	5.6
(mPEG$_{2k}$-*lin*-GA$_{30}$)-Lys	6.0	5.1	5.7	5.6
(mPEG$_{2k}$-*mik*-(GA$_{10}$)$_3$)-Lys	6.2	6.7	7.1	6.1
(vitB$_{12}$-PEG$_{3k}$-*lin*-polyGA)-Lys	4.9	4.8	7.3	6.4
(vitB$_{12}$-PEG$_{3k}$-*mik*-poly(GA)$_3$)-Lys	5.8	4.5	6.0	7.0

D_{90} represents the diameter below which 90% of the particle population lie.

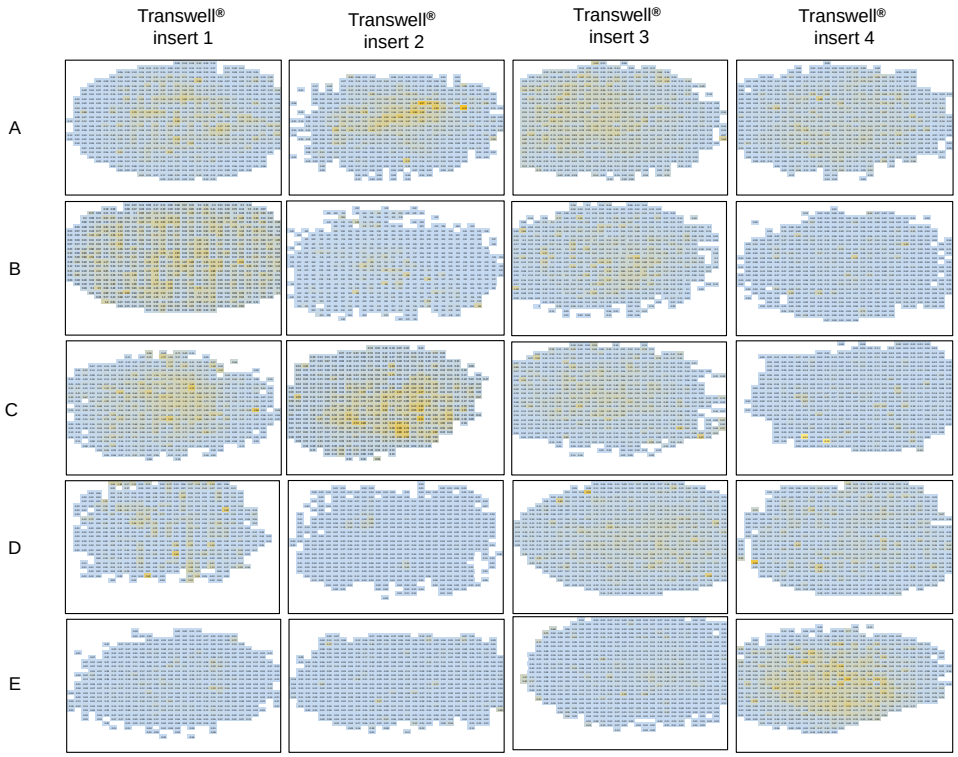


Figure 4.6. Dry powder distribution after spraying them using a Penn-Century® device onto Transwell® inserts. Four different Transwell® inserts were used at once for each formulation. Dry powders containing (A) un-complexed lysozyme, (B) mPEG$_{2k}$-*lin*-GA$_{30}$, (C) mPEG$_{2k}$-*mik*-(GA$_{10}$)$_3$, (D) vitB$_{12}$-PEG$_{3k}$-*lin*-polyGA and (E) vitB$_{12}$-PEG$_{3k}$-*mik*-poly(GA)$_3$-derived nanocomplexes. Each formulation was sprayed twice (2 mg per dose). Each square contains 900 small coloured images. These colours indicate the percentage of the Transwell® insert surface covered by particles. Blue: 0.01% of particles; orange: 5% particles; red: 10% particles. White small squares corresponds to 0% particles or focus issues with the microscope during the analysis. All dry powder contain 6.6% (*w/w*) phosphate buffer salts, 10% (*w/w*) leucine and up to 100% (*w/w*) trehalose.

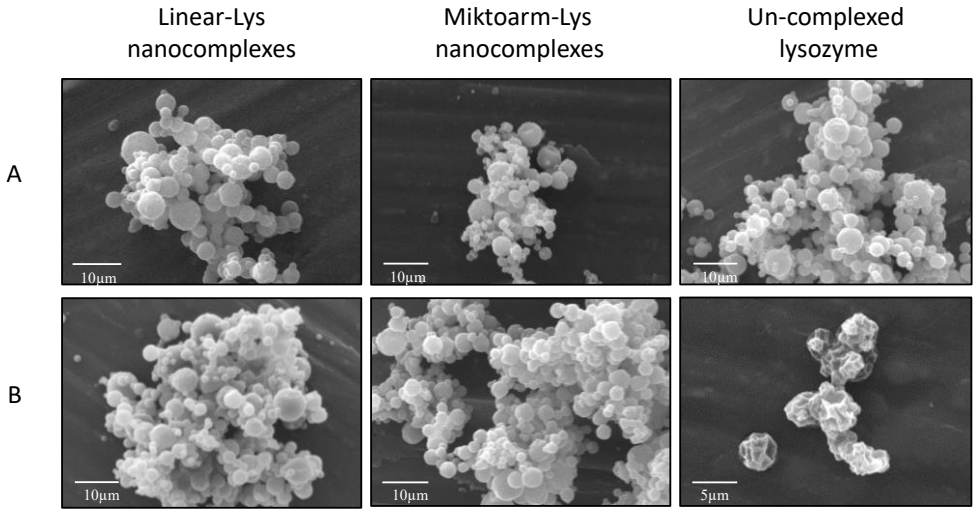


Figure 4.7. Representative scanning electron microscopy (SEM) images of dry powders before (A) and after (B) spraying them using a Penn-Century® device. "Un-complexed lysozyme" refers to formulations without copolymers. All dry powders contain 6.6% (*w/w*) phosphate salts, 10% (*w/w*) leucine and up to 100% (*w/w*) trehalose.

These results are, to the best of our knowledge, the first example where targeted polymer-protein nanocomplexes formulated into dry powder formulations, were able to increase protein uptake by the airway epithelium.

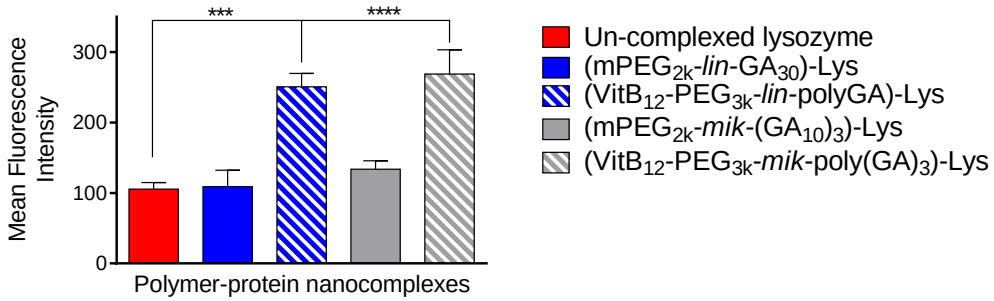


Figure 4.8. Cell uptake in Calu-3 cells of un-complexed lysozyme formulated into dry powders compared to lysozyme complexed with targeted vitB$_{12}$-PEG$_{3k}$-polyGA and non-targeted mPEG$_{2k}$-polyGA copolymers, both formulated into dry powders. All dry powder samples were directly applied on top of the Calu-3 cells grown in AIC conditions. "Un-complexed lysozyme" corresponds to dry powders without polymers. All dry powders contain 6.6% (*w/w*) phosphate salts, 10% (*w/w*) leucine and up to 100% (*w/w*) trehalose. One-way ANOVA was used for statistical analysis. *** $p < 0.001$, **** $p < 0.0001$.

4.3.3. Complement activation

The administration of protein therapeutics can produce undesirable immune responses which lead a decrease on the efficacy, anaphylaxis and sometimes life threatening autoimmunity (Baker et al., 2010). Complement activation system is a part of the innate immune system which is composed of a large number of different proteins. It enhances the ability to recognise and respond against pathogens, foreign particles and injured cells (Merle et al., 2015), inducing opsonisation and lysis of target cells (Noris and Remuzzi, 2013, Janeway, 2001). In addition, if activated, the complement system can induce unwanted side effects such as inflammation, pseudo-allergy and activation of cellular immune responses (Dobrovolskaia and McNeil, 2007, Zolnik et al., 2010).

As mentioned above, the lung may also act as local source of complement proteins (Pandya and Wilkes, 2014). However, in this study normal human serum was selected as a source of complement proteins, due to the ease of serum extraction compared to the extraction of complement proteins present in the human lungs. The ability of free lysozyme and lysozyme complexed with targeted nanocomplexes to activate the complement system was then evaluated. At the concentrations investigated (1.116 mg mL^{-1}), un-complexed lysozyme was found to activate the complement system to around 50% whilst targeted (vitB_{12}-PEG_{3k}-polyGA)-protein nanocomplexes decreased these values to 16 and 25% when linear or miktoarm copolymers were used, respectively (Figure 4.9). PEG is a well-known hydrophilic copolymer able to decrease

protein immunogenicity after polymer-protein conjugation (Filpula and Zhao, 2008). Therefore a diminished immunogenic response could be ascribed to the presence of PEG on the surface of these polymer-protein nanocomplexes. These results also suggest that the nanocomplexes investigated in this study could potentially decrease the immune response of immunogenic proteins. Interestingly, lysozyme complexed with linear copolymers showed lower immunogenicity than that observed with miktoarm copolymers probably due to better polymer-protein complexation, as shown in Chapter 2.

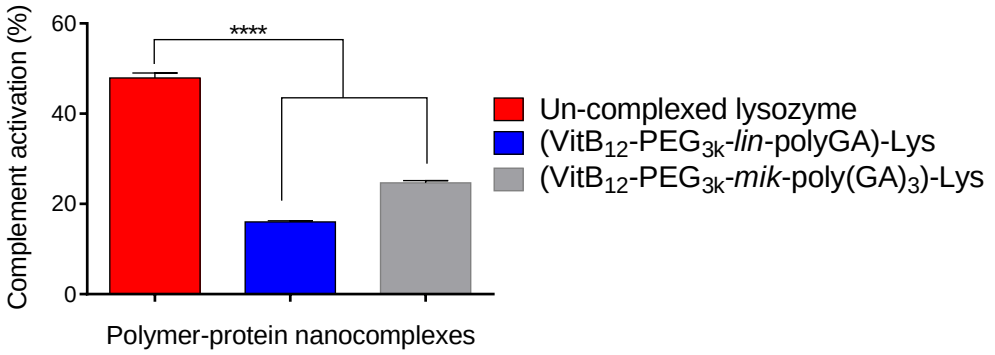


Figure 4.9. Complement activation at 37˚C by un-complexed lysozyme, (vitB$_{12}$-PEG$_{3k}$-*lin*-polyGA)-lysozyme and (vitB$_{12}$-PEG$_{3k}$-*mik*-poly(GA)$_3$)-lysozyme nanocomplexes. Lysozyme concentration was kept constant to 1116 µg mL^{-1} for all samples. "Un-complexed lysozyme" corresponds to formulations without copolymers. One-way ANOVA was used for statistical analysis. *** $p < 0.001$, **** $p < 0.0001$.

4.3.4. Local pulmonary tolerance of polymer-protein nanocomplexes-based dry powder formulations in healthy mice

One of the aims of this thesis work was to develop polymer-protein nanocomplexes-based dry powder formulations with a potential safe profile for inhalation. Here, we evaluated the safety profile of these dry powders *in vivo*, assessed in healthy mice by analysis of differential cell count and cytokine IL-1β, IL-6 and TNF-α concentrations in bronchoalveolar lavage fluids after dry

powder administration three times a week for three consecutive weeks. These experiments were materially carried out by our collaborators Drs Remi Rosière, Nathalie Wauthoz and Karim Amighi at the University of Brussels (Belgium), and discussed here for completeness.

It has been suggested that the presence of poorly water-soluble species such as leucine in inhaled formulations may induce local irritation and pro-inflammatory effects in the respiratory tract (Jones et al., 2014, Kumar et al., 2014). Also, the delivery of proteins into the lungs can in some cases induce immunogenicity, local irritation and toxicity (Fahy et al., 1999). Therefore, preliminary control experiments to study the pulmonary tolerance of unlabeled dry powder UDP (no polymer, no protein) and UDP-P formulations (with un-complexed lysozyme, no polymer) with 10% w/w leucine (see full composition in Table 4.2) in healthy mice was investigated together with UDP-L1 formulations (with targeted nanocomplexes).

Firstly, following endotracheal administration of dry powder formulations the potential inflammatory response was investigated by quantification of the concentration of IL-1β, IL-6, and TNF-α cytokines in the epithelial lining fluid of the lungs. These are pro-inflammatory cytokines that are implicated in pain, inflammation and autoimmune conditions (Gabay, 2006, Ren and Torres, 2009). As expected, mice treated with lipopolysaccharides (LPS, outer surface membrane components found in most Gram-negative bacteria, which are strong stimulators of innate or natural immunity in many eukaryotic species ranging from insects to humans (Alexander and Rietschel, 2001), positive

control) generated a significant increase of IL-1β, IL-6, and TNF-α compared to untreated mice (Figure 4.10). However, the levels of the three cytokines did not increase following endotracheal administration of dry powder formulations, compared to negative controls (untreated mice). These results were very encouraging as the presence of polymers in the lungs has previously shown to induce inflammatory responses (Beyerle et al., 2011).

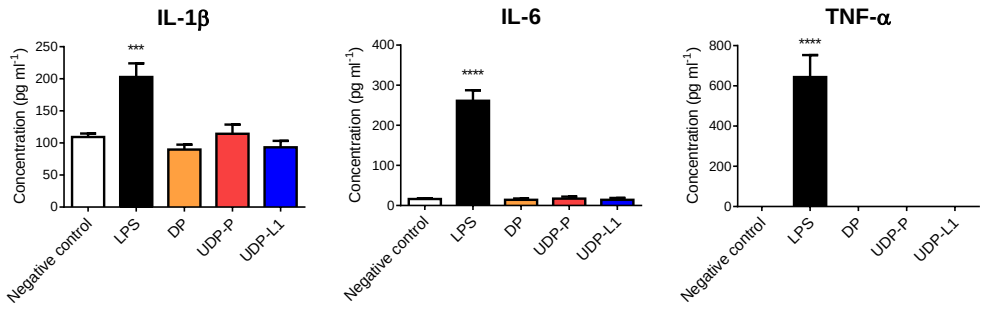


Figure 4.10. Pro-inflammatory cytokine IL-1β, IL-6, and TNF-α gene expression in lung tissues, following endotracheal administration of dry powder formulations. Results are shown for untreated mice, (negative control) or those treated with LPS (positive control), empty DP (no polymer, no protein), UDP-P (no polymer) and UDP-L1 (with targeted nanocomplexes). One-way ANOVA was used for statistical analysis. *** $p < 0.001$, **** $p < 0.0001$.

To further investigate the suitability of these dry powder formulations for pulmonary drug delivery, the differential cell count on alveolar macrophages (AM), polymorphonuclear neutrophils (PMN) and lymphocytes (LM) was also performed. Following LPS administration, the number of AM dramatically decreased to around 50% when compared to untreated mice, whereas the percentage of PMN increased to around 50%, indicating a pro-inflammatory reaction. However, all the dry powder formulations showed values for AM, PMN and LM in line to those found in untreated mice. These data were also qualitatively confirmed by optical microscopy (Figure 4.11).

Taken together these preliminary results suggested that (vitB_{12}-PEG-polyGA)-lysozyme nanocomplexes-based dry powder formulations (UDP-L1) were well-tolerated locally after dry powder administrations in healthy mice three times a week for three consecutive weeks, with no sign of toxicity or lung inflammation observed.

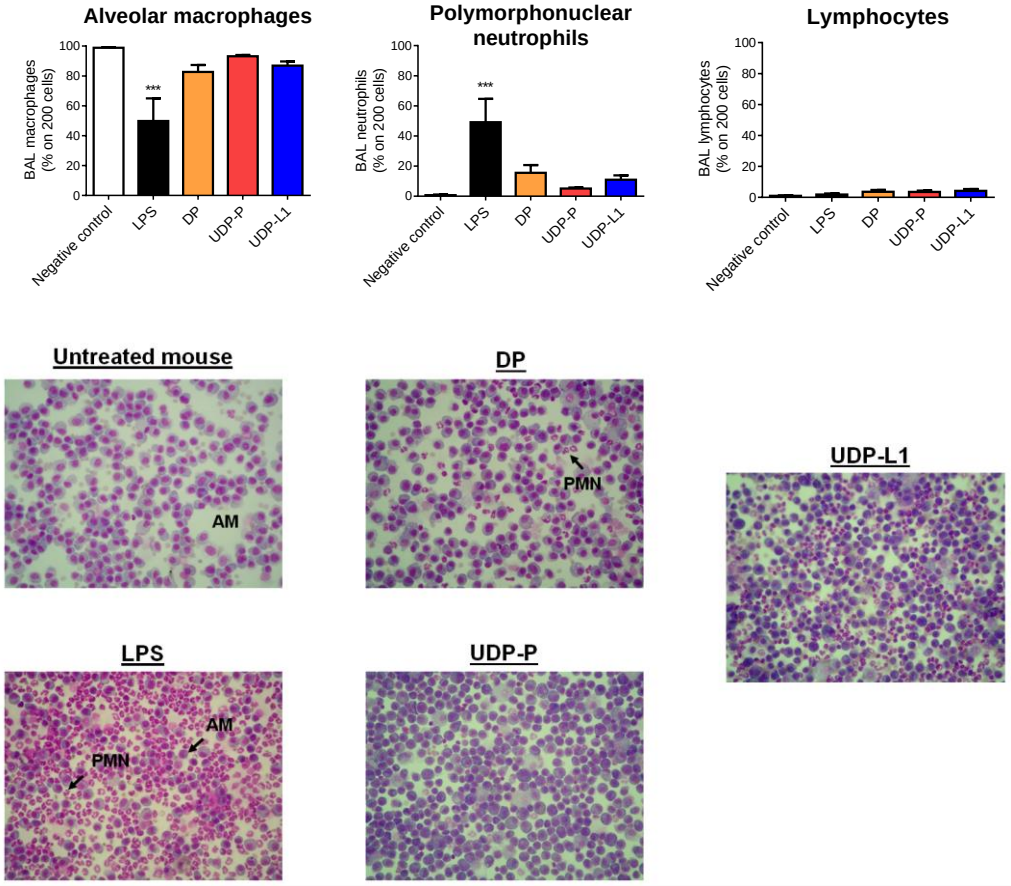


Figure 4.11. Bronchoalveolar lavage fluid analysis: differential cell count and representative images of the different cells found in the bronchoalveolar lavage fluid following endotracheal administration in healthy mice of dry powder formulations three times a week for three consecutive weeks (2 mg per dose). Mice were not treated (negative control) or treated with LPS (positive control), empty UDP (no polymer, no protein), UDP-P (no polymer) and UDP-L1 (with targeted nanocomplexes). One-way ANOVA was used for statistical analysis. *** $p < 0.001$, **** $p < 0.0001$.

4.3.5. *In vivo* pulmonary deposition and retention of polymer-protein nanocomplexes-based dry powder formulations in healthy mice

As discussed in Chapter 1, the therapeutic efficacy of pulmonarly-delivered biopharmaceuticals can be considerably decreased due to different particle removing mechanisms present in the lungs. Drug delivery systems can overcome the mucociliary escalator, proteolytic degradation and macrophage capture (El-Sherbiny et al., 2015). Therefore, the time of exposure of lung tissue to relevant protein therapeutics and the potential to exert their therapeutic action can be significantly increased. In this work, we evaluated the ability of targeted (vitB_{12}-PEG-polyGA)-lysozyme nanocomplexes to increase the deposition and the retention of proteins in the lungs with minimal toxicity.

Accordingly, 2 mg dose of each dry powder formulation were administered to healthy mice by the endotracheal route through a pulmonary delivery device. Under these experimental conditions, good uniformity in terms of mass delivered (RSD ≤ 25%) and optimal particle size (D_{50} ~4 μm) for efficient delivery into the mice were achieved for all formulations (Table 4.1). Figure 4.12 shows the lung distribution of Cy5-labelled lysozyme after pulmonary administration of labelled dry powder LDP-P (with un-complexed protein, no copolymer), LDP-L2 (with non-targeted nanocomplexes) and LDP-L1 (with targeted nanocomplexes) formulations. Immediately after endotracheal administration of dry powder formulations (time 0 h), mice were sacrificed and lungs were removed. Five non-serial cryo-sections of 7 μm per lung were prepared and then analysed by confocal microscopy. Images revealed that lysozyme was

homogeneously distributed in the lungs independently of the formulation used. This was in line with the literature where dry powder formulations with good aerodynamic properties were able to homogeneously distribute active ingredients in the lungs (Duret et al., 2012). However, the amount of lysozyme 3 h after the administration of dry powder formulations was significantly reduced for formulations without copolymers (LDP-P) probably due to pulmonary clearance mechanisms. No difference between formulations with targeted (LDP-L1) and non-targeted (LDP-L2) nanocomplexes was observed. However, after 14 h following treatment, LDP-L1 formulations (with targeted nanocomplexes) appeared to yield the best protein lung retention (Figure 4.12).

Whilst these experiments provided an initial estimation of protein lung retention, further studies will be needed to better understand protein lung distribution, and potential routes for cell uptake. However, taken together these initial *in vivo* experiments, suggested that targeted polymer-protein nanocomplexes may lead to a more efficient retention of lysozyme protein cargo in the lungs, compared to non-targeted nanocomplexes and un-complexed lysozyme-based formulations.

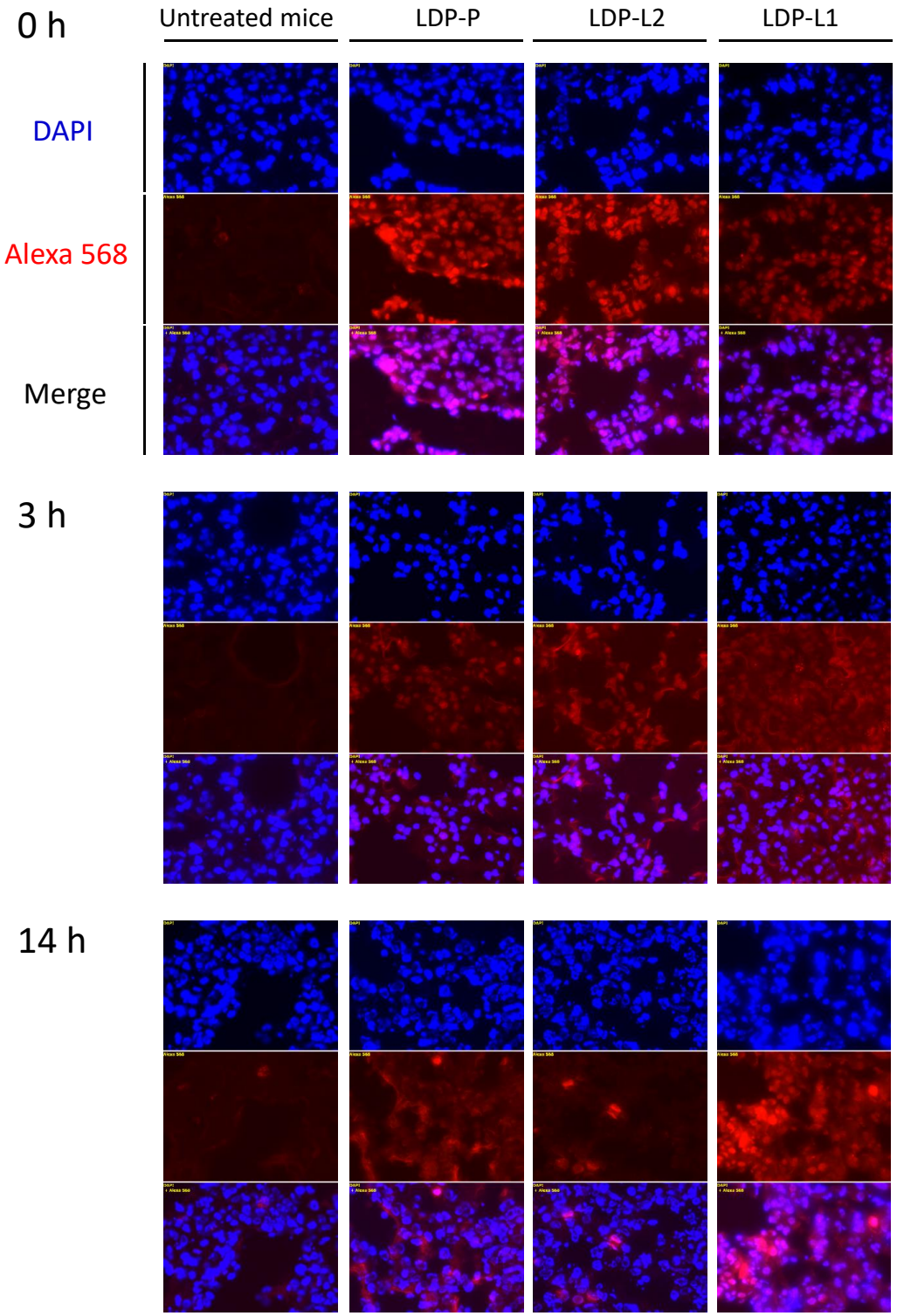


Figure 4.12. Distribution of fluorescent lysozyme in the lungs of healthy mice after 0, 3 and 14 h after pulmonary administration. Examples of a 7-µm longitudinal lung cryo-section that was observed using a fluorescent microscope at 200 x magnification. The images show the distribution of red labelled lysozyme-Cy5 (on an Alexa Fluor 568 filter) in the blue fluorescent lung tissue (on a DAPI filter) of healthy mice after administration of 2 mg dry powder formulations: (i) LDP-L1 (targeted nanocomplexes), (ii) LDP-L2 (non-targeted nanocomplexes) and (iii) LDP-P (no polymer) using the pulmonary delivery device.

4.4. Concluding remarks

In this part of our work, we have synthesised new targeted linear vitB_{12}-PEG_{3k}-*lin*-polyGA and miktoarm vitB_{12}-PEG_{3k}-*mik*-poly$(GA)_3$ copolymers to potentially increase the delivery of proteins into the lung epithelium.

Nanoparticle Tracking Analysis (NTA) showed that these copolymers were able to efficiently complex lysozyme model protein giving non-covalent conjugates with particle size in the 50-200 nm range. These nanocomplexes were then successfully formulated into dry powders containing 10% (*w/w*) leucine, 6.6% (*w/w*) buffer salts and up to 100% (*w/w*) trehalose as the main excipients.

Uptake studies on human airway epithelial cell line Calu-3 using both nanocomplex suspensions and dry powder formulations showed that targeted nanocomplexes were able to significantly increase lysozyme cell internalisation, compared to both non-targeted complexes and free lysozyme. Initial *in vivo* experiments suggested that targeted nanocomplexes were able to retain lysozyme in the lungs after 14 h treatment.

Finally, these dry powder formulations were well-tolerated in the lungs of healthy mice after chronic treatment as cytokine concentration (IL-1β, IL-6, and TNF-α) and differential cell counts (alveolar macrophages, polymorphonuclear neutrophils and lymphocytes) were similar to those found in untreated mice. Also, nanocomplexes were able to significantly decrease the immunogenicity caused by un-complexed lysozyme as assessed by the complement activation *in vitro* assay.

4.5. References

ALEXANDER, C. & RIETSCHEL, E. T. 2001. Bacterial lipopolysaccharides and innate immunity. *J Endotoxin Res,* 7**,** 167-202.

BAKER, M. P., REYNOLDS, H. M., LUMICISI, B. & BRYSON, C. J. 2010. Immunogenicity of protein therapeutics: The key causes, consequences and challenges. *Self Nonself,* 1**,** 314-322.

BEYERLE, A., BRAUN, A., BANERJEE, A., ERCAL, N., EICKELBERG, O., KISSEL, T. H. & STOEGER, T. 2011. Inflammatory responses to pulmonary application of PEI-based siRNA nanocarriers in mice. *Biomaterials,* 32**,** 8694-8701.

BIVAS-BENITA, M., ZWIER, R., JUNGINGER, H. E. & BORCHARD, G. 2005. Non-invasive pulmonary aerosol delivery in mice by the endotracheal route. *Eur J Pharm Biopharm,* 61**,** 214-8.

BOSE, S. & SEETHARAM, B. 1997. Effect of disulfide bonds of transcobalamin II receptor on its activity and basolateral targeting in human intestinal epithelial Caco-2 cells. *J Biol Chem,* 272**,** 20920-8.

BOSE, S., SEETHARAM, S., DAHMS, N. M. & SEETHARAM, B. 1997. Bipolar functional expression of transcobalamin II receptor in human intestinal epithelial Caco-2 cells. *J Biol Chem,* 272**,** 3538-43.

CHALASANI, K. B., RUSSELL-JONES, G. J., JAIN, A. K., DIWAN, P. V. & JAIN, S. K. 2007a. Effective oral delivery of insulin in animal models using vitamin B12-coated dextran nanoparticles. *J Control Release,* 122**,** 141-50.

CHALASANI, K. B., RUSSELL-JONES, G. J., YANDRAPU, S. K., DIWAN, P. V. & JAIN, S. K. 2007b. A novel vitamin B12-nanosphere conjugate carrier system for peroral delivery of insulin. *J Control Release,* 117**,** 421-9.

CINGOLANI, E. 2017. *In vitro investigation of factors affecting the fate of dry powders in the lungs.*

DIX, C. J., HASSAN, I. F., OBRAY, H. Y., SHAH, R. & WILSON, G. 1990. The transport of vitamin B12 through polarized monolayers of Caco-2 cells. *Gastroenterology,* 98**,** 1272-9.

DOBROVOLSKAIA, M. A. & MCNEIL, S. E. 2007. Immunological properties of engineered nanomaterials. *Nat Nano,* 2**,** 469-478.

DONDONI, A. 2008. The emergence of thiol-ene coupling as a click process for materials and bioorganic chemistry. *Angew Chem Int Ed Engl,* 47**,** 8995-7.

DURET, C., WAUTHOZ, N., MERLOS, R., GOOLE, J., MARIS, C., ROLAND, I., SEBTI, T., VANDERBIST, F. & AMIGHI, K. 2012. In vitro and in vivo evaluation of a dry powder endotracheal insufflator device for use in dose-dependent preclinical studies in mice. *European Journal of Pharmaceutics and Biopharmaceutics,* 81**,** 627-634.

EL-SHERBINY, I. M., EL-BAZ, N. M. & YACOUB, M. H. 2015. Inhaled nano- and microparticles for drug delivery. *Global Cardiology Science & Practice,* 2015**,** 2.

FAHY, J. V., COCKCROFT, D. W., BOULET, L. P., WONG, H. H., DESCHESNES, F., DAVIS, E. E., RUPPEL, J., SU, J. Q. & ADELMAN, D. C. 1999. Effect of aerosolized anti-IgE (E25) on airway responses to inhaled allergen in asthmatic subjects. *Am J Respir Crit Care Med,* 160**,** 1023-7.

FILPULA, D. & ZHAO, H. 2008. Releasable PEGylation of proteins with customized linkers. *Advanced Drug Delivery Reviews,* 60**,** 29-49.

FORBES, B. & EHRHARDT, C. 2005. Human respiratory epithelial cell culture for drug delivery applications. *European Journal of Pharmaceutics and Biopharmaceutics,* 60**,** 193-205.

FOSTER, K. A., AVERY, M. L., YAZDANIAN, M. & AUDUS, K. L. 2000. Characterization of the Calu-3 cell line as a tool to screen pulmonary drug delivery. *International Journal of Pharmaceutics,* 208**,** 1-11.

FOWLER, R., VLLASALIU, D., FALCONE, F. H., GARNETT, M., SMITH, B., HORSLEY, H., ALEXANDER, C. & STOLNIK, S. 2013a. Uptake and transport of B12-conjugated nanoparticles in airway epithelium. *Journal of Controlled Release,* 172**,** 374-381.

FOWLER, R., VLLASALIU, D., FALCONE, F. H., GARNETT, M., SMITH, B., HORSLEY, H., ALEXANDER, C. & STOLNIK, S. 2013b. Uptake and transport of B(12)-conjugated nanoparticles in airway epithelium(). *Journal of Controlled Release,* 172**,** 374-381.

FOWLER, R., VLLASALIU, D., TRILLO, F. F., GARNETT, M., ALEXANDER, C., HORSLEY, H., SMITH, B., WHITCOMBE, I., EATON, M. & STOLNIK, S. 2013c. Nanoparticle transport in epithelial cells: pathway switching through bioconjugation. *Small,* 9**,** 3282-94.

GABAY, C. 2006. Interleukin-6 and chronic inflammation. *Arthritis Research & Therapy,* 8**,** S3-S3.

GARCIA-VERDUGO, I., DESCAMPS, D., CHIGNARD, M., TOUQUI, L. & SALLENAVE, J.-M. 2010. Lung protease/anti-protease network and modulation of mucus production and surfactant activity. *Biochimie,* 92**,** 1608-1617.

GRAINGER, C. I., GREENWELL, L. L., LOCKLEY, D. J., MARTIN, G. P. & FORBES, B. 2006. Culture of Calu-3 cells at the air interface provides a representative model of the airway epithelial barrier. *Pharm Res,* 23**,** 1482-90.

HABRAKEN, G. J. M., PEETERS, M., DIETZ, C. H. J. T., KONING, C. E. & HEISE, A. 2010. How controlled and versatile is N-carboxy anhydride (NCA) polymerization at 0 °C? Effect of temperature on homo-, block- and graft (co)polymerization. *Polymer Chemistry,* 1**,** 514.

HUANG, Y. C., VIEIRA, A., HUANG, K. L., YEH, M. K. & CHIANG, C. H. 2005. Pulmonary inflammation caused by chitosan microparticles. *Journal of Biomedical Materials Research Part A,* 75A**,** 283-287.

HUSSAIN, A., ARNOLD, J. J., KHAN, M. A. & AHSAN, F. 2004. Absorption enhancers in pulmonary protein delivery. *Journal of Controlled Release,* 94**,** 15-24.

JANEWAY, C. A. 2001. *Immunobiology: The Immune System in Health and Disease*, Churchill Livingstone.

JONES, M. C., JONES, S. A., RIFFO-VASQUEZ, Y., SPINA, D., HOFFMAN, E., MORGAN, A., PATEL, A., PAGE, C., FORBES, B. & DAILEY, L. A. 2014. Quantitative assessment of nanoparticle surface hydrophobicity and its influence on pulmonary biocompatibility. *J Control Release,* 183**,** 94-104.

KAZATCHKINE, M., HAUPTMANN, G. & NYDEGGER, U. 1986. Techniques du complement. Paris: Inserm. 22-23.

KOBAYASHI, S., KONDO, S. & JUNI, K. 1994. Study on pulmonary delivery of salmon calcitonin in rats: effects of protease inhibitors and absorption enhancers. *Pharm Res,* 11**,** 1239-43.

KOBAYASHI, S., KONDO, S. & JUNI, K. 1996. Pulmonary delivery of salmon calcitonin dry powders containing absorption enhancers in rats. *Pharm Res,* 13**,** 80-3.

KOLB, H. C., FINN, M. G. & SHARPLESS, K. B. 2001. Click Chemistry: Diverse Chemical Function from a Few Good Reactions. *Angew Chem Int Ed Engl,* 40**,** 2004-2021.

KREFT, M. E., JERMAN, U. D., LASIČ, E., HEVIR-KENE, N., RIŽNER, T. L., PETERNEL, L. & KRISTAN, K. 2015. The characterization of the human cell line Calu-3 under different culture conditions and its use as an optimized in vitro model to investigate bronchial epithelial function. *European Journal of Pharmaceutical Sciences,* 69**,** 1-9.

KUMAR, A., DAILEY, L. A. & FORBES, B. 2014. Lost in translation: what is stopping inhaled nanomedicines from realizing their potential? *Ther Deliv,* 5**,** 757-61.

MACHIDA, M., HAYASHI, M. & AWAZU, S. 2000. The effects of absorption enhancers on the pulmonary absorption of recombinant human granulocyte colony-stimulating factor (rhG-CSF) in rats. *Biol Pharm Bull,* 23**,** 84-6.

MANTOVANI, G., LADMIRAL, V., TAO, L. & HADDLETON, D. M. 2005. One-pot tandem living radical polymerisation-Huisgens cycloaddition process ("click") catalysed by N-alkyl-2-pyridylmethanimine/Cu(i)Br complexes. *Chemical Communications***,** 2089-2091.

MERLE, N. S., CHURCH, S. E., FREMEAUX-BACCHI, V. & ROUMENINA, L. T. 2015. Complement System Part I - Molecular Mechanisms of Activation and Regulation. *Front Immunol,* 6**,** 262.

MORADI, E., VLLASALIU, D., GARNETT, M., FALCONE, F. & STOLNIK, S. 2012. Ligand density and clustering effects on endocytosis of folate modified nanoparticles. *RSC Advances,* 2**,** 3025-3033.

NORIS, M. & REMUZZI, G. 2013. Overview of complement activation and regulation. *Semin Nephrol,* 33**,** 479-92.

PANDYA, P. H. & WILKES, D. S. 2014. Complement system in lung disease. *Am J Respir Cell Mol Biol,* 51**,** 467-73.

PARK, S.-H., KWON, J.-H., LIM, S.-H., PARK, H. W. & KIM, C.-W. 2007a. Characterization of human insulin microcrystals and their absorption enhancement by protease inhibitors in rat lungs. *International Journal of Pharmaceutics,* 339**,** 205-212.

PARK, S. H., KWON, J. H., LIM, S. H., PARK, H. W. & KIM, C. W. 2007b. Characterization of human insulin microcrystals and their absorption enhancement by protease inhibitors in rat lungs. *Int J Pharm,* 339**,** 205-12.

PONS, L., GUY, M., LAMBERT, D., HATIER, R. & GUEANT, J. 2000. Transcytosis and coenzymatic conversion of [(57)Co]cobalamin bound to either

endogenous transcobalamin II or exogenous intrinsic factor in caco-2 cells. *Cell Physiol Biochem,* 10**,** 135-48.

PRIDGEN, E. M., ALEXIS, F., KUO, T. T., LEVY-NISSENBAUM, E., KARNIK, R., BLUMBERG, R. S., LANGER, R. & FAROKHZAD, O. C. 2013. Transepithelial Transport of Fc -Targeted Nanoparticles by the Neonatal Fc Receptor for Oral Delivery. *Science translational medicine,* 5**,** 213ra167-213ra167.

RAMANUJAM, K. S., SEETHARAM, S., RAMASAMY, M. & SEETHARAM, B. 1991. Expression of cobalamin transport proteins and cobalamin transcytosis by colon adenocarcinoma cells. *Am J Physiol,* 260**,** G416-22.

REN, K. & TORRES, R. 2009. Role of interleukin-1beta during pain and inflammation. *Brain Res Rev,* 60**,** 57-64.

RESPAUD, R., VECELLIO, L., DIOT, P. & HEUZÉ-VOURC'H, N. 2015. Nebulization as a delivery method for mAbs in respiratory diseases. *Expert Opinion on Drug Delivery,* 12**,** 1027-1039.

ROGER, E., KALSCHEUER, S., KIRTANE, A., GURU, B. R., GRILL, A. E., WHITTUM-HUDSON, J. & PANYAM, J. 2012. Folic acid-Functionalized Nanoparticles for Enhanced Oral Drug Delivery. *Molecular pharmaceutics,* 9**,** 2103-2110.

ROSIERE, R., VAN WOENSEL, M., MATHIEU, V., LANGER, I., MATHIVET, T., VERMEERSCH, M., AMIGHI, K. & WAUTHOZ, N. 2016. Development and evaluation of well-tolerated and tumor-penetrating polymeric micelle-based dry powders for inhaled anti-cancer chemotherapy. *Int J Pharm,* 501**,** 148-59.

RUGE, C. A., BOHR, A., BECK-BROICHSITTER, M., NICOLAS, V., TSAPIS, N. & FATTAL, E. 2016. Disintegration of nano-embedded microparticles after deposition on mucus: A mechanistic study. *Colloids and Surfaces B: Biointerfaces,* 139**,** 219-227.

RUSSELL-JONES, G. J., ARTHUR, L. & WALKER, H. 1999. Vitamin B12-mediated transport of nanoparticles across Caco-2 cells. *Int J Pharm,* 179**,** 247-55.

RUSSELL-JONES, G. J., WESTWOOD, S. W. & HABBERFIELD, A. D. 1995. Vitamin B12 mediated oral delivery systems for granulocyte-colony stimulating factor and erythropoietin. *Bioconjug Chem,* 6**,** 459-65.

SAEED, A. O., MAGNUSSON, J. P., MORADI, E., SOLIMAN, M., WANG, W., STOLNIK, S., THURECHT, K. J., HOWDLE, S. M. & ALEXANDER, C. 2011. Modular construction of multifunctional bioresponsive cell-targeted nanoparticles for gene delivery. *Bioconjug Chem,* 22**,** 156-68.

SAHALI, D., MULLIEZ, N., CHATELET, F., LAURENT-WINTER, C., CITADELLE, D., ROUX, C., RONCO, P. & VERROUST, P. 1992. Coexpression in humans by kidney and fetal envelopes of a 280 kDa-coated pit-restricted protein. Similarity with the murine target of teratogenic antibodies. *Am J Pathol,* 140**,** 33-44.

STRUNK, R. C., EIDLEN, D. M. & MASON, R. J. 1988. Pulmonary alveolar type II epithelial cells synthesize and secrete proteins of the classical and alternative complement pathways. *J Clin Invest,* 81**,** 1419-26.

TIWARI, V. K., MISHRA, B. B., MISHRA, K. B., MISHRA, N., SINGH, A. S. & CHEN, X. 2016. Cu-Catalyzed Click Reaction in Carbohydrate Chemistry. *Chemical Reviews,* 116**,** 3086-3240.

TUMA, P. & HUBBARD, A. L. 2003. Transcytosis: crossing cellular barriers. *Physiol Rev,* 83**,** 871-932.

VARSANO, S., KAMINSKY, M., KAISER, M. & RASHKOVSKY, L. 2000. Generation of complement C3 and expression of cell membrane complement inhibitory proteins by human bronchial epithelium cell line. *Thorax,* 55**,** 364-9.

VOLANAKIS, J. E. 1995. Transcriptional regulation of complement genes. *Annu Rev Immunol,* 13**,** 277-305.

VORTHERMS, A. R., KAHKOSKA, A. R., RABIDEAU, A. E., ZUBIETA, J., ANDERSEN, L. L., MADSEN, M. & DOYLE, R. P. 2011. A water soluble vitamin B12-ReI fluorescent conjugate for cell uptake screens: use in the confirmation of cubilin in the lung cancer line A549. *Chem Commun (Camb),* 47**,** 9792-4.

ZOLNIK, B. S., GONZALEZ-FERNANDEZ, A., SADRIEH, N. & DOBROVOLSKAIA, M. A. 2010. Nanoparticles and the immune system. *Endocrinology,* 151**,** 458-65.

CHAPTER 5

Concluding remarks and Future prospects

5.1. Concluding remarks and Future prospects

Biopharmaceuticals, especially protein-based products, are the fastest growing part of the pharmaceutical industry, with an annual growth rate of more than 8% (Otto et al., December 2014). Typically, proteins are delivered by parenteral administration, which is an invasive route that can lead to a reduced acceptance by patients (Klingler et al., 2009, Amidi et al., 2010). Alternatively, pulmonary delivery is receiving increasing attention as non-invasive route for the delivery of protein and peptide therapeutics, to treat both local and systemic diseases. However, the lungs present different physiological and immunological barriers that need to be overcome to achieve effective drug delivery (Depreter et al., 2013).

Polymer-based nanosystems are a promising strategy to address these challenges, as they can potentially protect proteins from degradation, enhance cellular uptake and reduce their immunogenicity. Poly(ethylene glycol) (PEG) has been covalently conjugated to a number of protein therapeutics, to give PEGylated macromolecular drugs, some of which have been on the market now for over two decades. However, this approach it is not suitable for all proteins as it can lead to reduced therapeutic efficacy. Within this context, the present work has aimed at developing an alternative approach where the added polymer could be only temporarily conjugated to a protein substrate which ideally would be then released at the required bodily target.

In Chapter 2, a family of structurally related block copolymers of $mPEG_{2k}$ - poly(glutamic acid) with linear A-B ($mPEG_{2k}$-*lin*-polyGA) and miktoarm A-B_3 ($mPEG_{2k}$-*mik*-$(polyGA)_3$) structure was synthesised by NCA polymerisation. PEG was chosen in this work to infer steric stabilisation to polymer-protein complexes and poly(glutamic acid) anionic blocks were utilised to complex positively charged amino acids in protein structure. Lysozyme, due to its high isoelectric point and stability in solution, was chosen as a protein model to assess the ability of these copolymers to bind proteins. Gel electrophoresis showed that for copolymers with the same number of glutamic acid repeating units, polymers with linear architecture were more efficient than their miktoarm analogues to complex lysozyme model protein. Polymer-protein complexes possessed particle size between 50 and 200 nm, independently from the polymer architecture. Importantly, upon polymer complexation the protein integrity appears to be conserved, and no detectable denaturation or reduced activity after de-complexation was observed. Also, this family of copolymers showed biocompatibility at concentrations up to 200 μg mL^{-1}, as assessed by MTS, LDH and Annexin V-FITC/propidium iodide apoptotic assays using A549 and Calu-3 cell lines.

Proteins are not always stable in aqueous solutions, and many degradation mechanisms are believed to be water-mediated. ($mPEG_{2k}$-polyGA)-lysozyme nanocomplexes were therefore incorporated into dry powder formulations as described in Chapter 3. To be efficiently delivered into the lungs, dry powders must possess specific aerodynamic diameters. To this aim, the effect of aerosol

excipients such as trehalose, mannitol and leucine was investigated. Excellent aerodynamic properties were found for formulations containing trehalose, leucine and polymer-protein nanocomplexes with fine particle fraction (FPF) values as high as 68%. In aqueous medium, dry powders rapidly disintegrated into the original polymer-protein nanocomplexes with an important ability to provide protection to the protein towards proteolytic degradation. Due to the difficulty of reproducing the lung conditions, a model polyionic macromolecule (poly(allyl amine)) and a model proteolytic enzyme (trypsin) were chosen in these studies to promote complex disassembly and investigate the ability of these complexes to protect proteins from proteolytic degradation. Further experiments with more complex systems able to reproduce the complexity of the respiratory system will be required to confirm these data.

After the optimisation of dry powder formulations, the next step was to investigate the ability of these complexes to deliver lysozyme into the airway epithelium and evaluate their immunogenic profile. To explore strategies potentially able to increase cell uptake of protein drug cargoes, $mPEG_{2k}$-polyGA were successfully modified with vitamin B_{12} ligand and the resulting functional copolymers utilised to assemble targeted polymer-protein complexes (Chapter 4). ($VitB_{12}$-PEG_{3k}-polyGA)-derived complexes were applied to Calu-3 cell monolayers and a significant increase of lysozyme uptake was observed compared to non-targeted nanocomplex or un-complexed lysozyme formulations. Also, *in vivo* experiments revealed that unlike non-targeted particles and lysozyme controls, $vitB_{12}$-PEG_{3k}-polyGA copolymers were able to

retain lysozyme in the lungs after 14 h treatment. Finally, (vitB_{12}-PEG_{3k}-polyGA)-lysozyme nanocomplexes-based dry powder formulations were well tolerated locally after intratracheal administration in healthy mice three times a week for three consecutive weeks, with no sign of toxicity or lung inflammation observed.

In summary, in this thesis we have developed a novel family of PEG-polyGA copolymers which are able to efficiently complex lysozyme model protein. These complexes can be incorporated into dry powder formulations with a crucial ability to protect proteins from proteolytic enzymes, increase protein cellular uptake in the lung epithelium and retain proteins in the lungs with minimal toxicity.

mPEG_{2k}-*lin*-GA_{30} copolymers showed the best characteristics for the delivery of lysozyme into the lungs. However, different copolymer lengths and/or architectures might be more appropriate for other types of protein therapeutics, thus a case-by-case optimisation of polymer chemistry and topology will likely be needed for the complexation of specific protein therapeutics.

Future work will focus on the development of new (PEG-polyGA)-derived complexes with new protein models and the assessment of their therapeutic effect on both *in vitro* and *in vivo* models. Also, the stability of polymer-protein complexes in the lungs should be investigated. The technology developed here appears to be general and applicable to other protein substrates. Preliminary

results have shown that PEG-polyGA copolymers are also able to complex other model proteins such as RNAse A. Ribonucleases are known to cleave ribonucleic acids, causing cell death. RNAse, is a member of this family, however it shows poor *in vitro* activity due to very poor cell uptake. In initial studies, not included in this thesis, we evaluated the ability of vitB_{12}-PEG_{3k}-polyGA copolymers to enhance the cell internalisation of RNAse A to selected cell lines. Complexation between (PEG-polyGA) copolymers and RNAse A was confirmed by NTA analysis, to give (PEG-polyGA)-lysozyme nanocomplexes with sizes in the 50-200 nm range (Figure 5.1). Cytotoxicity to Calu-3 cells was then evaluated by MTS assay. While un-complexed RNAse A was not toxic to Calu-3 cells, both linear and miktoarm (vitB_{12}-PEG_{3k}-polyGA)-derived complexes were able to promote cytosolic delivery of biologically active RNAse A, increasing cell death especially after 24 h treatment (Figure 5.2). In this case, no significant differences were observed between miktoarm and linear copolymers.

Taken together, the results discussed in this thesis and the preliminary results briefly summarised in this final chapter suggest that this technology could potentially be utilised as a general approach for the formulation and delivery of a wide range of protein therapeutics.

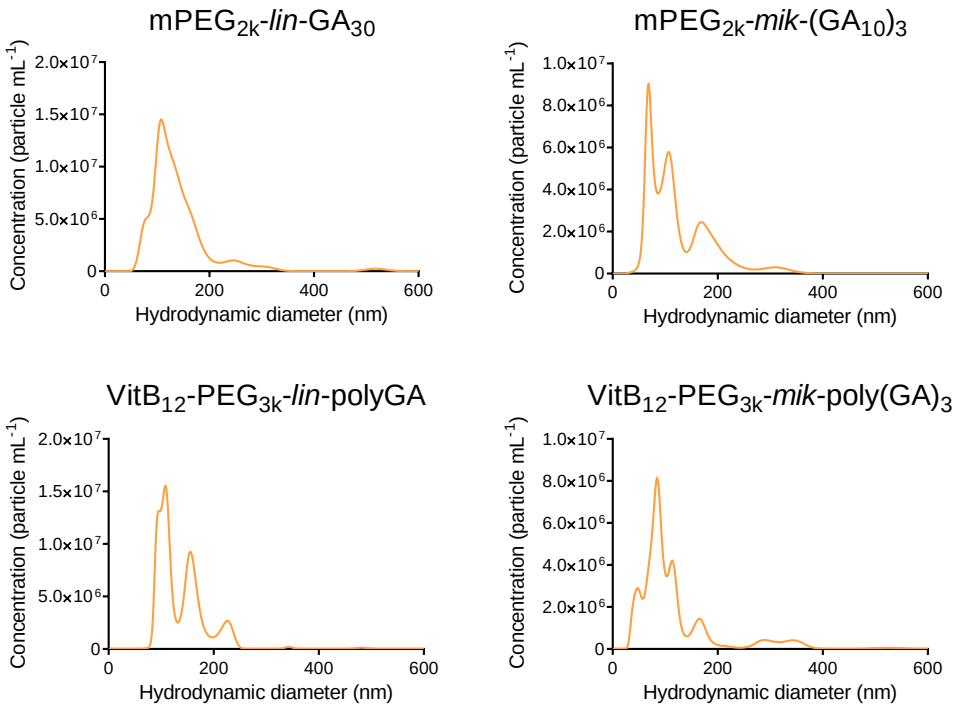


Figure 5.1. Particle size distribution of mPEG$_{2k}$-*lin*-GA$_{30}$, mPEG$_{2k}$-*mik*-(GA$_{10}$)$_3$, vitB$_{12}$-PEG$_{3k}$-*lin*-polyGA and vitB$_{12}$-PEG$_{3k}$-*mik*-poly(GA)$_3$-derived complexes with RNAse A at polymer-protein charge ratio 2.5. D_H is the average hydrodynamic diameter ± SD of polymer-protein nanocomplexes as assessed by nanoparticle tracking analysis (NTA). Protein concentration was kept constant (70 µg mL^{-1}) for all samples.

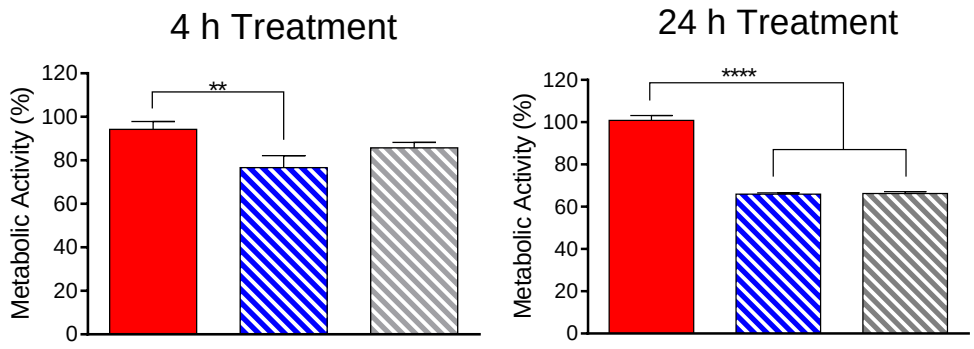


Figure 5.2. MTS assay in Calu-3 cells after 4 and 24 h treatment with un-complexed RNAse A (**red**), linear (**blue**) and miktoarm (**grey**) copolymers complexed with RNAse A. Polymer-protein nanocomplexes were composed of mPEG$_{2k}$-polyGA (85% mol:mol) and vitB$_{12}$-PEG$_{3k}$-polyGA (15% mol:mol) copolymers. RNAse A concentration was kept constant (200 µg mL^{-1}) for all the samples. One-way ANOVA was used for statistical analysis. ** $p < 0.01$, **** $p < 0.0001$.

5.2. References

AMIDI, M., MASTROBATTISTA, E., JISKOOT, W. & HENNINK, W. E. 2010. Chitosan-based delivery systems for protein therapeutics and antigens. *Adv Drug Deliv Rev,* 62**,** 59-82.

DEPRETER, F., PILCER, G. & AMIGHI, K. 2013. Inhaled proteins: challenges and perspectives. *Int J Pharm,* 447**,** 251-80.

KLINGLER, C., MULLER, B. W. & STECKEL, H. 2009. Insulin-micro- and nanoparticles for pulmonary delivery. *Int J Pharm,* 377**,** 173-9.

OTTO, R., SANTAGOSTINO, A. & SCHRADER, U. December 2014. *Rapid growth in biopharma: Challenges and opportunities* [Online]. Available: http://www.mckinsey.com/insights/health_systems_and_services/rapid_growth_in_biopharma.

Chapter 6

Supporting Information

Table of Contents

6.1. Material and Methods of Chapter 2.....191
6.1.1. Material.....191
6.1.2. Instrumentation.....192
6.1.3. Characterisation of copolymers and corresponding precursors.....194
6.1.4. TEM analysis.....204
6.1.5. Circular dichroism.....205
6.1.6. Synthesis of mPEG-lysozyme covalent conjugates.....205
6.1.7. Metabolic activity (MTS assay).....208
6.1.8. Membrane integrity (LDH assay).....208
6.1.9. Apoptosis assay (Annexin V-FITC/PI assay).....209
6.1.10. Stability of ($mPEG_{2k}$-polyGA)-lysozyme nanocomplexes in DMEM.....209
6.2. Material and Methods of Chapter 3.....210
6.2.1. Material.....210
6.2.2. Particle size distribution of nanocomplexes.....210
6.3. Material and Methods of Chapter 4.....211
6.3.1. Material.....211
6.3.2. Instrumentation.....212
6.3.3. Characterisation of copolymers and corresponding precursors.....214
6.3.4. Lysozyme-Cy5: Reaction conditions.....223
6.3.5. *In vivo* pulmonary deposition and retention of polymer-protein nanocomplexes-based dry powder formulations in healthy mice.....225
6.4. References.....229

6.1. Material and Methods of Chapter 2

6.1.1. Material

L-Glutamic acid γ-benzyl ester (≥ 99.0%), allyl bromide (97%), cysteamine hydrochloride (≥ 98%), triethylamine (≥ 99.0%), sodium phosphate dibasic (99.9%), sodium phosphate monobasic dihydrate (≥ 99.0%), phosphoric acid, *Micrococcus lysodeikticus* lyophilised cells, poly(allyl amine) solution (M_w ~17 kDa, 20 wt. % in H_2O), Tris-Acetate-EDTA buffer, agarose, acetonitrile (ACN, anhydrous, 99.8%), methoxypolyethylene glycol amine 2,000, dichloromethane (DCM, anhydrous, ≥ 99.8%), *N,N*-dimethylformamide (DMF, anhydrous, 99.8%), tetrahydrofuran (THF, anhydrous, ≥ 99.9%), deuterated chloroform (99.8 atom % D), deuterium oxide (99.9 atom % D), deuterated methanol (CD_3OD, 99.8 atom % D), Dulbecco's Minimal Essential Medium, Dulbecco's Minimal Essential Medium: Nutrient Mixture F-12, foetal bovine serum, L-glutamine (200 mM), antibiotic solution (100 U mL^{-1} penicillin, 0.1 mg mL^{-1} streptomycin), non-essential amino acids (100%), trypsin/EDTA solution, DPBS, triton X-100 and *in vitro* toxicology assay kit, lactic dehydrogenase based were purchased from Sigma Aldrich. Methyl 3,4,5-trihydroxybenzoate (98.0%), potassium carbonate anhydrous (≥ 99.0%), sodium hydroxide (≥ 97.0%), oxalyl chloride (98.0%), 2,2-dimethoxy-2-phenylacetophenone (DPAP) (99.0%), hydrochloric acid, ethidium bromide, magnesium sulphate dried, toluene, methanol, diethyl ether anhydrous, propan-2-ol, petroleum ether and ethyl acetate were supplied by Fisher Scientific. Triphosgene 98.0% and lysozyme molecular biology grade were

purchased from Alfa Aesar and AppliChem, respectively. All the chemicals were used as received without further purification. Anhydrous solvents were used as received and stored under dry and inert atmosphere. CellTiter 96® aqueous one solution cell proliferation assay (MTS) was supplied by Promega. A549 and Calu-3 cells were purchased from the American Type Culture Collection (USA). Phosphate buffer saline tablets were obtained from Oxoid (UK). Annexin V-FITC/PI was supplied by BD Bioscience. Thin layer chromatography (TLC) was carried out on pre-coated TLC sheets ALUGRAM®SIL G/UV254 purchased from Macherey-Nagel. TLCs were visualised by exposure to UV light (254 nm) followed by staining with $KMnO_4$.

6.1.2. Instrumentation

Characterisation of polymers and intermediates. ^{1}H and ^{13}C NMR spectra were recorded at room temperature on a Bruker DPX 400 MHz. Samples were prepared by dissolving products in suitable deuterated solvents ($CDCl_3$, CD_3OD or D_2O). All chemical shifts are reported in parts per million (ppm) and using residual solvent as an internal standard ($CDCl_3$: δH 7.26, δC 77.16; D_2O: δH 4.79; CD_3OD: δH 3.31). The mass spectrometric analyses were carried out using a Micromass LCT KC453 ESI-TOF spectrometer and an Ultraflex III MALDI-TOF spectrometer with N_2 laser of 337 nm and pulses of 3 ns, using DCTB as the matrix. FT-IR analyses were performed on a Nicolet IR200 FT-IR spectrometer (Thermo Fischer Scientific).

Size Exclusion Chromatography (SEC). Aqueous SEC was performed on a Shimadzu UPLC system fitted with a differential refractive index detector. The

mobile phase was aqueous 0.10 M $NaNO_3$, 0.02 (*w/v*) NaN_3, pH 10.0 at 35°C and a flow rate of 1.0 mL min^{-1}. The instrument was fitted with a Polymer Labs aquagel-OH guard column (50 x 7.5 mm, 8 µm) followed by three PL aquagel-OH columns (30, 40 and 50; 300 x 7.5 mm, 8 µm). Column calibration was achieved using PEG/ (PEO) narrow standards with Mp in the 0.2 – 130 kDa range. Molecular weights and dispersity values were calculated using Shimadzu LabSolutions software with SEC analysis add-on.

Transmission electron microscopy (TEM). TEM analysis was performed using a Tecnai G2 (FEI, Oregon, USA). Images were captured using Megaview III and analysed by Megaview III Soft imaging system. Samples were prepared by placing complexes suspension onto 3.05 mm Nickel grid, Formvar/Carbon supported film, 100 HEX. No staining was used in the sample preparation.

6.1.3. Characterisation of copolymers and corresponding precursors

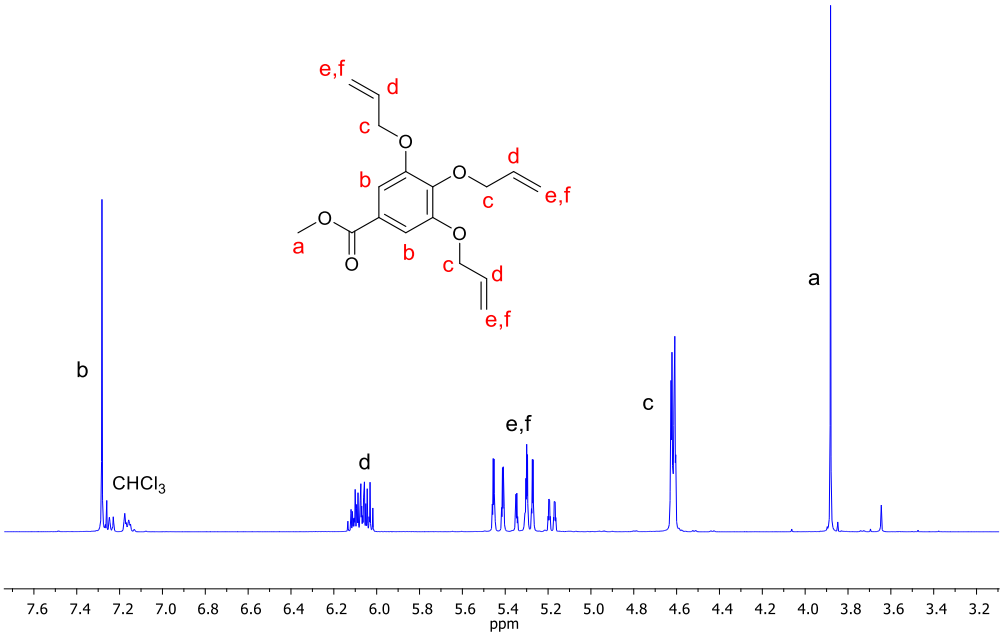


Figure S1. ^{1}H NMR spectrum of 3,4,5-tris(allyloxy)benzoic acid methyl ester **(1)** in $CDCl_3$.

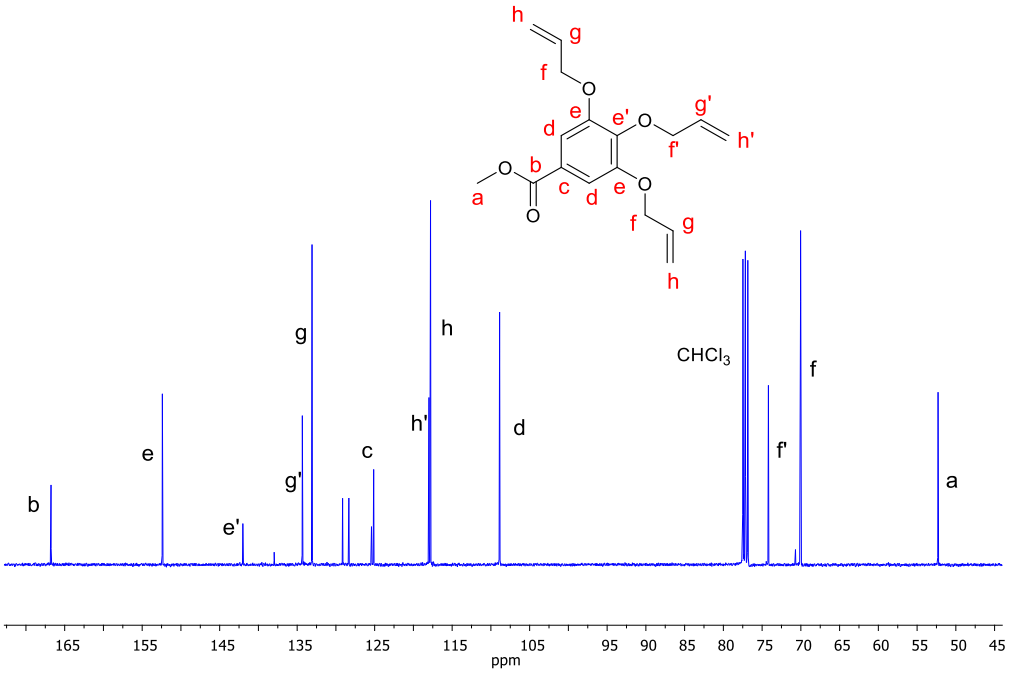


Figure S2. ^{13}C NMR spectrum of 3,4,5-tris(allyloxy)benzoic acid methyl ester **(1)** in $CDCl_3$.

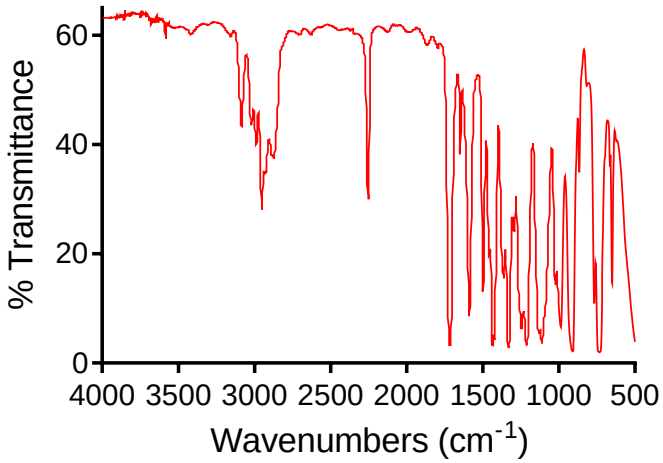


Figure S3. FT-IR spectrum of 3,4,5-tris(allyloxy)benzoic acid methyl ester **(1)** (neat).

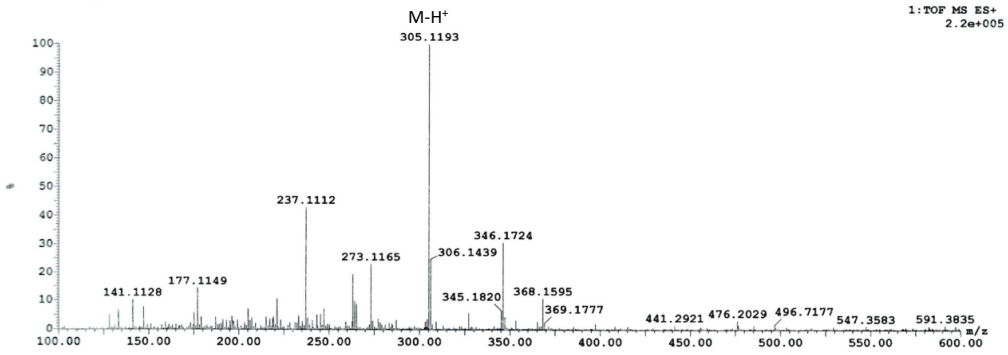


Figure S4. Mass spectrum (ESI-MS) of 3,4,5-tris(allyloxy)benzoic acid methyl ester **(1)**.

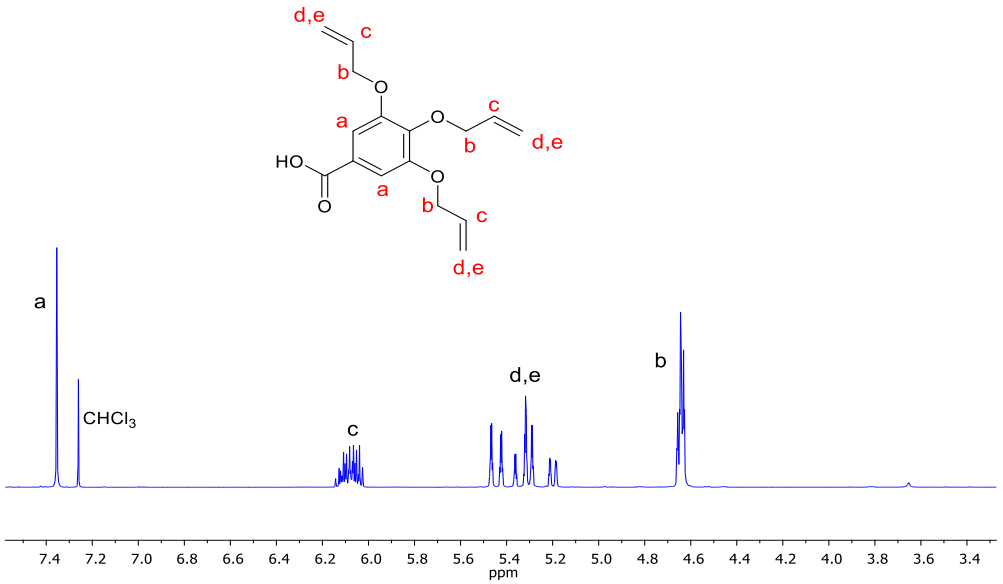


Figure S5. ^{1}H NMR spectrum of 3,4,5-tris(allyloxy)benzoic acid **(2)** in $CDCl_3$.

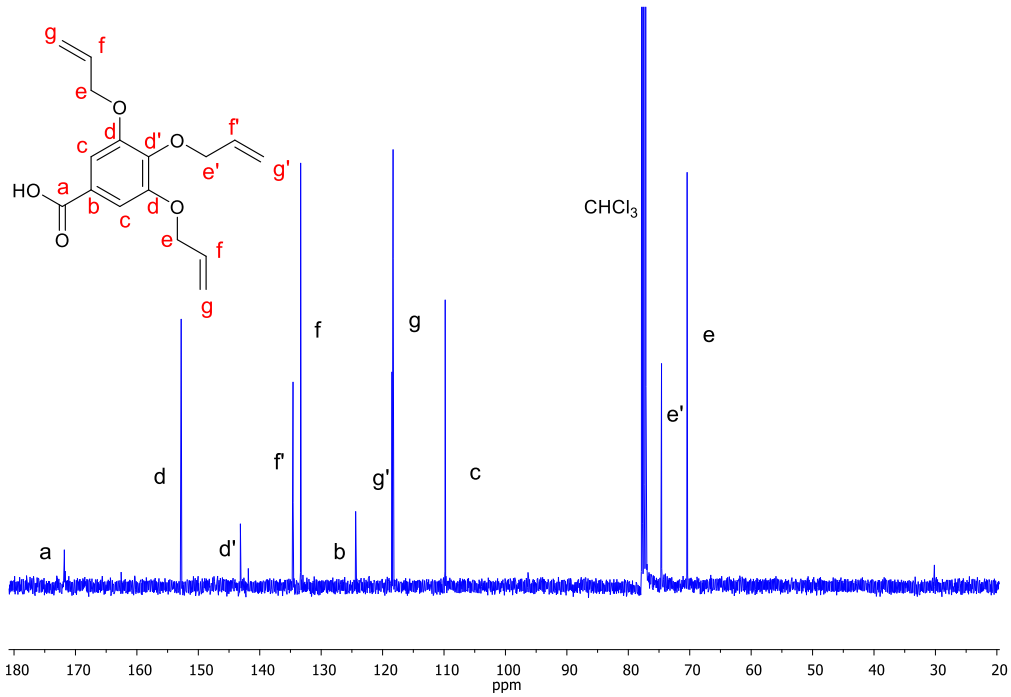


Figure S6. ^{13}C NMR spectrum of 3,4,5-tris(allyloxy)benzoic acid **(2)** in $CDCl_3$.

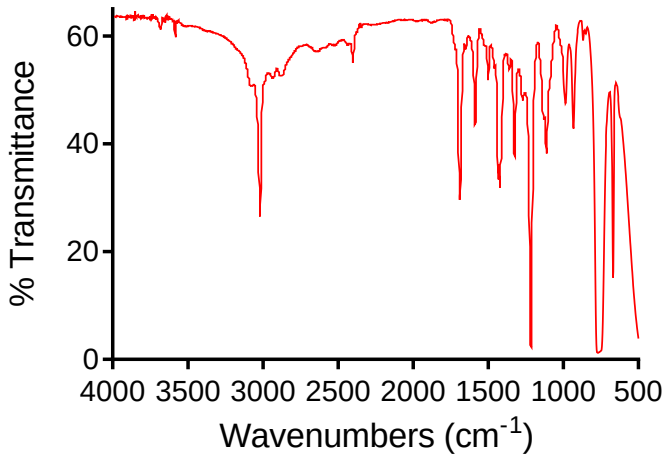


Figure S7. FT-IR spectrum of 3,4,5-tris(allyloxy)benzoic acid **(2)** (neat).

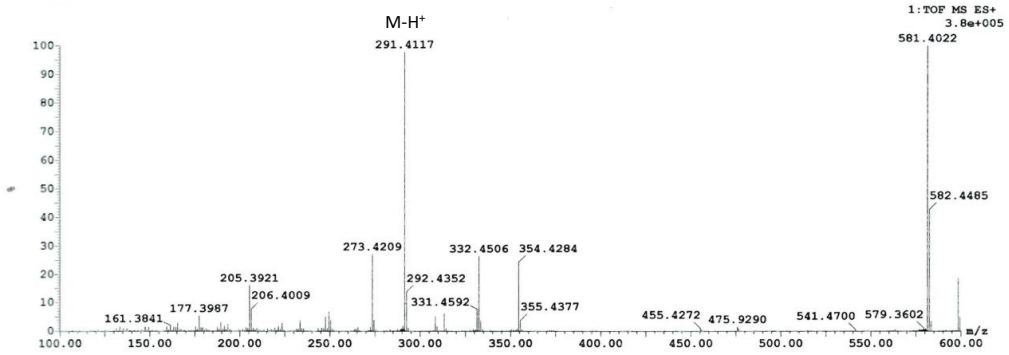


Figure S8. Mass spectrum (ESI-MS) of 3,4,5-tris(allyloxy)benzoic acid **(2)**.

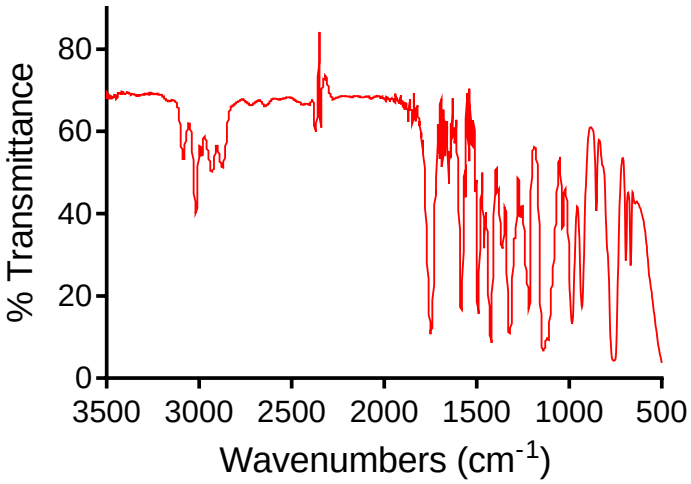


Figure S9. FT-IR spectrum of 3,4,5-tris(allyloxy)benzoyl chloride **(3)** (neat).

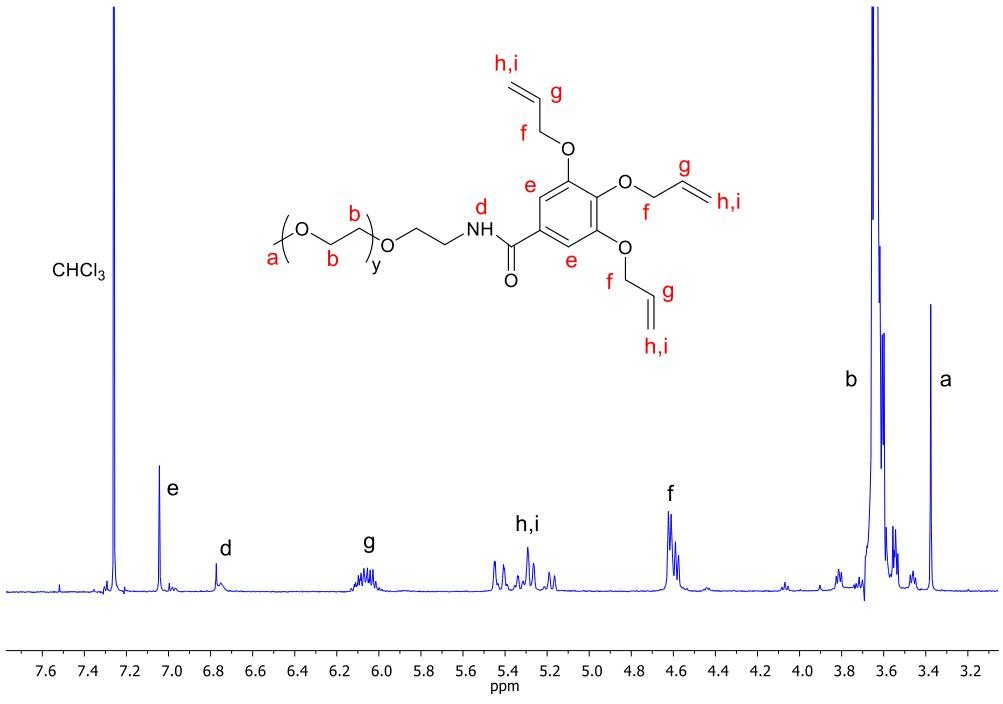


Figure S10. ^{1}H NMR spectrum of mPEG$_{2k}$ triallyl ether **(4)** in $CDCl_3$.

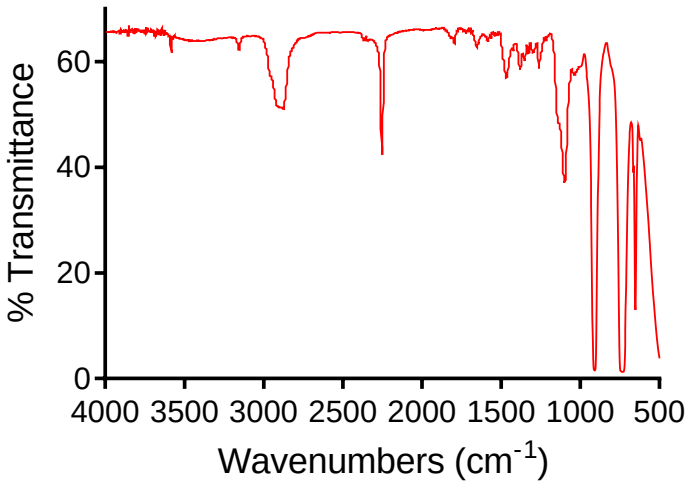


Figure S11. FT-IR spectrum of $mPEG_{2k}$ triallyl ether **(4)** (neat).

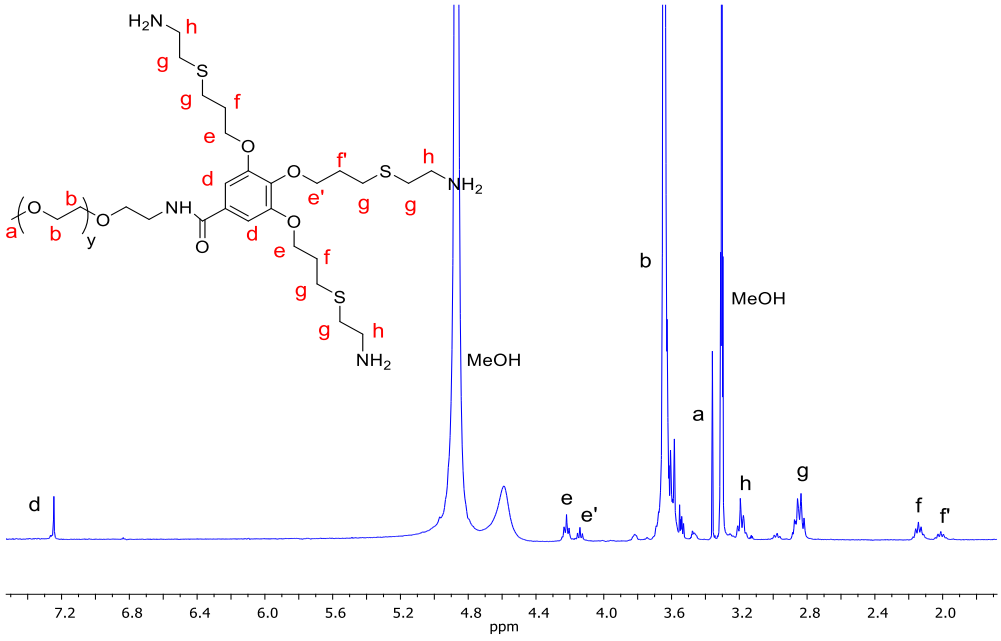


Figure S12. ^{1}H NMR spectrum of $triaminoPEG_{2k}$ **(5)** in CD_3OD.

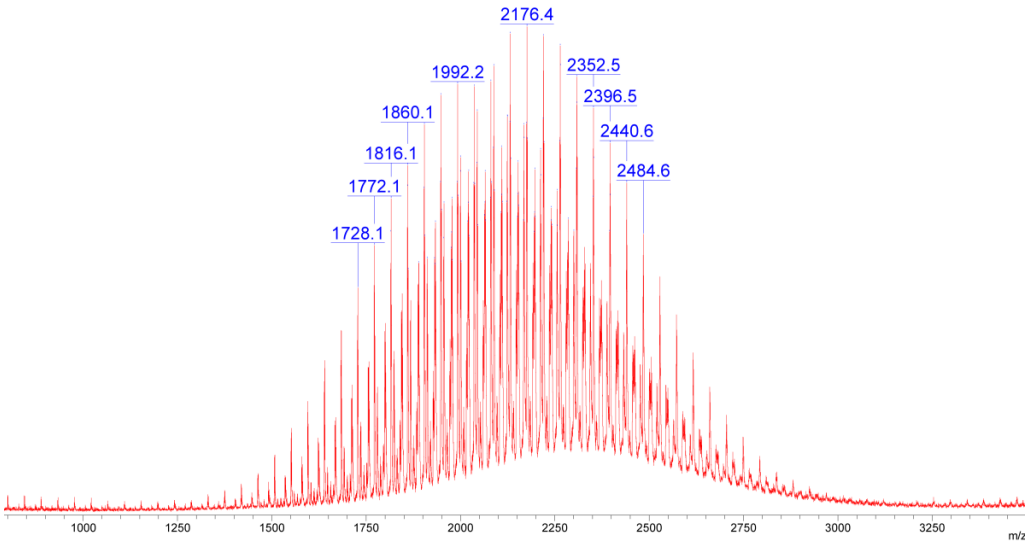


Figure S13. Mass spectrum (MALDI-TOF) of methoxypolyethylene glycol amine 2,000.

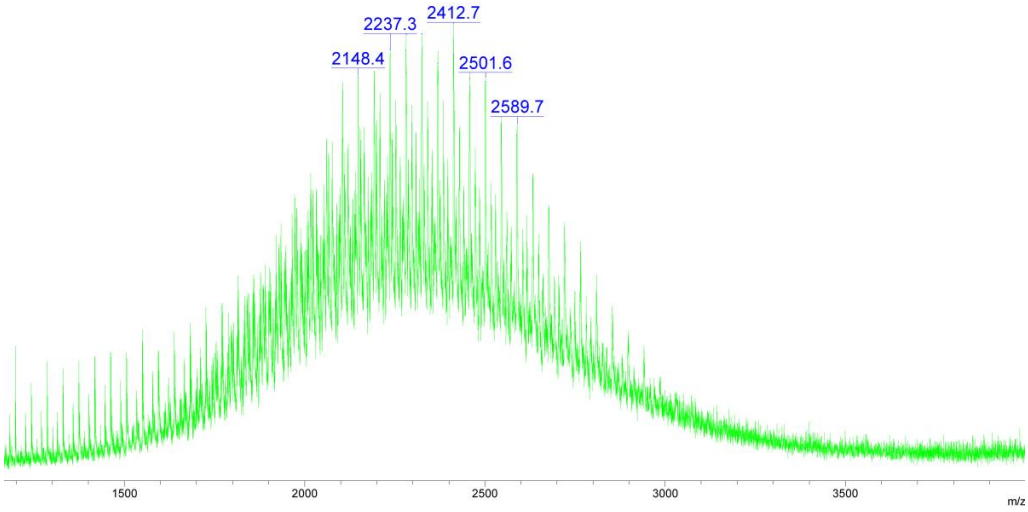


Figure S14. Mass spectrum (MALDI-TOF) of $mPEG_{2k}$ triallyl ether **(4)**.

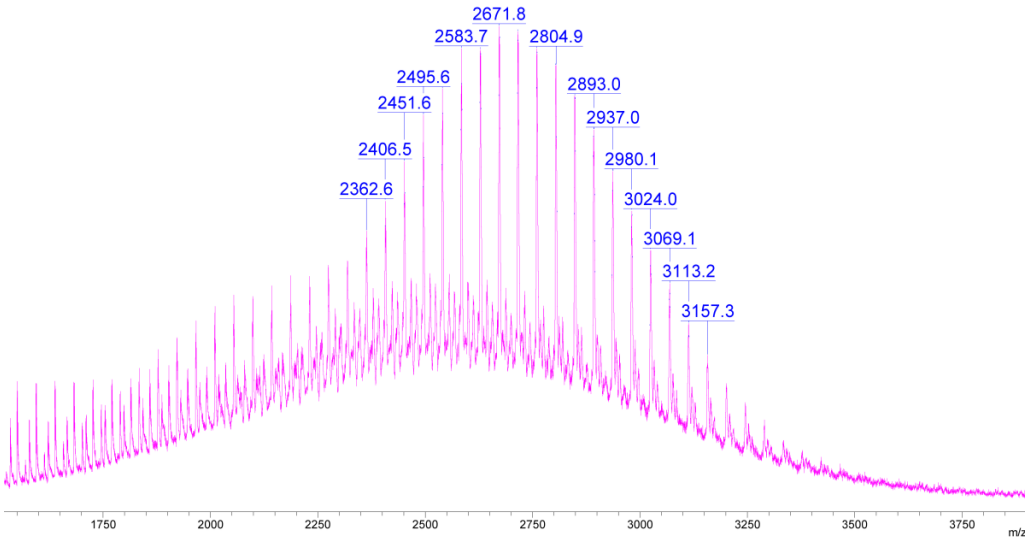


Figure S15. Mass spectrum (MALDI-TOF) of triaminoPEG$_{2k}$ **(5)**.

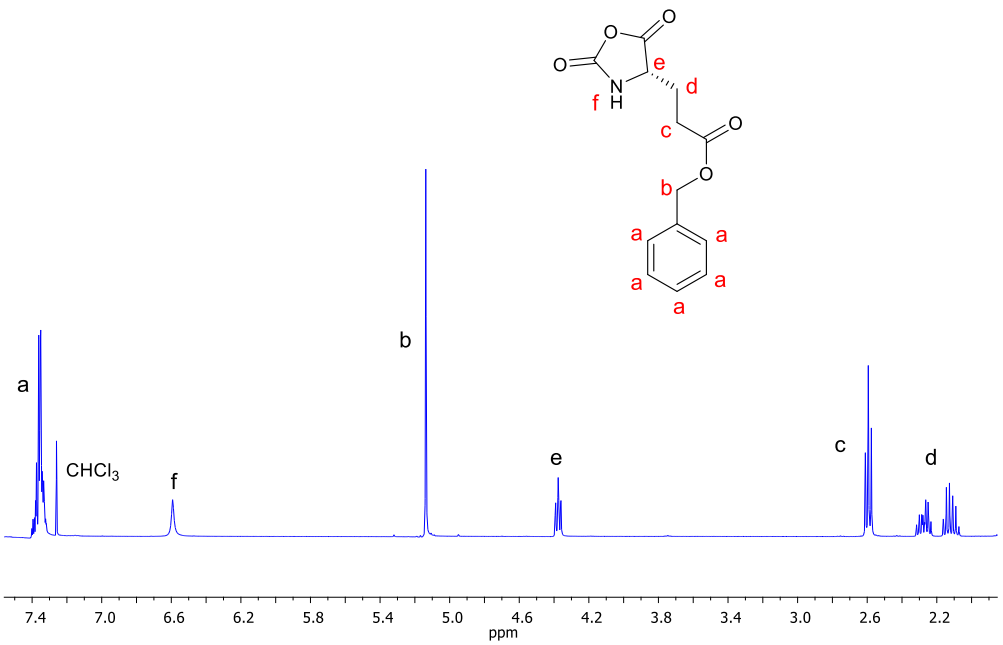


Figure S16. ^{1}H NMR spectrum of γ-benzyl-L-glutamate *N*-carboxy-anhydride (NCA) in $CDCl_3$.

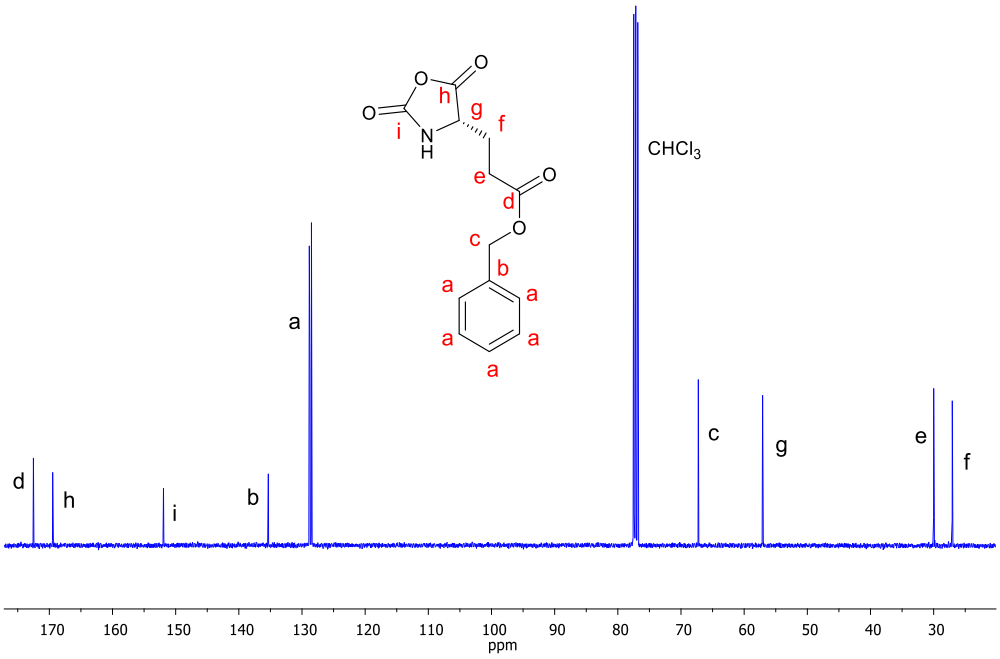


Figure S17. ^{13}C NMR spectrum of γ-benzyl-L-glutamate *N*-carboxy-anhydride (NCA) in $CDCl_3$.

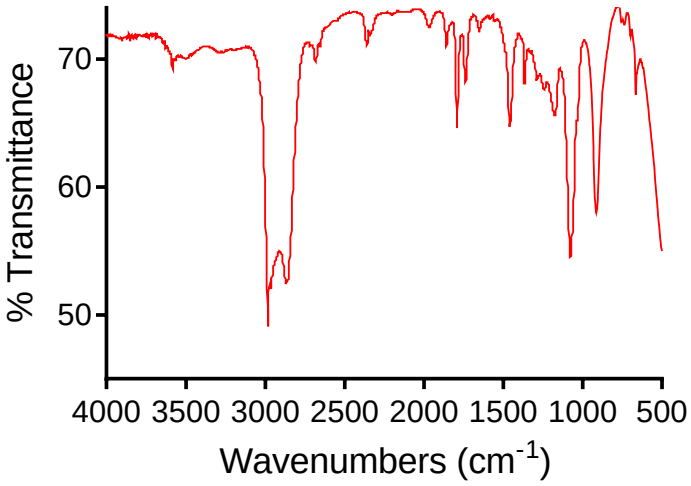


Figure S18. FT-IR spectrum of γ-benzyl-L-glutamate *N*-carboxy-anhydride (NCA) (neat).

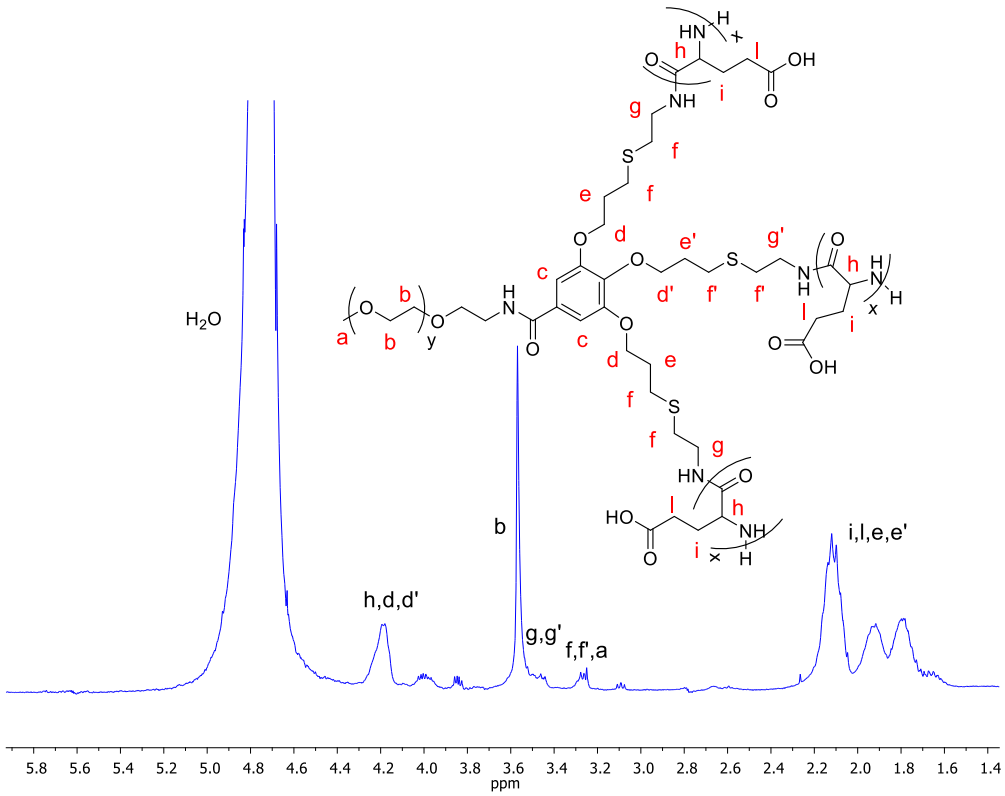


Figure S19. ^{1}H NMR spectrum of miktoarm mPEG$_{2k}$-*mik*-(GA$_{30}$)$_3$ copolymer in D_2O.

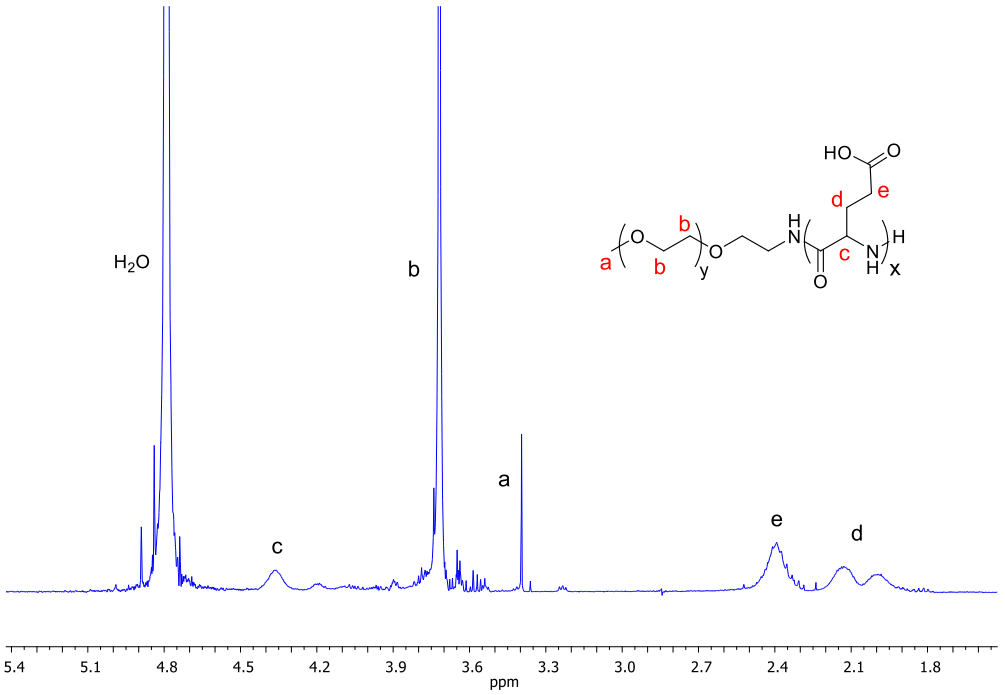


Figure S20. ^{1}H NMR spectrum of linear mPEG$_{2k}$-*lin*-GA$_{10}$ copolymer in D_2O.

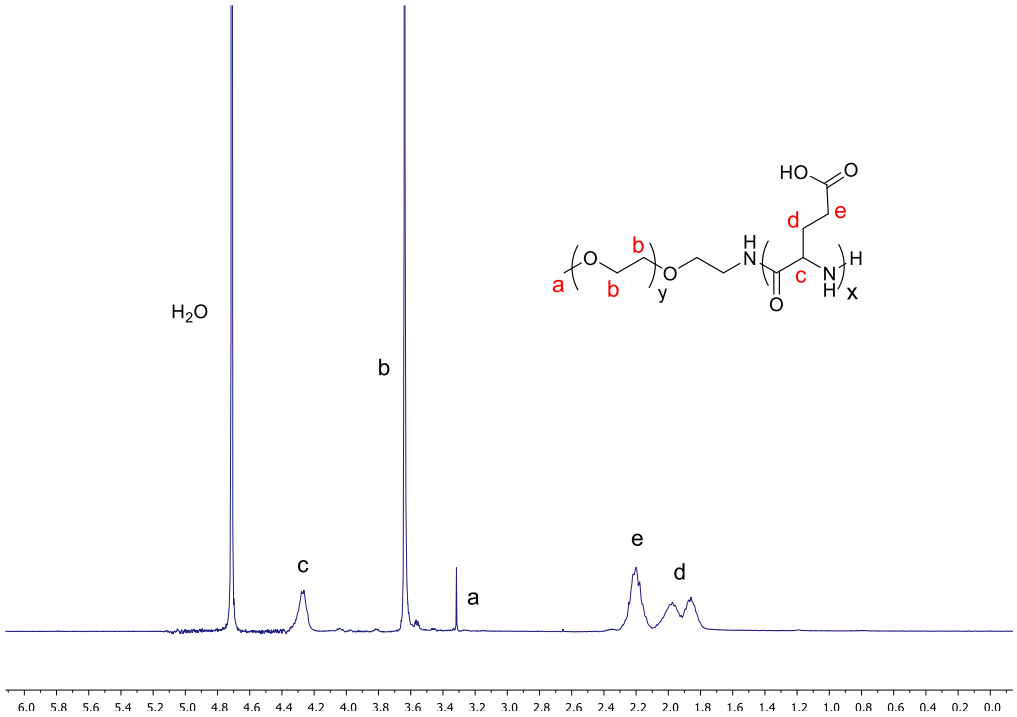


Figure S21. ^{1}H NMR spectrum of linear mPEG$_{2k}$-*lin*-GA$_{30}$ copolymer in D_2O.

6.1.4. TEM analysis

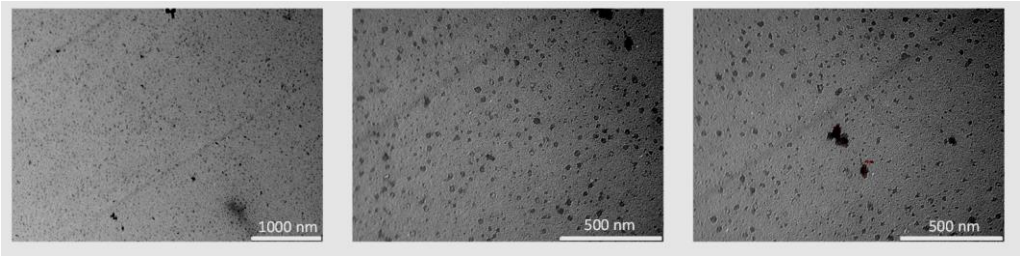


Figure S22. TEM images of (mPEG$_{2k}$-*lin*-GA$_{30}$)-lysozyme complexes prepared at *r*: 2.5, as described in instrumentation section (Supporting Information, section 6.1.2).

6.1.5. Circular dichroism

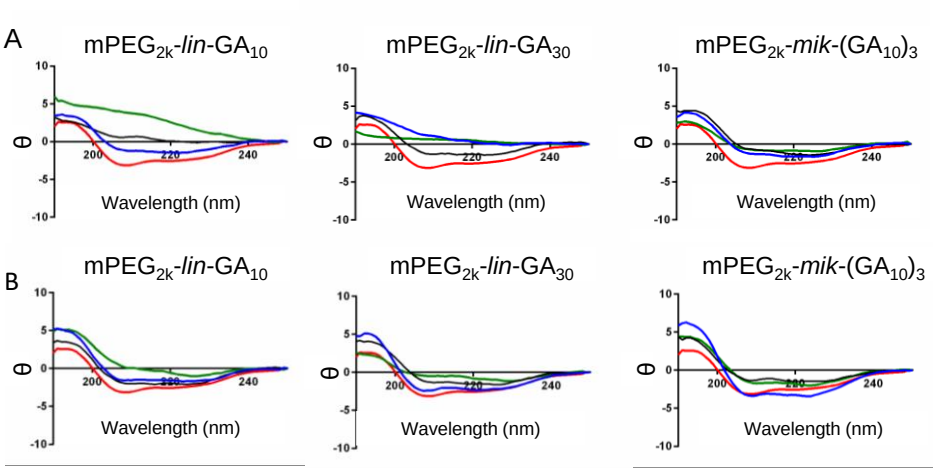


Figure S23. Circular dichroism spectra for free linear mPEG$_{2k}$-*lin*-GA$_{10}$, mPEG$_{2k}$-*lin*-GA$_{30}$ and miktoarm mPEG$_{2k}$-*mik*-(GA$_{10}$)$_3$ copolymers (A) and their respective complexes with lysozyme (B). Complexes were prepared at different charge ratios *r*: 0.1, 1.0 and 2.5. Free lysozyme (**red**), *r*: 0.1 (**blue**), *r*: 1.0 (**black**) and *r*: 2.5 (**green**).

6.1.6. Synthesis of mPEG-lysozyme covalent conjugates

Lysozyme (143.1 mg, 10.00 µmol) was dissolved in 10 mM phosphate buffer, pH 8.0 (14.3 mL) and different amounts of methoxy PEG succinimidyl carbonate 1.9 kDa (Miron and Wilchek, 1993) (95 mg (50 µmol), 190 mg (100 µmol), 380 mg (200 µmol), or 570 mg (300 µmol)) were added to the solution. Final protein concentration was always kept constant at 10 mg mL^{-1} before addition of PEG succinimidyl carbonate 1.9 kDa. The reaction was kept under slow agitation for 1 day, and PEGylated lysozyme conjugates were purified by dialysis (MWCO: 10.0 kDa) against 10 mM phosphate buffer, pH 7.4.

The number of conjugated PEG polymer chains *per* lysozyme was estimated by titrating the residual lysozyme primary amino groups (unmodified chicken egg white lysozyme possess 6 lysine residues and 1 *N*-terminal amine) by

TNBS assay. Accordingly, the dialysed PEGylated protein solutions were incubated with 410 µL of 0.10 M borate buffer (pH 9) and 0.1% (*v/v*) TNBS reagent in the dark, at room temperature for 30 minutes. The absorbance was then recorded at λ = 420 nm using a TECAN microplate reader, and the number of unreacted amino groups was calculated using a calibration curve built using unmodified lysozyme at different concentrations. A final 65, 74, 89 or 90% of lysozyme amino groups – corresponding to 4.5, 5.2, 6.2, 6.3 mPEG chains per protein – were found to be reacted following incubation with 5, 10, 20 or 30 $mPEG_{2k}$ equivalents, respectively (Table S1).

Table S1. Percentage of lysozyme amino groups reacted with $mPEG_{2k}$, as estimated by TNBS assay.

$mPEG_{2k}$:Lysozyme molar ratio in the reaction feed	Percentage of lysines reacted with PEG (%)	Average number of $mPEG_{2k}$ per lysozyme
5	65	4.5
10	74	5.2
20	89	6.2
30	90	6.3

SDS-PAGE was performed using a BioRad mini-PROTEAN Tetra Cell. The sample was prepared under reducing conditions for application on a gel consisting of 6 and 15% stacking and resolving gel, respectively. Coomassie blue staining was used to visualise the protein bands.

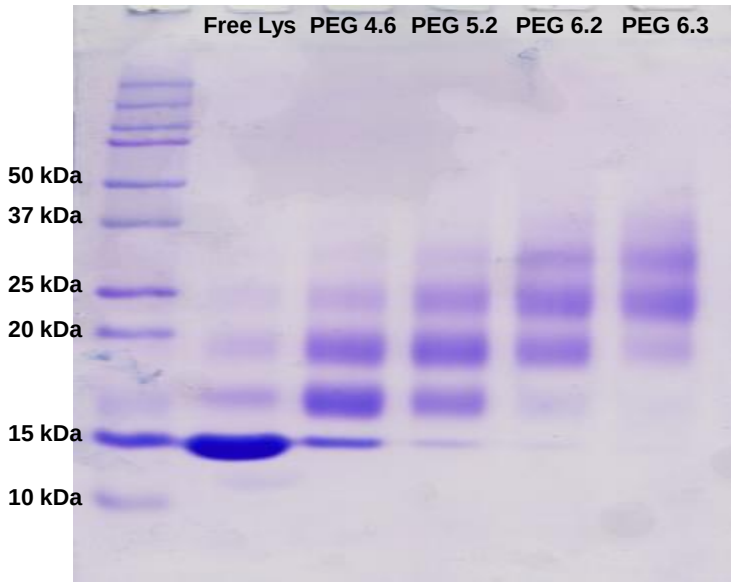


Figure S24. SDS-PAGE of dialysed PEGylated lysozyme at different $mPEG_{2k}$-lysozyme molecule ratios (4.6, 5.2, 6.2, 6.3), as determined by TNBS assay.

The enzymatic activity of the various PEGylated lysozyme conjugates was evaluated. Lysozyme-$(mPEG_{2k})_{4.6}$ conjugate sample was not utilised in this part of our study because it still contained a non-negligible amount of unmodified enzyme. A lysozyme concentration of 37 μg mL^{-1} was utilised in all enzymatic assay tests. 10 mM phosphate buffer, pH 7.4 (20 mL) was added to 10 mg of *Micrococcus lysodeikticus* lyophilised cells. 300 μL of the resulting suspension were added to 150 μL of sample solution and the decrease in optical density at λ = 460 nm was measured as a function of time. All enzyme digestion experiments were carried out in triplicate.

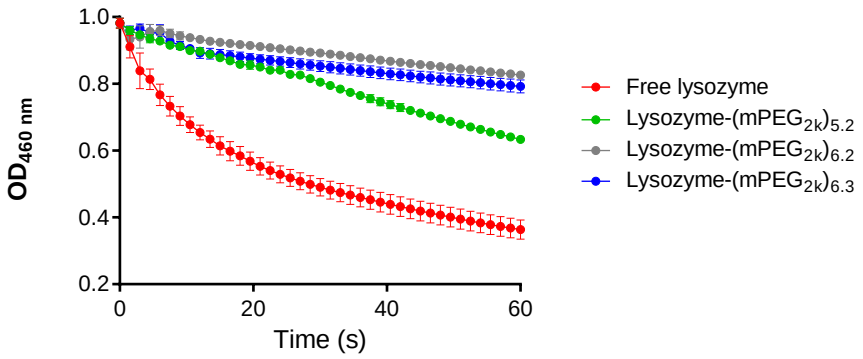


Figure S25. Enzymatic activity of lysozyme-$(mPEG_{2k})_{5.2}$, lysozyme-$(mPEG_{2k})_{6.2}$, lysozyme-$(mPEG_{2k})_{6.3}$ conjugate PEGylated proteins containing different amounts of $mPEG_{2k}$ chains per lysozyme molecule: 5.18, 6.23 and 6.30. All experiments were carried out in triplicate.

6.1.7. Metabolic activity (MTS assay)

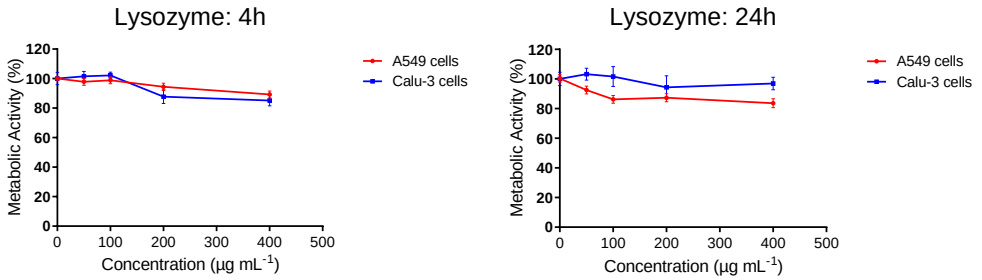


Figure S26. MTS assay in A549 and Calu-3 cells after 4 and 24 hours treatment with un-complexed lysozyme.

6.1.8. Membrane integrity (LDH assay)

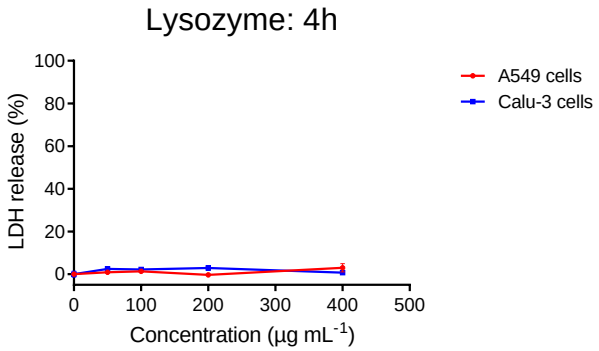


Figure S27. Percentage of total LDH released from A549 and Calu-3 cells after 4 hours treatment with un-complexed lysozyme.

6.1.9. Apoptosis assay (Annexin V-FITC/PI assay)

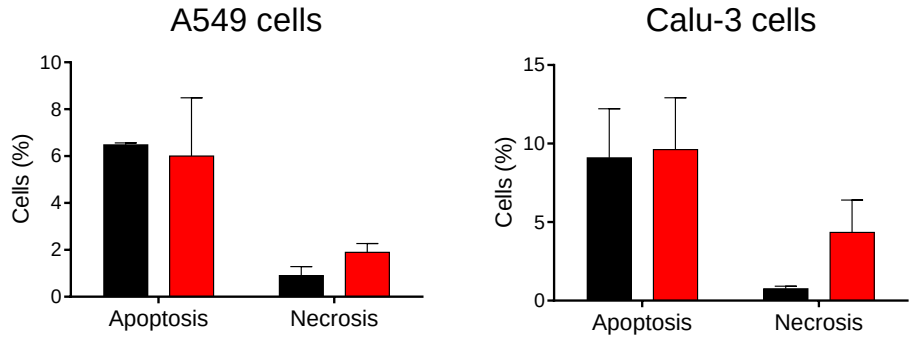


Figure S28. Percentage of apoptosis and necrosis in A549 and Calu-3 cells after 4 hours treatment with un-complexed lysozyme. Control untreated cells (**black**) and un-complexed lysozyme (**red**).

6.1.10. Stability of (mPEG$_{2k}$-polyGA)-lysozyme nanocomplexes in DMEM

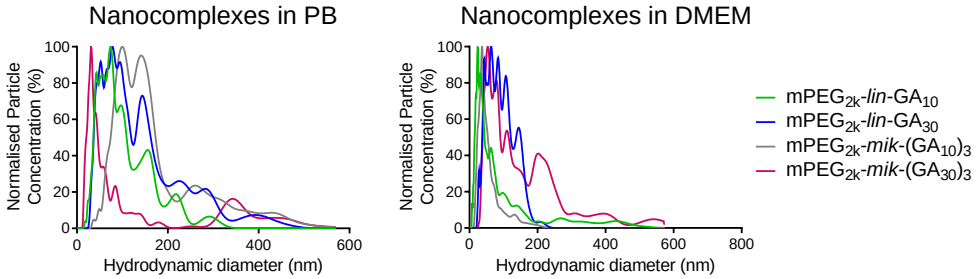


Figure S29. Particle size distribution of (mPEG$_{2k}$-polyGA)-lysozyme nanocomplexes in phosphate buffer (PB) and phenol red-free DMEM. Polymer-protein nanocomplexes were prepared in PB and then diluted (40x) either in phenol red-free DMEM or PB. Polymer-protein nanocomplexes were incubated for 4 h at 37°C prior analysis by NTA. Final protein concentration was kept constant (70 µg mL^{-1}) in both media.

6.2. Material and Methods of Chapter 3

6.2.1. Material

Sodium phosphate dibasic (99.9%), sodium phosphate monobasic dihydrate (≥ 99.0%), phosphoric acid, *Micrococcus lysodeikticus* lyophilised cells, trypsin from bovine pancreas (≥ 9,000 BAEE units/mg protein), poly(allyl amine) solution (Mw 17,000 g mol^{-1}), L-leucine, D-mannitol and D-(+)-trehalose dihydrate were purchased from Sigma Aldrich. Lysozyme molecular biology grade and BCA protein assay kit was supplied by AppliChem and ThermoFisher Technologies, respectively.

6.2.2. Particle size distribution of nanocomplexes

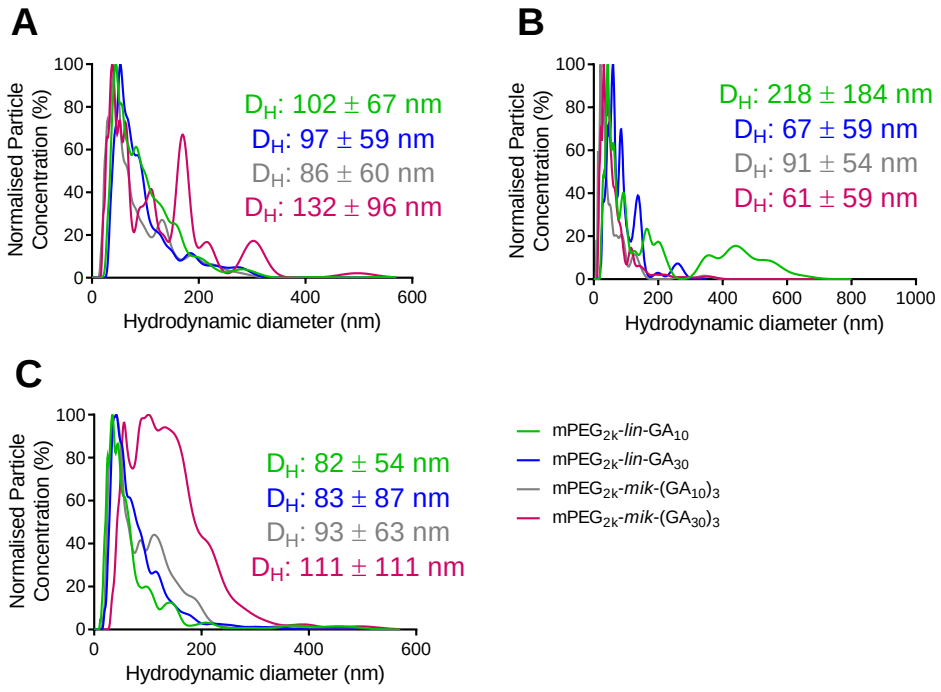


Figure S30. Nanoparticle tracking analysis (NTA) of dry powder formulations following incubation in phosphate buffer (PB, 10 mM, pH 7.4) at 70 µg mL^{-1} protein concentration in ($mPEG_{2k}$-polyGA)-lysozyme nanocomplexes for 15 min. Particle size distribution of nanocomplexes recovered from (A) trehalose, (B) trehalose + leucine and (C) mannitol-based dry powders. $mPEG_{2k}$-*lin*-GA_{10} (**green**), $mPEG_{2k}$-*lin*-GA_{30} (**blue**), $mPEG_{2k}$-*mik*-$(GA_{10})_3$ (**grey**) and $mPEG_{2k}$-*mik*-$(GA_{30})_3$ (**pink**)-derived complexes.

6.3. Material and methods of Chapter 4

6.3.1. Material

L-Glutamic acid γ-benzyl ester (≥ 99.0%), allyl bromide (97%), cysteamine hydrochloride (≥ 98%), 4-(4,6-Dimethoxy-1,3,5-triazin-2-yl)-4-methylmorpholinium chloride (DMTMM), p-toluenesulfonyl chloride (≥ 99.0%), trimethylamine (≥ 99.0%), sodium bicarbonate, sodium azide (≥ 99.0%), cyanocobalamin (≥ 98.0%), 1,1'-carbonyldiimidazole (CDI), dibenzocyclooctyne-amine, sodium phosphate dibasic (99.9%), sodium phosphate monobasic dihydrate (≥ 99.0%), L-leucine, D-(+)-trehalose dehydrate, 1-butanol, ammonia hydroxide solution, acetonitrile (ACN, anhydrous, 99.8%), dichloromethane (DCM, anhydrous, ≥ 99.8%), tetrahydrofuran (THF, anhydrous, ≥ 99.9%), methanol (MeOH, anhydrous, 99.8%), dimethyl sulfoxide (DMSO, anhydrous, ≥ 99.9%), deuterated chloroform (99.8 atom % D), deuterium oxide (99.9 atom % D), deuterated methanol (CD_3OD, 99.8 atom % D), Dulbecco's Minimal Essential Medium: Nutrient Mixture F-12, foetal bovine serum, L-glutamine (200 mM), antibiotic solution (100 U mL^{-1} penicillin and 0.1 mg mL^{-1} streptomycin), non-essential amino acids (100%), trypsin/EDTA solution, DPBS and Hanks' Balanced Salts (HBSS) were purchased from Sigma Aldrich. Methyl 3,4,5-trihydroxybenzoate (98.0%), potassium carbonate anhydrous (≥ 99.0%), sodium hydroxide (≥ 97.0%), 2,2-dimethoxy-2-phenylacetophenone (DPAP) (99.0%), hydrochloric acid, magnesium sulphate dried, toluene, methanol, diethyl ether anhydrous, propan-2-ol and petroleum ether were supplied by Fisher Scientific.

Triphosgene 98.0% and lysozyme molecular biology grade were purchased from Alfa Aesar and AppliChem, respectively. *O*-(2-aminoethyl)polyethylene glycol 3.0 kDa and sulfo-cyanine 5 NHS ester were supplied by Iris Biotech and Lumiprobe, respectively. Sheep erythrocytes and rabbit anti-sheep erythrocytes were purchased from Eurobio. All the chemicals were used as received without further purification. Anhydrous solvents were used as received and stored under dry and inert atmosphere, unless stated otherwise. Thin layer chromatography (TLC) was carried out on pre-coated TLC sheets ALUGRAM®SIL G/UV254 purchased from Macherey-Nagel. TLCs were visualised by exposure to UV light (254 nm) followed by staining with $KMnO_4$. Calu-3 cells were purchased from the American Type Culture Collection (USA). Phosphate buffer saline tablets were obtained from Oxoid (UK). CellTiter 96® aqueous one solution cell proliferation assay (MTS) was supplied by Promega.

6.3.2. Instrumentation

Characterisation of polymers and intermediates. ^{1}H and ^{13}C NMR spectra were recorded at room temperature on a Bruker DPX 400 MHz. Samples were prepared by dissolving products in suitable deuterated solvents ($CDCl_3$, CD_3OD or D_2O). All chemical shifts are reported in parts per million (ppm) and using residual solvent as an internal standard ($CDCl_3$: δH 7.26, δC 77.16; D_2O: δH 4.79; CD_3OD: δH 3.31). Mass spectrometric analyses were carried out using a Micromass LCT KC453 ESI-TOF spectrometer. FT-IR analyses were performed on a Nicolet IR200 FT-IR spectrometer (Thermo Fischer Scientific).

Size Exclusion Chromatography (SEC). Aqueous SEC was performed on a Shimadzu UPLC system fitted with a differential refractive index detector. The mobile phase was aqueous 0.10 M $NaNO_3$, 0.02 (*w/v*) NaN_3, pH 10.0 at 35°C and a flow rate of 1.0 mL min^{-1}. The instrument was fitted with a Polymer Labs aquagel-OH guard column (50 x 7.5 mm, 8 µm) followed by three PL aquagel-OH columns (30, 40 and 50; 300 x 7.5 mm, 8 µm). Column calibration was achieved using PEG/ (PEO) narrow standards with Mp in the 0.2 – 130 kDa range. Molecular weights and dispersity values were calculated using Shimadzu LabSolutions software with SEC analysis add-on.

SEC analysis to evaluate the purity of targeted vitB_{12}-polyGA copolymers was carried out with a Wyatt down 8^+ 1200 infinity series in a system equipped with an Agilent PL aquagel-OH 8 µm SEC column. DPBS was used as the mobile phase, with a flow rate of 1 mL min^{-1} and UV detection at λ = 360 nm. The resulting chromatograms were analysed using ASTRA® software V.6.1.2.84 (Wyatt Tech Corp).

Reverse Phase - High Performance Liquid Chromatography (RT-HPLC). The purity of alkyne vitamin B_{12} was evaluated using a Shimadzu HPLC system (LC-20 AP pump). A Jupiter C18 300 Å (250 x 4.6 mm) column (Phenomenex, Macclesfield, UK) was used, with 50 µL samples being injected each time, with water/acetonitrile as the mobile phase in gradient from 5% to 90% (*v/v*) of acetonitrile and with UV detection at λ = 360 nm.

6.3.3. Characterisation of copolymers and corresponding precursors.

^{1}H and ^{13}C NMR, FT-IR, and MS spectra of intermediates **(1)**, **(2)** and γ-benzyl-L-glutamate *N*-carboxy-anhydride (NCA) are reported above (section 6.1 Material and Methods of Chapter 2).

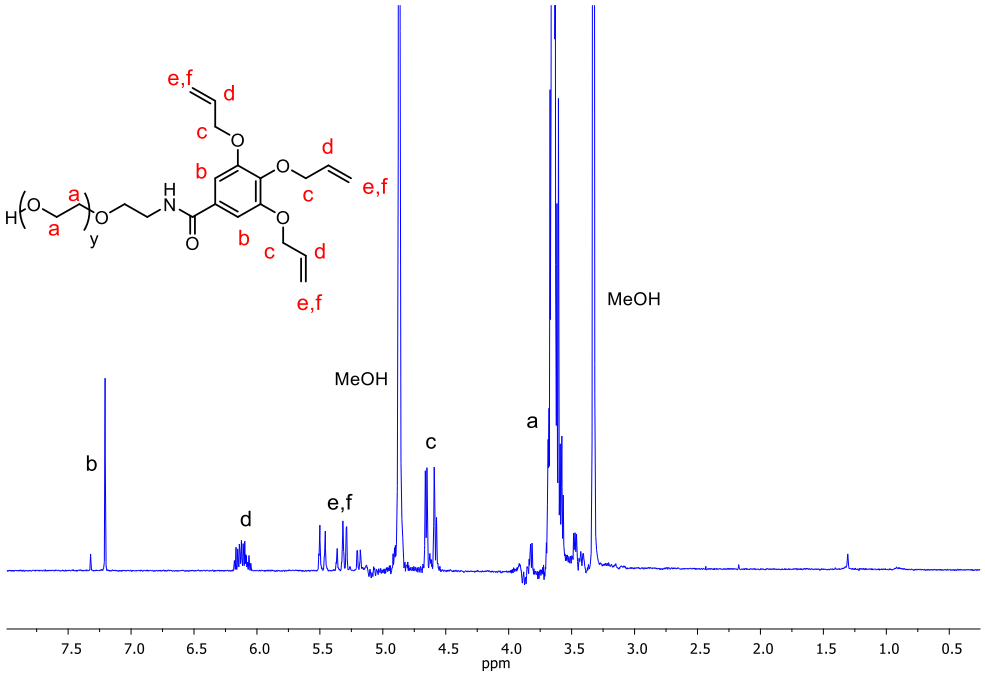


Figure S31. ^{1}H NMR spectrum of hydroxyl-PEG_{3k} triallyl ether **(6)** in MeOD.

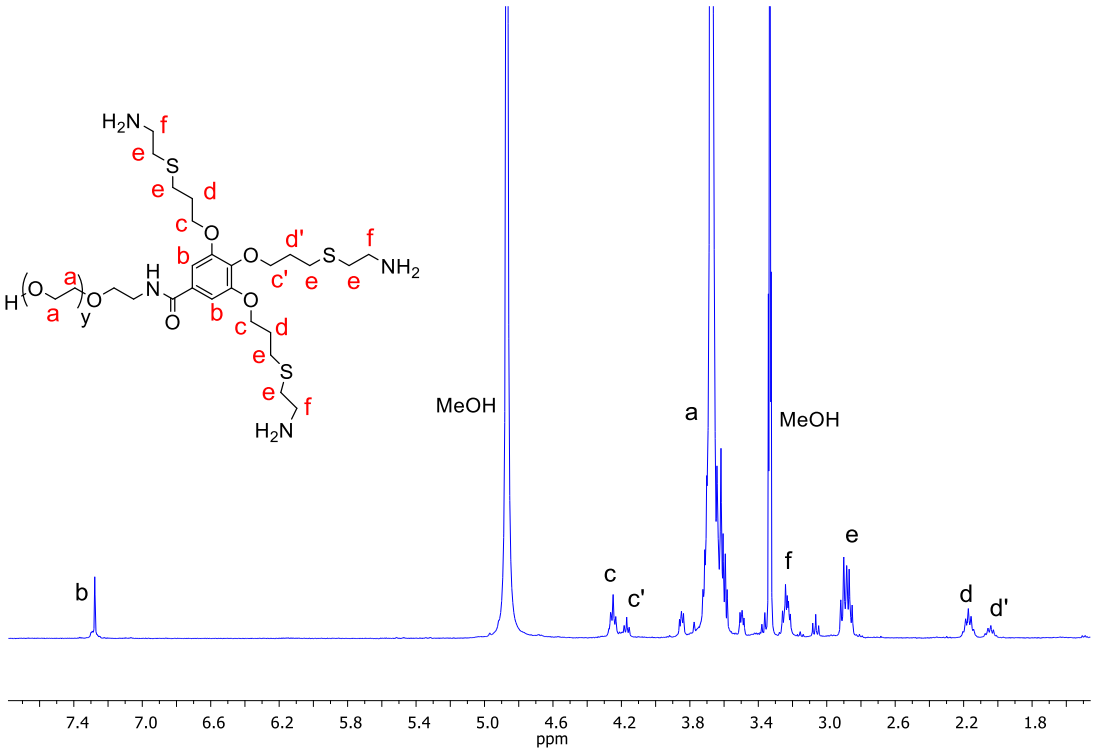


Figure S32. ^{1}H NMR spectrum of triamino-hydroxyl-PEG$_{3k}$ **(7)** in MeOD.

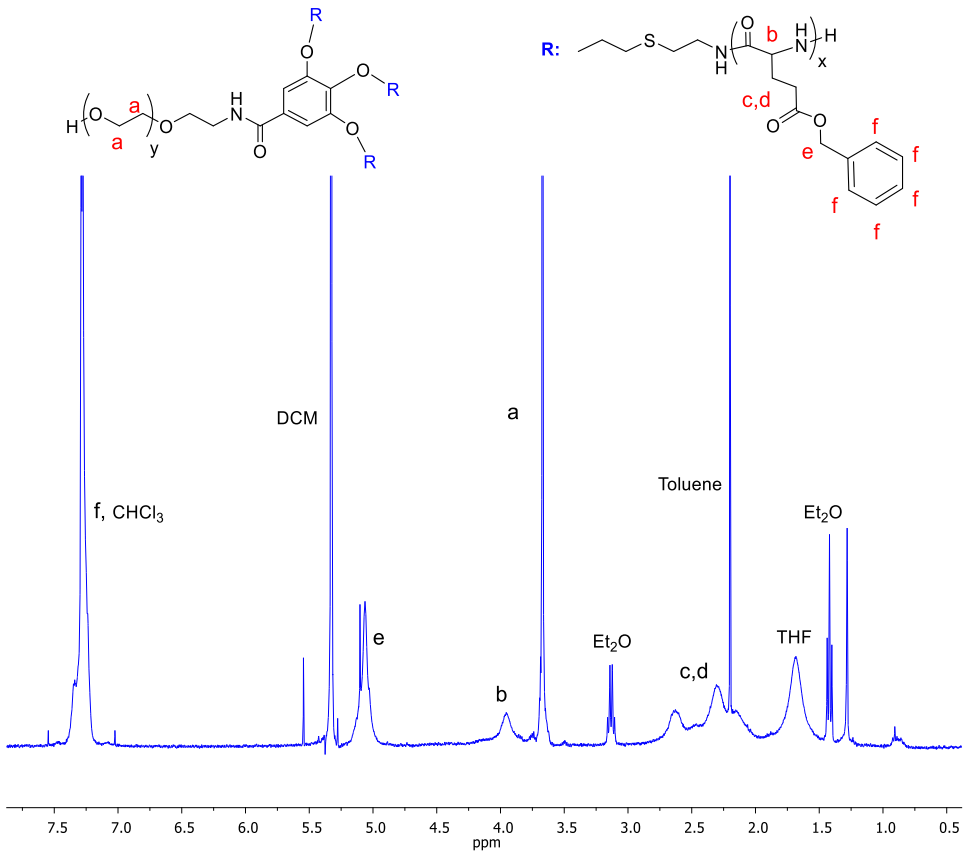


Figure S33. ^{1}H NMR spectrum of hydroxyl-PEG$_{3k}$-*mik*-poly(benzyl-glutamic acid)$_3$ **(8)** in $CDCl_3$.

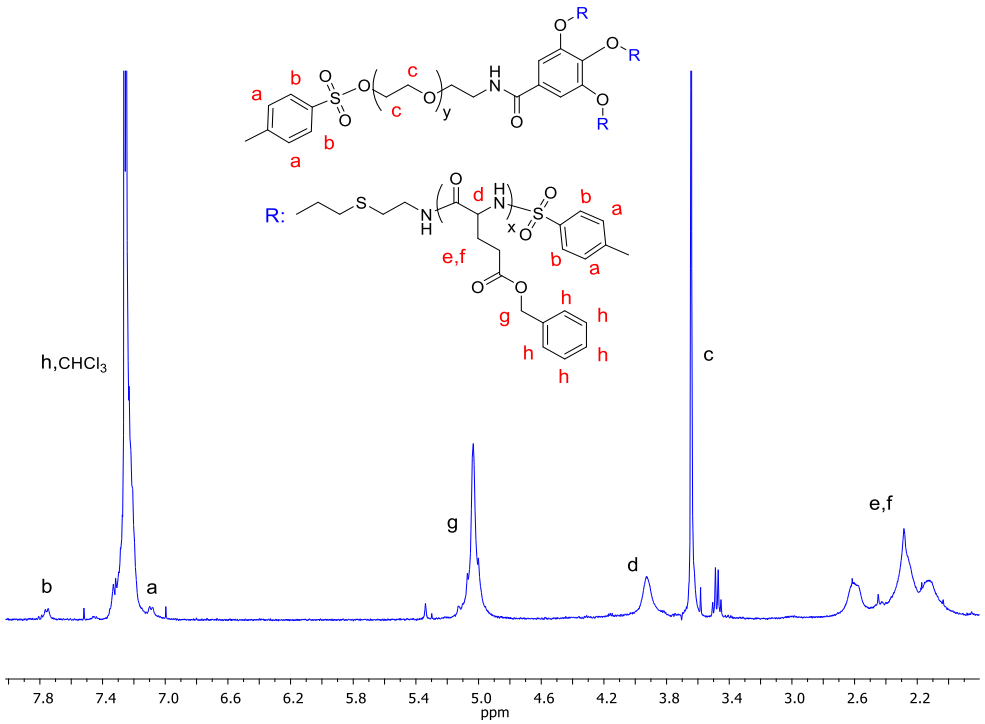


Figure S34. ^{1}H NMR spectrum of *p*-toluenesulfonyl-PEG$_{3k}$-*mik*-poly(benzyl-glutamic acid)$_3$ **(9)** in $CDCl_3$.

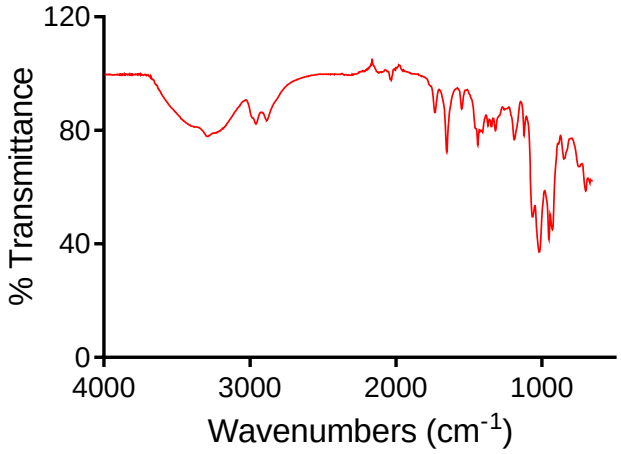


Figure S35. FT-IR spectrum of azide-PEG$_{3k}$-*mik*-poly(benzyl-glutamic acid)$_3$ copolymer **(10)** (net).

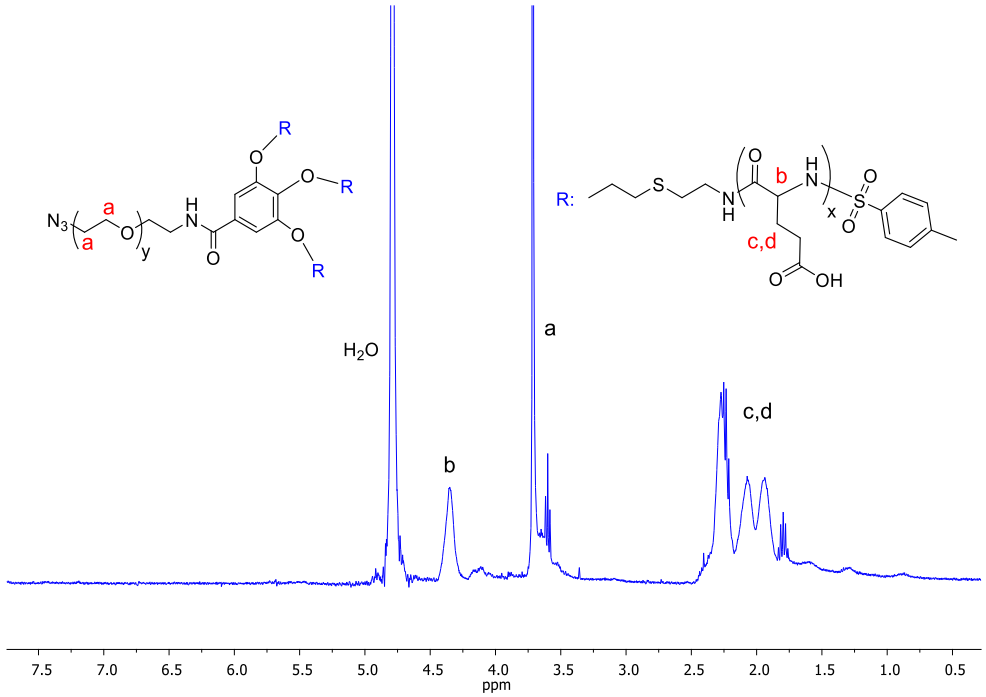


Figure S36. ^{1}H NMR spectrum of azide-PEG$_{3k}$-*mik*-poly(glutamic acid)$_3$ **(11)** in D_2O.

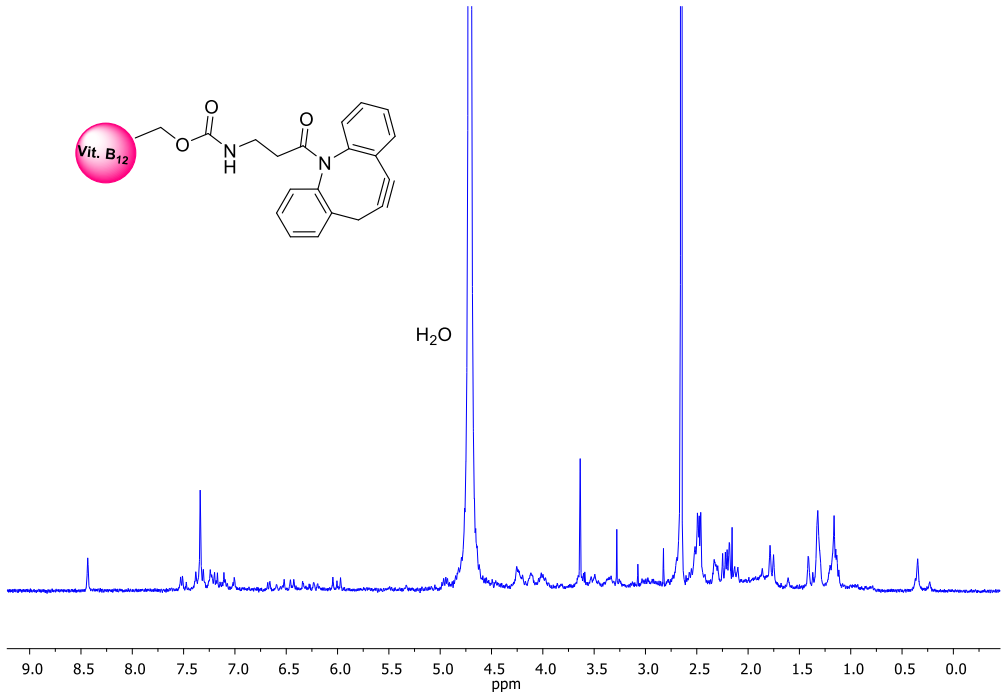


Figure S37. ^{1}H NMR spectrum of alkyne vitamin B_{12} **(12)** in D_2O.

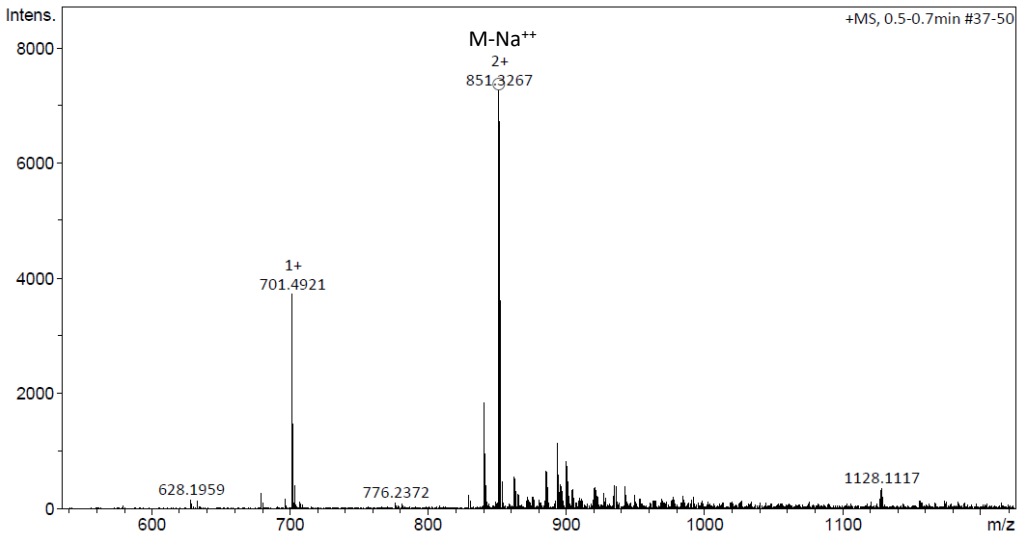


Figure S38. Mass spectrum (ESI-MS) of purified alkyne vitamin B_{12} **(12)**.

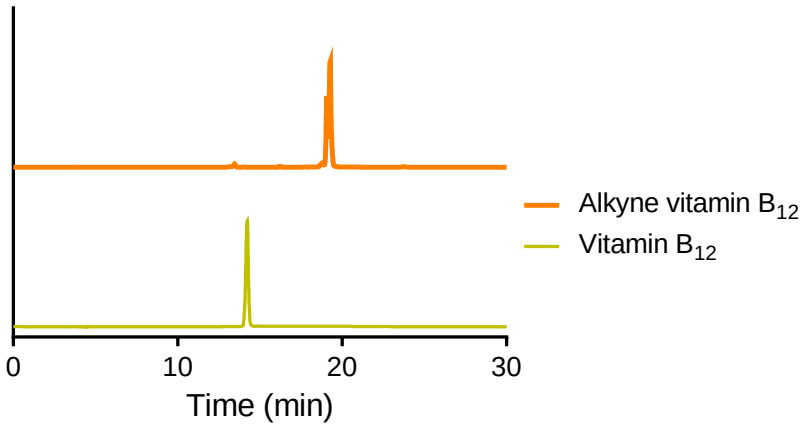


Figure S39. RP-HPLC chromatographs of alkyne vitamin B_{12} (top) and vitamin B_{12} starting material (bottom). Water/acetonitrile was used as the mobile phase in gradient from 5% to 90% (*v/v*) of acetonitrile and UV detection at λ = 360 nm.

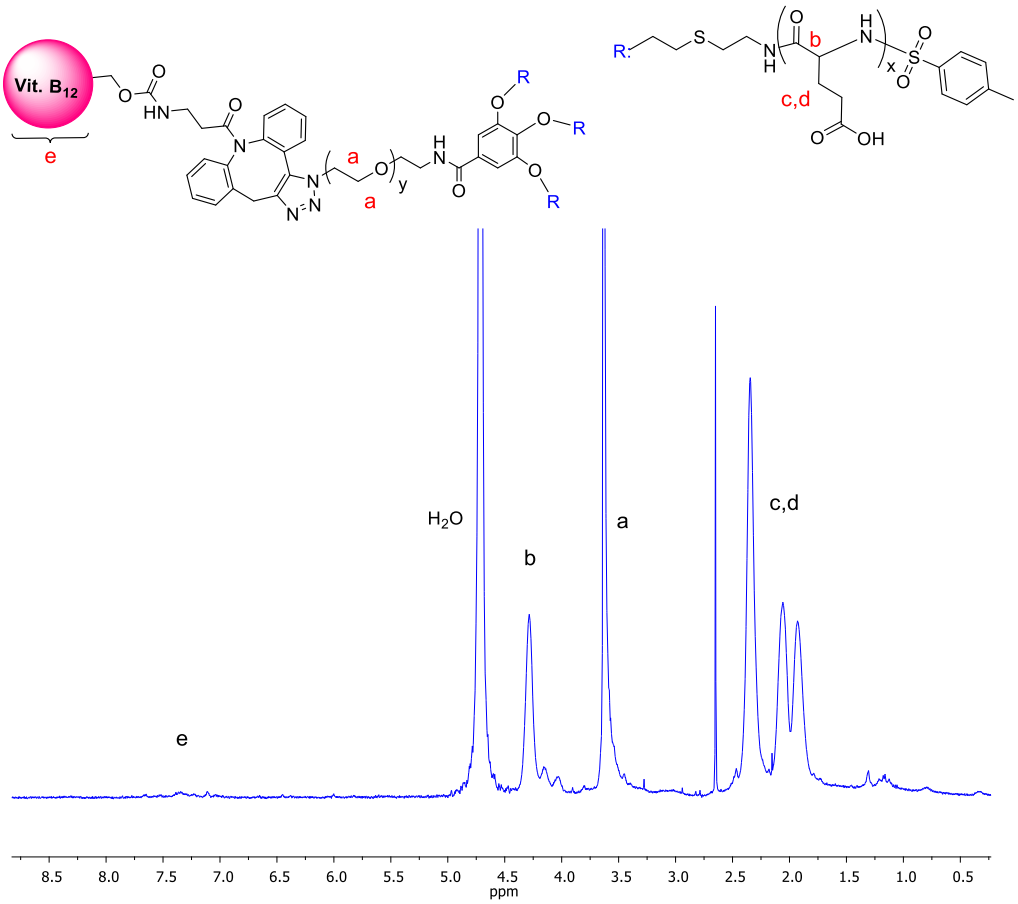


Figure S40. ^{1}H NMR spectrum of vitB$_{12}$-PEG$_{3k}$-*mik*-poly(glutamic acid)$_3$ in **(13)** D$_2$O.

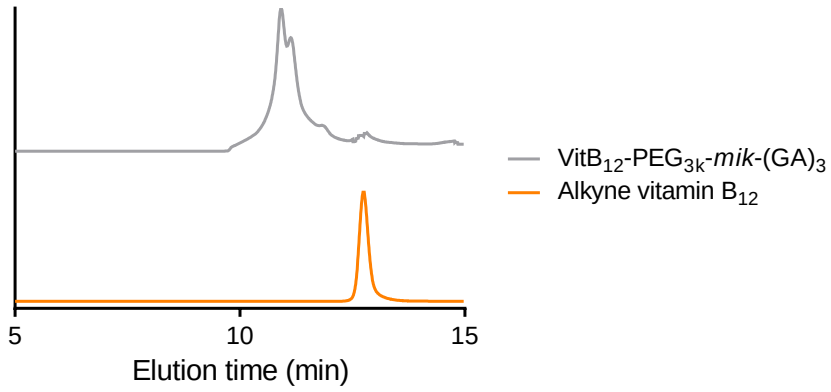


Figure S41. SEC chromatogram of vitB$_{12}$-PEG$_{3k}$-*mik*-poly(GA)$_3$ copolymer (top) and alkyne vitamin B$_{12}$ (bottom). Water/acetonitrile was used as the mobile phase in gradient from 5% to 90% (*v/v*) of acetonitrile and UV detection at λ = 360 nm.

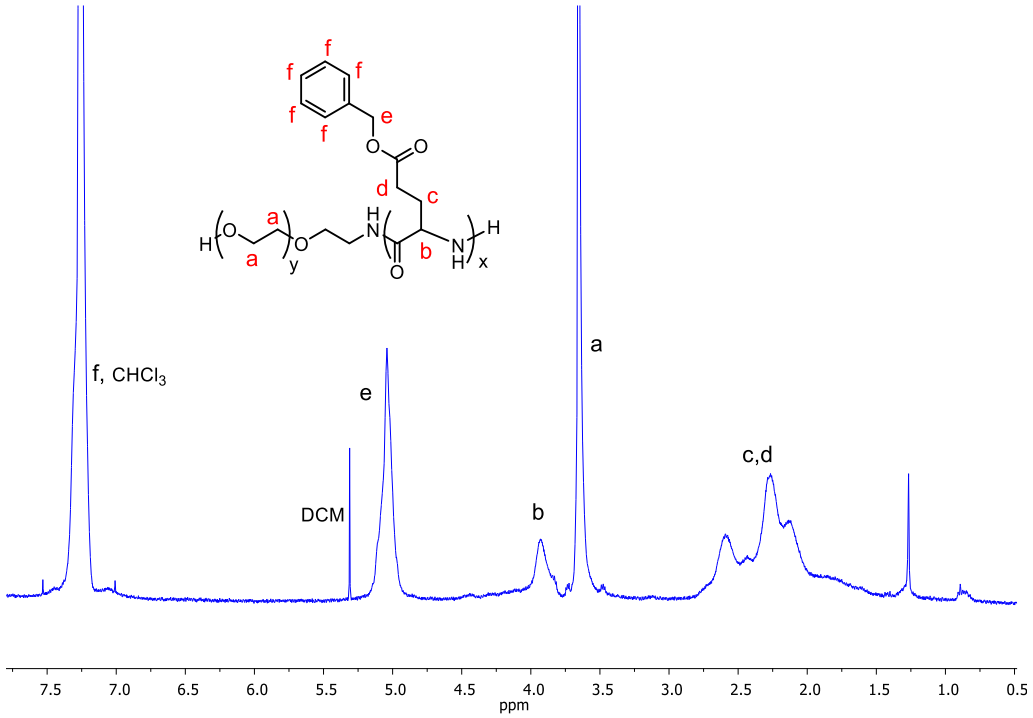


Figure S42. ^{1}H NMR spectrum of hydroxyl-PEG$_{3k}$-*lin*-poly(benzyl-glutamic acid) **(14)** in $CDCl_3$.

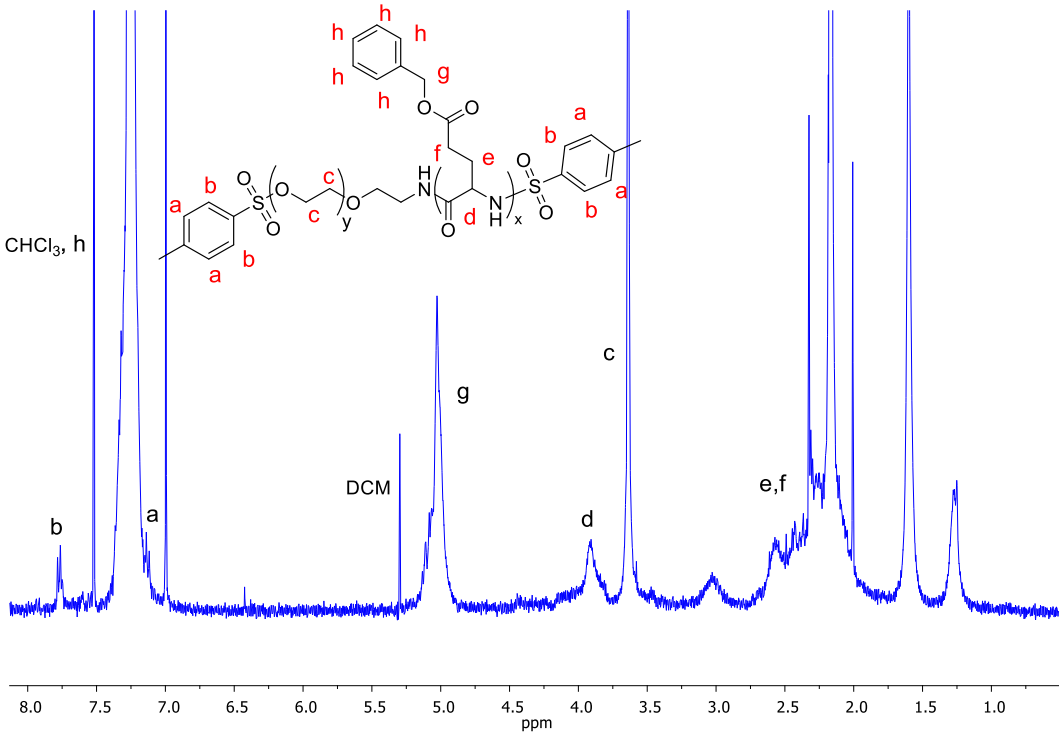


Figure S43. ^{1}H NMR spectrum of *p*-toluenesulfonyl-PEG$_{3k}$-*lin*-poly(benzyl-glutamic acid) **(15)** in $CDCl_3$.

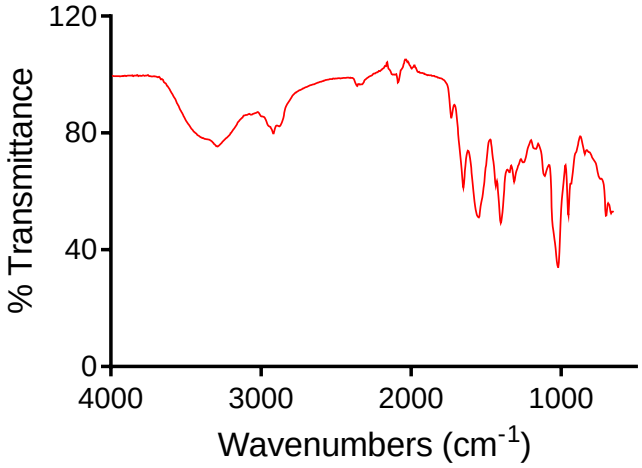


Figure S44. FT-IR spectrum of azide-PEG$_{3k}$-*lin*-poly(benzyl-glutamic acid) **(16)** copolymer (net).

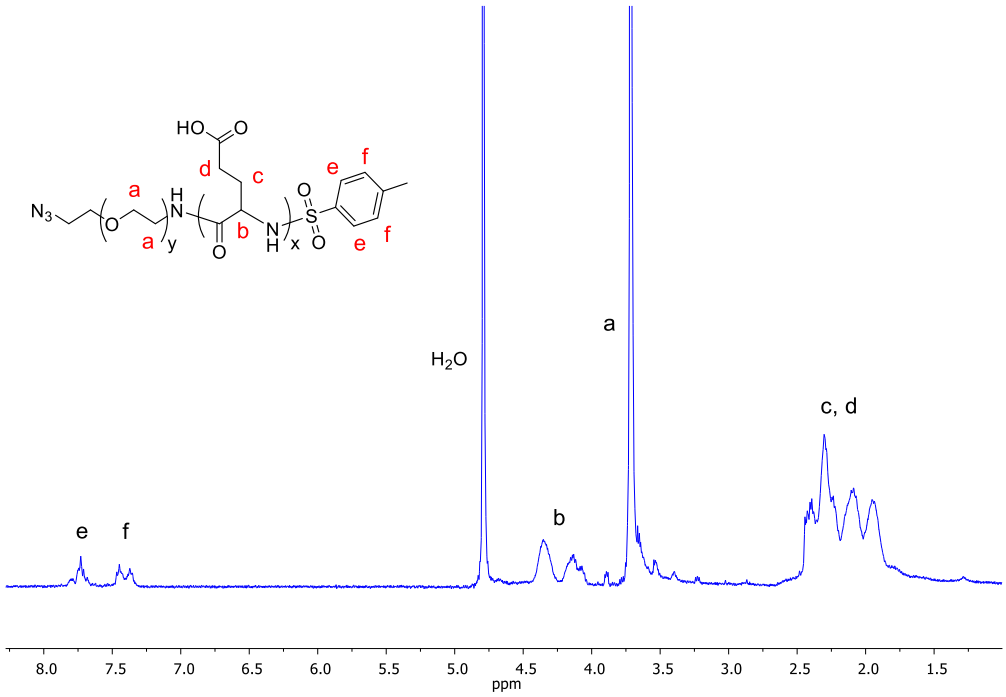


Figure S45. ^{1}H NMR spectrum of azide-PEG$_{3k}$-*lin*-poly(glutamic acid) **(17)** in D_2O.

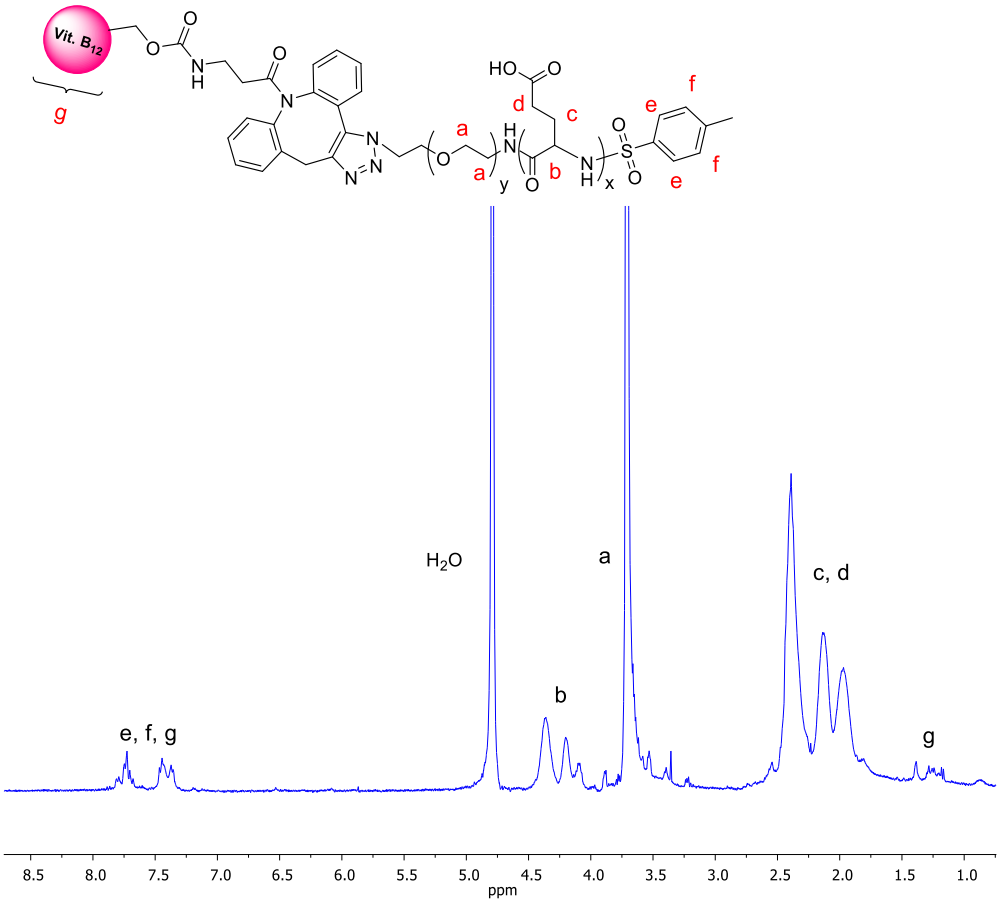


Figure S46. ^{1}H NMR spectrum of vitB$_{12}$-PEG$_{3k}$-*lin*-poly(glutamic acid) **(18)** in D$_2$O.

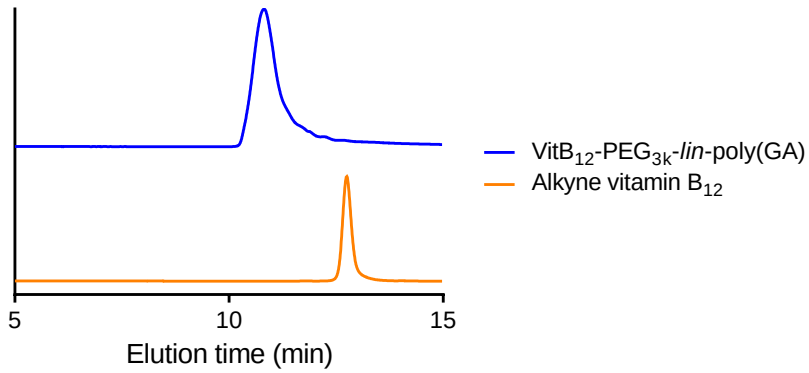


Figure S47. SEC chromatogram of vitB$_{12}$-PEG$_{3k}$-*lin*-poly(GA) copolymer (top) and free alkyne vitamin B$_{12}$ (bottom). Mobile phase water/acetonitrile in gradient from 5% to 90% (*v/v*) of acetonitrile and UV detection at λ = 360 nm.

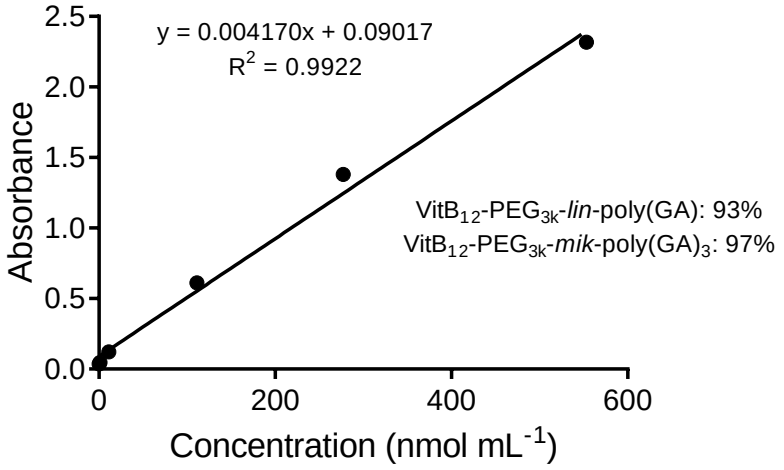


Figure S48. Percentage (%) of PEG_{3k}-polyGA copolymers end-functionalisation with vitamin B_{12} as estimated by UV-vis spectrophotometry with detection at λ = 540 nm. Graphic shows the calibration curve utilised for this calculation, built using serial dilutions of cyanocobalamin. Samples of known copolymer concentration were analysed at λ = 540 nm and the resulting reading was compared to the theoretical value calculated assuming 100% vitamin B_{12} end-functionalisation.

6.3.4. Lysozyme-Cy5: Reaction conditions

Lysozyme (40 mg, 2.8 µmol, 1.0 eq.) was dissolved in 4.5 mL of a 100 mM sodium bicarbonate solution at pH 8.4. Sulfo-Cyanine 5 NHS ester (5 mg, 6.4 µmol, 2.3 eq.), dissolved in 0.5 mL DMSO, was then slowly added to the solution and the reaction was left overnight under very gentle stirring and protected from the light. The mixture was then dialysed (MWCO 10.00 kDa) against phosphate buffer (PB, 10 mM, pH 7.4). The absence of free dye was confirmed by SEC. SEC was run at a flow rate of 1 mL min^{-1} and DPBS as the mobile phase, with simultaneous fluorescence ($\lambda_{max,ex}$ = 647 nm; $\lambda_{max,em}$ = 665 nm) and UV (λ = 280 nm) detection. Lysozyme concentration and degree of labelling (DOL) were calculated as follows:

$$A_{protein} = \varepsilon_{\text{protein}} * \text{path lenght} * \text{protein concentration}$$

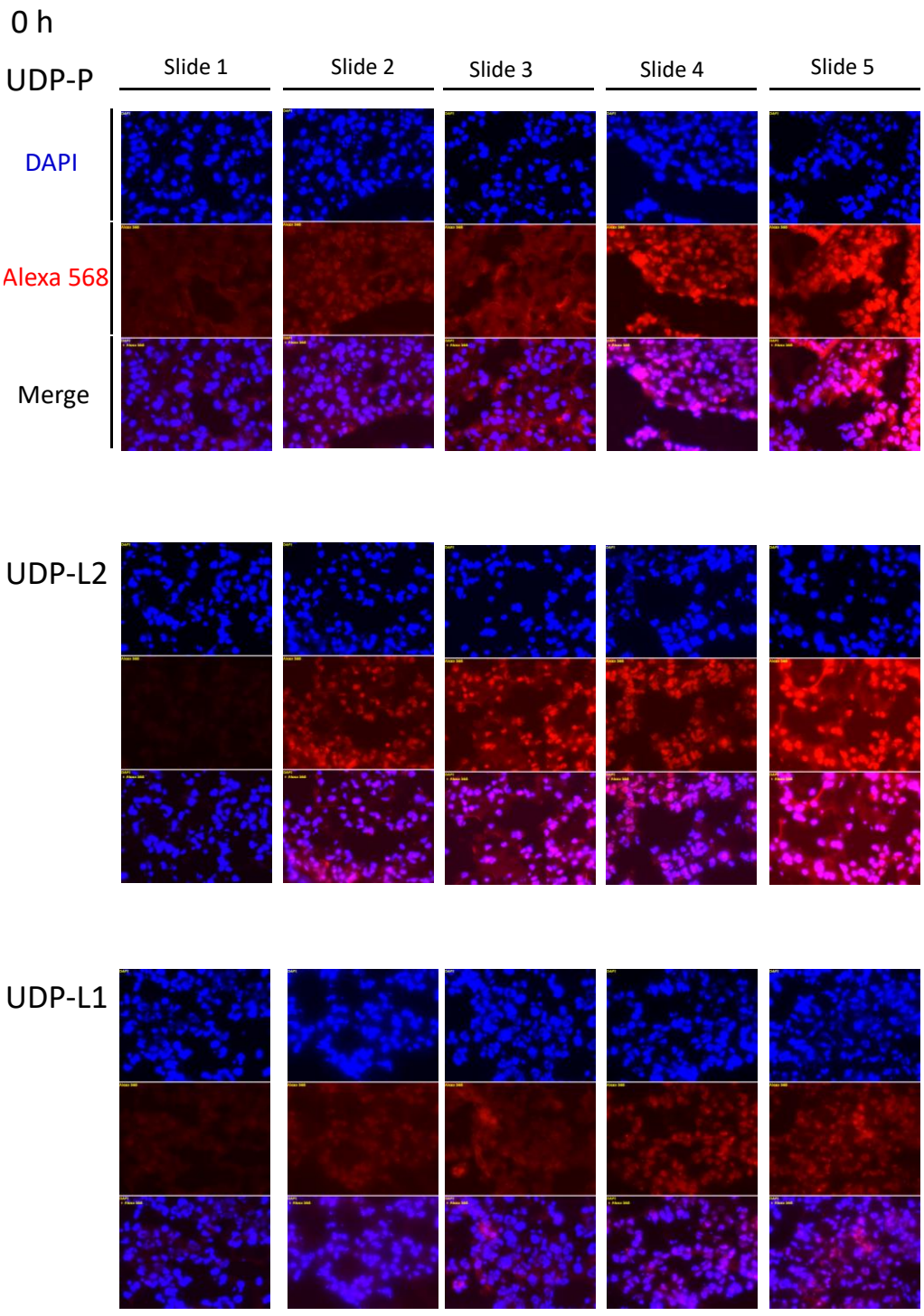
$$A_{protein} = A_{280} - (A_{max} * CF)$$

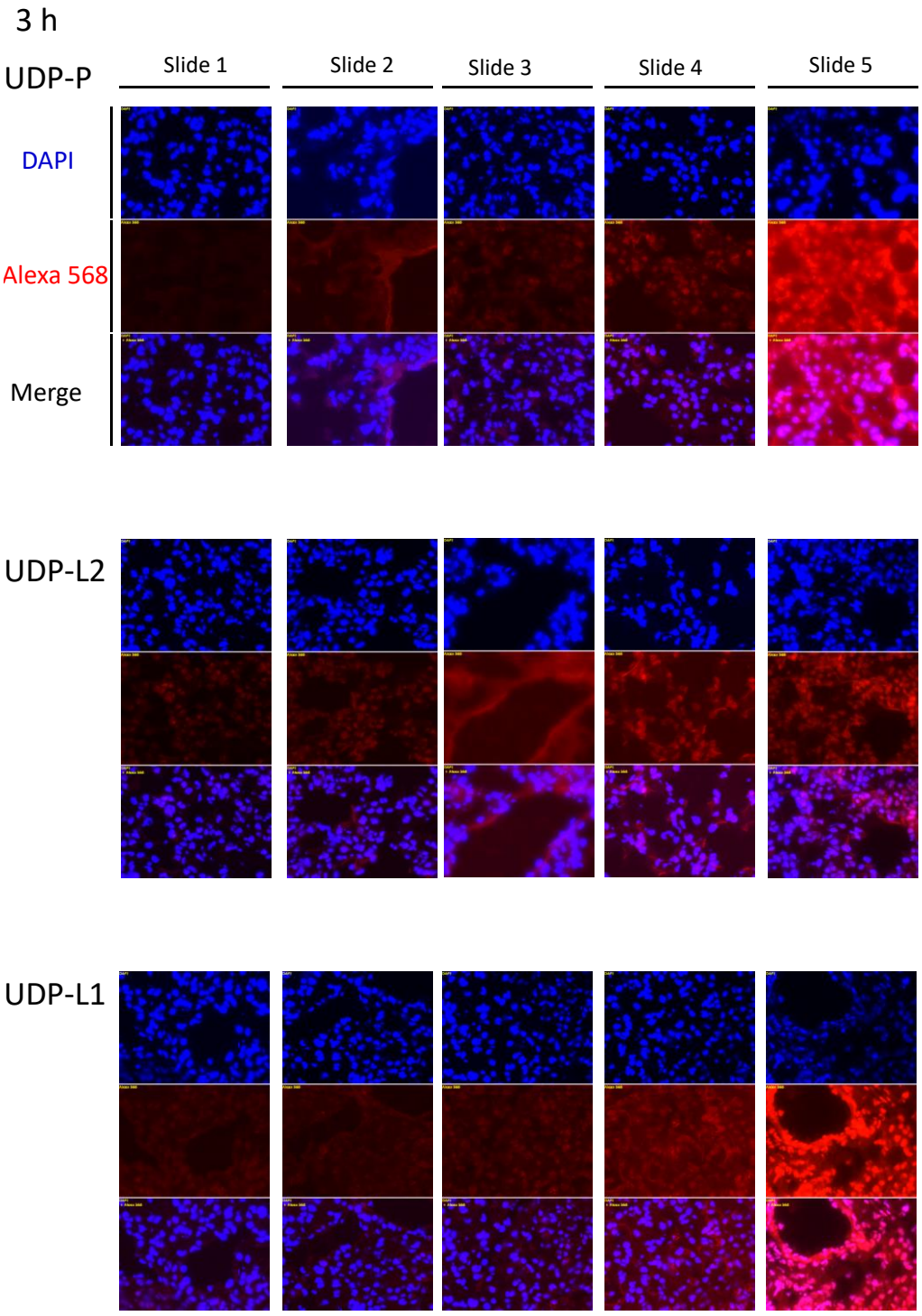
$$DOL = \frac{(A_{max} * Mw_{protein})}{(Protein\ concentration * \varepsilon_{Cy5})}$$

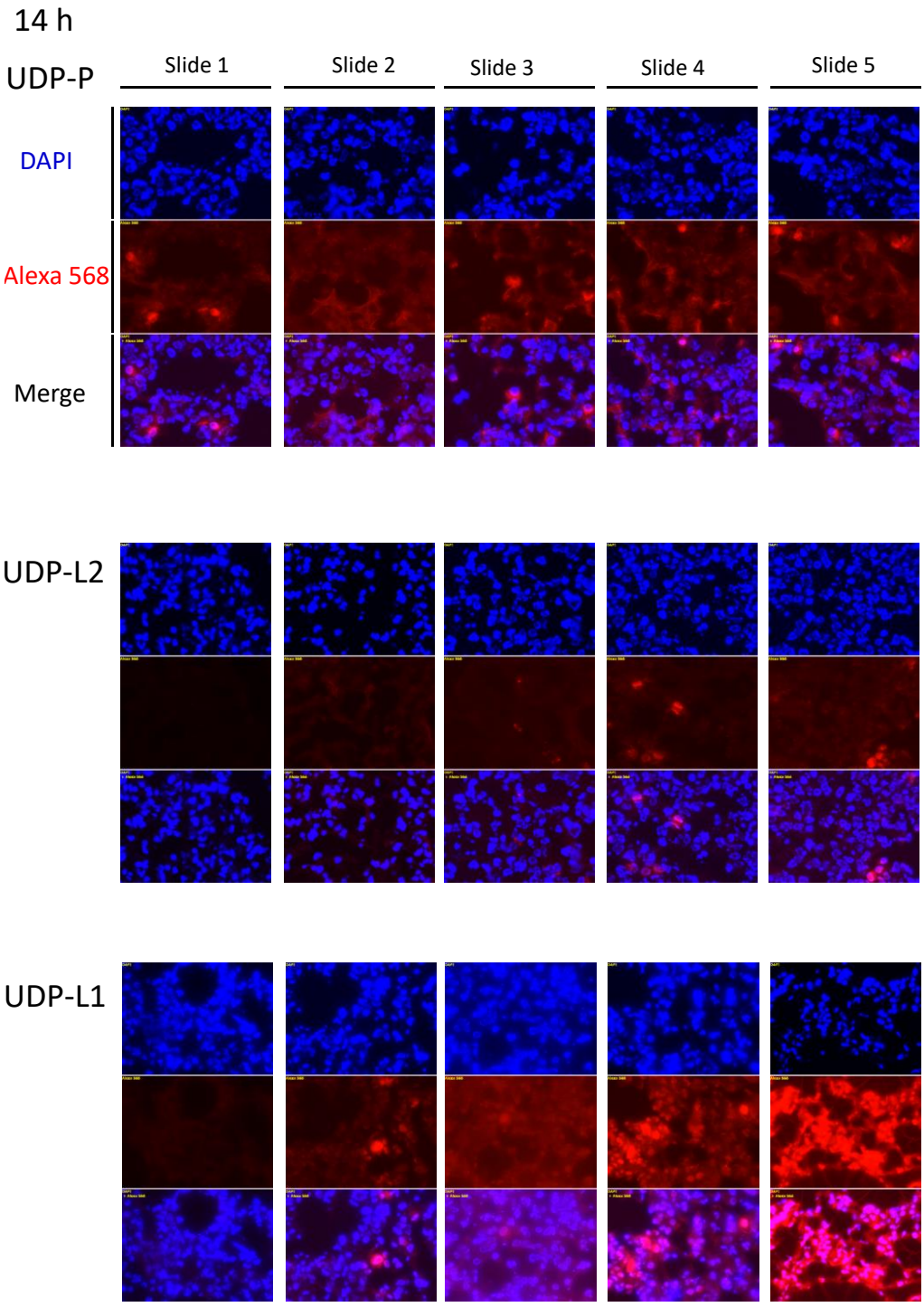
where A is the absorbance, ε is the extinction coefficient and CF is correction factor.

The degree of labelling of lysozyme was ~ 70% for all the experiments carried out in this work.

6.3.5. *In vivo* pulmonary deposition and retention of polymer-protein nanocomplexes-based dry powder formulations in healthy mice




3 h
UDP-P
Slide 1
Slide 2
Slide 3
Slide 4
Slide 5
DAPI
Alexa 568
Merge
UDP-L2
UDP-L1


14 h
UDP-P
Slide 1
Slide 2
Slide 3
Slide 4
Slide 5
DAPI
Alexa 568
Merge
UDP-L2
UDP-L1

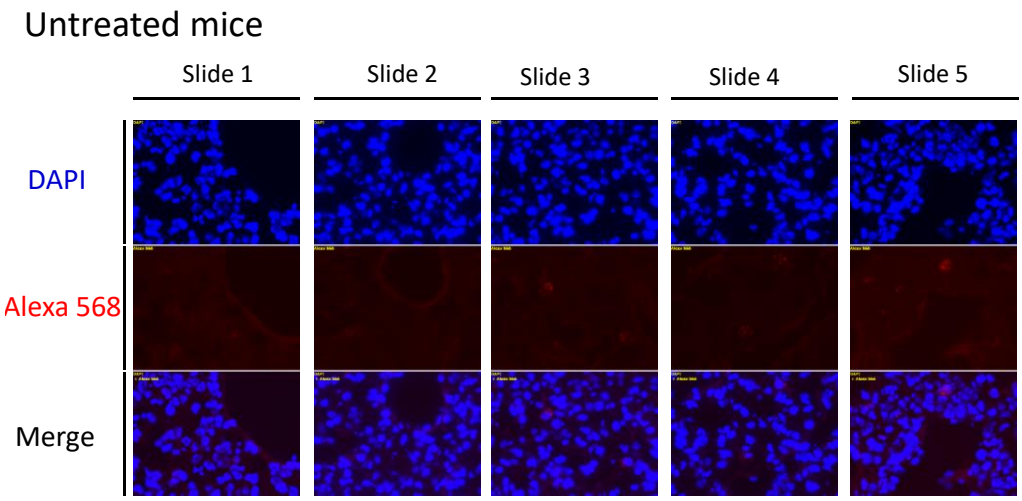


Figure S49. Distribution of fluorescent lysozyme in the lungs of healthy mice after 0 h, 3 h and 14 h pulmonary administration. Each slide represents a 7-µm longitudinal lung cryo-section that was observed using a fluorescent microscope at 200 x magnification. The images show the distribution of red labelled lysozyme-Cy5 (on an Alexa Fluor 568 filter) in the blue fluorescent lung tissue (on a DAPI filter) of healthy mice after administration of 2 mg dry powder formulations: (i) LDP-L1 (targeted nanocomplexes), (ii) LDP-L2 (non-targeted nanocomplexes) and (iii) LDP-P (no polymer) using the pulmonary delivery device.

6.4. References

MIRON, T. & WILCHEK, M. 1993. A simplified method for the preparation of succinimidyl carbonate polyethylene glycol for coupling to proteins. Bioconjugate Chemistry, 4**,** 568-569.